Development of short fiber C/C-SiC material for rocket nozzle applications

Manufacturing analysis and material characterisation resulting in a CMC nozzle prototype

AE5711: Thesis Aerospace Structures & Materials

Yestin van Haaren

Delft University of Technology

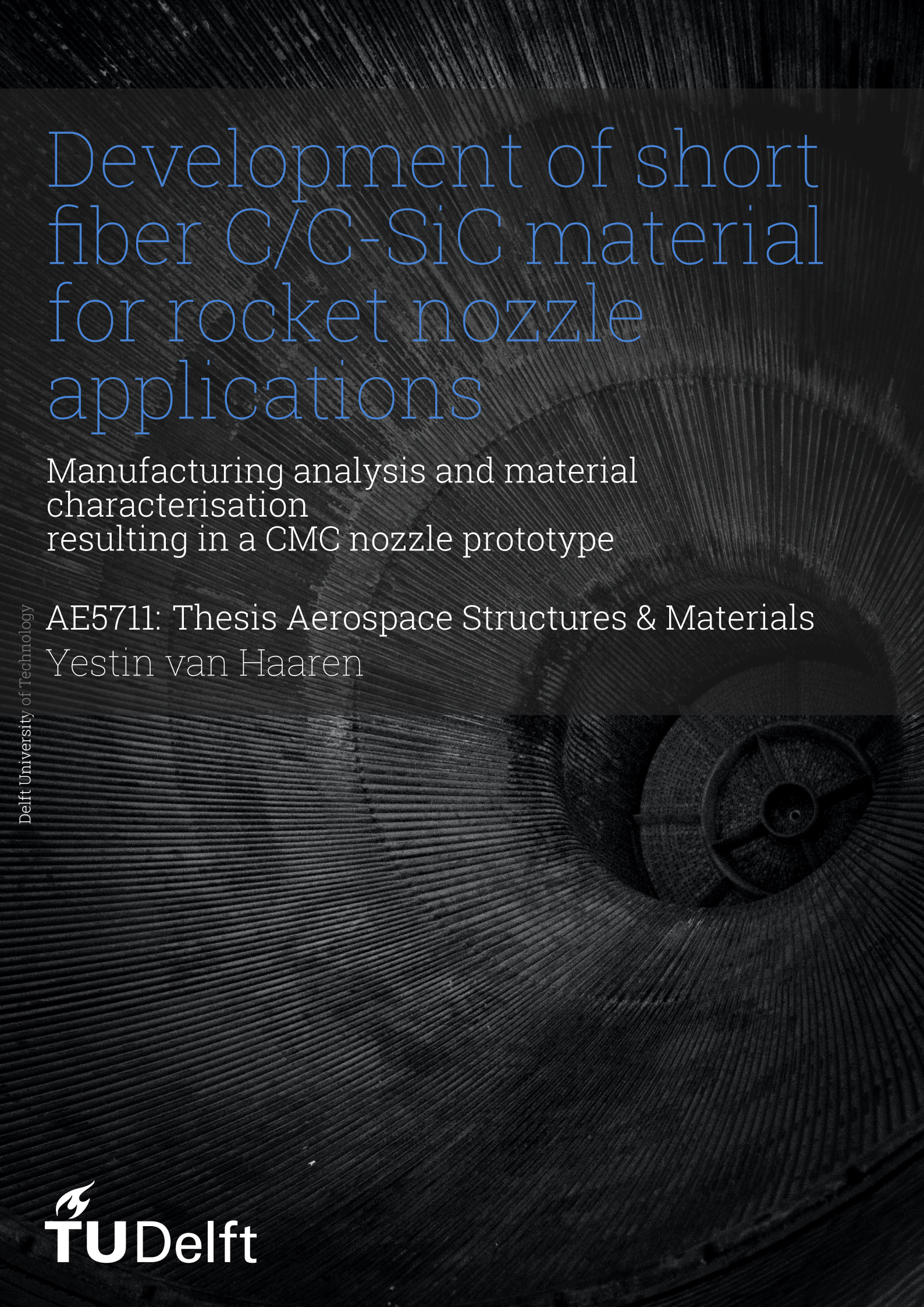

TU Delft

Development of short fiber C/C-SiC material for rocket nozzle applications

Manufacturing analysis and material characterisation resulting in a CMC nozzle prototype

by

Yestin van Haaren

Student Name	Student Number
Yestin Jacobus van Haaren	4667581

First supervisor:	Dr. Ir. Otto Bergsma
Second supervisor:	Rahul Shirke
Graduation committee:	Dr. D. Zarouchas
	Dr. B.V.S. Jyoti
Project Duration:	February 2022 - January 2023
Faculty:	Faculty of Aerospace Engineering, Delft

Cover: Engine bell of the F-1 Engine from the Saturn V rocket, Photo by Hafidh Satyanto on Unsplash: `unsplash.com/photos/AMOMZ34mGiY`

TU Delft

Preface

"3 When I look at your heavens, the work of your fingers, the moon and the stars, which you have set in place,
4 what is man that you are mindful of him, and the son of man that you care for him?"
—Psalm 8:3-4

"Great are the works of the LORD, studied by all who delight in them."
—Psalm 111:2

From a very young age, space and spaceflight have been my fascination. As the years went by, this interest never ceased, but only grew, eventually leading to my enrolment in the aerospace bachelor and subsequently master at TU Delft. Many hours of lectures, projects and exams followed and have led up to this point: my master's thesis. After this, I will be proud and honoured to call myself, an aerospace engineer. In the last eleven months, my passion for rockets took on a practical form and research into it became my day-to-day job. The culmination of this research now lies before you as a finished master's thesis.

This thesis would not have happened and would not have been the same without the help and involvement of many people, to whom I want to offer my gratitude. First of all to Arceon and its members: Rahul, Rahul and Bernhard. You offered me this opportunity and helped me with knowledge, expertise and suggestions every step of the way. Moreover, you made this an enjoyable time: with your enthusiasm, your openness and with the many interesting conversations we had over the months, thesis related and otherwise. The same goes for my fellow students at Arceon: Danny, Darspreet, Efthymios and especially Ebrar. Thank you for the nice working environment you provided and for the good times we had together. Particularly all the talks we had about our different backgrounds, religions and cultures have been valuable and interesting. From the faculty of Aerospace engineering, I extend my utmost gratitude to my supervisor Dr Otto Bergsma, who helped me, challenged me and always gave valuable suggestions and insights during the process. He was very supportive and stood behind my every step. Also thanks to all the staff members of the aerospace lab, who were kind and patient and helped me with all the tests I did.

Other people who cannot be thanked enough are my friends and family. To my friends inside TU Delft and outside, thank you for all the nice times we continue to have together, which really helped to unwind from this thesis and show that life is way more than just your education and career. To my family, who supported me throughout my education and helped me wherever they could. And most of all to my wife Henriëtte, who was always there for me and supported me in everything: Thank you from the bottom of my heart. Above all, gratitude is offered to God, who gave me the strength to do this. He helped me when things were tough, and gave me joy when things were good. Everything I have, I owe to Him. Soli Deo Gloria.

Yestin van Haaren
Delft, January 2023

Summary

C/C-SiC is a type of ceramic matrix composite. This material consists of a silicon carbide matrix phase, combined with reinforcing carbon fibers. Also, some residue carbon (and oftentimes silicon) is left in the material as a result of the manufacturing process. This residue carbon is referred to by the second ”C” in the material name. The used route for manufacturing the C/C-SiC material starts with fabricating a CFRP part. In the second step, this part is pyrolyzed, resulting in a porous C/C preform. In the last step, this preform is infiltrated at high temperature with liquid silicon, which reacts to form the silicon carbide matrix. This three-step process is called liquid silicon infiltration and is preferred over other manufacturing routes due to its cost and processing time advantages.

Ceramic matrix composites are a material group which boasts high specific strength and stiffness, good damage tolerance, as well as excellent thermal properties. These include high working temperature, high creep resistances and high thermal shock resistance. It is commonly applied in environments where these properties are utilized, such as thermal protection systems, engine components and refractory industry parts. Thus also rocket nozzles, which contain a highly mechanically and thermally stressed environment, have been made with the use of ceramic matrix composites.

This thesis is aimed at adding to the research on C/C-SiC for rocket nozzle applications. Specifically, using pitch-based short fibers as a reinforcing stage. This has the potential to have manufacturing, cost and performance benefits over other materials, however, this has never before been developed. To guide research into this area, the following research question was set up: ”What is the influence of manufacturing and material composition parameters on the properties of short fiber C/C-SiC material for rocket nozzle applications?”. The thesis answers this question in three phases. First manufacturing parameters are researched, by making many samples and determining and optimizing their properties. Secondly, composition parameters are investigated, where samples of different compositions are fabricated and compared with each other. Lastly, this knowledge is combined to suggest the ideal nozzle material and a detailed plan is set up for validation by the manufacturing of a proof-of-concept rocket nozzle from short fiber C/C-SiC material.

In the manufacturing phase, samples were made and assessed on their density and porosity. Trials were performed to assess the influence of parameters such as the oven characteristics, the accuracy of used tools, the excess resin amount and the temperature and pressure cycles. Also, data gathering techniques were developed and resin analysis using TGA and rheology was performed. This led to the conclusion that the temperature cycle, the moment of pressure application, excess resin amount and resin division in the mould were the parameters that had the largest influence on part quality. A way to optimize these parameters was described. Next to this, four other parameters of minor influence were also identified and described.

After this, the material composition was studied. The influence of fiber type, length, volume fraction and resin type was investigated. The effect of these on physical properties, microstructure and mechanical properties was determined. It was found that changing fiber type from PAN to pitch-based increases density, but also decreases porosity and greatly increases flexural strength, stiffness, coefficient of thermal expansion and ablation resistance of the material. Increasing fiber length mainly increases strength, while decreasing stiffness. Fiber volume fraction increases density and porosity, while it also slightly increases flexural strength, stiffness and coefficient of thermal expansion. Changing the resin type from liquid to powder causes lower porosity and a decrease in fiber bundle spreading.

Lastly, a plan for a nozzle prototype was developed. Based on conclusions from the second phase, the optimal composition was decided, namely 25 mm, pitch-based fibers with powder resin. A detailed manufacturing and validation plan was set up for a nozzle prototype, with which the thesis was concluded.

Contents

Nomenclature

Abbreviations

Abbreviation	Definition
ANOVA	Analysis Of Variance
ASTM	American Society for Testing and Materials
C/C	Carbon/Carbon
C/C-SiC	Carbon/Carbon-SiliconCarbide
CFRP	Carbon Fiber Reinforced Polymer
CMC	Ceramic Matrix Composite
CPR	Closed Pore Ratio
CSV	Comma Separated Values
CT	Computed Tomography
CTE	Coefficient of Thermal Expansion
CVI	Chemical Vapour Infiltration
DIC	Digital Image Correlation
DIMOX	Direct Melt Oxidation
DSC	Differential Scanning Calorimetry
EDS	Energy Dispersive Spectroscopy
EDX	Energy-dispersive X-ray spectroscopy
FVF	Fiber Volume Fraction
GFRP	Glass Fiber Reinforced Polymer
L/D	Span to Depth ratio
LEAP	Leading Edge Aviation Propulsion
LPI	Liquid Polymer Infiltration
LSI	Liquid Silicon Infiltration
PAN	Poly Acrylo Nitrile
PIP	Polymer Infiltration and Pyrolysis
SEM	Scanning Electron Microscopy
SiC	Silicon Carbide
TGA	Thermogravimetric analysis
UHTCMC	Ultra High Temperature Ceramic Matrix Composite

Symbols

Symbol	Definition	Unit
CPR	Closed pore ratio	[-]
b	Width	[m]
D	Deflection	[m]
d	Diameter	[m]
d	Depth	[m]
E	Young's Modulus	[MPa]
F	Force	[N]
FVC	Fiber volume content	[%]
FVF	Fiber volume fraction	[%]
FVF_a	Acquired fiber volume fraction	[%]
FVF_{seop}	Fiber volume fraction excluding open pores	[%]

Symbol	Definition	Unit
G'	Storage modulus	[Pa]
G''	Loss modulus	[Pa]
k	Spring constant	[N/m]
l	Length	[m]
L	Length	[m]
L_s	Sample length	[m]
m	Stress-strain slope	[N/m]
m_{air}	Dry mass	[g]
m_{cp}	Closed pore gas mass	[g]
m_f	Fiber mass	[g]
m_r	Resin mass	[g]
m_s	Soaked mass	[g]
m_w	Wet mass	[g]
P	Applied force	[N]
P_U	Ultimate force	[N]
PF	Porosity fraction	[%]
S_U	Ultimate stress	[MPa]
T	Torque	[Nm]
t_s	Sample thickness	[m]
t_{seop}	Sample thickness excluding open pores	[m]
V_f	Volume of fibers	[m^3]
V_{op}	Volume of open pores	[m^3]
V_s	Volume of sample	[m^3]
V_{seop}	Volume of sample excluding open pores	[m^3]
W_s	Sample width	[m]
ϵ	Strain	[-]
λ	Thermal conductivity	[W/(m K)]
ρ_f	Fiber density	[g/cm^3]
ρ_r	Resin density	[g/cm^3]
ρ_s	Sample density	[g/cm^3]
ρ_{seop}	Sample excluding open pores density	[g/cm^3]
ρ_T	Theoretical sample density	[g/cm^3]
ρ_{Tseop}	Theoretical sample density excluding open pores	[g/cm^3]
ρ_w	Water density	[g/cm^3]
σ	Stress	[MPa]

1

Introduction

In the last decade, the spaceflight industry has seen tremendous growth. Many new companies have successfully launched orbital rockets, while important novel capabilities such as the re-usability of rockets have been developed and matured. One of the reasons why this is possible is the continual research into and development of new materials and applications. By making rocket parts lighter, performance increases and cost goes down. One of the areas where there is still great potential for improvement is that of rocket nozzles. These important and extreme parts are highly stressed with both thermal and mechanical loads. Because of this, they are commonly still made from high-density metal super-alloys. One promising candidate for replacing this material is the low-density material class of ceramic matrix composites. However, for this to be implemented, first a greater understanding of its properties and their dependence on composition and manufacturing has to be acquired. When this is achieved, the material can more easily be applied to rocket nozzle applications, which can lead to launch systems with higher performance and lower cost, making space greener, cheaper and more accessible for everyone.

To address this problem, this report will answer the following research question: What is the influence of manufacturing and material composition parameters on the properties of short fiber C/C-SiC material for rocket nozzle applications? This will be done by manufacturing samples of this material with different compositions and using different manufacturing techniques, after which the resulting properties of the material will be assessed. Short fiber C/C-SiC material will be used, as the easily available material components and cost-effective manufacturing routes associated with it have great promises with regards to bringing down cost and increasing accessibility to this technology for more people.

The report is set out as follows. First relevant background information is provided in chapter 2. After this, motivation and methodology will be elaborated on in chapter 3. This is followed by research into manufacturing parameters in chapter 4. Then, material composition parameters are discussed in chapter 5. Lastly, all of the gained knowledge is brought together in chapter 6 regarding nozzle development. The report is ended with conclusions and recommendations in chapter 7.

2

Background information

This chapter will contain background information on ceramic matrix composites and rocket nozzles. This is to familiarize the reader with the terminology and concepts utilized in the rest of the report. In section 2.1, ceramic matrix composites will be discussed, followed by a short elaboration on rocket nozzle design in section 2.2. The information found here is based on the literature study performed before the thesis. This literature study can be found attached in Appendix B.

2.1. Ceramic matrix composites

2.1.1. Properties and applications

As the name implies, ceramic matrix composites (CMCs), are a group of composite materials with a ceramic material as the matrix phase. This ceramic matrix phase distinguishes them from the more well-known polymer-based composites, such as CFRP or GFRP. Ceramic matrix composites aim to combine the desirable properties of ceramics and polymer-based composites. It aims to improve on ceramics by adding more strength and ductility, as found in CFRP. It aims to improve on polymer composites by implementing the properties of ceramics, namely a high working temperature and a good thermal shock and scratch resistance. Since the density of the ceramic is, like polymers, low, the composite material will still have high specific properties. This makes that it has the ability to compete with metal super-alloys, which it aims to replace in the application of a high-temperature structural material.

Similar to polymer composites, the choice and combination of fiber and matrix dictate the properties of the composite. Some commonly made categories can be mentioned. In the matrix category, the distinction is often made between oxide and non-oxide ceramics. A common oxide ceramic used is alumina, while silicon carbide (SiC) is an often used non-oxide ceramic. Other notable examples are CMCs using zirconium, hafnium or boron-based ceramics. These have a very high working temperature and thus are often applied in so-called ultra-high temperature ceramic matrix composite materials (UHTCMCs).

Considering the fibers, the following can be said. The most commonly applied reinforcement in ceramic matrix composites is carbon fiber, similar to polymer composites. It is used in all the available forms: 3D braids, 2D fabrics, 1D filaments as well as in chopped form. The continuous fibers will provide better mechanical properties such as strength and stiffness, however, often come at a high cost and increased production complexity. Next to carbon fibers, also other fibers are used, most notably SiC fibers. The choice for these is made when the composite will be applied in high temperature, oxidizing environments. Here SiC provides a large benefit over carbon fiber, since carbon will deteriorate quickly in these conditions. However, this performance increase comes with a large increase in material cost.

To give some examples of where and how ceramic matrix composites are and have been applied, the following list is compiled. This is done based on the work of Krenkel [1] and Heidenrich [2][3].

- Thermal protection systems: Due to their excellent high-temperature thermal and mechanical

properties, CMCs have often been applied as shielding for spacecraft and re-entry vehicles. Especially in places of peak thermal stress, for example nose cones or leading edges, few other alternatives exist[4]. An example which can be given is the NASA X-38, an experimental re-entry vehicle which had a nose cap and body flaps constructed from CMC material [5].

- High-temperature engine components. Another area where the high-temperature properties are utilized is jet and rocket engines. Here parts like thrust vector control vanes, which sit in the rocket exhaust, or complete nozzles or nozzle extensions have been made. An example is the nozzle extension used on the Ariane 5 rocket [6]. Also, jet engine and gas turbine components have been made[7][8] [9] [10]. An example of jet engine applications is the LEAP engine, used on recent generations of both Airbus and Boeing aeroplanes. The CMC components increased the working temperature and thus removed the need for cooling, leading to an increase in engine efficiency [11].
- Brake systems: Ceramic matrix composites are also unique in their good tribological characteristics, which they maintain at high temperatures. This has led to the development of CMC brake disks and pads, which are applied in sports and racing cars [12][13], as well as aircraft[14] and emergency brake systems[15] for example in trains, elevators and cranes. This was the first application where serial production of CMC components was seen, which was achieved by the use of short carbon fibers. These made it possible to make complex geometries, like ventilated disks, in a cost-efficient and near-net-shape way [16]. Also, the use of short fibers made the process easy to automate, decreasing the cost even more. Several ways of automation have been developed, like tape laying [17] and injection moulding [18][19].
- High precision structures: Depending on their exact composition, CMC materials can have a coefficient of thermal expansion close to zero. Also given that they have a low density and high stiffness, gives them the ideal properties for use in high precision structures. Applications of this are calibration plates [20] or satellite tubes. An example is the telescope tube of the TerraSAR-X satellite, which was made from a ceramic matrix composite. Other desirable properties for this application which CMCs display are low susceptibility to environmental conditions and the absence of hysteresis behaviour.
- Refractory industry: At high temperatures, CMCs have better durability than many other materials. This makes that they have potential to be used in the refractory industry. Here moving parts like slide gates have to be replaced often due to the high production numbers present in the refractory industry. Using CMC materials for this application can increase the lifetime of these components and decrease downtime.

2.1.2. Manufacturing routes

Ceramic matrix composites can be made in multiple ways, each with its own advantages and disadvantages. Three of these manufacturing routes have been deployed at an industrial scale. To get a better understanding of the manufacturing, as well as the microstructure of the material, these three routes will be explained in more detail. The different ways will be explained assuming C/C-SiC as the CMC, as this material will be the focus of the thesis. However, other ceramic matrix composites can be fabricated using the same or similar techniques. The three manufacturing routes are called chemical vapour infiltration (CVI), polymer infiltration and pyrolysis (PIP) and liquid silicon infiltration (LSI), which will each be detailed in a separate section. The explanations will be based on the work of Krenkel[1], Heidenrich [3] and Kopeliovich [21], who have all detailed and discussed these processes in their papers. Lastly, also some alternative manufacturing techniques will be quickly summarised. It is important to note that the used manufacturing technique has a large influence on the properties of the material, caused by the effect it has on the microstructure. To illustrate this point, and to give some feeling for the material characteristics, properties of C/C-SiC created using different routes are given in Table 2.1, as taken from Heidenrich [2].

Table 2.1: "Typical material properties of C/SiC and C/C-SiC materials in dependence of the manufacturing method.", taken from Heidenrich [2]

Manufacturing route		CVI	CVI	LPI	LSI	LSI	LSI
Material		C/SiC	C/SiC	C/SiC	C/C-SiC	C/C-SiC	C/SiC
Manufacturer		SPS (SNECMA)	MT Aerospace	EADS	DLR	SKT	SGL (9)
Density	g/cm3	2.1	2.1-2.2	1.8	1.9-2.0	>1.8	2/2.4
Porosity	%	10	10-15	10	2-5	-	2/<1
Tensile strength	MPa	350	300-320	250	80-190	-	110/20-30
Strain to failure	%	0.9	0.6-0.9	0.5	0.15-0.35	0.23-0.3	0.3
Young's Modulus	GPa	90-100	90-100	65	50-70	-	65/20-30
Compression strength	MPa	580-700	450-550	590	210-320	-	470/250
Flexural strength	MPa	500-700	450-550	500	160-300	130-240	190/50
Inter-laminar shear strength	MPa	35	45-48	10	28-33	14-20	-
Fiber content	Vol. %	45	42-47	46	55-65	-	-
Coefficient of thermal expansion ||	E-6/K	3(1)	3	1.16(4)	-1-2.5(2)	0.8-1.5(4)	-0.3/1.8(5)
Coefficient of thermal expansion $\perp$	E-6/K	5(1)	5	4.06(4)	2.5-7(2)	5.5-6.5(4)	-0.03-1.36(6) /3(7)
Thermal conductivity ||	W/mK	14.3-20.6(1)	14	11.3-12.6(2)	17.0-22.6(3)	12-22	23-12(8) /40-20(8)
Thermal conductivity $\perp$	W/mK	6.5-5.9(1)	7	5.3-5.5(2)	7.5-10.3(3)	28-35	-
Specific heat	J/kgK	620-1400	-	900-1600(2)	690-1550	-	-

|| and $\perp$ = Fibre orientation; (1) RT - 1000 °C ; (2) RT - 1500 °C; (3) 200 - 1650 °C; (4) = RT - 700 °C; (5) 1200 °C; (6) 200 – 1200 °C; (7) 300 – 1200 °C; (8) 20 °C – 1200 °C; (9) values for fabric/short fibre reinforced material.

Chemical Vapour Infiltration

Chemical vapour infiltration is the process in which the ceramic matrix composite is created by infiltrating a preform with a gas which carries and then deposits the ceramic matrix. This manufacturing technique comprises the following steps. First, a preform of the reinforcing fibers needs to be made. This can be done by winding or braiding techniques, or by densifying fibers in a press mould. These fibers then form a porous preform. In the second step, the interphase between the matrix and fibers is formed. This is a crucial step regarding the final material properties, as the interphase dictates the fracture behaviour and toughness of the material. This interphase is created by the deposition of (pyrolytic) carbon on the preform, which is done using chemical vapour deposition. This thin layer provides the material with toughness mechanisms such as fiber pullout and crack steering. In the last step, the matrix is formed by gaseous infiltration. The part is put in an infiltration chamber, where it is heated up and a SiC carrying gas is introduced, usually methyltrichlorsilane (MTS). This gas is reacted with hydrogen gas to form solid SiC. The SiC is deposited directly on the fibers, forming a so-called C/SiC material, with only carbon fibers and SiC matrix present in the final material.

Two different types of chemical vapour infiltration are used, namely isothermal CVI and gradient-CVI. In the first one a single, uniform temperature is used, usually around 800-900 °C, under a low pressure of 50-100 hPa. The matrix is then deposited by diffusion. This type leads to high quality parts and can be used with complex part shapes. However, as deposition happens, pores start to close, which

limits the part thickness to approximately 3 mm. If thicker parts are to be infiltrated, the part has to be removed from the oven and the edges of the part need to be machined to open the pores again, after which infiltration can be resumed. The main disadvantage of this type of chemical vapour infiltration is the processing time, which is a few weeks up to a few months for very thick parts.

Gradient-CVI[22][23] was developed to reduce the process time and thus remove this disadvantage. This is done by applying a pressure or temperature gradient over the part, to speed up the infiltration process. This is commonly done by establishing a temperature difference between both ends of the part by heating one end to around 1000-1100 °C, while keeping the other at 800-900 °C. With this technique, the processing time can be brought down to less than one week. Part complexity however becomes much more limited and thus this technique is only used on simple shapes such as tubes.

The manufacturing route of chemical vapour infiltration boasts high matrix purity and quality and gives excellent material properties in terms of strength, stiffness and high temperature performance. The process gives the ability to very precisely control the steps which form the interphase and the matrix. However, this process is also associated with long process times and thus high costs. Next to this, due to the closing of the pores, porosity of the final part is often high, in the range of 10-15%.

Polymer Infiltration and Pyrolysis

In the polymer infiltration and pyrolysis technique, the ceramic matrix is formed by the pyrolysis of ceramic polymers, which are infiltrated in the matrix. This technique is also called liquid polymer infiltration (LPI). The process consists of the following steps. First, a CFRP part is made. Similarly to the CVI process, different fiber types can be used. Again, fibers are coated to form the interphase of the material. As a resin a preceramic precursor is used, often polycarbosilane or polysilane polymers. Optionally SiC particles are added to this, forming a slurry. Fibers will be infiltrated with this resin, after which a part is created by using layup or wet filament winding. This part is then cured in an autoclave. In the second step, this CFRP part is pyrolyzed, in which the polymer is converted to a ceramic, forming the matrix of the CMC. Again, since only SiC and fibers are present in the part, the material is labeled C/SiC. The pyrolysis step happens between 1100 °C and 1600 °C, where higher temperatures are preferred as they result in lower porosity. However, due to the shrinkage of the part during pyrolysis, as well as due to the volatiles from the polymer, a high porosity is left after this step. To reduces this, re-infiltration with the polymer happens, after which pyrolysis is repeated. This cycle often happens between 4-10 times before the desired density is acquired. Still, porosity is often high, though below 10%. Due to the cyclic nature of this manufacturing route, process times are long with one part taking multiple weeks to multiple months.

This route results in a high quality matrix, as well as good fiber quality. This is due to the fact that process temperatures are low and thus fibers are not damaged during the forming of the material. Also, this route creates near-net shape parts, with part size and complexity only limited by oven size. The disadvantages of this route are the very long (and thus expensive) cycles, as well as the high cost of the materials involved. Also, the relatively high final porosity reduces the mechanical properties.

Liquid Silicon Infiltration

Liquid silicon infiltration is a form of reactive melt infiltration (RMI) with silicon as reactive metal. In RMI, the CMC is formed by infiltrating the fiber preform with a liquid metal, which then reacts with the preform to create the ceramic matrix. In case of C/C-SiC, a C/C preform is used with liquid silicon as a metal, hence the name LSI. The manufacturing process is summarized in the following steps. In the first step, a CFRP part is formed, for which conventional composite manufacturing techniques can be used, such as filament winding, resin transfer moulding or hot pressing. It is important to note that the polymer used has to have high carbon yield after pyrolysis, and thus often phenolic resins are used. The fibers used can be coated in the same way as during the CVI and PIP process, however, this is not a requirement. After a CFRP part is created, the second step follows which is the pyrolysis of this preform. The part is put in an inert atmosphere oven, where it is heated to temperatures up to 1000 °C. During this, the polymer gets converted to pure carbon, as part of it vaporizes. Also, due to the difference in thermal expansion coefficient between the fiber and polymer, the part will crack. This leads to a porous C/C part. This step can be done in one to two days for parts with very isotropic fiber

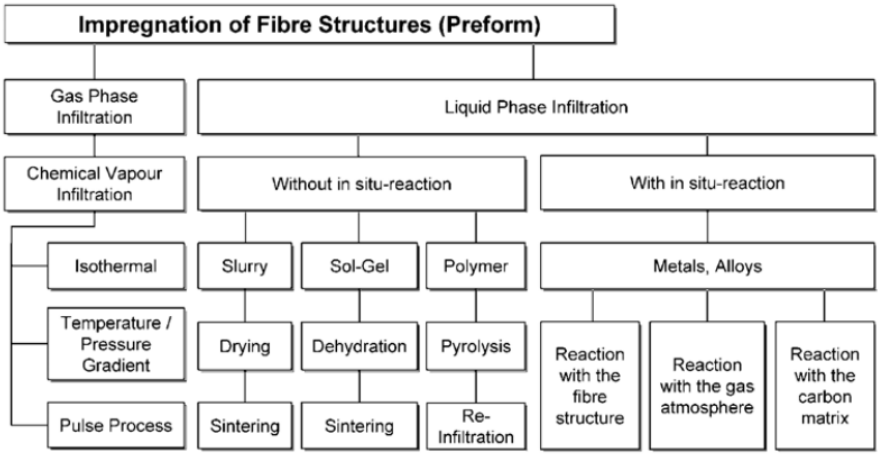

Figure 2.1: "General overview of the manufacturing processes for CMC materials", taken from Krenkel [1]

distributions, such as when using chopped fibers. However, for more anisotropic reinforcements, such as fabric or braids, lower heating rates are used to prevent delaminations and excessive warpage. In this case the step can take up to two weeks. The last step in the LSI process is the infiltration with liquid silicon. The C/C preform is put in a tub with silicon granulates, which is then put in a vacuum oven and heated to around 1600 °C. Above 1414 °C, the silicon starts melting and infiltrates the part by capillary action. As the silicon encounters the carbon, it reacts to form SiC and in this way forms the matrix of the CMC. The infiltration stops when the entire part is filled and all pores are closed. This process takes one to two days. Some amount of unreacted carbon, as well as residue silicon, will be left in the part. This is why CMCs produces using this route are called C/C-SiC, pointing to the unreacted carbon. More technically correct would be C/C-SiSiC, however, this is never used.

This manufacturing route has the advantage of being far cheaper than the other two. This since there are few process steps, which are shorter in duration and require less expensive materials. Another advantage of this technique is the low resulting porosity, commonly (well) below 4%, as the liquid fills up almost all voids. This route also has no real part complexity, shape or size requirements, except for the oven size. Another interesting addition in this process is the ability to join parts during the siliconization stage: this is done by pyrolyzing parts separately and then joining them using a carbonaceous paste or felt. After this, they are siliconized together, and a strong bond is formed. This gives the ability to make complex parts by combining simple CFRP shapes. The main disadvantage of this technique is the lower control over the microstructure, as well as lower mechanical properties. This is caused by the unreacted elements which stay behind in the material, as well as by the liquid silicon attacking and converting some of the carbon fibers, reducing their strength.

Other techniques

The three techniques detailed above are the most used ones and also the only three which have been industrialized. However, research has also suggested alternative techniques, each with its own benefits and drawbacks. These will now be listed. A clear overview of the different techniques and their relation to one another was made by Krenkel and can be seen in Figure 2.1, taken from Krenkel [1].

Firstly, direct melt oxidation (DIMOX), which is also a form of reactive melt infiltration. However, instead of reacting with the preform, it reacts with a gas which is introduced in the chamber. This technique is used for manufacturing alumina CMCs.

Secondly, slurry infiltration, where the matrix is formed by powders which are dissolved in a liquid, a slurry. Similarly to PIP, fibers are infiltrated with this slurry before a preform is formed. The next step is pressing and sintering, which results in the CMC part. The route is proven to work with matrices of silica, alumina or glass, but also research on silicon carbide or nitride has been done.

Thirdly, sol-gel infiltration, where sols are used to form the matrix, which are then later converted to gels and to ceramics afterwards. Sols are liquids containing particles that exhibit gelation when heated up. At relatively low temperatures, this gel can be converted to a ceramic. Due to low yield, the

infiltration, gelation and drying cycle has to be repeated several times. When the desired properties are reached, the part is sintered in an oven to form the CMC.

Lastly, combined methods, where some of the above described routes are combined. This is done in an effort to combine the advantages of multiple methods. Some examples are combinations of slurry infiltration with PIP or LSI, as well as combining CVI and LSI or PIP and LSI. For a more detailed explanation on these, please refer to the mentioned literature. Here these methods will not be further elaborated on, as these will not be used in the further of the thesis.

2.2. Rocket nozzle design

The function of a rocket nozzle is to transform heat energy into more usable kinetic energy, meaning the rocket will produce thrust. The environmental conditions for nozzles are extreme, with high thermal, mechanical and chemical loads. In this section, a short summary will be given of the main design drivers in rocket nozzle design and the potential for CMC materials in this.

Three different design drivers can be distinguished: performance, aerodynamics and dimensions [24]. In the first category, the environmental characteristics on the inside of the nozzle can be found: exhaust gas speed and temperature, chamber pressure, thrust level and thrust time. In the second category, much of the shape of the nozzle is defined, based on the aerodynamic requirements. Also, good shape stability is required, especially near the throat region. Lastly, strict weight and size requirements are present on the design. These conditions and drivers result in the loads and stresses that form the basis of the design. Notable stresses specific to rocket nozzles are high shear stresses and high thermal gradients inside the material. To cope with these, different materials are considered, with common ones being graphite, ceramics or refractory metals.

Already early on in CMC development, their potential for use in rocket nozzles was recognized. CMCs

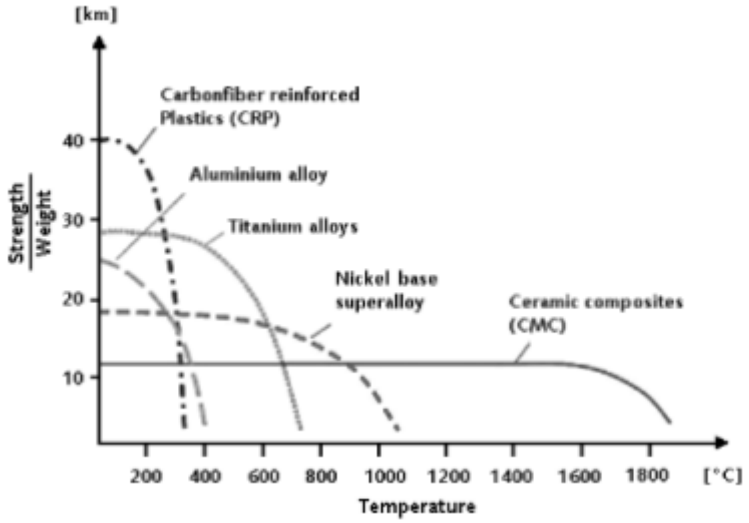

Figure 2.2: Comparison of strength to weight ratio over temperature for different nozzle materials, taken from Schmidt et al.[25]

have major advantages over ceramics, as they have higher toughness and improved damage tolerance. Compared to metals they show better resistance against thermal gradients and a much higher maximum allowable temperature, where they still have good specific properties. This is illustrated in Figure 2.2 below, as taken from Schmidt et al. [25]. The better high temperature performance leads to a reduction of cooling requirements, sometimes leading to the removal of a cooling subsystem altogether. The main disadvantages of ceramic matrix composites which should be overcome are their low mechanical values at room temperature and the bad oxidation resistance of carbon based CMCs. This last problem is relevant in uncoated carbon based CMCs when in an oxygen rich environment. However, graphite materials or metals can also encounter problems in these types of flow. A large

amount of exploratory work on the application of CMCs for rocket nozzles was done by the DASA company (turned into Astrium, then EADS-ST and is now part of the Airbus Group). They manufactured and tested rocket nozzles, nozzle extensions and combustion chambers using CMCs, proving them to work under real-world conditions [25][26]. Their test indicated that CMCs can withstand the encountered loads and often have lower mass than other nozzle alternatives.

3

Motivation and methodology

In this chapter, the research question stated in the introduction will be used to explain the setup of this thesis. Also, the motivation behind this research question will be explained. To repeat, the research question was stated as: What is the influence of manufacturing and material composition parameters on the properties of short fiber C/C-SiC material for rocket nozzle applications? Now first, the motivation behind this question will be explained. This thesis is performed at the company Arceon, a startup company developing ceramic matrix composites and bridging the gap between research and industry. They have worked together with a variation of partners in both academy and industry, and are constantly innovating to improve the material and find new areas of application. As described in the background chapter, CMC materials have great potential in rocket nozzle applications. Knowing this and having gotten multiple requests from the industry, Arceon wants to do research to better understand how CMC material can be used in this application. From this point of view, the question was set up, with the goal to develop a deeper understanding of the material, which can then be used to persuade the space industry to accept this technology. This can lead to higher performance launch vehicles, as well as increased sustainability, as less fuel and material resources have to be used for each launch.

Arceons speciality is the C/C-SiC ceramic matrix composite, which is fabricated using the LSI process. This is the material the thesis will focus on. This is of course partially because of the affinity of the company with this material. However, in general, there are good reasons to explore this material for nozzle applications. Firstly, because there is a research gap here. As far as the student and the company are aware, there are no examples of rocket nozzles made from C/C-SiC created using short, pitch-based, carbon fibers. There are good reasons to explore this research gap: Pitch-based carbon fiber CMCs have been proven to have higher stiffness than their PAN-based counterparts, as well as a vastly different microstructure. The microstructure of pitch-based C/C-SiC has fibers more embedded in and surrounded by SiC material, which gives it better oxidation resistance. This could mean that it can withstand the environment inside the rocket nozzle without any additional coating or processing, greatly reducing the complexity of the entire process. The reason for researching short-fiber materials is similar. They are more embedded in the matrix and therefore show better oxidation resistance. Also, they are cheaper and their handling and manufacturing characteristics are better. This again means that, if proven successful, this material has the potential to greatly reduce complexity in the fabrication of rocket nozzles. This means less energy, effort, material and cost needs to be used, leading to more sustainable and more accessible parts.

Now the methodology of the research done in this thesis will be outlined. To answer the research question, three major phases will be considered. In the first phase, the effect of manufacturing parameters will be researched. Here many parts will be made and by checking the resulting properties, conclusions will be drawn. A gradual increase in complexity is sought, so first prepreg samples will be made, followed by PAN short-fiber samples, followed by pitch short fiber samples. The aim is to at the end of this phase understand what manufacturing parameters matter and to have a reliable and optimal way of manufacturing high-quality C/C-SiC materials. In the second phase, the effect of material composition will be investigated. Using the manufacturing process developed in the first stage, many

samples will be made using different material compositions. The properties of these materials will then be compared and assessed to understand what parameters have what effect on the final part. Once this phase is finished, a fundamental knowledge of the material will have been obtained, from which predictions can be made regarding the properties of C/C-SiC based on its composition. This will then lead to the third phase, in which this knowledge will be used to select the best parameters for rocket nozzle applications. A rocket nozzle will be made as a proof of concept to finish the thesis. In this nozzle, both the knowledge of the manufacturing and material effects will be combined, validating the knowledge gained in the thesis. This nozzle can then be used as starting point for further research.

4

Manufacturing characterization

This chapter will detail the first phase of the thesis research, namely the research into the effect manufacturing has on material properties. First, in section 4.1, the used manufacturing steps will be explained. Then, all of the manufacturing parameters discovered will be detailed in section 4.2. After this, the way in which all the data was collected is discussed in section 4.3. This is followed by an elaboration on resin characterization in section 4.4. All of the samples made and knowledge gained from this is listed in section 4.5. Lastly, a summary of the entire process is given in section 4.6.

4.1. Production procedure

To give a better idea of the production procedure, and thus of the manufacturing parameters encountered, first a detailed description is given of the process. Note that not all the steps shown here are consistent for all the iterations. The point of the iterations was to find the best way of manufacturing, so some things changed. However, this will be explained in more detail in section 4.5. The current section aims to make sure the reader understands all the terminology and concepts which will be used in the later sections. Thus also the detailed reason behind most of these steps will be explained in section 4.5.

Firstly, the moulding technique will be explained. There are many ways to produce CFRP parts, such as filament winding, resin transfer moulding or using an autoclave. At Arceon however, currently, one technique is being used, namely press moulding. In this technique, the material is being placed in a mould, which is then closed using bolts and nuts. These are used to apply the required pressure during the curing of the part. The temperature is applied by putting the mould in an oven. This technique has some advantages and disadvantages. A detailed discussion of these and a reason for using this technique is given in subsection 4.2.1. Here the steps for using this type of technique will be discussed.

The mould used consists of five parts, which can be seen in Figure 4.1. Here, part one is called the bottom plate, two is the pressure plate, three is the top plate, four is the spacer and five is the frame. The setup of the mould is as follows. The frame is put on top of the bottom plate and connected with four countersunk screws into threaded holes on the bottom plate. The pressure plate is connected to the top plate with four countersunk screws into threaded holes on the pressure plate. The spacer is can be put on top of the frame, after which the top and pressure plate are placed on top. Then, the entire mould can be tightened by placing eight bolts in the through holes which go through the top plate, frame and bottom plate. Nuts are placed on the other end to tighten the entire assembly. The spacer will determine the thickness of the cavity left inside the mould. Different spacers can thus be used to have different part thicknesses. The mould in a connected stage, but before closing, can be seen in Figure 4.2.

The procedure to make a part during this mould will now be explained using both words and pictures. If a part is made using prepreg, the following steps are taken. First is the preparation phase:

1. A lab coat, safety shoes, nitrile gloves and a mouth mask are worn.

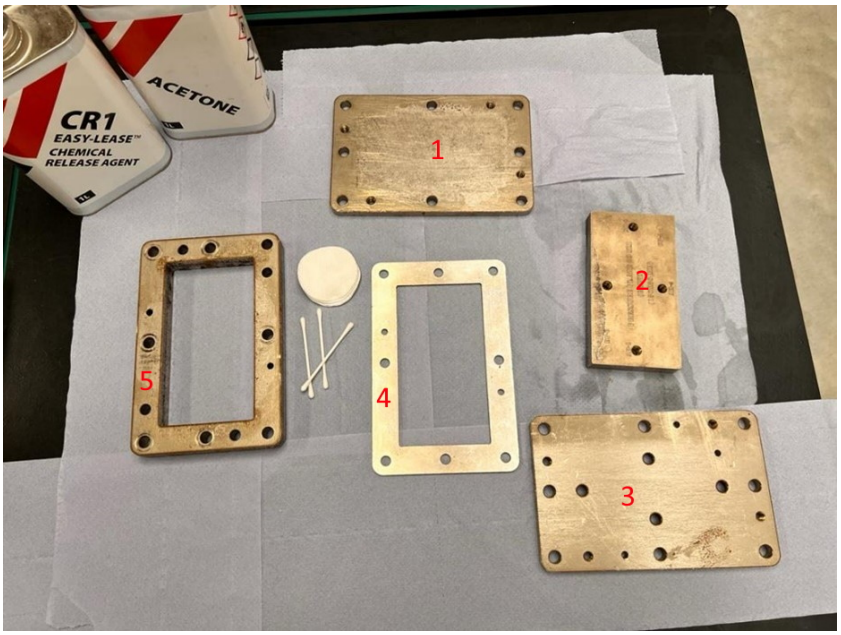

Figure 4.1: Parts of the used press mould

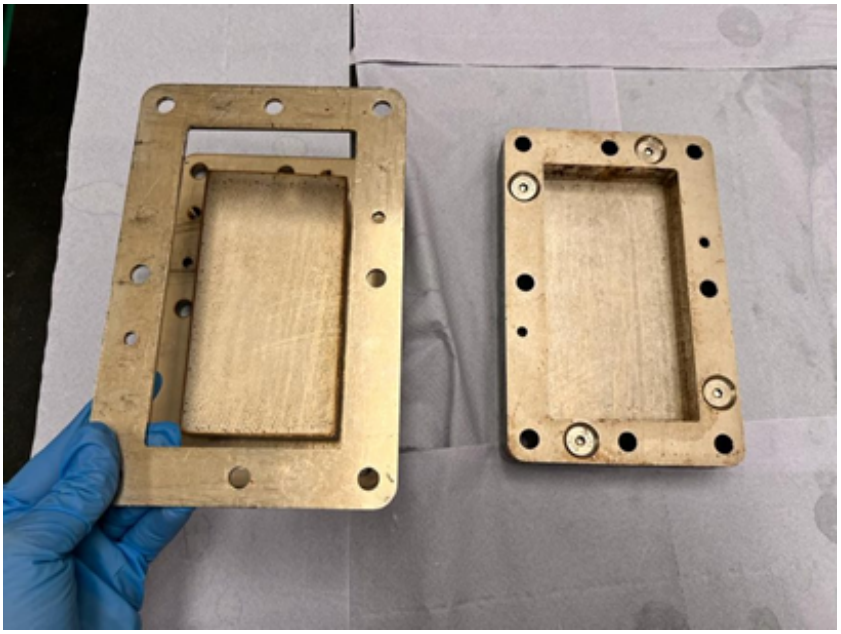

Figure 4.2: Assembly of the mould, before closing

2. The preparation table is cleaned and a clean, protective cover is placed.
3. All the required mould parts, bolts and nuts are gathered and laid out, see Figure C.1.
4. The ventilation hood is brought over to the working area and turned on to collect any fumes or particles released while working.
5. Using acetone and cotton pads, the mould parts are cleaned and allowed to dry.
6. Using cotton pads, a release agent is applied to the mould parts. First strokes are made in horizontal direction, then in vertical direction. Inside the holes release agent is applied by use of cotton swabs. The release agent is allowed to dry.
7. All the bolts and nuts are placed in a cup, with a small amount of release agent. The cup is closed and shaken to apply the release agent. The bolts and nuts are removed from the cup and allowed to dry.
8. The frame is connected to the bottom plate and the top plate is connected to the pressure plate, see Figure 4.2.

The manufacturing phase follows:

9. A prepreg is taken out of the freezer, the plastic bag preventing moisture buildup is removed and layers are measured out, drawn with a marker and then cut with scissors, see Figure C.2. The plastic bag is placed back and the roll is placed back in the freezer. Time out of the freezer is recorded.
10. For each prepreg layer, the white protection cover is carefully removed and the layer is placed in the mould. The layer is flattened with a spatula to ensure its flatness. Then the blue protective cover is removed. Any remaining wrinkles are removed by using the blue protective cover with the spatula on top. Care is taken to not touch the prepreg itself at any point in the process. Not with the spatula, nor with the gloves.
11. To measure the temperature inside the mould, a thermocouple is attached to the pressure plate with Kapton tape, see Figure C.3. To measure the temperature outside, a thermocouple is connected to the top plate, see Figure C.4.
12. The mould is placed in the oven, however, no pressure is applied yet. The first part of the cycle is programmed into the oven and started. More information on the cycle will be discussed in subsection 4.2.6.
13. After the first part of the cycle, the mould is taken out of the oven and pressure is applied using a torque wrench set to a specified value, see Figure C.5. More information on the pressure will be discussed in subsection 4.2.7. After this, the mould is placed back in the oven and the curing cycle is programmed and started.

Lastly the post-manufacturing stage:

14. The part has to be demoulded. First, all the bolts and nuts are removed.
15. Four bolts are placed in threaded holes on the top plate. These are tightened and in this way will push apart the top plate and pressure plate from the spacer and frame.
16. The spacer is removed. The bolts connecting the frame to the bottom plate are removed. The bottom plate is removed.
17. A demoulding block is placed on the sample, and then the top plate and pressure plate are placed on top of this. Bolts and nuts are used to connect the top plate to the frame.
18. These bolts are tightened, pushing out the sample from the frame.
19. The sample is placed back in the oven, and weights are put on top of it, see Figure C.6. The oven is programmed and a post-curing cycle is started.
20. At the end of this cycle, the part is completed, and the edges are cut off using a diamond-coated blade.
21. The moulds are cleaned with a spatula and acetone, scraping off any excess resin.
22. All items are placed back in storage, with all chemicals being placed in a dedicated, safe place.

The procedure when fabricating short-fiber based parts uses the same mould, however, some steps differ. These will now be explained. The preparation phase remains the same. Then the manufacturing stage:

9. The required amount of resin and fiber is calculated, based on the fiber volume fraction, mould size and density of constituents. This will be explained in more detail in subsection 4.2.4.
10. A filling strategy is decided upon. In this example, the filling strategy with two fiber layers and three resin layers in a 25/10/65 division will be shown. Also here Teflon paper assistance was used as part of the strategy.
11. Resin is put in a cup and placed on the weighing scale with a stick inside, see Figure C.7. This resin is then spread out on a piece of Teflon paper to have a uniform resin layer and a good surface finish, see Figure C.8.
12. Fiber is put in a cup and measured on a scale, see Figure C.9. This is then put on top of the resin and spread out as uniformly as possible, see Figure C.10.
13. The middle resin layer is weighed and placed on top of the fiber, in this case around the edge with the use of a dripping stick or syringe, see Figure C.11.
14. The top fiber layer is weighed and placed, see Figure C.12.
15. The top resin layer is weighed, spread on Teflon paper and put on top, see Figure C.13.
16. The thermocouple is connected and the mould is put in the oven. The top plate is put next to the frame, see Figure C.14. The first part of the cycle is started.
17. After the first part of the cycle is finished, the oven is opened and the top plate is placed on top of the frame. No bolts or pressure is used, see Figure C.15. The second part of the cycle is started.
18. After the second part of the cycle, the mould is taken out of the oven, bolt and nuts are put in and the mould is closed to a specified pressure using a torque wrench, see Figure C.16. The mould is placed back in the oven for the final part of the curing cycle.

After this, the post-manufacture phase comes, which is the same as described above.
All of the above-described steps belong to phase one of the LSI process: the creation of a CFRP green body. After this, the other two steps follow. These are outsourced to an external company and no pictures of these are available. However, the steps can still be explained. After the parts arrive at the external company, the parts are measured and weighed and a pyrolysis cycle is decided on. The parts are put in a pyrolysis furnace and optionally graphite plates are put on top of the part to prevent warpage. The furnace is closed and vented multiple times to replace the atmosphere with inert nitrogen gas. Then the pyrolysis cycle is started. At the end of this cycle, parts are taken out of the oven and weighed and measured again. Optionally a second pyrolysis cycle is created and performed. Otherwise, a siliconization cycle is created. The plates are put vertically in a crucible filled with a layer of silicon granulates. This crucible is then placed in the siliconization furnace. The furnace is degassed and pumped to a preset vacuum level. The cycle is started and at some point, the silicon granulates start to melt and become liquid. Infiltration and siliconization start. After the end of the cycle, the parts are measured and weighed again and shipped back to Arceon.

4.2. Manufacturing parameters

Now that the production process is understood, the manufacturing parameters which were discovered and researched will be outlined in this section. Which parameters were found, what their influence was and how this was assessed will be explained.

4.2.1. Method and motivation

Firstly, the reason for using this type of moulding technique will be explained. As mentioned before, it has some benefits and some drawbacks. This process mimics the hot pressing technique, however, it is less automated. Instead of having a device which constantly controls the temperature and pressure of the part, only temperature is controlled, and this using an indirect route. Pressure is not monitored but just set to a specific value at one point. The drawbacks of this are obvious, namely that it is harder to apply the exact pressure and temperature needed at every point in time: there is simply less process control opportunity. Also, the process is more labour-intensive than when using a warm press. However, there are also some advantages. First of all the lower cost, which leads to other benefits as well. A hot press is a large and expensive machine, mostly in acquisition but also in operation. Secondly,

though it cannot be proven that this way of working is a complete novelty, it is at least rarely used and not properly researched or understood. If it can be better understood and proven to work, it can bring down costs and make technology more accessible. This has advantages both in large and small industries. For large industries, it gives the possibility for fast iteration and more innovation, without the need for more expensive machinery. In the case of small industries, it enables more people with innovative ideas to test them and possibly bring them to market. In a world where big challenges have to be faced, speeding up innovation and making high-quality technology available for more people is seen as vital development. Thus, the potential for valuable development and lower costs are reasons for deciding to use and research this way of making CFRP components.

4.2.2. Assessment parameters and procedure

Secondly, before a discussion on the effect of manufacturing parameters can be done, a way of quality assessment needs to be established. There should be metrics for deciding if a part is different or better from other ones. The optimal way of doing this from a material properties point of view would be to convert them to C/C-SiC parts and test their mechanical properties. However, this is not a sustainable, practical or cost-effective way of work. It cannot be considered sustainable if a lot of energy is used in the pyrolysis and siliconization, as well as high amounts of silicon material, just to convert parts which are then found to be of very poor quality. It is not practical as the total time for parts to be converted, including packing and transit, is around two to three weeks. Ideally, a new part is made by doing improvements based on data from the old part. This ensures that no parts are made that are worse than previous ones. Thus, if only one part could be made every two to three weeks, evaluation would be really slow and very little research and very few improvements can be made. It is also not a cost-effective way of working, again because transit and conversion come with high energy and material usage, and thus also high cost. Therefore an intermediate and easier to measure property was taken for the evaluation of different parts, namely density and porosity. These are properties that are easy to measure (the exact procedure will be explained shortly), but also very relevant for the final properties of the CMC part. This was researched more thoroughly in the literature phase, with details to be found in subsection B.6.3. Summarizing the following can be stated. The final infiltration of silicon into the porous C/C preform happens through cracks and pores. The amount and dimensions of these pores are important and have a large influence on the quality of infiltration and thus the part properties. Most pores form during the pyrolysis, however, pores in the CFRP stage will also be present after pyrolysis and thus carry over directly to the infiltration phase. If the porosity is high and large pores are found, then this will negatively influence the final part's properties. Another reason for choosing density and porosity, next to the two mentioned above, is that it gives a good indication of the understanding of the process. High density and low porosity will rarely happen by chance, as most defects or errors in the process will induce porosity. Thus, having very low porosity shows that there is a good understanding of all relevant process parameters.

The way in which the density and porosity are calculated is as follows. For this, the ASTM C20-00 standard is used. Normally this is for burned refractory brick, however, it was found to also work well for CFRP. The decision was made to deviate from the more common standards for density and porosity measurements for CFRP. This since in these standards porosity is often calculated in a destructive way, such as by burning or dissolving the polymer stage of the matrix. This was not acceptable, because if a good sample was manufactured, the goal was to send it to be converted to C/C-SiC, which cannot happen if it is destroyed during evaluation. Doing density and porosity measurements consisted of the following steps:

1. Samples are put in the oven, which is then heated up to 110 °C and remains there for two hours. This is to remove any moisture from the samples
2. The samples are taken out and weighed. This is their dry mass or mass in air.
3. Samples are put in cups, see Figure C.17, which are filled with demineralized water, see Figure C.18.
4. The cups are covered with aluminium foil which is perforated, see Figure C.19. This is to prevent excessive boiling of the water.

5. These cups are put in the oven and made to boil for two hours. Afterwards, the samples are kept submerged in the water for another twelve hours. This is to ensure all gases inside the sample are removed.
6. A scale with a density kit, also using demineralized water is set up, see Figure C.20. Water temperature and air temperature are recorded. Samples are taken out of their cups and put onto the balance which is submerged in the water, see Figure C.21. Their mass is recorded, which is their wet mass.
7. The sample is taken out of the water. The water film on the surface is carefully removed by dabbing the sample with a cloth. After this, the sample is put on the top of the scale, weighing its mass in air, see Figure C.22. This mass is recorded as the soaked mass of the sample.

From this, the samples' open porosity and density are determined using the following equations, derived from the standard:

$$\rho_s = \frac{m_{air}\rho_w}{m_s - m_w} \tag{4.1}$$

and

$$PF = \frac{m_s - m_{air}}{m_s - m_w} \tag{4.2}$$

Here ρ_s is the sample density in g/cm^3, ρ_w the water density in g/cm^3, m$_{air}$ the dry mass in gram, m$_s$ the soaked mass in gram, m$_w$ the wet mass in gram and PF the porosity fraction in %.

4.2.3. Oven characteristics

The first possible parameter to consider is the characteristics of the oven. The used oven is a Thermo Scientific Heratherm OMH 60. This 60 liter oven has multiple functionalities, namely setting a temperature, and controlling the fan speed and the damper level. Most importantly however, it has the ability to store programs in which all of these things can be set and automatically run. It is important to understand the characteristics of the oven to ensure it does not affect part quality. From the oven manual, the following numbers were obtained, as seen in Table 4.1.

Table 4.1: Heratherm OMH 60 oven characteristics

Process	Value
Maximum temperature (°C)	330
Spatial temperature deviation from set value at 150 °C Max value/Typical value (K)	± 2 / ± 1.5
Temporal temperature deviation from set value at 150 °C Max value/Typical value (K)	± 0.25 / ± 0.2
Heat-up time (empty, form 25 °C to 150 °C) Max value/Typical value (min)	20/18
Recovery time (empty, door open for 30 s, at 150 °C) Max value/Typical value (min)	3/4

To confirm these, a test was performed in which a number of parameters were evaluated, namely:

- Heating and cooling rate: Testing the maximum heating and cooling rate of the oven.
- Response: The amount of overshoot, as well as the time to reach a stable value.
- Temperature accuracy: How close is the temperature the oven reports to the actual temperature?

To test this, a thermocouple was placed in the oven and a program was created with high heating rates and temperatures close to the maximum of the oven. Also, the mould was placed in the oven to assess the effect of the extra thermal mass provided by the mould. The results of the test can be seen in Figure 4.3. The spikes in this graph can be ignored, as they are a result of the data processing. For more details, refer to section 4.3 on data gathering below. From the oven test, the following conclusions could be made:

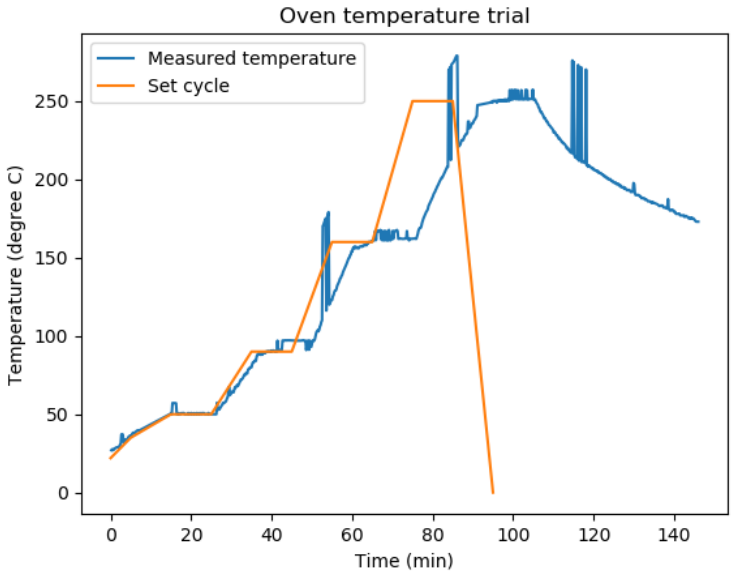

Figure 4.3: Oven characterization test

- Heating and cooling rate: This should be at least 6.25 K/min for an empty oven, according to the manual. However, it was found that in practice, with some thermal mass, this maxed out at around 5 K/min. It can be seen that the oven was still mostly able to reach the 4.0 K/min slope between 50 and 90, however, the 7.0 and 9.0 K/min slopes between 90 and 160 and between 160 and 250 could not be matched. Instead, an average slope of 5 K/min was found. The cooling rate is dependent on the conditions, such as the fan speed, damper level and door opening, however in this case, with a closed damper and closed door, was found to be around -1.9 K/min, and becoming smaller as the temperature difference with the outside environment decreases.
- Response: Good response conditions were recorded, with no overshoot and therefore no real measurable time to reach stability. After a certain temperature was reached, it stayed within 0.1 K, which is even better than given by the oven manual.
- Temperature accuracy: The temperature recorded during the dwell periods was around 1-2 degrees higher than given by the oven, however, this falls in the range of the spatial temperature deviation as given in the manual.

With this, the oven was understood better, with the main takeaway being to avoid very high heating rates as the oven will not be able to replicate these. Also, an important observation is the fact that the oven will extend each step until the conditions are reached, after which the next step is fully performed again. This leads to an extension of the cycle. It is well illustrated by the graph: The oven was slightly behind in reaching the 90 °C dwell, but performed this dwell fully, thus starting the heat up to 160 °C later. If this happens multiple times, the cycle gets shifted severely and dwells can happen significantly later than originally planned, as can be seen in the graph.

After the oven was characterized, the relationship between the mould and the oven was explored. The main research topic here was: What is the thermal lag caused by the mould, i.e. how does the temperature outside compare to the temperature inside? For this, a thermocouple was placed inside the mould, as well as one outside. The same program with high temperatures and high heating rates was used. The results are illustrated in Figure 4.4 below. Again, the spikes are a result of data processing and can be ignored. As can clearly be observed, the inside of the mould lacks a lot behind the outside of the mould. Thus the program should be adapted for this, with longer dwells and lower heating rates. Especially if the temperature difference between the inside and outside of the mould is low, heating rate is limited. It can be calculated that in the first hour of this trial, the heating rate inside the mould was around 0.5 K/min. In the second hour, when temperature differences were (much) larger, the heating rate increased to 1.9 K/min. These values give a starting point for cycle design.

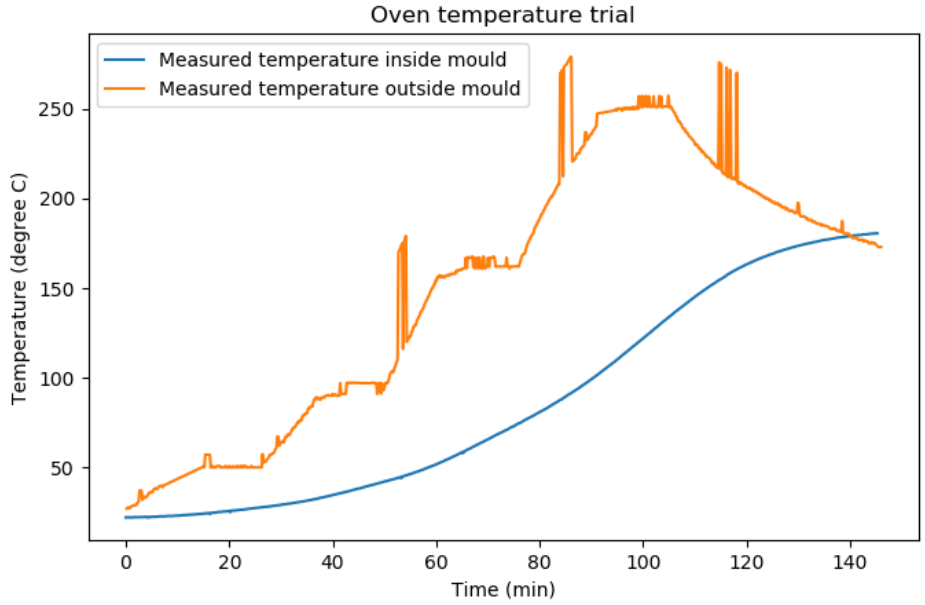

Figure 4.4: Comparison between the temperature inside and outside the mould

4.2.4. Excess resin

The next parameter is the procedure for the determination of components for short fiber production, especially the excess resin amount. For short fiber manufacturing, both fiber and resin have to be weighed separately and thus a procedure for determining these weights to get the desired mixture is required. This is done using the following steps:

1. Calculate the mould cavity area. The mould used in this thesis has an area of 150 times 80 mm^2, with a thickness of 3 or 5 mm.
2. Look up the density of the resin and fiber used.
3. Decide on a fiber volume fraction, excess resin percentage and number of resin and fiber layers for filling
4. Determine resin and fiber area by multiplying the mould area by one minus the fiber volume fraction or the fiber volume fraction respectively.
5. Determine the fiber mass by multiplying the fiber area with its density. Determine the mass per layer by dividing the mass by the number of layers (assuming equal distribution over all layers, note that this is not always the case).
6. Determine the resin mass by multiplying the resin volume with its density. Increase this value with the excess resin percentage chosen. Divide by the number of layers to find the mass per layer, (assuming equal distribution over all layers, note that this is not always the case).

Most of the parameters in this procedure are known or given. The mould area can be measured. The density of fiber and resin is given by the manufacturer, however, it is useful to check the density of resin empirically as well, as it can change with temperature and humidity. More information on this can be found in section 4.4 on resin characterization below. The fiber volume fraction is one of the material parameters tested for and thus decided before production. The number of layers is part of the mould filling strategy, which will be discussed in more detail in section 4.5. The excess resin will be discussed here. Excess resin is, as the name implies, additional resin added to the amount needed according to the calculation. Adding resin is done for a number of reasons. Firstly to compensate for volatiles in the resin. These boil off during the manufacturing process and thus decrease the mass of the resin. The amount of volatiles is dependent on the resin used. The second reason is the uniformity of the material. When excess resin is used, resin will be forced to move and flow during the application of pressure. This ensures that resin will fill the part completely and uniformly. A downside of using excess resin is of

course additional material usage, but also more trouble closing the mould. This is especially relevant when too much excess resin is used. As this resin will all have to be pushed out of the way for the mould to close, a large amount of force will be needed. This can not always be acquired, leading to incomplete closure and thus increased part thickness and decreased fiber volume fraction. Therefore, a balance has to be found between too little and too much excess resin. One important aspect of this is that there should be a way for the excess resin to escape, otherwise it will remain in the part and closing will be impossible. In the used mould this was accommodated by leaving a small gap between the pressure plate and the frame. A good indication if the amount of excess resin was good was to see if this gap was completely filled with resin after demoulding. When this was not the case, more resin needed to be used. Too much resin was identified by problems with closing, as well as seeing a large amount of resin outside of the mould after the curing.

4.2.5. Accuracy of used tools

Another parameter during manufacturing which can influence the part quality is inaccuracy of used tools. Two important tools were identified, namely the syringe, used to fill liquid resin in the mould, and the weighing scale, used to weigh off fibers and resin. To test the accuracy of the volume markings of the syringe, a certain amount of resin was filled to a certain volume, after which this volume was released in a cup and measured on a high-precision, calibrated scale (Radwag PS 200/2000.R2). This procedure was repeated 10 times, for different volume markings. Using this, the resin density was calculated and compared to the known resin density. Results showed that using the syringe had a deviation of on average 3.3%, that is on average the syringe added 3.3% resin weight to the sample. This is small enough to not have a large influence on the sample and is in the same range of error introduced by things like temperature or humidity levels. These small deviations are acceptable for the current manufacturing method, which is focused on ease of manufacturing, low cost and accessibility, not on extremely high precision.

Next to this, the weighing scale was tested. Though a high precision weighing scale is available, this is not used during manufacturing, as it is too slow for and big for this, and also is not allowed to get too dirty. Therefore a small, cheap scale is used during manufacturing with a resolution of 0.1 gram. Different weights were placed on the high accuracy scale and after that on the manufacturing scale and readings were compared. The manufacturing scale was found to always be within 0.1 grams of the high precision scale, which is a good and acceptable result.

4.2.6. Temperature cycle

To properly cure a CFRP part, the correct cycle has to be used. For a given resin, the cycle is normally provided by the manufacturer. However, as discussed in subsection 4.2.3 about oven characteristics, there is a large temperature lag and difference between the oven temperature and inside the mould. Therefore, the temperature cycle has to be adapted to account for this. First, a temperature test with an empty oven was performed, after which a test with an empty mould in the oven was done, as seen in Figure 4.3 and Figure 4.4. This was followed by two tests performing the real cycle with an empty mould. However, data processing was not possible due to a wrong setup and thus only a guess could be done about the correct cycle. A new cycle was proposed and tested, this time with prepreg also in the mould, to also assess the effect of this. This time data was available, with the resulting graph shown in Figure 4.5 (exact values can be requested from the thesis supervisor). As can be seen, though the inside temperature did follow the ideal cycle more closely, still some errors were present, meanly in the first heating up phase, as well as the height and length of the dwells. So based on this, a new oven cycle was proposed, as can be seen in the graph. This new cycle was then tested, again with a sample inside the mould. The result of this test can be seen in Figure 4.6 (exact values can be requested from the thesis supervisor). As can be seen, here the cycle is followed much closer. Based on the overshoots programmed here, other cycles can be determined.

4.2.7. Pressure cycle

Another important part of the curing cycle is the application of pressure. Again, this is given by the manufacturer, however, mostly with autoclave manufacturing in mind. In an autoclave, the required pressure can easily be set and controlled. However, for the press mould technique utilized here, this is more complex. One way of determining the applied pressure is the following. The area of the

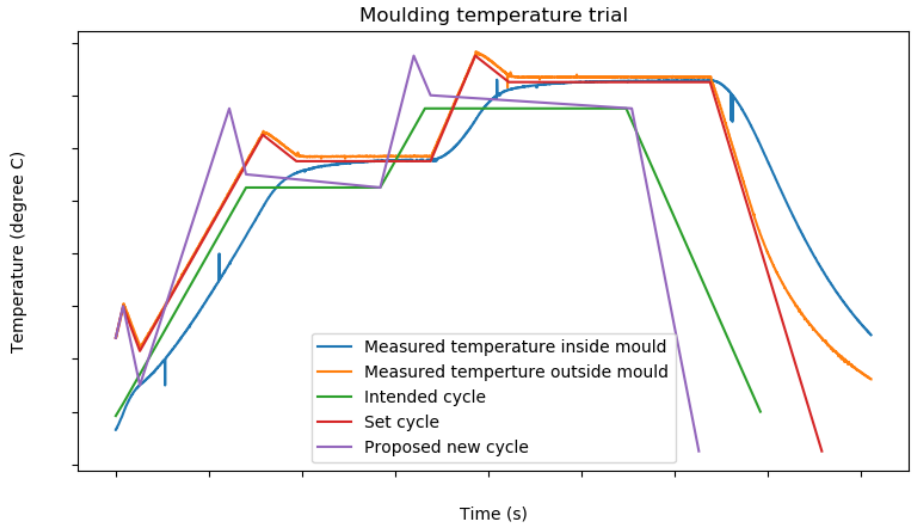

Figure 4.5: First sample trial and cycle development

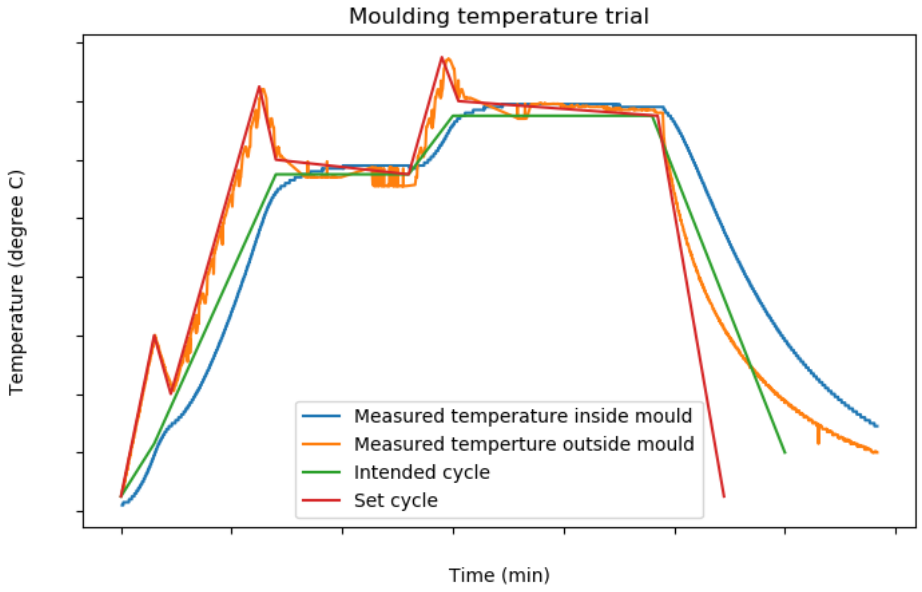

Figure 4.6: Second sample trial and cycle iteration

pressure plate can be determined and combined with the force applied on the bolts, the pressure can be calculated. However, no direct way of measuring the force applied on the bolts was available, so the force was estimated based on the torque using [1]:

$$F = \frac{T}{K \cdot d \cdot (1 - l/100)} \tag{4.3}$$

Where F is the force applied by the bolt in N, T is the torque in Nm, d is the nominal bolt diameter in m, K is a non dimensional constant and l is the lubrication factor in percentage. K can be assumed to be 0.2 for these normal, dry steel bolts, and l can be 0 when no lubricant is applied. To problem with this calculation is that it assumes that force does not go into anything else. From the moment that the top plate touches the spacer, this assumption is invalid. From that point, the load generated by the bolts will divide itself between the CFRP part and the spacer and frame. This can be considered as a parallel spring system, where the frame and spacer have a certain spring stiffness and the part has a certain spring stiffness. The amount of force that goes into each is related to the difference in magnitude of the spring stiffness of the parts. It can be captured in an equation as:

$$\frac{F_1}{F_2} = \frac{k_1}{k_2} \tag{4.4}$$

Where F_1 and k_1 relate to the force in and spring stiffness of the frame and spacer, while F_2 and k_2 relate to the force in and spring stiffness of the CFRP part. The spring stiffness of the frame can be estimated using the materials' Young's modulus, however, for the CFRP part no modulus is available. Also, since it is at an elevated temperature and undergoing the curing reaction, this stiffness will be changing with every passing second and is therefore impossible to accurately predict. This is why the estimation of pressure using bolt force is inherently flawed.

Another factor coming into play here is the thermal expansion of the mould. After the closing of the mould and bolts, the mould will heat up again, leading to thermal expansion in both the mould and the bolts, as well as the CFRP part. The thermal expansion of the mould leads to more constriction of the part and thus a higher applied pressure. Thermal expansion of the bolts leads to some reduction in applied pressure. This means that more uncertainties are added, which cannot be easily quantified. Thus again, the exact pressure applied to the CFRP part is hard to estimate.

A possible way of trying to estimate the pressure is by putting a load cell inside the mould instead of the CFRP part, after which the cycle is followed as normal. The problem with this is that, as explained above, force follows stiffness. The stiffness of the load cell will not be the same as the CFRP part and thus it will attract a different amount of force, meaning that the results will not be applicable to the CFRP part. Another, better way of estimation is by using pressure film. Pressure films are small pieces of film with minuscule ink pockets, which burst after a predetermined amount of pressure. The hue of the film after exposure to pressure can then be correlated to the magnitude of the pressure. This was tested using Prescale Pressure measurement film from Fujifilm. They have different films, correlating to different pressure ranges. If this film could be put in between the pressure plate and the top plate during the closing of the mould, the exact amount of pressure going into the CFRP could be measured. However, after some validation tests in which known pressure was applied using weights, it was found that the film was not accurate enough to do useful measurements. The hue was very difficult to read off properly, and small changes in humidity could have a large influence on the results. It was concluded that this film is more useful for finding pressure distributions (its original use case) and is not easily applicable for doing precise pressure measurements. Images of the pressure film experiment can be seen in Figure 4.7.

Another possible solution was offered in making a simulation in Solidworks, however, it was quickly concluded that again, since the material properties during closing are not known nor constant, it is impossible to get proper data out of this. Also, it is questionable whether this data would have more value than simply using the above mentioned equation. Therefore, this effort was quickly abandoned.

[1] `https://www.engineeringtoolbox.com/bolt-torque-load-calculator-d_2065.html`, retrieved on 14-11-2022

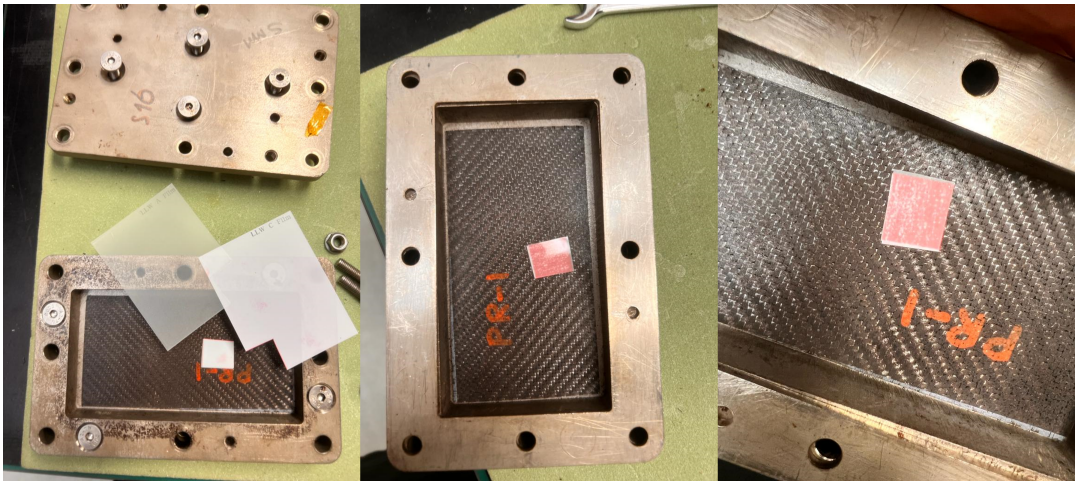

Figure 4.7: Pressure film experiment

The last aspect to consider in the pressure cycle is its influence on part thickness. If low pressure is applied, part thickness will be higher, while if very high pressure is applied, the spacer (which normally limits the thickness), will deform and part thickness will decrease. In the end, part thickness is a very important characteristic, as it dictates many part properties. From the above discussion, it can be inferred that pressure control and thickness control are mutually exclusive. Either thickness can be controlled with high precision, but then the amount of pressure will not be equal to the amount required by the resin manufacturer. Or the correct amount of pressure can be applied, but then the thickness might be different from desired. From inspection of the parts, it was determined that thickness control is both easier and more desirable than pressure control. Thickness control is done by simply closing the mould until the top plate reaches the spacer at all points. In parts made using this way, no problems with the curing of the resin or porosity of the parts were observed, from which it could be concluded that the different pressure had little to no influence on the resin cycle. This while higher thickness did have an influence on the part properties, as porosity was often higher, leading to lower mechanical properties. Therefore, in the end, it was concluded that during the manufacturing the pressure required by the manufacturer would be waived and instead thickness control would be applied.

4.2.8. Pyrolysis and siliconization cycles

Also in the pyrolysis and siliconization cycles, pressures, temperature and heating rates have to be considered as manufacturing parameters. During pyrolysis, two main concerns are present: warpage and porosity. Warpage is mainly a concern in fabric based plates, but also short fiber based parts can suffer from warpage. To prevent this, two methods are used. Firstly, heating rates are limited to make sure stresses in the material are slowly built up and can be relieved through cracking and moving of the matrix with respect to the fibers. Secondly, pressure application is done by using graphite plates. These plates are put on top of the samples, in this way limiting their out-of-plane movement and thus making warpage harder. Another concern for fabric based plates is the risk of delamination. To avoid this, heating rates should be limited, especially in temperature ranges where mass loss rate, and thus shrinking rate, are high. In general it can be stated that heating rates are coupled with part size and complexity, as again large sizes and complex geometries can lead to unwanted stresses in the material during shrinkage. The second concern is porosity, which is directly linked to siliconization. Porosity is caused by the removal of the resin matrix, as well as cracking of the part due to shrinkage. If the temperature is not high enough for long enough, a too low amount of the matrix will be lost and converted, leading to a high amount of resin based carbon left. Though this might increase ductility, it will also decrease the mechanical properties, meaning that after some point it is undesirable. To prevent this, a second, higher temperature pyrolysis cycle can be used after the first one. However, generally, pyrolysis is stopped after the mass loss rates stagnates, which for most resin is between 600 to 900 °C. This is discussed in more detail in section 4.4.

During siliconization, also both temperature and pressure are important. Temperature affects the vis-

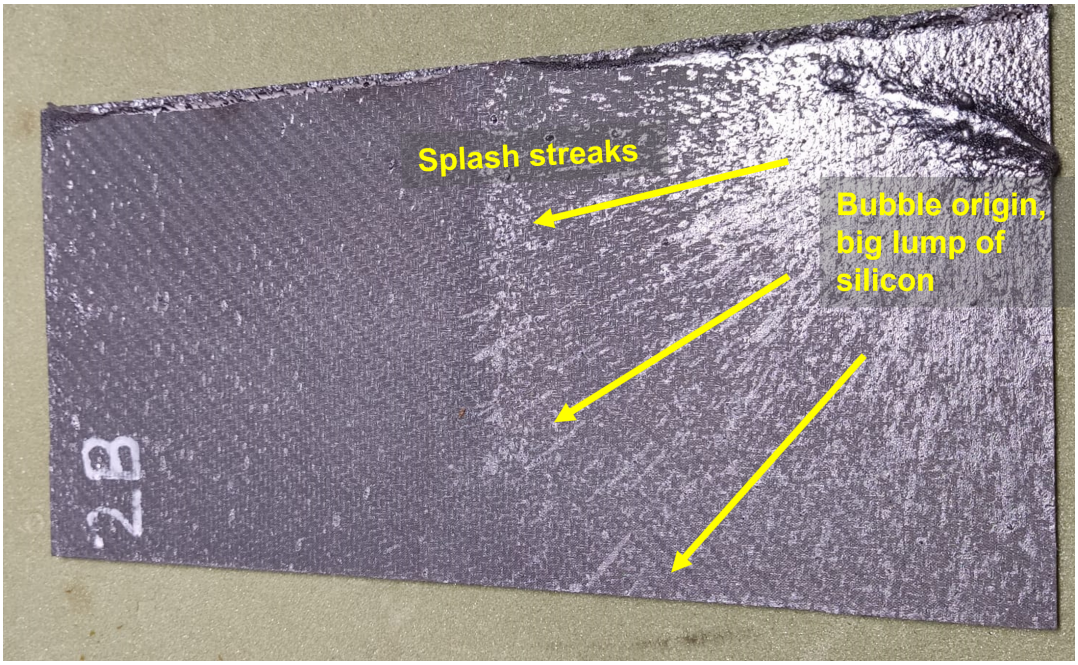

Figure 4.8: Result of exploded Si bubble

cosity of the liquid silicon and thus the infiltration. Often with higher temperatures, better infiltration happens with lower remaining porosity and higher mechanical properties. For this reason, the infiltration temperature is set around 1600 °C, around 200 °C higher than the melting point of silicon (1414 °C). Next to temperature, pressure is also important. In this case, that refers to the pressure inside the chamber. Infiltration happens under a vacuum, but the exact amount of vacuum pressure does matter. The vacuum is beneficial for the infiltration, as it increases capillary forces, however, if the pressure drops too low, it was found that there is a risk of bubbles forming in the liquid silicon reservoir. When these bubbles pop, they throw out silicon onto the plates, which leaves a high amount of liquid silicon on the surface. This is unwanted and hard to remove without damaging the part itself. An example of a popped bubble can be seen in Figure 4.8. Using a slightly higher vacuum pressure, this can be prevented. Also, the vacuum level will influence the boiling point of the silicon, which is taken into account in cycle design. Most of the time, the cycle is limited by the capabilities of the siliconization furnace.

4.3. Data gathering

This section will detail how the data used in the previous section was gathered. This is mainly with regard to the temperature data gathering, but also sizes and thicknesses of parts will be discussed. The weights and densities have already been discussed in subsection 4.2.2.

Firstly, the temperature logging. This was done using commercially available K-type thermocouples, a common and cheap type of thermocouple with a wide measuring range, from -220 to 1350 °C. As shown in Figure C.3 and Figure C.4, two thermocouples were used, one taped to the outside of the mould and one taped to the inside. For the one taped on the inside, the wire was threaded through an unused alignment hole, after which half of the frame was crossed and the cavity was reached. To prevent influence on the part uniformity and thickness, the thermocouple wire was stripped down as much as possible. However, though the wire had a thickness of 0.64 mm, it was still found that it influenced the part quality, with the part thickness on the side of the wire being higher than on the other side. Thus, to prevent this, a small groove was cut with a diamond-coated blade, which provided a route for the thermocouple wire, without influencing part quality. This can be seen in Figure 4.9. With this, the influence of the thermocouple on part quality was removed.

To get the temperature data from the thermocouple, a Proster digital thermocouple thermometer was available, see Figure 4.10. This device has the ability to read data from two thermocouples, which was

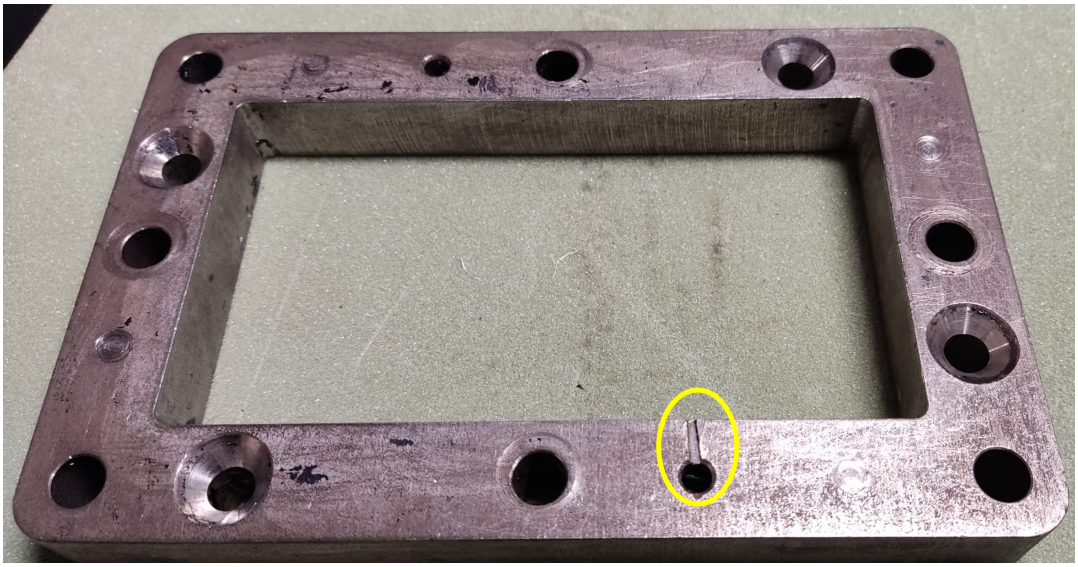

Figure 4.9: Groove created for thermocouple insertion

ideal for the used test setup. However, the device does not log the data, meaning that to create a graph, the thermometer had to be constantly monitored and recorded. This was seen as a very impractical and inefficient process, thus a different solution was found. Using a webcam linked to a laptop, pictures were taken of the Proster every ten seconds. These pictures were then saved on the laptop and later exported. Using a Python program, these images were processed to create the desired graph. This was done in the following way. First, a good image was selected and loaded into a calibration program. This program loads the image on the screen and then asks the user to click on the top left corner of each number, after which one number is selected, from which the user is asked to select the centre of each of the seven segments of the seven segment display of the number. All these locations are stored for both rows of thermometer data. From this, the location of each segment of each number is obtained. Now a new program is run, in which all pictures of the test are loaded. A grid is defined, which defines all the numbers based on which segments are identified. From the pictures, the time duration of the test is calculated. Then, some defined functions are used which convert the images to black and white, based on a set light level, from which then the coordinates are used to determine if each segment is on or off. Mapping this to the grid gives the numbers associated with each picture. Some post-processing is done to increase the number of correctly identified pictures (for example converting all detected leading 7's into 1's, as no temperatures in the 700 range can be measured, so all leading 7's are misidentified leading 1's). After this, the data is plotted. Both programs can be found in the appendix, with the calibration program in section A.1 and the second program in section A.2.

Though this technique of image taking and processing did work, it was still found to be too time-consuming and also filled up a large amount of storage space with the pictures. Thus, a different solution was desired. For this, an Arduino microcontroller was purchased. The Arduino MKR WiFi 1010 was used in combination with the MKR Therm Shield. This shield could connect to a thermocouple. A simple code was used, similar to the one given in the documentation [2]. The Arduino exported its data directly into a csv file, which could then be loaded into Python.

Figure 4.10: Used Proster thermometer

However, again this solution was not found to be optimal. The Arduino generated a high amount of noise when connected to a power outlet, and the setup was still quite complex and time-consuming. If this system was to be used for both inside and outside thermocouples, the system had to be upgraded with new and different mod-

[2] https://docs.arduino.cc/tutorials/mkr-therm-shield/mkr-therm-shield-basics, retrieved 21-11-2022

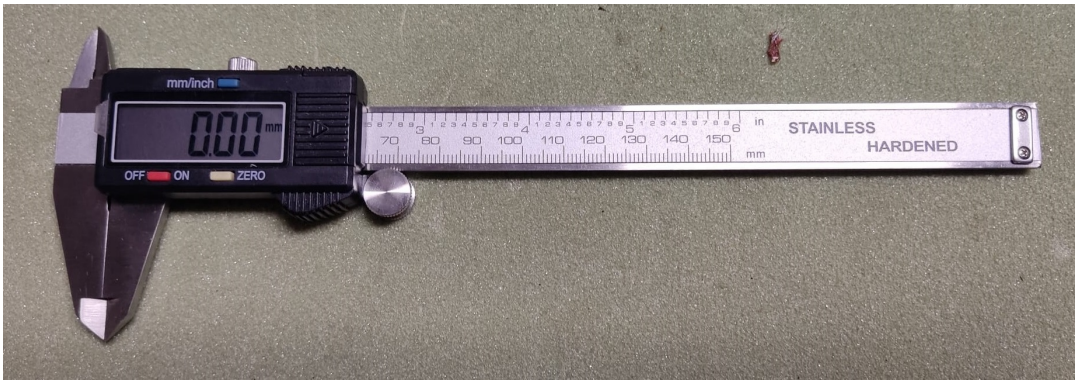

Figure 4.12: Used electric caliper

ules, which would be time-consuming again. Therefore, it was decided to choose a different, off-the-shelf option, namely, Voltcraft DL-240K data loggers, see Figure 4.11. These data loggers work as follows. They have a single USB outlet, which can be plugged directly into a computer. Online a file can be generated which defines things such as the start condition, measurement frequency and end conditions. This file is transferred to the data logger, after which it can be used. On top, a single thermocouple is connected, after which the data logger can be started and stopped using its buttons. While running, it displays the current temperature. At the end of a run, an easy to use csv file is generated, which is turned into a graph using Python. The code used for this can be found in section A.3.

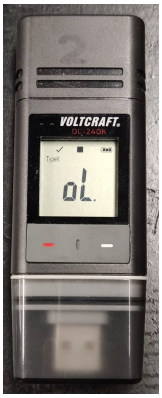

Figure 4.11: Used Voltcraft thermocouple datalogger

Next to gathering data on temperature, some other things were measured as well. Firstly the weight of components and samples using a high precision (Radwag PS 200/2000.R2) weighing scale, as was mentioned before. Next to this, the size of each sample was also determined. This was done using an electric caliper, as seen in Figure 4.12. Always multiple points were used, after which an average was taken. Using this, the width and length of samples was determined. For the thickness, an electric micrometer was used. This allowed point measurements for thickness, also on the inside of the part where the caliper sometimes cannot reach. Many points around the perimeter and more on the inside of the samples were assessed and an average was taken. Also, note was taken on the uniformity of the thickness. If one side was clearly higher in thickness than another, the reason for this was looked for.
Another way in which size and area were determined, was by taking a picture of a part with a ruler next to it, after which this picture was imported into paint.net. Here, using the ruler, the ratio between number of pixels and cm was defined, after which the program could be set to cm and every size could be easily measured by selecting it. This was especially helpful when parts or pieces of prepreg were not completely square: In those cases, a magic wand tool in the program was used, which selects an area based on the contrast with its surroundings. This allowed taking easy area measurements of non-square shapes. Note should be taken that lens distortion played a role in these images, with objects in the centre of the picture seeming bigger than those near the edges. Therefore, the accuracy of using this method was found to be limited, though if care was taken with how the images were taken, it was still a useful tool.

Lastly, for measuring and applying torque during closing, a torque wrench was used. This device can be set to a limited torque, which is then applied. The used Wera wrench can be seen in Figure 4.13[3]. A problem encountered with this wrench was its lowest torque level, which was 2.5 Nm. Using Equation 4.4, it can be determined that for 8 bolts and 2.5 Nm, the pressure applied to a 150x80 mm^2 part is 10.2 bar. This while from the manufacturer the required pressure was 8 bar. However, it was assumed

[3]Retrieved from `https://bit.ly/WeraWrench` on 15-11-2022

Figure 4.13: Used torque wrench

that the rest of this force is carried by other mould parts. For a more detailed discussion, please refer to subsection 4.2.7 above.

4.4. Resin characterization

In the previous sections, it was explained how the manufacturing parameters were discovered, researched and optimized, mostly in an empirical way. Though this is not a bad way of doing research, a more structured approach can also be taken, especially by analyzing the material properties of the used resin. As part of the thesis research, this was also done. However, it was found that the empirical approach was more valuable and easier, which is the reason it is listed earlier. Still, interesting lessons were also taken from the analysis of the resins, which will now be detailed.

First of all, thermogravimetric analysis (TGA) will be discussed. In this type of analysis, a piece of material is heated, while continually its weight is measured. Doing this for a resin can first of all help identify how much volatiles are present and thus how much weight the resin loses during curing. This can then be added as additional weight during the manufacturing stage. Secondly, the temperature at which major weight loss occurs can help identify when the volatiles will go away and by extension, the volatile type can be identified. Also curing temperature can sometimes be identified. Lastly, looking at the high-temperature mass loss can help define the pyrolysis cycle as it can be estimated how much carbon the resin will deposit for certain temperatures. For these tests, the TGA4000 from Parker Elmer was used.

Two types of tests were done both using between 32 and 64 mg of resin. This resin was put in a crucible and weighed on a high-precision scale, after which the crucible was put in the test chamber and a predetermined cycle was run. Firstly, a low-temperature test was done. A low heating rate was used, to be able to precisely see at what temperature changes happen. This test is mostly focused on CFRP production. Secondly, a high temperature test was done. Multiple runs were done for each test. The result of the low temperature tests can be seen in Figure 4.14, and the result of the high temperature test in Figure 4.15 (exact values can be requested from the thesis supervisor).

For the low temperature test, a high amount of scattering between different tests was observed. This can be the result of small impurities or the amount of cure and solvent of the resin samples used. One way to get closer data is to increase the heating rate, as then the effect of these small deviations is smaller, as can be seen in the high temperature test. In general, it can be identified that the resin experiences a large and fast decrease in mass at a definable temperature point. This can point to some solvent boiling away or a chemical reaction like curing happening. At a slightly higher temperature, this process has mostly stopped and additional mass loss is very gradual. The mass loss at the curing temperature, the highest temperature experienced by the resin during production, can be read off and defined. This loss in mass should be accounted for during production.

For the high temperature test, the same behaviour and mass loss at low temperature is found. After this, a major mass loss process can be identified starting at two points in approximately in the center off the graph. This can be identified as the area where the hydrocarbon volatiles from the phenolic resin emerge. The total mass loss can also be defined. This can be used for the pyrolysis cycle design. Especially the area in the center of the graph is relevant, as here mass loss rate is very high. This means that the part shrinkage here will also be very quick, so it is good practice to slow down the heating rate during this period. This is done to prevent delaminations or other mistakes from happening. Ideally,

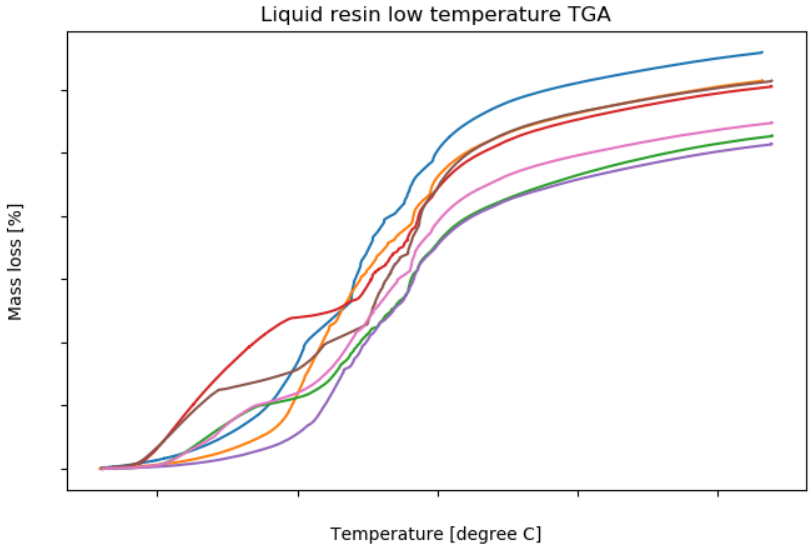

Figure 4.14: Multiple low temperature TGA runs for the used resin

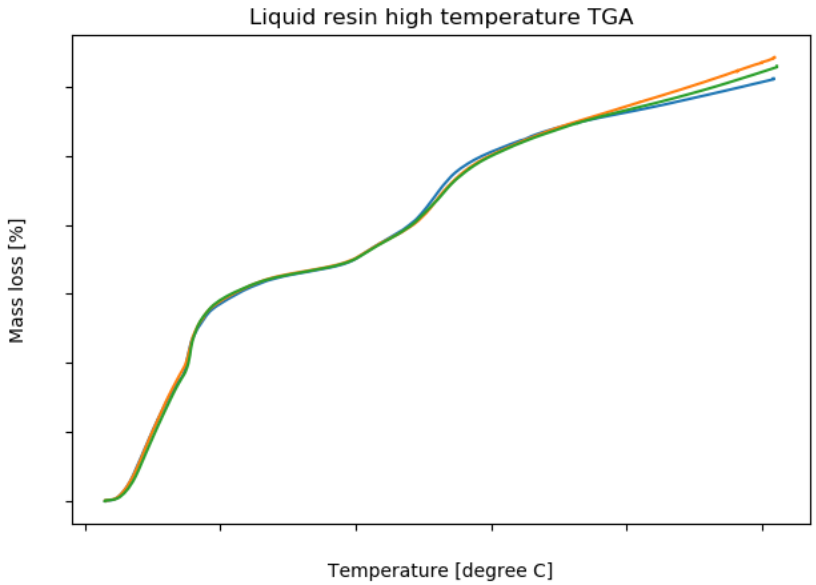

Figure 4.15: Multiple high temperature TGA runs for the used resin

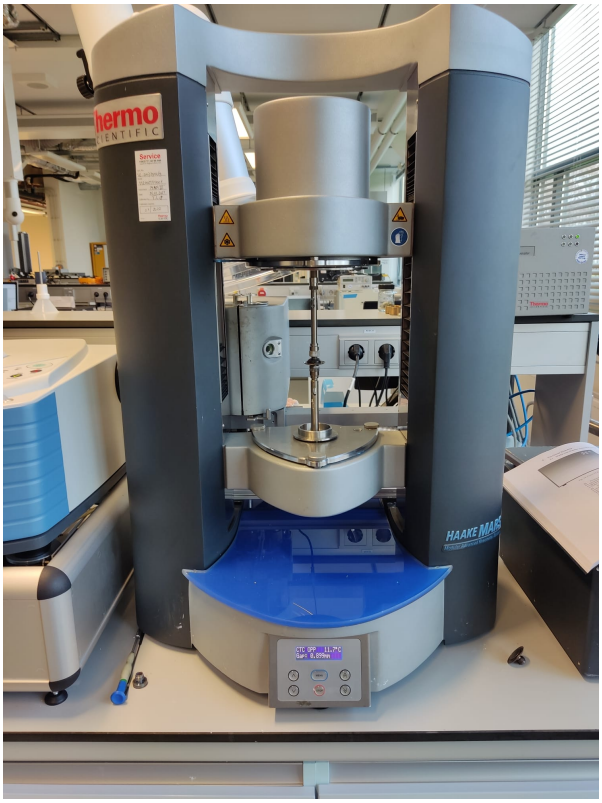

Figure 4.16: Used HAAS MARK III rheometer

the test should be repeated with a cured resin sample, as then the effect of curing is removed. It would thus be easier to design the pyrolysis cycle, as the same source material, cured CFRP, is presented. However, this is left for future research.

A second characterisation test which was performed was rheology. Here the storage and loss moduli of the material are measured. If this is done over a temperature range, then from this gel temperature and curing characteristics can be precisely determined, as well as a viscosity curve. To perform this test the ThermoScientific HAAS MARK III rheometer was used, as can be seen in Figure 4.16. A heating measurement was performed from a low to a high temperature. Flat, round plates with a 20 mm diameter were used. From literature, test parameters were derived which were used for a similar resin. These were for a rotating, oscillatory rheometer, which this is. A frequency of 10 Hz was used, with a deflection angle of 0.01 °. From this, the following graph was obtained, as seen in Figure 4.17 (exact values can be requested from the thesis supervisor).

Some problems with this test were identified. First of all, it is expected that as the material cures and turns solid (which it was after the test), the storage and loss modulus lines cross over. This cross-over point then defines the gel point. However, this never happened. Also, it can be seen that the data for G" is very noisy below 120 °C. This leads to unusable data, and since the viscosity is derived from G' and G", the viscosity in this region also cannot be used. This while one of the most important reasons for doing this test is to determine the point of lowest viscosity before curing, as this gives an indication as to when the mould is best closed. Now, the only useful observation which can be made from this graph is the rapid increase in viscosity and moduli. This gives a strong indication that at this point the material solidified and thus represents the curing point. The reason for the low quality of data in the rest of the graph is likely the use of wrong testing parameters. To determine better parameters, a number of tests should be performed on the resin in the rheometer like an oscillation frequency sweep, an oscillation amplitude sweep and a deflection angle sweep. The resulting graphs can then be analyzed to determine what parameters will give the most accurate results. Also, the heating rate will have to be

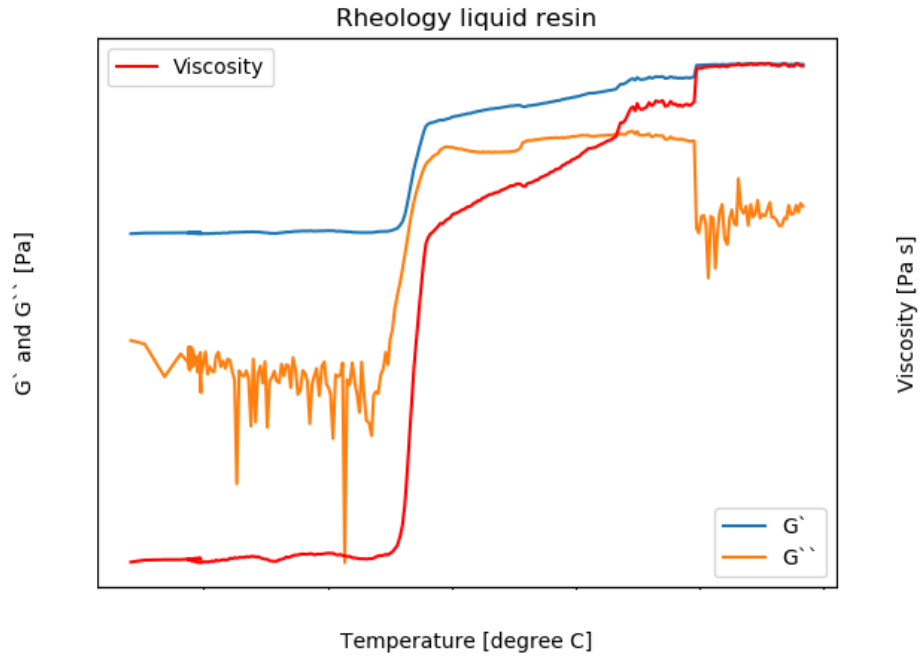

Figure 4.17: Rheology test results

reconsidered. As these tests would have required a large amount of time and research into rheology testing, it was decided not to do them, but to determine the optimal manufacturing parameters in a more empirical approach, as was already explained. However, these tests are still valuable to consider performing in some form of future research, which is more focused on resin characterization instead of manufacturing and C/C-SiC material understanding.

To get a better understanding of the ideal mould closing point, meaning the point where resin most easily spreads among the fibers, as well as the ideal dwell length, two viscosity trials were done. The first trial was set up as followed. Resin was put in a partly assembled mould, on top of which fibers were placed. Just the bottom plate connected to the frame was used. This was placed in the oven and every ten minutes pictures were taken to see if the fibers would sink into the resin. Also, the temperature of the resin was recorded. Some relatively random amount of resin was placed in the mould and the amount of fibers corresponding to 55% fiber volume fraction (including 10% excess resin) was determined and placed in the mould as well. This was quite a large amount, so it was slightly compressed before being put into the oven. For this 3 mm PAN based short fibers were used. The test was performed using the DE20 resin. The amount of resin used was 64.3 g + 6.8 g excess. 119.4 grams of fiber were used, which corresponded to a fiber volume fraction of 55%. This amount corresponded to a theoretical plate thickness of around 10 mm. The test results are summarized in Table 4.2 below. An image showing the test setup can be found in Figure 4.18.

This test was not successful. This was due to the large number of fibers on top of the resin. Due to this, no changes could be observed and no conclusions drawn. For this reason, a second trial was done. This time instead of a mould, an aluminium tray was used. Also not 55% fiber volume was used, but just a small amount of fibers with a large amount of resin. The following procedure was followed: A certain amount of resin was put on an aluminium tray. A small amount of fibers were put on top. This was put in the oven and the sinking of the fibers into the resin was checked approximately every 10 minutes. At every check, multiple pictures were taken. A thermocouple was put inside the resin to monitor its temperature. The amount of resin used was 61.0 g, while only 1.8 of fiber was used to be able to properly observe the infiltration (corresponding to a theoretical fiber volume fraction of approximately

Table 4.2: Viscosity trial 1 results

Time [hh:mm]	Resin temperature [°C]	Action or observation
00:00	Room temperature	Mould put in oven, oven set to 80 °C.
00:25		Oven damper closed as temperature got stuck at 77 °C.
00:27		Oven at 80 °C.
00:30	57	No changes visible.
00:41	64	No changes visible.
00:51	68	No changes visible.
01:04	72	No changes visible.
01:14	74	No changes visible.
01:28	76	No changes visible.
01:41	77	No changes visible.
01:54	78	No changes visible.
02:06	79	No changes visible.
02:22	79	No changes visible.
02:35	80	No changes visible.
02:37	80	No changes visible Experiment end.

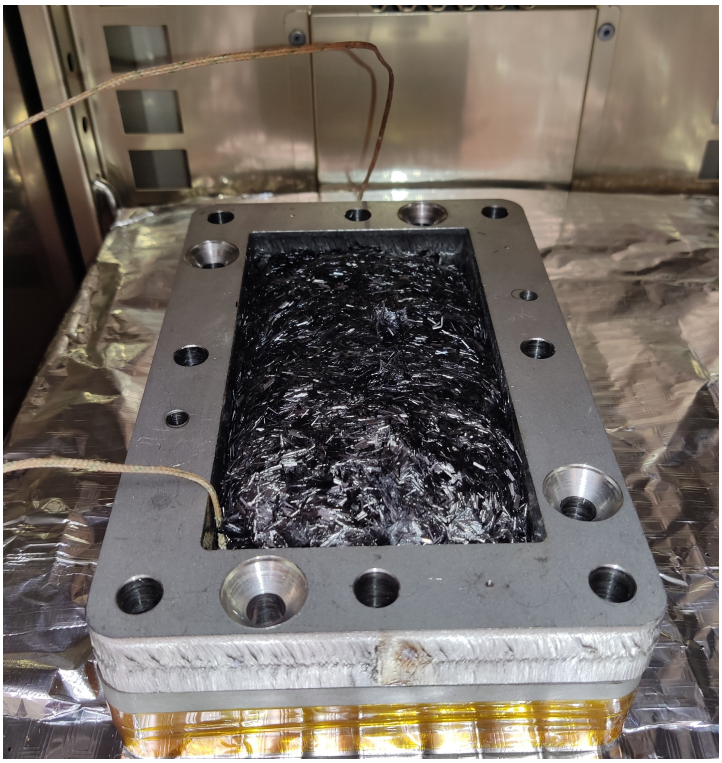

Figure 4.18: Viscosity trial 1 test setup

Table 4.3: Viscosity trial 2 results

Time [hh:mm]	Resin temperature [°C]	Action or observation
00:00	Room temperature	Tray was put in oven, oven set to 80 °C.
00:07	55	Oven at 80 °C. No fibers yet inside the resin.
00:14	68.6	Significant amount of fibers in resin, though mainly the shortest ones.
00:25	74.0	Majority of fibers inside resin.
00:35	75.1	Almost all fibers inside resin.
00:46	75.3	1 dry spot left, 4 major 'bumps' where fibers are wet but the resin surface is not yet flat.
01:03	76.9	No dry spots, all fibers a bit wetter, 5 major 'bumps'
01:18	76.4	No change visible.
02:06	80.1	All fibers a bit more sunken into the resin, but no major changes. Experiment end

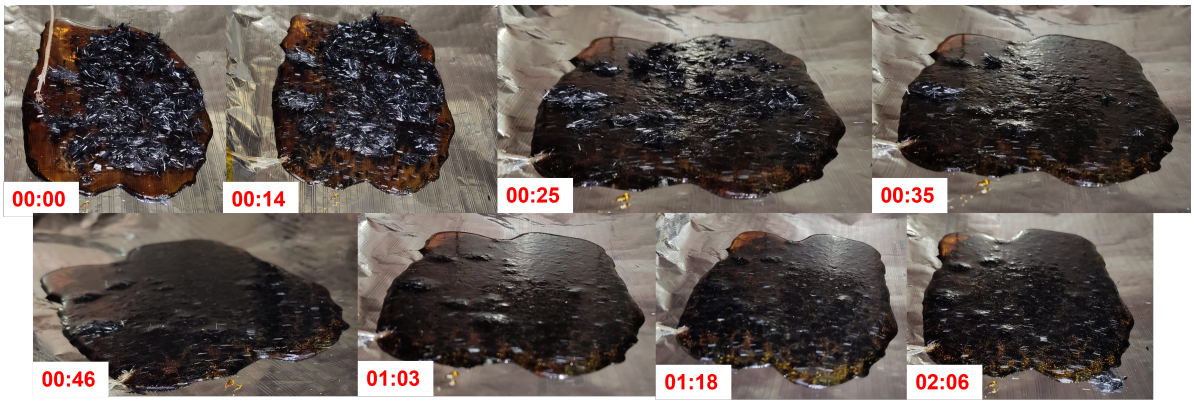

Figure 4.19: Viscosity trial 2 images

2%). The approximate resin area was 124.4 cm^2, corresponding to an approximate average thickness of 4.3 mm for this resin layer. The test results are summarized in Table 4.3 below. The images of this test can be seen in Figure 4.19.
This test gave a lot more insight into the speed of fibers infiltration in the resin and the temperature at which this starts. Based on this, it was decided to add a dwell to the short fiber cycle.

Lastly, a test was performed to determine the density of the NO 09 powder resin. The density is important for calculations on how much resin to use when manufacturing. However, the density given by the manufacturer (0.365 g/cm^3) was deemed incorrect. Also, since this is a powder resin, a large change in density will occur during the phase transition from powder to liquid. Therefore, using the powder density will not lead to successful parts. To solve this, a density test was set up to determine the resin density at different temperatures. The setup will now be described. A beaker with volume markings was filled with the powder resin and put in the oven. A thermocouple was put inside the resin to monitor the temperature. The oven temperature was increased in a step-wise fashion. Periodically the beaker was taken out of the oven, the volume was estimated using the scale on the beaker and the weight was taken. The thermocouple had to be taken out every time this happened, and once the resin solidified, it could not be put back in. The results of this test can be found in Table 4.4. The numbers in brackets behind the volume measurement give the range of uncertainty. So 80 (-5) means the value is likely 80, but could be as low as 75. The thermocouple data from this test can be seen in Figure 4.21. Pictures of the experiment can be found in Figure 4.20.

Table 4.4: NO 09 resin density experiment

Time [min]	T [°C]	Volume [ml]	Weight [g]	Resulting density [g/cm^3]	Notes
0	21	80 (-5)	47.634	0.60	Powder form, resin was compacted by shaking
17	40	80 (-5)	47.609	0.60	Powder form, resin was compacted by shaking
33	60	75 (-5)	47.526	0.63	Resin is solidifying
45	83	50 (?)	47.439	0.95	Resin is completely solid
65	98	35 (-5)	47.412	1.35	Resin is liquid but still very sticky
73	111	30 (-0)	47.409	1.58	Resin is liquid, less sticky, a smooth surface has formed
78	135	30 (-0)	47.417	1.58	Resin is liquid, more sticky, surface is not smooth anymore heating going very fast at this stage
90	149,130	115 (+-10)	47.187	0.41	Temperature increased to 150 °C, then dropped to 130 °C. Volume has greatly increased. The resin is still quite liquid but is creating foam
100	155	150 (+-15)	47.681	0.32	Resin is mostly solid. Experiment end.

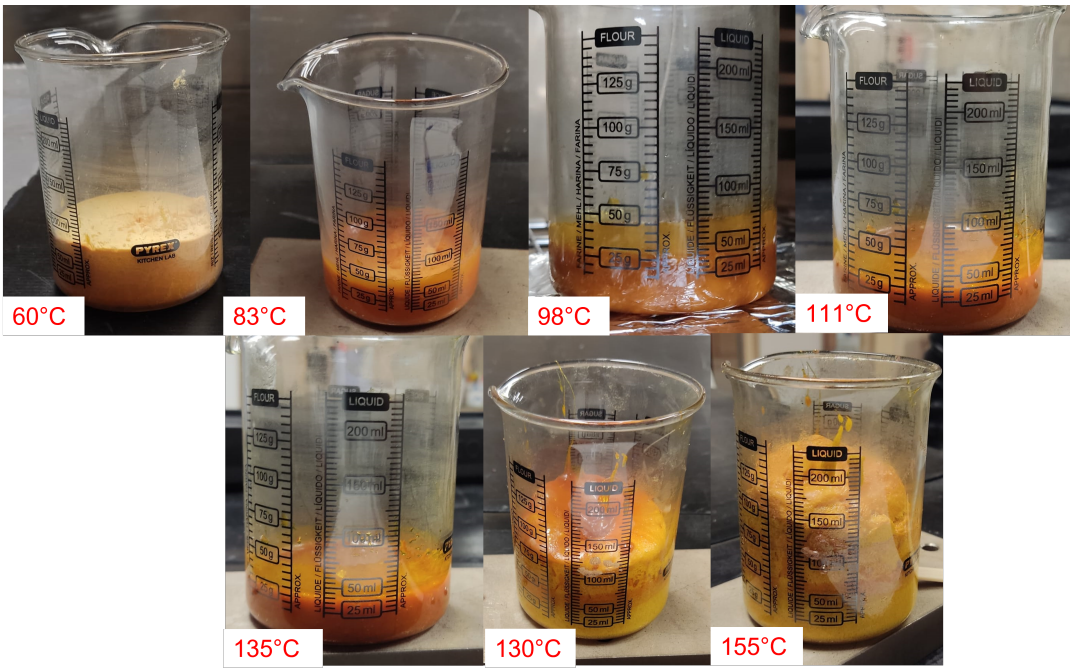

Figure 4.20: Pictures of NO 09 resin density test

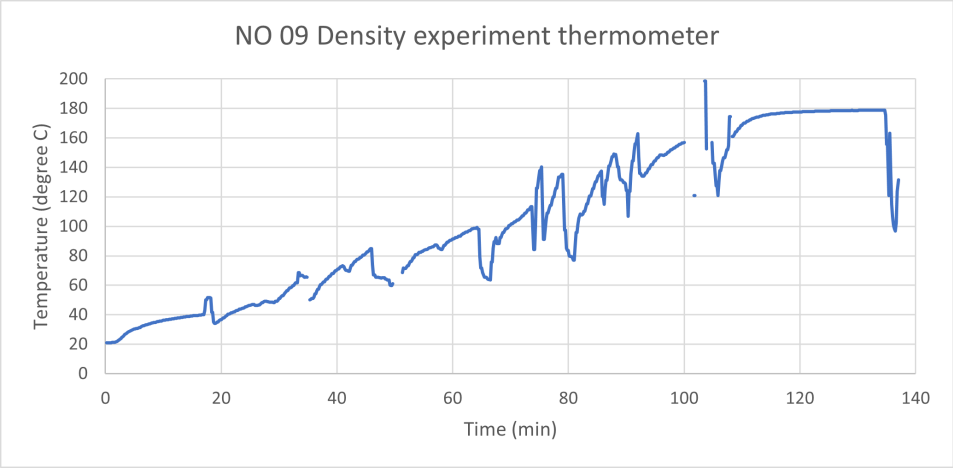

Figure 4.21: Thermocouple data from NO 09 density experiment

At the end of the experiment, the volume did not change anymore (as the resin was curing and thus becoming solid). The temperature of the (solid) foam at the start of this phase was estimated at 125 °C. The resin was left to cure. After this, it was completely solid. By then the foam temperature had increased to around 135 °C. Based on this test it was found that the real density of the resin is around 1.55 g/cm^3. This value was to be used for further manufacturing calculations with this resin.

4.5. Performed iterations

Finally, in this section, a detailed overview will be given of all the tests performed, which parameters were discovered and how they were improved upon. The goal of the thesis is to also do experiments with pitch-based short fibers, as these are promising for rocket nozzle applications and have never been used there. However, due to their high cost and the high amount of energy needed to produce them, it was decided to do the exploration of manufacturing parameters as much as possible with other materials. For this reason, the first trials were performed with prepreg material. Once all relevant parameters with this material were understood, the step to PAN-based short fiber was made. Only after these were fully understood, the step to pitch-based fibers was made. The samples manufactured and manufacturing parameters researched in each of these three phases will now be explained. Pictures of the manufactured samples can be seen in Appendix C

4.5.1. Prepreg

In the first phase of manufacturing research, seven prepreg samples were made. The properties of the prepreg material used can be found in Table 4.5. The general characteristics of the samples can be found in Table 4.6 below. A short summary of the reasoning behind each sample, as well as the steps and parameters found, shall now be given.

1. The main goal with this sample was to test the new process cycle, which was designed with overshoots to better adapt to the temperature difference between the inside and outside of the mould. The first manufacturing parameter discovered was the prepreg size. Prepreg was cut well to size, however as 12 layers were stacked on top of each other, it became harder to keep them fully inside the mould. Therefore, for the next production, the prepreg layer size was slightly reduced. The intended, set and measured cycle for this sample can be seen in Figure 4.5. The resulting density and porosity for this sample were not in an acceptable range. The manufacturing parameters discovered were temperature cycle (which was improved afterwards), moment of pressure application (was changed afterwards), prepreg size and solvent boiling point (cycle was changed for this afterwards).
2. This second sample aimed to try and decrease the porosity and increase the ease of closing. This was attempted by increasing the first dwell temperature. Again the sample was closed at

Table 4.5: Fabric properties

Property	Unit	Value	Property	Unit	Value
Fabric name	[-]	Efabrics-e462	Resin name	[-]	DE20
GSM	[g/cm^2]	245	Resin type	[-]	Phenolic
Weave	[-]	2/2 Twill	Resin form	[-]	Liquid
Stabilization material	[-]	None	Matrix volume	[%]	45
Orientation	[°]	0/90	Density at 20°	[g/cm^3]	1.14
Thickness	[mm]	0.254	Viscosity at 20°	[mPa s]	1000 $\pm$ 200
Fiber name	[-]	HTA40	pH at 20°	[-]	7.6
Fiber type	[-]	PAN	Water content	[%]	<3
Density	[g/cm^3]	1.7			
Linear density	[Tex]	200			
Filament diameter	[µm]	7			
Sizing	[%]	1.3			
Sizing type	[-]	E13			
Tensile strength	[MPa]	4100			
Tensile modulus	[GPa]	240			

Table 4.6: Prepreg samples general properties

Sample number	Sample size (mm^3)	Actual thickness (mm)	Porosity (%)	Torque (Nm)	Torque application
1	150x80x3	2.74	11.3	2.5	Before in oven
2	150x80x3	2.71	13.0	2.5	Before in oven
3	150x80x3	Not recorded	Not recorded	2.5	After second dwell
4	150x80x3	2.73	1.63	2.5	After second dwell
5	150x80x3	2.69	1.92	2.5	After second dwell
6	150x80x3	3.13	12.0	2.5	After second dwell
7	150x80x3	2.76	2.31	2.5	After second dwell

the beginning of the cycle. The cycle for this sample can be seen in Figure 4.6. For this sample, porosity was found to be even higher. Afterwards, this was likely due to the fact that at the increased temperature, the sample already started curing (as confirmed by the rheology tests) and therefore, there was no point for the solvent to boil off. The use of smaller layer sizes was successful, as filling the mould was significantly easier. Also, the changed set cycle led to the fact that the internal cycle of the mould was very close to the intended cycle, as can be seen in the graph.

3. The goal of this sample was still to reduce porosity by finding a good way to let the solvents boil off. Since increasing the dwell temperature was not effective, a new route was designed, in which first a dwell at a lower temperature was added to the cycle and only afterwards the mould was closed and pressurized. This was done with the idea that with lower pressure, the boiling point of the solvent would be lower and thus at a lower temperature it could boil off, without the curing process starting in the sample. The used cycle for this sample can be seen in Figure 4.22. After this sample was cut and post-cured, large delaminations were observed. Because of these obvious defects, it was assumed that this new cycle had not been effective and thus no further tests were done. However, later investigation showed that these delaminations were likely caused by bad post-cure practices in which too high heating and cooling rates had been used. Thus another parameter was discovered and implemented in sample 5.
4. This sample was made with the exact same procedure as sample 3. With this, the reproducibility of the process was investigated. This is important, since if the process was found to not be reproducible, then it meant that the process was not yet understood. If reproducibility is proven, then it can be assumed that all process parameters are discovered and that one has a good understanding of the workings of the process. The porosity and density of this sample were in the acceptable range and a great improvement over the first two samples, however, reproducibility could not be proven, due to the complications with sample 3. For this sample better post-cure practices were used (though mostly by accident), which is likely the reason that this sample did not suffer the faults which sample 4 showed. The cycle for this sample however did show another manufacturing parameter. The cycle data can be observed in Figure 4.23 (please ignore the spikes in the outside mould data, bad image quality made the processing of this data difficult). As can be seen here, the inside temperature deviated from the intended temperature during the second heat-up phase. This can directly be linked to the fact that also the outside temperature deviated. The reason for this was found to be the following. When the mould is taken out of the furnace for closing and pressurization, the temperature inside the furnace drops. Then, when the mould is placed back in the furnace, the furnace needs time to recover to its previous temperature. However, if the next cycle is started before the furnace has recovered, it will start at a lower temperature and thus affect the entire cycle. This is what can be seen to have happened for sample 4. Thus, the parameter discovered from this run is about how the furnace operates. The conclusion to be drawn is that the furnace should always be allowed to recover before the next cycle is started. Another noticeable point is that even though the cycle was not perfect, the sample properties were still very good. This shows that there is some margin for error in the cycle, indicating the cycle as conservative. Though this implies that the cycle is not optimal, conservative cycles are often desirable, especially when a product is still being developed.
5. This sample was made in the same way as sample 4 to check for reproducibility. The only difference is that from this sample onward, the post-curing heating and cooling rates were reduced to prevent delaminations. For the same reason, post-curing pressure was increased (from 1.8 kg on top of a sample plate to 5 kg on top of a sample plate). With properties almost identical to that of sample 4, the reproducibility test was deemed successful.
6. At this point, the only remaining concern for the prepreg samples was their low thickness. The mould should provide 3 mm thick samples, however, all samples produced were closer to 2.7 mm. A hypothesis was that this was due to too much pressure. To test this, a sample was made with one less layer of prepreg material, in theory leading to less pressure being applied and thus a thicker plate. The result of this test was that indeed plate thickness did increase, however, porosity also greatly increased, as there was too much room for gases left in the mould cavity. Since high porosity is not desirable, it was decided that the old setup was better, even though it had a slightly lower thickness.

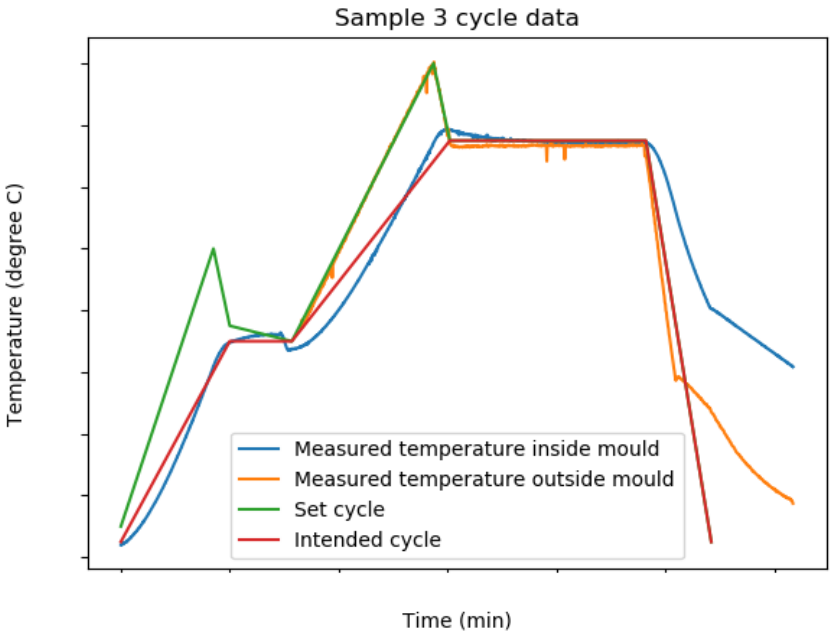

Figure 4.22: Sample 3 cycle information

7. This last sample was again a reproducibility check with the same parameters as sample 4. Again reproducibility was proven.

After these seven samples, the consensus was that the manufacturing process was well understood, especially since it was proven that several consistent samples with good properties could be produced. During prepreg manufacturing, a number of valuable processing parameters were discovered and implemented, which could be used directly for short fiber fabrication as well.

4.5.2. PAN based short fiber

After the prepreg manufacturing was well understood, short fiber based manufacturing was started. Since pitch fibers are very costly and use a lot of resources, manufacturing was initially done using more affordable PAN-based short fibers. The fibers used were 3 mm chopped carbon fibers from R&G Faserverbundwerkstoffe. Details regarding the fibers used can be found in Table 4.7. The resin used was the same as for the prepreg material, thus information for that one can be found in Table 4.5. A summary of the properties of all the samples produced can be found in Table 4.8. All samples were made with an intended fiber volume fraction of 55% and with an intended dimension of 150x80x3 mm^3. In the following list, a short summary will be given of all samples manufactured, the reason behind each and the parameters researched. The cycle used for short fiber manufacturing has three dwells. The last two dwells are taken directly from the prepreg cycle, as described above. However, before this, an additional dwell is added to allow the resin to infiltrate the fibers. Also, the mould is put in the oven without top or pressure plate for this dwell. Then the top plate is put on, but not yet pressurized for the next dwell. Then after this dwell, the top plate is pressurized, similarly as happens in the prepreg cycle. Then the sample is heated up to the curing dwell.

1. The first two samples were used to compare two different ways of manufacturing short fiber CFRP, namely mixing the resin and fiber before filling, or filling them separately. In the first sample, no mixing was used, instead, first the resin was put in the mould, with the fibers on top. As explained before, this was then put in the oven without a top plate. After this, the top plate was put on and the mould returned to the oven. After this, the mould is tightened and put in the oven, after which it is heated for the curing stage. Some lessons were learned from this sample. Firstly that more excess resin should be used. This is because on top of the sample, still, unimpregnated spots of fibers were visible after demoulding. Secondly that the resin should be divided over both

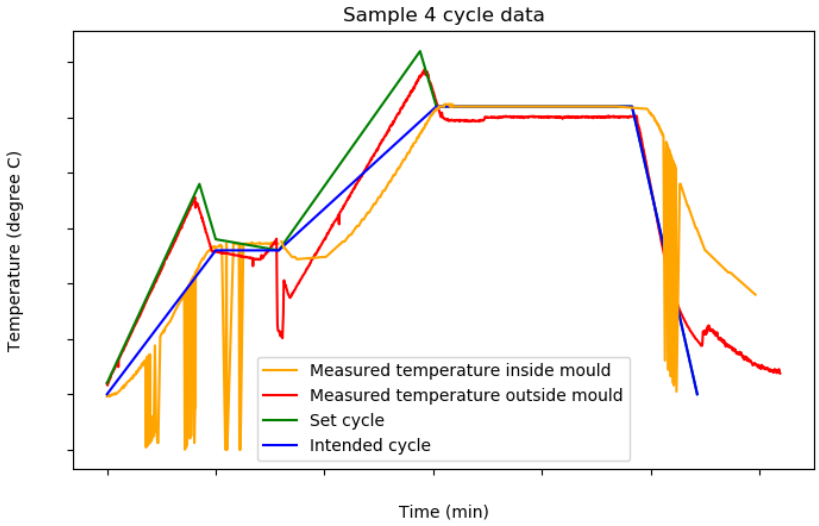

Figure 4.23: Sample 4 cycle information

Table 4.7: PAN-based short fiber properties

Property	Unit	Value
Fiber name	[-]	R&G3mm
Fiber type	[-]	PAN
Density	[g/cm^3]	1.7
Linear density	[Tex]	-
Filament diameter	[µm]	7
Sizing	[%]	1.4
Sizing type	[-]	Unknown
Tensile strength	[MPa]	3500
Tensile modulus	[GPa]	230

Table 4.8: PAN-based short fiber samples general properties

Sample number	Thickness (mm)	Excess resin (%)	Density (g/cm^3)	Porosity (%)	Torque (Nm)
1	3.47	10	1.19	25.5	2.5
2	4.12	6.5	0.68	58.9	2.5
3	3.22	20	1.34	12.1	2.5
4	3.42	40	1.27	16.2	2.5
5	3.44	60	1.31	12.9	2.5
6	3.44	60	1.36	8.5	2.5
7	3.50	60	1.37	8.3	5.0
8	3.41	60	1.39	6.4	2.5
9	3.30	60	1.35	11.1	2.5
10	3.58	100	1.30	15.1	2.5
11	3.55	60	1.36	6.4	2.5
12	3.23	60	1.40	5.8	5.0
13	3.23	60	1.40	6.2	5.0
14	3.34	60	1.41	6.6	5.0

the top and bottom of the fibers, instead of just the bottom. This will lead to better and easier infiltration. Thirdly that the top plate should already be put in the oven during the lowest dwell, just not on the part. Since then it will have the time to heat up. Now after this lowest dwell, the frame and sample had a reasonable temperature but were quickly cooled due to the introduction of a room temperature pressure plate and top plate. Lastly, the oven cycle should be improved with overshoots, similar to prepreg manufacturing. Even though the top plate might not be on the sample, the sample still needs time to heat up, so there is still a difference between the intended and set temperatures. The large disruptions caused by the bad cycle can be seen in Figure 4.24. Do note that the parts where the inside temperature drops and rises quickly are during mould opening where the thermocouple measures air temperature instead of sample temperature. Also note that in this sample, again the mistake was made to start the oven cycle before the oven had recovered. This also was a cause of the bad cycle.

2. This second sample was made at the same time as the first sample, with the same cycle (and also with the same procedural mistakes described above). However, here material loading was done differently. All fiber and resin were put in a cup and manually mixed before being put inside the mould cavity. Here it was pressed into shape using a roller. For this sample, large dry spots were found everywhere in the sample. Likely, a significant amount of resin had not transferred from the mixing cup to the mould. In general, it was found that mixing the fibers homogeneously and filling them correctly in the mould was very difficult and time-consuming, due to the very sticky resin. Therefore, it was chosen to use the no-mixing technique for further samples, as this was easier and seemed to produce better samples.
3. For this third sample, the manufacturing parameters discovered and assessed from the first two samples were improved, and a lot of changes were implemented. Firstly, more excess resin was used, namely 20%. Also, the total resin amount was split in two, with half of it put in the bottom of the mould and the other half on top of the fibers. Creating a uniform resin distribution on top was found to be difficult. Also now a new cycle with overshoots was used and the top plate was put in the oven from the start of the cycle to also heat it up. Afterwards, it was found that the programmed overshoots were still too small, as a large deviation from the intended cycle could still be observed. Nevertheless, it was a large improvement over the first two samples. The cycle data can be found in Figure 4.25. The sample seemed to have better microstructure, though some dry spots could be observed near the sample edges, especially near the top surface. Thus improvement plans for the next sample included an updated cycle, more excess resin and alternative filling strategies.
4. Here again, parameters assessed from the last sample were used to improve. The cycle was not updated as the data from the last sample had not yet been processed. However, more excess resin was used (40%) and a different resin division was made, with 30% of the resin below the fibers and 70% on top. The effects of this could not be properly assessed though, as the sample had bad quality due to an error with the thermocouple instalment during manufacturing. This led to a very uneven pressure distribution in the sample. It was observed however that there were still dry spots around the edges, meaning that resin uniformity was likely still a problem.
5. For this sample again excess resin amount was increased, to 60%. Apart from this, the same procedure as the previous sample was used. This was done to try and assess the effect of the higher excess resin amount. However, due to the problems with the previous sample, no real conclusions could be drawn.
6. For this sample a new cycle was used, also the 60% excess resin was maintained. The way the thermocouple was installed was improved to have less effect on sample quality. To improve the resin uniformity, a test was done where the resin was spread out on a piece of Teflon paper, which was then put on top of the fibers, see also Figure C.13. This was found to be really helpful, with the quality of the top surface regarding dry spots and surface finish greatly improving. Also, the new cycle was successful in getting the inside temperature close to the intended temperature, see Figure 4.26. The improvements in this sample could also be seen in a drop in porosity.
7. One of the problems that was still present at this point was the high plate thickness. 3 mm was desired, but the samples were closer to 3.4 mm. To try and improve this, a higher pressure was used for this sample. Apart from this, the same procedure as sample 6 was used. However, the pressure application for this sample was unsuccessful due to problems with bolt length. Therefore, no conclusions could be drawn.

8. Due to the positive effect the Teflon paper had on surface quality, it was decided for this sample to also use it on the bottom surface. In a different attempt to bring down the plate thickness, the second dwell was reduced in time, hypothesizing that possibly during this dwell the resin solidified too much, making complete closing of the mould problematic. The use of Teflon paper on the bottom was successful, with the surface finish improving. The reduction of the second dwell was inconclusive, with a slightly lower thickness found, but it was unsure if this was related to the dwell reduction or by chance.
9. To test the hypothesis that the resin was solidifying during the second dwell and that this was causing the high thickness, the dwell was removed entirely for this sample. It was pressurized after the first dwell. Also, since still some dry spots were observed near the middle of the sample, the resin distribution was changed, with 25% at the bottom 10% in the middle plane, mostly along the edges, and the remaining 65% on top. The hypothesis tested was found to be false, as no extreme decrease in plate thickness was observed, it was still well above 3 mm. Also, the porosity increased significantly. Therefore the experiment was deemed as not successful and for other samples, the second dwell was included again.
10. This sample was made at the same time as sample 9 with the same goal of testing the hypothesis of the second dwell. However, for this sample, the excess resin was also increased again to see the effect of this. However, a very high amount of resin outflow was observed after the curing and surface quality had decreased, as well as porosity increased. Therefore, also the hypothesis that a higher excess resin amount could be beneficial was rejected.
11. This sample and the next were made with reduced second dwell times to attempt to reduce thickness. The dwell was set at 20 minutes, instead of 45. However, during manufacturing, some unexplained problems with the oven cycles were encountered. Firstly, the first cycle step ended too early, leading to large cooling of the sample before the second cycle step was initiated. Also, the oven greatly increased its curing dwell time. It was investigated but could not be found why these problems occurred. Because of these problems, no meaningful conclusions could be drawn from the samples.
12. This sample had similar parameters as sample 12, however, it used a higher pressure. It suffered the same problems as sample 12.
13. This sample was the second try of sample 12, however now without oven problems. In this run, only a single sample was made and put in the oven (instead of the more common two samples at the same time), to better inspect and control the process. The sample gave good properties, with the lowest thickness observed until this point (though still too high), as well as low porosity. By comparing the cycle data of sample 12, see Figure 4.27, and sample 13, see Figure 4.28, it can be seen that indeed the time the oven was open was greatly reduced, leading to lower temperature drops in the material. However, since the properties of these two samples are almost identical, it was concluded that these differences in temperatures had little influence on the final product. For this sample, the influence of the thermocouple was studied and it was found that it still had a significant influence on part thickness uniformity. Thus in future samples, a way should be found to prevent this.
14. This last sample was a reproduction of sample 7 to see if with the new experience the parameters used there could also give good results. However, during manufacturing too small pieces of Teflon paper were used, which caused large dry spots near the edges of this sample. Therefore, no real conclusions were drawn.

After these experiments, manufacturing was started using a fixed set of parameters. The found thickness and porosity for samples 12 and 13 were found to be in the acceptable range. Also, it was determined that any further improvements would come with great effort and would require high time and cost. This is because all big improvements had already been made, thus only small steps could still be done. However, it was decided to first see if these samples would give good properties after siliconization, before much more effort was put into optimizing CFRP samples which were already in the acceptable range.

4.5.3. Pitch-based short fiber

The last phase in the research on manufacturing parameters was studying parameters in pitch-based short carbon fiber composites. Seven samples were produced. Details of the fibers used can be found

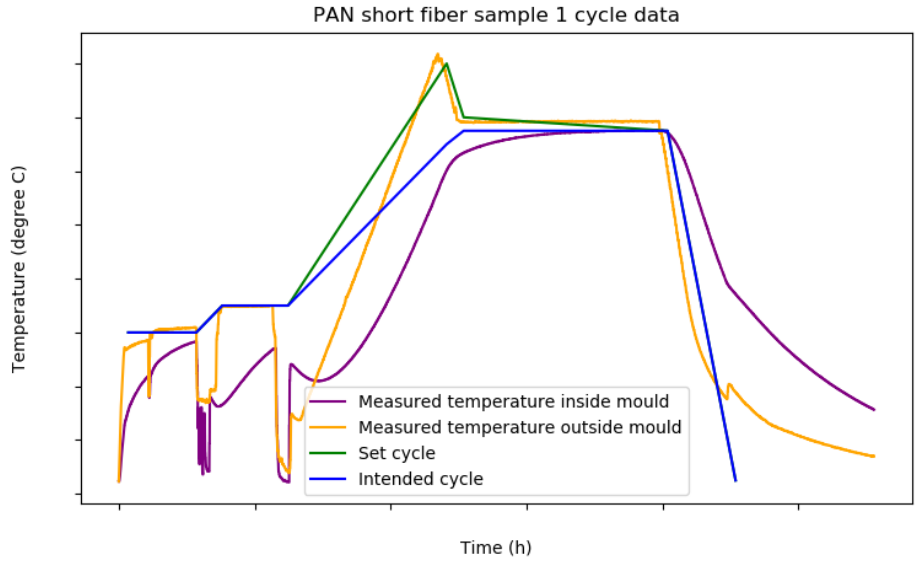

Figure 4.24: First PAN short fiber sample cycle information

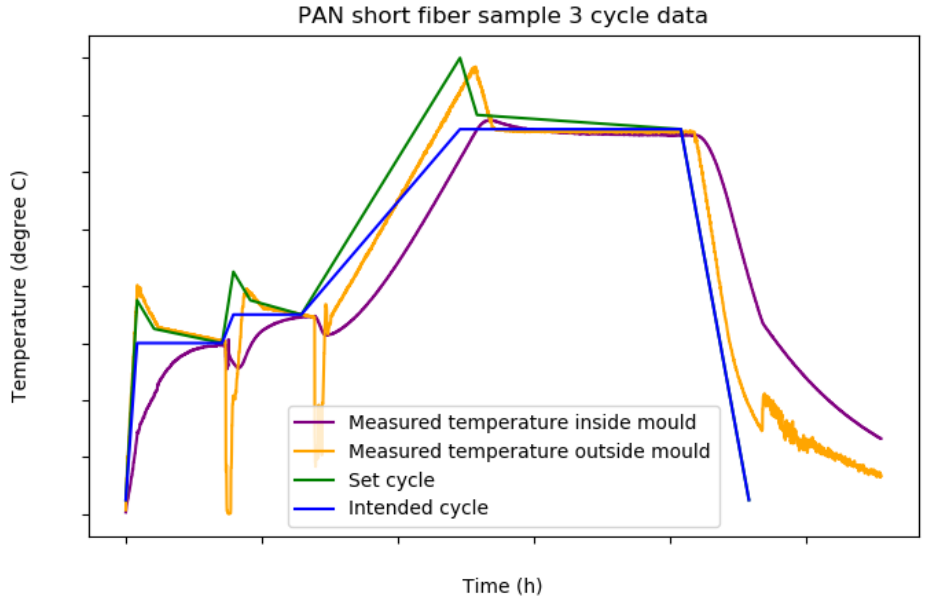

Figure 4.25: Third PAN short fiber sample cycle information

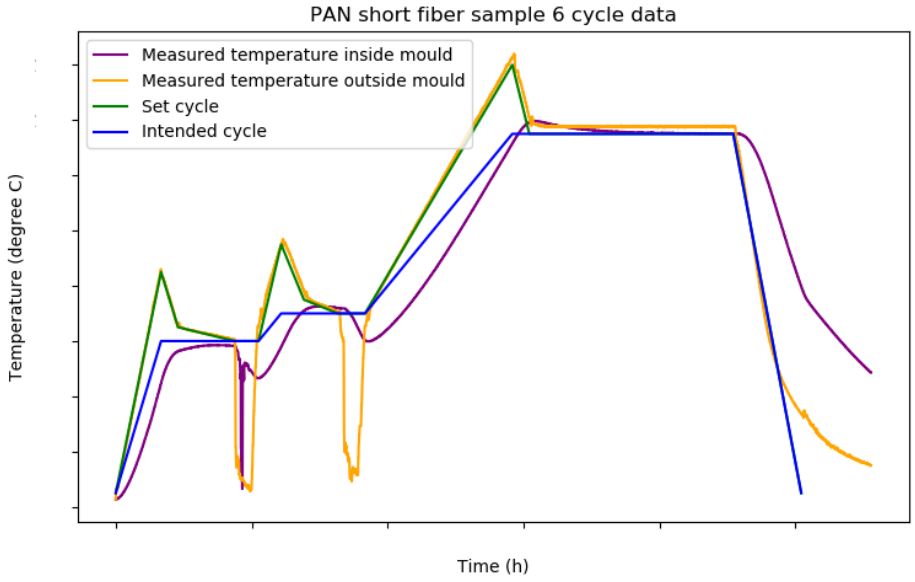

Figure 4.26: Sixth PAN short fiber sample cycle information

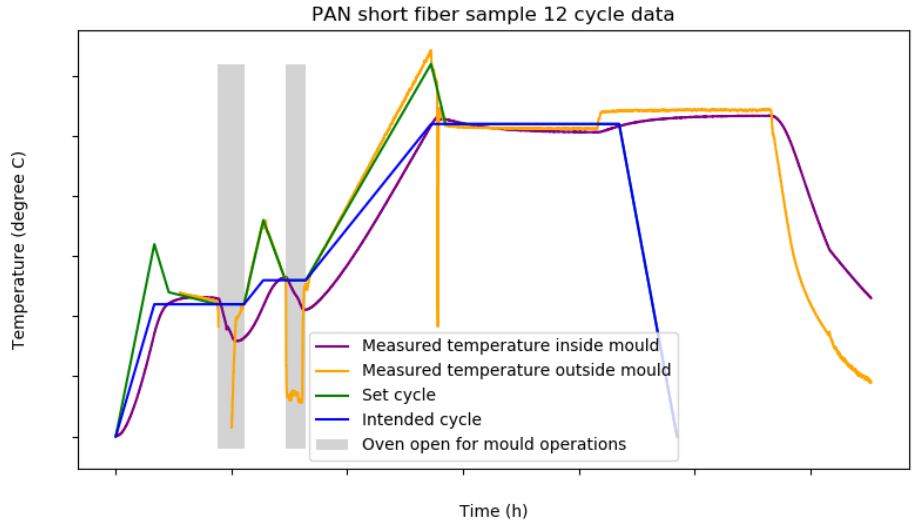

Figure 4.27: Twelfth PAN short fiber sample cycle information

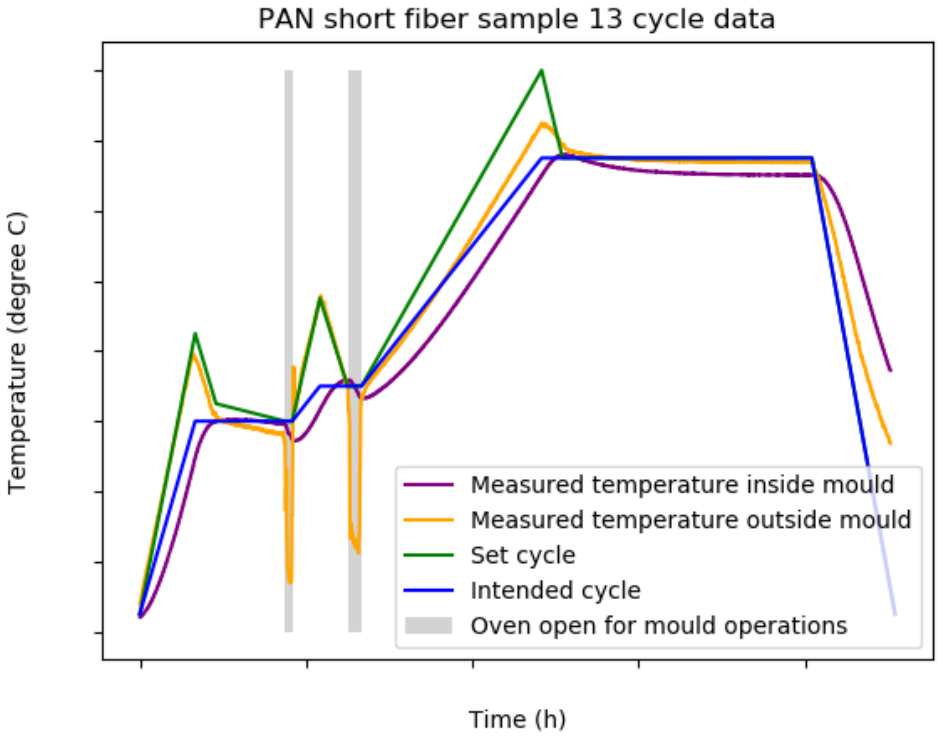

Figure 4.28: Thirteenth PAN short fiber sample cycle information

in Table 4.9. The resin is the same as for PAN-based short fiber manufacturing. Again, all samples were made with an intended fiber volume fraction of 55% and with an intended dimension of 150x80x3 mm^3. The cycle used has the same characteristics as the cycle for PAN-based short fibers. A list with all samples and all manufacturing parameters found and researched will now be given.

1. This is the first pitch-based sample produced, using 6 mm long fibers, the shortest available. The same cycle was used as sample 13 from the PAN-based samples. Also, 5 Nm pressure was used. 45% excess resin was used instead of 60% due to a calculation error during production. Also, the pressure plate was placed on top from the beginning. This is because of the fiber structure: These fibers had more of a woolly structure, instead of the more pallet based structure of the PAN fibers. This made that a lot of air got trapped and the mould was very hard to close. After demoulding, a high, very nonuniform thickness was observed and a lot of dry spots.
2. A second attempt using 60% excess resin was done, however, the same problems were encountered as sample 1.

Table 4.9: Pitch-based short fiber properties

Property	Unit	Value
Fiber name	[-]	XN-100-12Z
Fiber type	[-]	Pitch
Density	[g/cm^3]	2.22
Linear density	[Tex]	-
Filament diameter	[µm]	?
Sizing	[%]	None
Sizing type	[-]	Not applicable
Tensile strength	[MPa]	NotAV
Tensile modulus	[GPa]	NotAV

3. A third attempt was done with a smaller theoretical area. Instead of the amount of material needed or 150x80 mm^2, the calculation was based on 140x70 mm^2. This means that less resin and fiber were present in the mould cavity. Also here, the sample still had large dry spots.
4. Now the Teflon paper was removed, with the idea that possibly the air in between the fibers would be able to escape better. To accommodate this, also the resin distribution was changed to 50% on the bottom and 50% on top. However, this also did not solve the problem, as still thickness was high and infiltration poor.
5. Since no real progress and understanding was made for these 6 mm fibers, the choice was made to switch to 12 mm fibers. These instead of the woolly structure had a pallet structure. The difference between the structure of the different fibers is illustrated in Figure 4.29. For this sample, 60% excess resin and a distribution of 33/33/33 was used. This sample was much easier to fill and close. After demoulding, good infiltration and surface finish were found. Some pores could be seen between the fiber bundles though. The thickness was 3.26 mm, around the same as the best PAN-based fiber samples. After this sample, data from all samples were grouped and options for improvement, as well as reasons for the remaining problems, were discussed. Looking at this sample, it was seen that there was still room left in the cavity during demoulding and that the fibers near the edges sometimes came loose. Based on this, it was decided to increase the excess resin amount.
6. For this sample the excess resin amount was increased to 200%. Instead of using a set torque to apply pressure, the pressure was applied until the mould was fully closed. This was done using the bolts, as well as two clamps that were placed on the mould. A lot of resin outflow was observed during this closing. After demoulding, the thickness of the sample was found to be 2.75 mm. This meant that a good but too aggressive step in the right direction was made. Therefore, the ideal parameters would be in the middle.
7. Based on the information from the previous samples it was decided to use 150% excess resin for this sample, as well as 5 Nm of pressure, combined with the clamps. After demoulding it was found that the sample looked really good, infiltration looked proper and the surface finish and sample thickness were close to ideal. The porosity was measured as 6.5%, similar to that of the best PAN-based samples. After this sample, no big improvements were deemed necessary and the manufacturing research was stopped.

With the creation of a good, pitch-based, plate, the manufacturing research was finished. All the knowledge gained and relationships found were written down and can be used in future research. The conclusions from this manufacturing research provide valuable data for understanding the influence of manufacturing on sample quality. By quantifying this, the methods developed here can be used by other people and in other research and thus in this way it is making manufacturing and research more accessible.

4.6. Summary

All of the knowledge gained from the research into the effect of manufacturing parameters on sample quality, specifically when considering the press-mould manufacturing technique, will be summarized here. The parameters found to most influence sample quality were the following:

- Temperature cycle: Bad temperatures cycle was found to lead to greatly reduced part quality, with higher thickness, lower density and higher porosity. Several important parameters regarding the temperature cycle were found, firstly the usage of correct overshoots to link the internal and external temperatures of the mould. Next to this the influence of solvent boiling point: above this temperature, a dwell should be implemented to allow the solvent to evaporate. Thirdly the dwell time for infiltration, which was optimized and set at a the determined value.
- Moment of pressure application: It was found that too late pressure application leads to significantly increased void content, as well as increased sample thickness. This was found to be the result of the resin starting to cure. Too early pressure application also leads to increased void content. This is due to the fact that this leads to volatiles becoming trapped in the part. An optimum pressure application point is after solvents have boiled, but before the resin starts curing. This can be found semi-empirically by determining the solvent type and its boiling part, after which

Figure 4.29: Different short fiber types, note their structure

multiple trials are performed. Another option is by finding the temperature at which viscosity is minimal, from rheology data, and use this as the moment of closing.

- Excess resin: Regarding the amount of additional resin it was found that firstly, the additional resin has to compensate for mass loss of resin during curing, which was found to be around 30%. On top of this, it also functions as a homogeneity method, as excess resin forces resin (and fibers to some extent) to move through the mould from high concentration to low concentration locations, leading to a more uniform part. However, it was also found that too much excess resin negatively influences part thickness and in extension porosity characteristics. The optimal point was determined as around 60% for short, 3 mm, fibers, while for larger, 12 mm fibers, 150% was preferred.
- Resin division: A good resin division was found to greatly increase uniformity and decrease the porosity of the final part. Bad division was found to lead to too little resin spreading and thus dry spots in some areas of the part. The ideal division was found to be 33% on the bottom, 33% at the midplane and 33% on top.

Next to these, some other parameters were also found, however of lesser influence:

- Prepreg size: When the margins of prepreg size were too low, accurate manufacturing became more difficult, often leading to reduced part quality. Thus more significant margins are advisable.
- Heating-cooling rates: The oven as well as the mould was found to have limited heating and cooling rates, which should be taken into account for cycle design. However, often during cycle design, these values will not be required.
- Furnace closing: Bad procedures around the furnace closing, especially when it was not allowed to return to its previous temperature, were found to have large influences on the temperature cycle. However, only minimal influence on part quality was observed. Also, these errors can easily be avoided by setting up proper procedures.
- Mould pre-heating: When cold moulds were combined with hot moulds, it was found to negatively influence the heat-up capability of the part, as well as temperature uniformity inside the part. This led to reduced part quality close to the cold mould part. This can be prevented by heating all mould parts at the same time and with the same heating rate.

5

Material characterization

With the effect of manufacturing well understood, and a reliable manufacturing method developed, research could be done into the material itself. By varying the material composition and performing tests afterwards, the effect of different material compositions could be quantified. In this chapter, that process will be described. Firstly, the different parameters available and chosen will be discussed in section 5.1. After this, what samples were actually manufactured using these parameters will be shown in section 5.2. The physical properties of the samples will be detailed in section 5.3. Investigation into the microstructure is elaborated on in section 5.4. Mechanical properties are discussed in section 5.5, followed by an assessment of thermal properties in section 5.6. The chapter is concluded with a summary in section 5.7.

5.1. Parameter selection

There are many different types of parameters that can be considered for study, however, a selection has to be made. Four main parameters were selected to be studied in detail. These parameters and the background behind them will now be explained.

Firstly, fiber type. In a composite material, two main parts can be easily distinguished, namely the matrix and the fiber. In the fiber category, many different parameters can be considered, partly because there are many different fibers. Also in the category of carbon fibers, often groups are created for example based on modulus or heat treatment temperature. One way to divide carbon fibers is on their material type, namely PAN (Poly Acrylo Nitrile) or pitch. These fibers are made from different resources and using different routes. Therefore, they also exhibit different properties. This makes for an easy but informative way to split them. It is especially relevant for C/C-SiC, as here the pitch fibers will interact differently with the silicon carbide matrix compared to the PAN fibers. This is due to the additional layer of active carbon often found on their surface. This creates a good interphase source, which is desirable to have when wanting to prevent silicon attacks on the fibers. More details about the influence of fiber type in CMCs can be found in subsection B.4.2. The main differences in the fibers used in this thesis are summarized in Table 5.1 below. As can be seen, there are large differences in strength, stiffness and density. It will be interesting to research and quantify how these differences express themselves when the fibers are made into a C/C-SiC material. That is the reason to choose fiber type as one of the parameters for the study.

The second parameter, also identifiable in the table, is fiber length. There is always a balance to be found in fiber length. On one hand, it is known that in CFRP products mechanical properties such as strength and stiffness reduce with shorter fiber length. However, workability and handling, as well as material uniformity often increase. Quantifying the differences in mechanical strength between different fiber lengths gives the possibility to make a more informed choice on what fiber to choose. Also, it leads to the possibility of creating predictions as well as models for this material, in which properties might be predicted for any fiber length, which could be a valuable design tool.

Table 5.1: Properties of short fibers used

Fiber name	Units	R&G3mm	T700	XN-100-6Z	XN-100-12Z	XN-100-25Z
Fiber type	[-]	PAN	PAN	Pitch	Pitch	Pitch
Fiber length	[mm]	3	12	6	12	25
Filament diameter	[µm]	7	7	10	10	10
Density	[g/cm^3]	1.7	1.80	2.22	2.22	2.22
Sizing	[%]	1.4	1.3	None	None	None
Sizing type	[-]	Unknown	Epoxy	None	None	None
Tensile strength	[MPa]	3500	4400	3430	3430	3430
Tensile modulus	[GPa]	230	240	780	780	780

Table 5.2: Properties of resins used

Resin name	Units	DE20	NO 09
Resin phase at 20°C	[-]	Liquid	Solid (powder)
Melting point	[°C]	-	85
Density at 20°C	[g/cm^3]	1.14	0.6

The third parameter is fiber volume fraction, a common material characteristic in CFRP production. However, its influence on the properties of C/C-SiC should also be understood, especially since other factors come into play. Commonly in polymer composites, higher fiber volume fractions lead to higher strength and stiffness, often easily estimated using the rule of mixtures. However, in CMCs the volume fraction will also have an effect on the infiltration properties, possibly leading to differences in infiltration and microstructure. Also, because of the infiltration, high strength and stiffness are not guaranteed for high fiber volume fractions, as with less resin, the risk will be higher that the silicon will react with the carbon fibers and thus degrade their strength and stiffness.

Lastly, resin type is selected. Naturally, many different resin types can be selected, however, this is not what will be focused on. Due to the nature of the pyrolysis and siliconization process and the requirements for the infiltration, the choice of resins is relatively limited, with most often phenolics being used. However, one clear distinction that can be made within phenolic resins is their phase. Some of them are in liquid phase at room temperature while some of them are in powder form. This changes the way manufacturing is done and thus influences handling properties, as well as the uniformity of the resin. It can also influence how well the resin is infiltrated into the fibers. All of these things can have effects on the final pyrolysis and siliconization steps and thus the properties of the material. Therefore, the difference between powder and liquid resins will be studied. The details of the two resins used can be found in Table 5.2.

While these are the defining and important parameters, one additional minor parameter will be tested, namely plate thickness. This is not a material composition characteristic and in an ideal case the plate thickness should not influence the mechanical properties of a material. However, from a manufacturing and handling point of view, it is interesting to see if this indeed is the case. When a rocket nozzle is made, it would be valuable to be able to give some insight into what effect the wall thickness will have on strength of the part. It is especially relevant since it has been noted in literature that many geometric values of samples can have an effect on measurements. For more details on this, please refer to subsection B.3.2. Therefore, also some samples of higher thickness will be manufactured.

5.2. Manufactured samples

Based on the chosen parameters described above, a number of samples was manufactured which could be used for testing. Even if only four variations are made in each of the four parameters mentioned above, already 16 different material compositions arise. Since resources in this project were limited, both in time and material, a selection of these 16 compositions was made. Also, due to the testing accuracy problems sometimes encountered with this material, see subsection B.3.2, of some important

Table 5.3: Summary of sample variations manufactured for testing

Variation number	Fiber type (-)	Fiber length (mm)	Resin type (-)	Fiber volume fraction (%)	Number of samples (-)
1	PAN	3	Liquid	55	4
2	PAN	12	Liquid	55	11
3	PAN	12	Powder	55	1
4	PAN	12	Powder	40	7
5	Pitch	12	Liquid	55	7
6	Pitch	12	Powder	40	1
7	Pitch	25	Liquid	55	1
8	Pitch	25	Liquid	40	1

Table 5.4: Comparisons possible with manufactured plates

Variations to be compared	Parameter to be compared	Number of plates for comparison
1 to 2	Fiber length	4
2 to 3	Resin type	1
3 to 4	Fiber volume fraction	1
2 to 5	Fiber type	7
5 to 6	Resin type	1
5 to 7	Fiber length	1
7 to 8	Fiber volume fraction	1

variations many samples were made to be able to set a solid baseline. A summary of which samples were manufactured can be found in Table 5.3 below. A few notes should be made. Firstly, due to some mistakes in manufacturing, not all samples are usable. Of variation 2, 2 samples were not usable, while for variation 4, 4 samples were not usable. Also, as described above, some samples were made with high thickness, namely 2 samples of variation 2, which have a 5 mm plate thickness. All other samples have a 3 mm plate thickness. The exception to this is the plate of variation 8, which by mistake also has a 5 mm plate thickness. It thus needs to be seen if this plate can be used in the comparison. Based on these manufactured plates, the following comparisons can be made regarding the material composition parameters. This is summarized in Table 5.4. Again note should be made that this last comparison might be difficult to make, as two parameters are changing instead of one. And also, one additional comparison can be made, namely comparing the effect of plate thickness using the 2 5 mm plates of variation 2.

5.3. Physical properties

In this section, the physical properties of the manufactured samples will be discussed and compared. Also, the methods in which these properties were measured will be discussed, if this was not already done beforehand.

First of all, the density and porosity of the samples will be listed. These can be considered in CFRP stage, C/C stage and C/C-SiC stage. The way in which this is measured was discussed in subsection 4.2.2. The density and porosity for the C/C and C/C-SiC stage were determined by an external company, namely where also the pyrolysis and siliconization is done. The density shown here is the skeletal density, meaning the density of the parts with the open pores excluded. The porosity for all variations in the various process stages can be seen in Figure 5.1. The density can be found in Figure 5.2. Based on these, the following comparisons can be made, using Table 5.4 as reference. Firstly it can be noted that for all variations with multiple samples, the standard deviation is relatively small. This makes making statistically significant comparisons easier and also gives confidence that the variations with only one plate also provide representative data. Firstly the CFRP stage can be compared. Regarding porosity, it can be seen that variation 1 has a very low porosity, while variations 2, 7 and

8 have a high porosity. This is not ideal, as it was expected that the low porosity of variation 1 could be achieved for other variations as well. However, the difference does not seem to carry over to the C/C and C/C-SiC stage. When the different variations are compared, no general statements can be made on the influence of resin type or fiber volume fraction, as different comparisons point in different directions. However, fiber length does seem to have a large influence, as the 3 mm fibers have lower porosity than 12, while 12 have lower than 25. This is understandable from a physical point of view, as long fiber are harder to spread homogeneously, and air gets trapped between them easier, leading to higher porosity. Another notable observation is the decrease in porosity from PAN to pitch based fiber, by comparing variations 2 to 5. No immediate physical reason for this could be determined, however, it was hypothesized that the fibers are packed in a different way, leading to higher trapped air amount inside the fiber bundles for the PAN based fibers.

In the CMC stage, the porosity can be found to be low for all samples, well below 5%. This again proves the effectiveness of the LSI process. The only exception is the single plate of variation 7, which has a high resulting porosity of over 10%. The reason for this is due to incomplete infiltration, which can be clearly seen in the x-ray image Figure C.88. For unclear reasons the infiltration seems to have stopped, possibly due to the pores closing, leading to the upper part of the plate containing no silicon or silicon carbide and thus high porosity. Comparing the different variations, the only noticeable result is the slight decrease in porosity when switching from liquid to powder resin. This could be caused by the better uniformity in the CFRP stage, leading to more optimal infiltration paths and thus lower porosity.

Regarding density the following can be noted. Firstly, the difference due to fiber type is clearly visible, as the samples with pitch based fibers have higher densities than those with PAN based fibers. This is easily correlated with the higher fiber densities of the pitch based fibers compared to their PAN based equivalents. Secondly, the fiber volume fraction can also be observed to have a direct influence on density, with lower FVF leading to lower densities. This is again easily explained by the fact that resin has a much lower density than fiber. A density difference due to fiber volume fraction would also have been expected between variations 7 and 8, however this is lower than the other variations. This is likely due to the fact that the actual fiber volume fraction of the sole plate of variation 8 is closer to 55% than to 40%, as a result of a too high applied pressure during manufacturing, which led to a low thickness of the part.

In the C/C stage, the density of all variations increases. However, relative to each other, the densities do not change much. As mentioned before, the density is calculated excluding the pores. The increase in density is due to the shrinkage of the part in this process stage. The amount of density increase from the CFRP stage is between 5 and 17% for the different samples. It is observed that the density increases more with shorter fibers, with powder resin compared to liquid and with pitch fibers compared to PAN. Shorter fibers create a less strong part and thus will give more room for fibers to move and thus for the part to shrink. For powder resin, the reason is not clear. Pitch fibers can have a different shrinkage behaviour from PAN fibers, leading to this result.

Lastly, in the CMC stage, density increases again. This is due to the infiltration of silicon and the formation of silicon carbide, both of which have a high density. The change in density differs for each sample and is largely determined by the resulting microstructure of the part. Parts with more carbon will have a lower density, while parts with high amounts of residue silicon will have a higher density. The resulting division of the components will be discussed in more detail in the next section.

The samples with higher plate thickness were also compared in the above ways, however, no significant changes in any of the mentioned parameters could be observed.

An interesting footnote regarding these results and mainly the measurement technique is the following. When talking about porosity, always open porosity is referenced. This means that only the pores are considered that can be reached from the outside of the part. However, for both the CFRP and C/C-SiC stages, it is likely that there are also closed pores. These are important to also consider, since they will have an influence on part properties. However, this is hard to determine accurately in a non-destructive

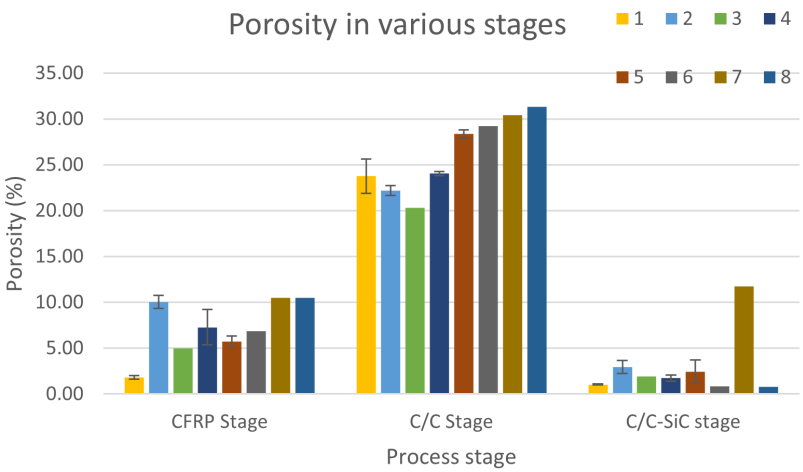

Figure 5.1: Porosity of manufactured samples

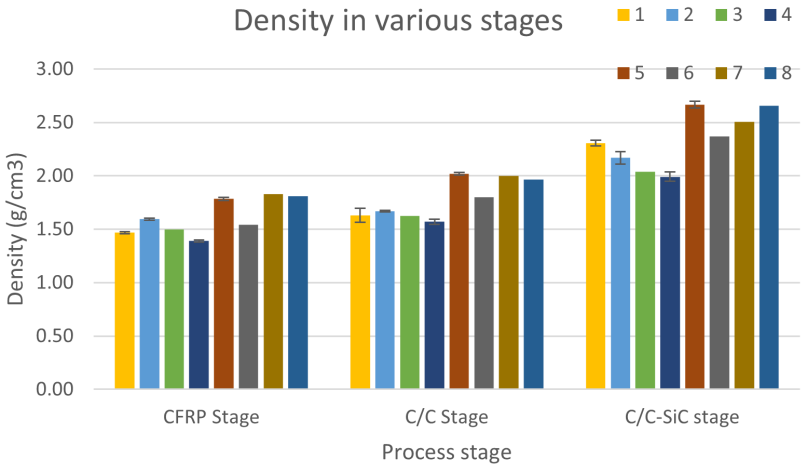

Figure 5.2: Density of manufactured samples

way, as often either burning processes are used, or an approximation is acquired by microscopic analysis.

To solve this problem, an attempt was made to acquire the closed pore content approximately using an analytical process. This will now be shown. The following terminology is used: the dry weight in air as m_{air}, the soaked weight of the sample in air as m_s and the weight of the sample in water as m_w. Now from this, density and open porosity are usually calculated in the following way. Firstly, the weight in air can be defined as:

$$m_{air} = m_f + m_r + m_{cp} \tag{5.1}$$

where m_f is the fiber mass and m_r the resin mass, with m_{cp} the mass of the gas filling the closed pores. This last value is usually assumed to be 0. The weight in water can be defined as:

$$m_w = m_{air} - V_{seop} \cdot \rho_w \tag{5.2}$$

where V_{seop} is the volume of the sample excluding open pores and ρ_w is the water density. The soaked weight can be defined as:

$$m_s = m_{air} + V_{op} \cdot \rho_w \tag{5.3}$$

where V_{op} is the volume of the open pores. The total sample volume is then defined as:

$$V_s = V_{seop} + V_{op} \tag{5.4}$$

We can define sample density simply as:

$$\rho_s = m_{air}/V_s \tag{5.5}$$

From Equation 5.2 one can write:

$$-V_{seop} \cdot \rho_w = m_w - m_{air} \tag{5.6}$$

giving

$$V_{seop} = \frac{m_{air} - m_w}{\rho_w} \tag{5.7}$$

Also from Equation 5.3 one can write:

$$V_{op} \cdot \rho_w = m_s - m_{air} \tag{5.8}$$

giving

$$V_{op} = \frac{m_s - m_{air}}{\rho_w} \tag{5.9}$$

The porosity percentage can be defined as:

$$\text{porosity fraction} = \frac{V_{op}}{V_s} \tag{5.10}$$

Combining Equation 5.7 and Equation 5.9 using Equation 5.4 and Equation 5.5:

$$\rho_s = m_{air}/(\frac{m_{air} - m_w}{\rho_w} + \frac{m_s - m_{air}}{\rho_w}) = m_{air}/\frac{m_s - m_w}{\rho_w} = \frac{m_{air}\rho_w}{m_s - m_w} \tag{5.11}$$

And combining Equation 5.9 and Equation 5.7 using Equation 5.4 and Equation 5.10:

$$\text{porosity fraction} = \frac{m_s - m_{air}}{\rho_w}/(\frac{m_{air} - m_w}{\rho_w} + \frac{m_s - m_{air}}{\rho_w}) = \frac{m_s - m_{air}}{\rho_w}/\frac{m_s - m_w}{\rho_w} = \frac{m_s - m_{air}}{m_s - m_w} \tag{5.12}$$

These last equations are also given in the ASTM standard and used for density and open porosity determination.

Now to get an estimate of the closed porosity, a theoretical and actual density of the sample excluding

open pores should be defined. Now the density of the sample excluding open pores can similarly be defined as the density of the complete sample, but now using Equation 5.7:

$$\rho_{seop} = m_{air}/V_{seop} = m_{air}/\frac{m_{air} - m_w}{\rho_w} = \frac{m_{air} \cdot \rho_w}{m_{air} - m_w} \tag{5.13}$$

Normally a theoretical density can be defined based on the fiber volume fraction. If 0% porosity is assumed, density can be calculated using:

$$\rho_T = FVF \cdot \rho_f + (1 - FVF)\rho_r \tag{5.14}$$

Where ρ_T is the theoretical sample density, FVF the fiber volume fraction, ρ_f the fiber density and ρ_r the resin density.

When making the sample, an ideal fiber volume fraction is aimed at and resin and fibers are added accordingly. During the operations, excess resin is added to account for any resin evaporation and outflow. This does however mean that the fiber volume fraction is less exact. However, the final acquired fiber volume fraction can be calculated with:

$$FVF_a = V_f/V_s \tag{5.15}$$

Where V_f is the fiber volume and V_s is the sample volume. Since no fibers leave the mould after the start of the moulding process, the V_f can be determined by weighing the fibers beforehand and dividing this by the fiber density. The sample volume can be accurately determined using the known mould dimensions and by measuring the average thickness over the part. It can be written as:

$$V_s = W_s \cdot L_s \cdot t_s \tag{5.16}$$

This actual fiber volume fraction can then be used to get an accurate theoretical density.

Now this theory of fiber volume fraction and theoretical density can also be applied to the sample excluding open pores as well. To do this, a new part thickness is defined, namely the t_{seop}. This thickness can be seen as the thickness of the sample if all the open pores would be removed. This can be determined by:

$$t_{seop} = t_s/(1 - \text{porosity factor}) \tag{5.17}$$

now using this, the FVF_{seop} can be defined:

$$FVF_{seop} = W_s \cdot L_s \cdot t_{seop} \tag{5.18}$$

Now using this FVF in Equation 5.14:

$$\rho_{Tseop} = FVF_{seop} \cdot \rho_f + (1 - FVF)\rho_r \tag{5.19}$$

This thus gives a theoretical density which can be compared to the actual density calculated using Equation 5.13. Since the theoretical density assumes no porosity, it should always be higher than the actual density, since this will have some closed porosity. An estimate of the porosity can be made by assuming the closed pores are filled with air. The density of the sample can then be written as:

$$\rho_{seop} = CPR \cdot \rho_{air} + (1 - CPR)\rho_{Tseop} \tag{5.20}$$

Where CPR is the closed pore ratio. This can be rewritten as:

$$CPR = \frac{\rho_{seop} - \rho_{Tseop}}{\rho_{air} - \rho_{Tseop}} \tag{5.21}$$

This was seen as an elegant solution to get an estimate of the closed porosity. However, the following problem was encountered: For every sample on which these formulas were applied, a CPR of between -5% and 0% was gotten, which cannot be correct. Though it is expected that this indicates a low closed porosity content, it should still be explained why negative values are encountered. An error in the derivation or underlying assumptions was assumed, but after a thorough investigation, no such error was found. Some of the assumptions that were considered were:

- The density calculations are sometimes done on smaller parts of the sample, while the theoretical density is based on the volume of the entire sample. Thus a possible explanation could be that the fiber spreading throughout the entire mould is not uniform, leading to wrong theoretical values. Though this is true, the average then should still be correct, which is not the case.
- The fiber mass is constant during the process. Though this is not fully correct as sometimes some fiber escapes, this is a very small amount, so this cannot explain the results.
- The thickness of each sample piece is uniform. Since the thickness of each piece is used for the calculation, wrong measurements of these could lead to wrong values. While the sample pieces are definitively not uniform and the thickness might be incorrect for some pieces, to explain the result obtained, the thickness should be underestimated for every single piece. This is very unlikely.
- Closed pores are filled with air. Though this is likely not true, the density of other types of gasses is similar. Also changing this value has a very small influence on the CPR results.
- Measurements are done correctly: probably some errors are here as well, but again these are likely random errors, which cannot lead to the observed result (only if there were big systematic errors could this be explained).
- Sample fills the entire cavity and is exactly 150*80 mm. The sample does fill the entire cavity and the accuracy of the cavity is quite high.
- Fiber and resin densities which are used (as given by the manufacturers) are correct. Though this cannot be checked, the fact that Equation 5.14 often correlates with the empirical density measurements indicates that these values are likely correct.

Thus, sadly enough no reason for the erroneous results could be found and thus these equations were not used for further analysis. However, they are still included in the thesis report to add to the general body of scientific knowledge. This way, in the future possibly somebody else can reconsider this and find a good reason to completely reject it or to correct it and build upon it.

Another way in which physical properties were tested was subjection to typical environments in rocket thrusters, specifically, reaction to rocket fuel. This was done at and by an external company. To test this, two samples were taken, one of variation one and one of variation five. These were put in a tube furnace, which was then heated to 1600 °C. After this, exhaust gases of an undisclosed green propellant were introduced into the furnace. The presence of these gases at this temperature represents conditions experienced by a rocket nozzle during actual performance very well. The samples were subjected to these conditions for two hours, after which their mass loss was determined. It was found that for the variation one sample, the mass loss was 3%, while for the variation five sample, mass loss was 1%. This shows promising results regarding the use of these materials in nozzle applications, as both of these are in the acceptable range for rocket nozzle performance. The reason for the lower mass loss shown by the variation five sample is likely the higher silicon carbide content caused by the fiber architecture. This will be explained in more detail in the next section. Another notable observation is the formation of small SiO spots on the surface, a result of the oxygen present in the propellant reacting with the silicon in the material.

5.4. Microstructure

The second point of comparison is the microstructure of the C/C-SiC plates. By investigating the microstructure, already many predictions can be made regarding the properties of the material. Especially when the ratio and placement of the carbon, SiC and Si stages can be identified and quantified, a lot of information is gained. It shows the quality of the infiltration process and determines properties such as mechanical strength, ablation and oxidation resistance and other thermal properties. Two ways of microstructure assessment will be done and explained. Firstly, scanning electron microscopy in combination with energy dispersive spectroscopy (SEM with EDS) will be discussed. Secondly, x-ray radiography will be elaborated on.

Scanning electron microscopy is an imaging technique where electrons are used as the main information carriers. An electron beam is generated and directed towards the sample surface. When the beam hits the surface, secondary electrons are generated by the surface, which are then collected by

a scanner to form an image. Energy dispersive spectroscopy is an additional module used in combination with SEM. Due to the electron beam, the surface will become ionized, which results in the material emitting photons. These can be captured and analyzed and correlated to the atom numbers, as each atom type will emit photons with a different energy level. This way, the elemental content of the surface can be qualified and quantified to some extent. This can be useful for the identification of different phases in the SEM images, especially when filler materials are present. However, for this thesis, the use of EDS was found to not be required.

The used SEM was the JEOL-JSM 7500F, which is shown in Figure 5.3. To analyze samples using the SEM, first, they have to be prepared. The first step is selecting an interesting region and cutting a small piece, as the sample size in the machine is limited to approximately 2.5 cm by 4.5 cm. For cutting the sample a Sectotom-10 with a Streuers M1D20 diamond cut-off wheel was used. A diamond-coated tool is required due to the high hardness of the material. Whenever possible, the device was used in automatic mode with a low feed speed of 0.2 to 0.5 mm/s. However, when the samples were too large, manual cutting was done. The cutting already gives a reasonable surface finish, however, it was found that still grinding and polishing were needed to get the desired image quality. This was done on a grinding and polishing rotating disk. Samples were ground in multiple steps, first using #180, #360, #600, #1000 and #1200 SiC grinding papers. This was followed by using a polishing disk with a diamond paste, going from 6 µm to 3 µm to finally 1 µm. After this, the samples could be put into the machine. Often, it is recommended to coat samples with a conductive gold layer, however, for C/C-SiC this is not needed, since it is conductive by itself. It is actually desirable not to coat the samples, as a lack of coating will make it easier to recognize the different material components. For each variation, one or two plates were selected for SEM analysis. From each plate, two small samples were cut from opposite sides of the plate. Each sample was polished on two sides. And from each side, multiple pictures were taken, often between 3 and 6. Thus, in total, between 12 and 48 pictures were taken and analyzed for each variation. This was done to gain confidence that the acquired data would be representative of the entire variation.

Now the microstructure of the different variations will be shown and compared. This is first done qualitatively, followed by quantitative analysis. Representative overview images of all variations can been seen in the following figures. Variation 1 and 2 are shown in Figure 5.4, 3 and 4 in Figure 5.5, 5 and 6 in Figure 5.6 and 7 and 8 in Figure 5.7. More SEM images can be found in section C.4.

These images should be understood in the following way. The black areas represent carbon fibers or carbonaceous resin residue. The white or light grey areas show residual silicon, while the (dark) grey areas in between show the silicon carbide. Some cracks or other imperfections also show up in white, due to the way they scatter the electron beam. Seeing the location of these phases with respect to each other gives important information. In the first two variations, the following pattern can be observed: It can be seen that the carbon fiber bundles stayed together, however, silicon carbide did get in between the fibers, which means the fiber did get attacked and some got converted to silicon carbide. Between the fiber bundles, large spots of silicon carbide are observed, within which some smaller parts of silicon can be seen. At some intersections of differently orientated fiber bundles, larger spots of silicon are observed. It is not unlikely that these large areas of unreacted silicon are at the locations where the pores used to be in the CFRP part. Here the fact that the fibers got partly converted will have an influence on the mechanical strength and stiffness. However, since the fibers are more surrounded by silicon carbide, the ablation resistance will be improved slightly. The large patches of free silicon are undesirable, as they do not provide the same amount of ablation resistance or mechanical strength as the matrix or fibers.

Variations three and four show a different structure. Here the fibers have stayed together and no silicon carbide is found inside the bundles. This is to be attributed to the powder resin, as this is the major change from the first two variations. Possibly already in the CFRP manufacturing stage, the resin was less infiltrated inside the fiber bundles than was the case for variations one and two which used liquid resin. This structure is more similar to the microstructure of woven C/C-SiC material, where also the fiber bundles and matrix stay seperated. This seperation will have a positive influence on the mechanical strength of the material, but a negative influence on its ablation resistance. The amount of

free silicon, especially for variation three, seems low, which points to a good infiltration process where the infiltration pathways were not too large.

Comparing the last four variations to the first four, large differences can be observed. No real fiber bundles can be seen anymore and silicon is infiltrated between all of the individual fibers. This is due to the change in fiber type and in line with the expectation, as literature also describes this effect. The fibers here are better shielded from attack because of an additional graphite layer on the outside of the fibers, as explained before. Also, since the stiffness of these fibers is much higher, some loss of fibers will still result in acceptable stiffness values. Because of this more uniform microstructure, the effects of other changes such as resin type or fiber length are hard to observe.

Secondly, more quantitative data can also be obtained from these images. This is done by performing colour recognition on the images using image editing software, for example, paint.net. Here one colour is selected and the number of pixels of this colour and neighbouring colours is counted. By doing this for black, grey and white, the volumetric division of carbon, SiC and silicon can be estimated. Afterwards, the areas can be filled with more contrasting colours to give a better overview of the location of each phase. An example of doing this can be seen in Figure 5.8. Similar pictures for the other variations can be found in section C.4. It was done for all images to determine the average composition for each variation. The results of this can be found in Figure 5.9. Also here some notes can be made. Again the largest difference is observed between the pitch and the PAN-based variations. For the pitch based variations, a higher amount of silicon carbide is formed. This is due to the graphite layer around the fibers getting converted, as well as the fibers being more completely surrounded. Like mentioned before, this will negatively influence properties like strength and fracture toughness, as these are mainly provided by the fiber. However, thermal properties like ablation resistance are increased, as the silicon carbide will shield the fibers from recession. Another thing to note is the relatively high amounts of free silicon present in almost every variation. Though it is hard to completely remove free silicon without additional processing steps, it should be minimized to at least below 10%. This is because the free silicon will not benefit the structural or thermal properties of the material. The fact that still large amount of free silicon can be observed, means that improvements in the manufacturing technique are still possible and desirable. Reduction in free silicon can be achieved by improving the C/C microstructure with smaller pathways. This can likely be done by more uniform fiber distributions, lower CFRP porosity and changes in the pyrolysis cycle.

Next to SEM, also X-Ray inspection is performed. In this form of radiographic testing, the sample is placed between a radioactive x-ray source and a detector. The thickness and amount of material at each location of the sample determine the number of X-rays that pass through the sample. This thus gives a good image of the microstructure, with pores and inhomogeneities easily identifiable. These X-ray tests are outsourced to an external company that does the test and then sends the X-ray images. Analysis and evaluation are not performed by this company. For LSI parts this technique is most valuable to check the quality of infiltration since badly infiltrated areas will very clearly show up on the pictures, due to their lack of silicon and silicon carbide. Two inspections will now be shown. Firstly, in Figure 5.10, an image of a plate of variation 1 can be seen. Though not perfectly homogeneous, there are no large spots that have much more fiber or matrix than others. Therefore, this is an example of a good sample. Notable is the dark line on the right side of the image. This represents an area with a high amount of residue silicon. This is due to the fact that here the plate was immersed in the silicon granulates, thus after cooling down, a small line of silicon got stuck to the sample.

An image containing three plates of variation 5 can be seen in Figure 5.11. Here a clear difference is observed between the left plate and the other two. The left plat is mostly uniform in colour and thus represents a well-infiltrated plate. The other two have areas on their top left side which show up very white. These areas have not been properly infiltrated. That means that here the carbon phase will be dominant, and thus mechanical, thermal and physical properties will be different. These plates cannot in their entirety be considered good CMCs, and thus when testing these, the areas that are badly infiltrated should be avoided. In section C.5, X-ray images of all plates can be found. It can be observed that almost all plates show good infiltration, with the exception of the variation 7 plate. An investigation

Figure 5.3: Used scanning electron microscope

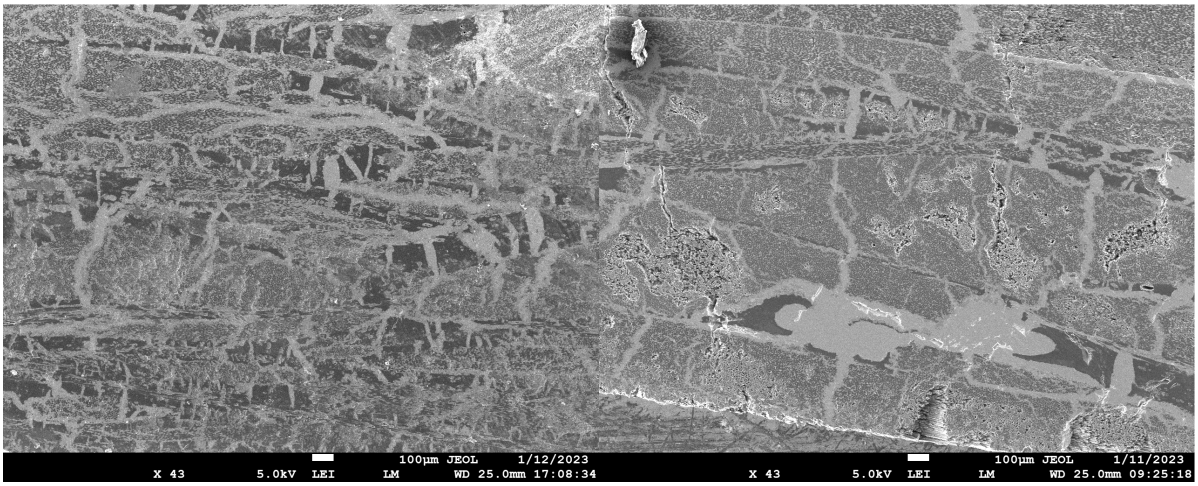

Figure 5.4: Overview SEM image, Variation 1 (left) and 2 (right)

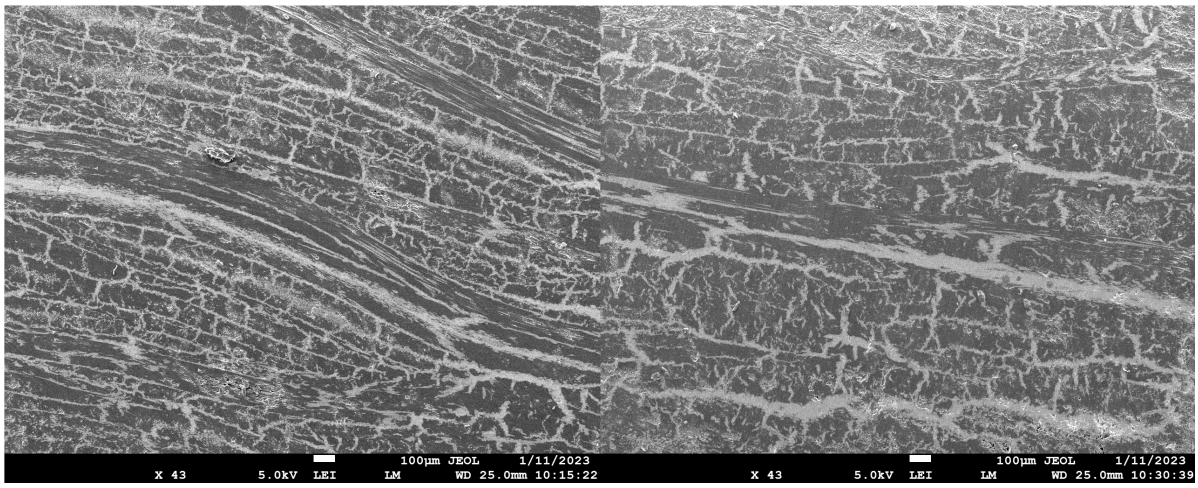

Figure 5.5: Overview SEM image, Variation 3 (left) and 4 (right)

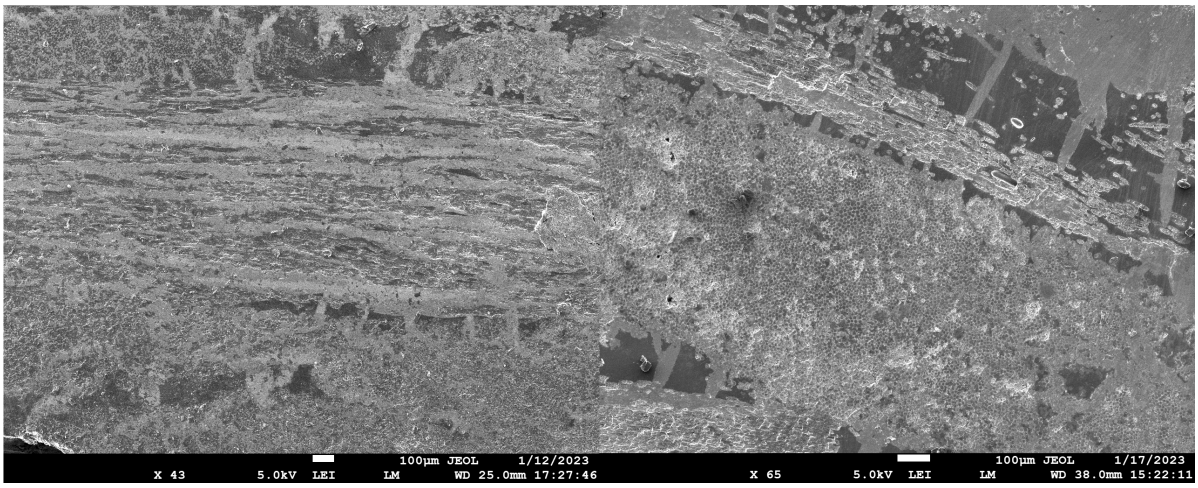

Figure 5.6: Overview SEM image, Variation 5 (left) and 6 (right)

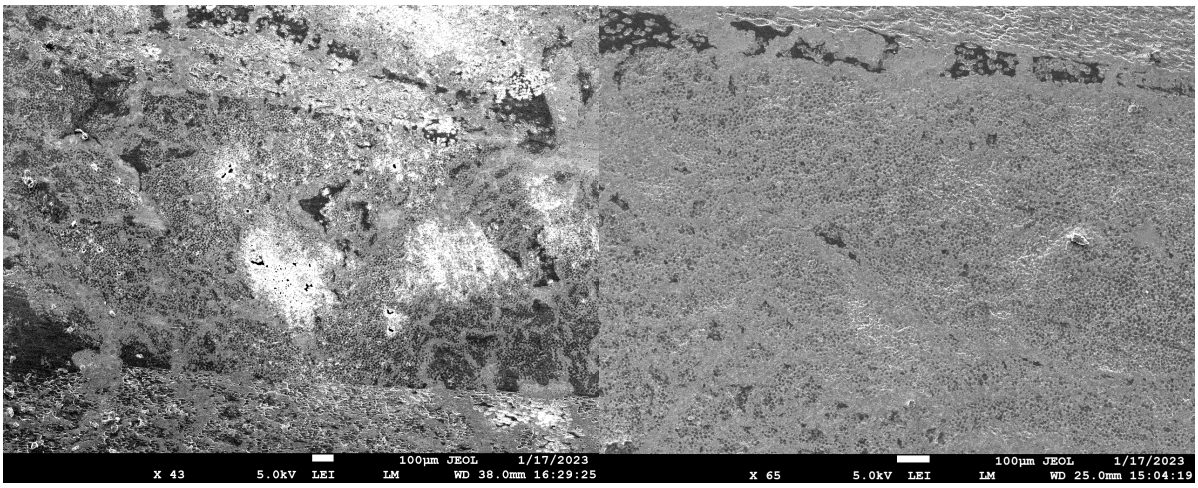

Figure 5.7: Overview SEM image, Variation 7 (left) and 8 (right)

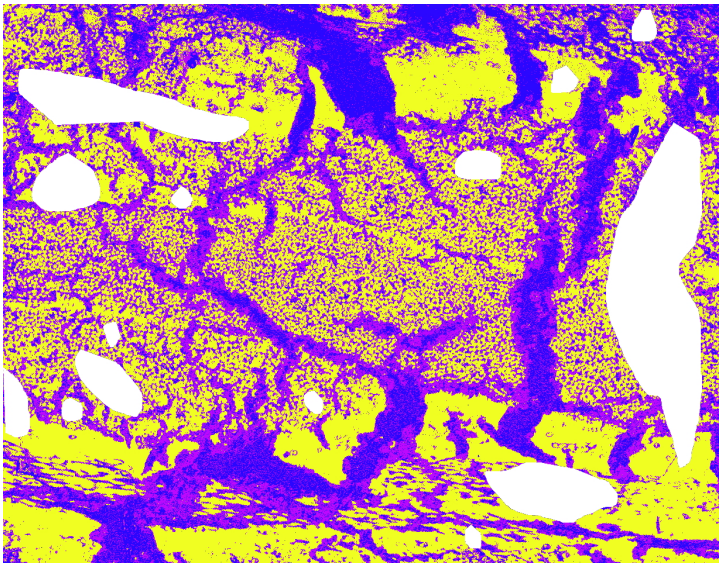

Figure 5.8: Example of a processed SEM image

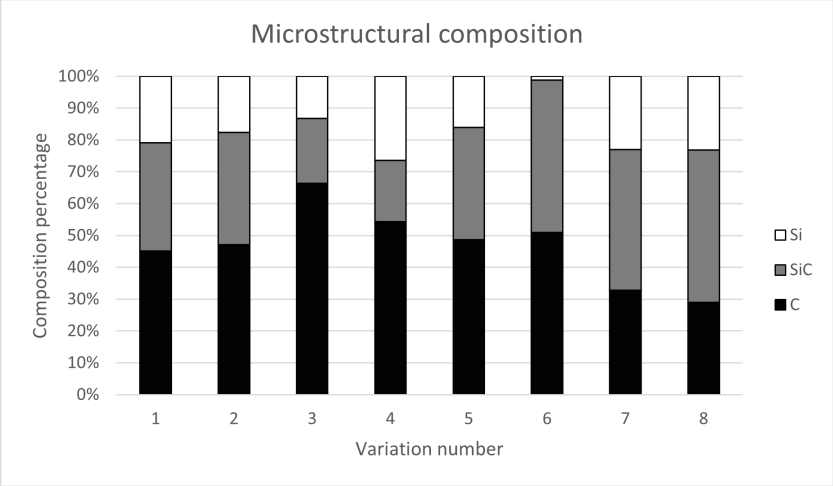

Figure 5.9: Comparison of phase composition of different variations

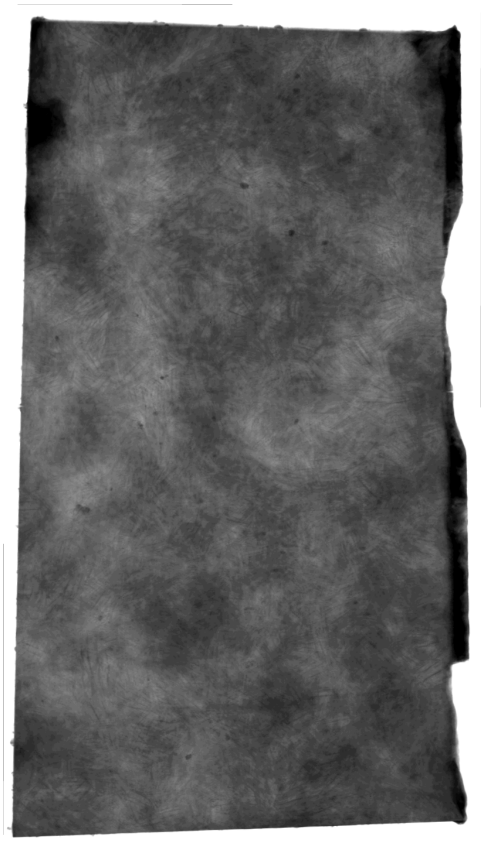

Figure 5.10: X-ray inspection of a variation 1 plate

was done into the reason why incomplete infiltration happened. It was concluded that this is most likely caused by inhomogeneous fiber distribution in the sample. At some locations, fiber had clumped together with little resin, and these regions thus did not provide good cracks and pathways for infiltration, leaving the regions beyond it uninfiltrated. To avoid this, better care should be taken to spread fiber and resin homogeneously when creating samples. This is especially important when longer fibers are used, as these can more easily be accidentally aligned in one direction. Another notable difference in the X-ray images that can be observed is the sample thickness, which makes the X-ray look darker (for example variation 4, sample 4, which was 2 mm thicker than the other variation 4 samples). Also, the distinction between pitch and PAN based fibers can be seen, with the former showing darker and less contrasting fiber architectures in the X-rays. Differences in resin type, fiber length or fiber volume fraction cannot be easily detected in the X-ray images.

5.5. Mechanical properties

Here the mechanical characterisation tests done will be explained and the results shown and discussed. First, the methods used and the motivation behind these will be discussed. After this, the test procedure will be elaborated on. Lastly, the results of the tests will be shown and analysed.

Mechanical characterisation represents a large field in which many material properties are available as well as many different ways of determining these. For many materials such as metals or polymer composites, the most commonly evaluated properties are tensile strength and modulus. These are tested using a tensile test bench. The choice for these is evident, since these values play a large role in design, and are relatively straightforward to determine. Next to tensile tests, compressive tests are sometimes also performed, though these are less common as geometric considerations start playing a large role: A dedicated test setup is needed to avoid materials failing in buckling at much lower strength

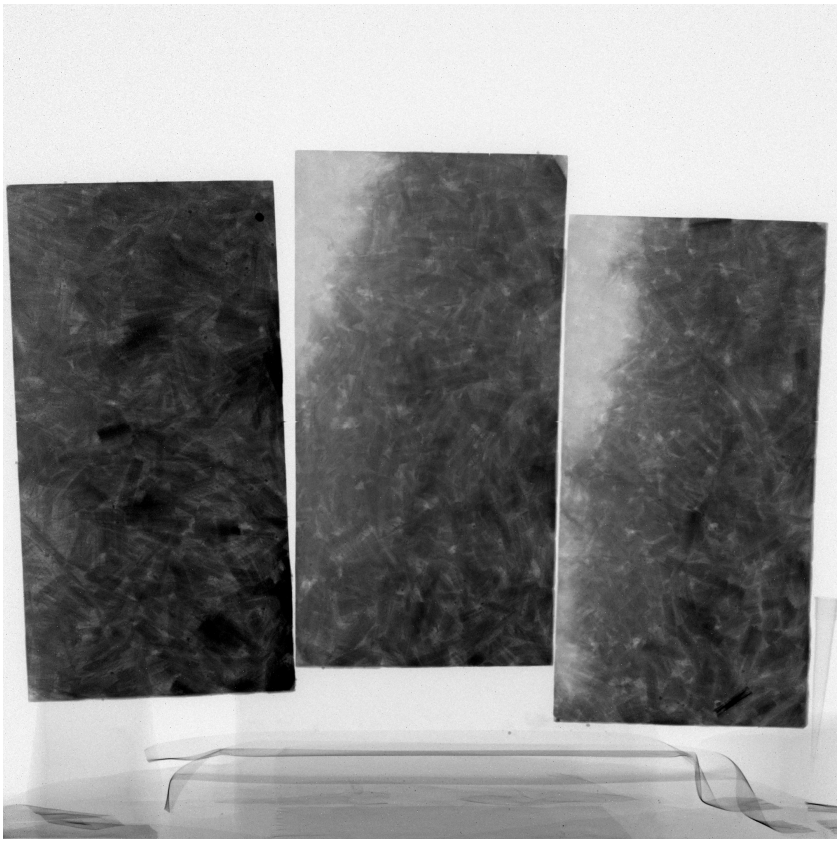

Figure 5.11: X-ray inspection of three variation 5 plates

than the actual material strength. However, for ceramics and ceramic matrix composites, other considerations are at play. Ceramics have very strong bonds, which leads to minimal plastic deformation ability. This leads to low fracture toughness and thus to high defect sensitivity. This means the type of tensile testing performed for metals or polymers is not applicable, as the ceramic will fail due to small flaws at much lower levels than its actual strength. To avoid this, historically it has been common to test the tensile strength of ceramics using flexural tests [27]. This practice has also been adapted for ceramic matrix composites, for similar reasons [28]. However, here tensile strength cannot be easily determined from flexural strength anymore, due to the fibers providing different failure mechanisms. Thus, instead of listing flexural strength data as tensile data (as is common for ceramic testing), it is listed as flexural strength for CMCs. In this way, flexural strength has become the most common way of comparing different CMC materials with each other.

For these reasons, this thesis also uses flexural tests for CMC evaluation. These tests are relatively straightforward to perform and having this data is required if comparisons with literature have to be done. However, there are still some large problems associated with these tests, which are important to understand. First of all, bending tests introduce a complex stress state in the material, combining tensile, compression and shear stresses. To make comparisons possible, it should be ensured that each specimen fails in the same way. Even then, the presence of this complex stress state will lead to a large spread in test data, an undesirable characteristic. Also, significant size and testing procedure effects have been observed during these tests, as described in more detail in section B.3. However, as also shown there, switching to other types of tests, such as tensile tests, will bring its own problems, mainly with the need for high precision alignment and gripping of the specimen.

For short fiber based CMC materials, no test standards exist. Therefore, the standards for continuous fiber CMCs are used as guidelines, as done by other authors. The ASTM C1341-13 is the standard that is used, in a three-point bending setup. Since the specimens have a thickness of 3 mm, a specimen width of 9 mm is used. According to the standard, a specimen length of at least 60 mm is needed for

Figure 5.12: Zwick Z010 used for flexural testing

this to attain the minimal L/D of 16. The L/D (span-to-depth ratio) is used to estimate the stress state inside the material. If the L/D is too low, there will be an increased likelihood that the specimen will fail in shear, which invalidates the test. To optimize the area from the manufactured plates, specimens were cut along the width of the plates. This resulted in specimens with a length of around 73 mm. This means that the L/D is approximately 21, thus above the 16 required for the test. However, it is below the 32 recommended by the standard, thus still some specimens can possibly fail in shear. Due to the size and geometry effects described by other authors (summarized in subsection B.3.2), it was decided to also have some specimens with higher width, around 15 mm. This is not according to test standards, however, it is likely that this will give less scattered test results and is therefore worth trying.

The procedure, equipment and preparation will now be detailed. The specimens are prepared by measuring the desired dimensions, which are then marked on the plate. This plate is then cut to size using the Sectotom-10 with a Streuers M1D20 diamond cut-off wheel. Whenever possible, the device was used in automatic mode with a low feed speed of 0.2 to 0.5 mm/s. However, when the samples were too large, manual cutting was done. After this, all samples were measured using an electric caliper to determine their test volume. Width and thickness measurements were taken on the top, middle and bottom of the samples and an average was taken. The used testing machine was a Zwick Z010, a 10 kN test bench, see Figure 5.12. This device was used in a three-point bending setup with a 500 N Zwick Xforce P loadcell. Samples were loaded into the device, making sure they were as centred as possible. The device was set in displacement control mode with a speed of 1 mm/min until a preload of 0.1 N was reached. After this, the test speed was set to 0.04 or 0.06 mm/s. This was in line with the test standard, which recommended that specimens fail in 5 to 10 seconds after the test start. With these test speeds, specimens often failed between 6-7 seconds. Furthermore, the test was set to stop after a force drop of 95%. This was done to also have the option of seeing the post-failure behaviour of the material. After the test was started, force and displacement were measured at high frequency and finally exported to a CSV file, which could be used for further processing.

The data has to be converted to stress and strain to remove the influence of specimen size. This is done using the following equations, also given in the standard. The equation for flexural strength and

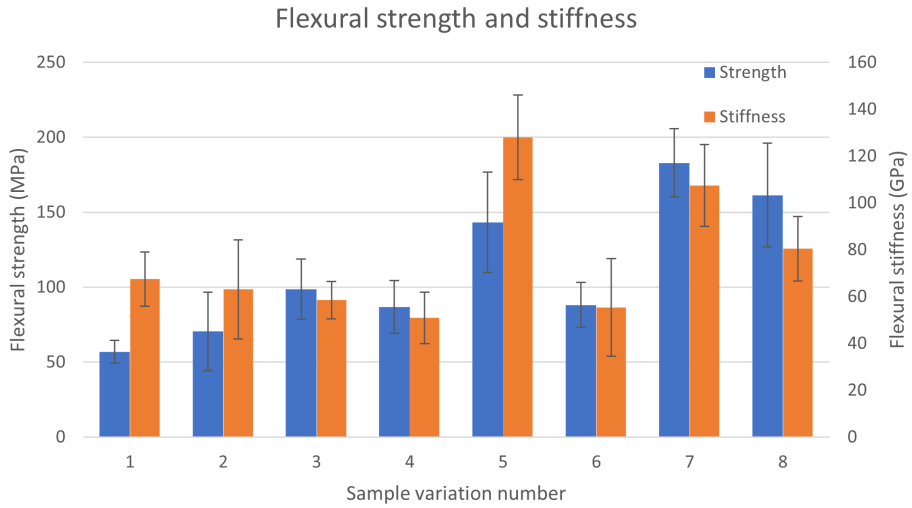

Figure 5.13: Flexural strength and stiffness of different variations, including STD

modulus of elasticity are also given.

$$\sigma = \frac{3PL}{2bd^2} \tag{5.22}$$

$$\epsilon = \frac{6Dd}{L^2} \tag{5.23}$$

$$S_U = \frac{3P_U L}{2bd^2} \tag{5.24}$$

$$E = \frac{L^3 m}{4bd^3} \tag{5.25}$$

Here σ is the maximum stress on the outer edge of the material in MPa, ϵ the maximum strain at the outer edge, L the outer support span in mm, d the sample thickness in mm, b the sample width in mm, D the deflection measured by the testing device in mm, P the measured force in N, P_U the maximum force experienced during the test in N, E the flexural modulus in MPa, m the slope of the linear part of the stress-strain curve in N/mm and S_U the flexural strength in MPa.

By processing the data like this, the strength and stiffness of different variations can be compared. The resulting strength and stiffness of each variation, as well as the standard deviation in the error bars, can be seen in Figure 5.13. The data processing code can be found in section A.5.

Using Table 5.4, the effect of different material compositions will now be discussed. First of all, the effect of fiber length is considered. It can be deduced from the test that an increase in fiber length, both for PAN and for pitch fibers, has two effects. On one hand, the strength of the material increases, however, on the other hand, the stiffness decreases. The increase in strength can be contributed to the fact that more of the stress experienced by the material is carried directly by the fibers, instead of the matrix. The longer the fiber length, the closer the strength values will be to that of a continuous fiber material. This effect is also well documented in literature, see subsection B.4.4 for more details. The effect of fiber length on modulus is less well understood, and in the past different results have been found. It should also be noted that for the PAN based fibers, the difference is very small. For the pitch based fibers, however, this is not the case. This author suggests the following hypothesis to explain this effect: With the longer fiber lengths, the fiber-matrix bonding becomes weaker due to the fact the fibers are harder to spread and separate from each other and therefore become less fully embedded in the matrix. This weaker interface leads to more movement between fiber and matrix, that is, higher strains, which then leads to a lower modulus. It is understood that normally the bonding mostly plays a role in the failure region of the material, however, it is not unthinkable that it also influences the material behaviour earlier on in the stress-strain curve. Nevertheless, to prove or reject this, more tests should

be done to look into this specific effect.

Regarding resin type, no single clear conclusion can be drawn. When considering the PAN based fibers, the resin type leads to slightly increased strength and similar modulus, however when considering pitch based fibers, both strength and modulus greatly decrease. This means that either other factors were at play in these specific samples, or that the influence of resin type is depended on the fiber type as well. It is important to note that the increased strength of variations three and four compared to one and two corresponds with the observations done on the microstructure. The powder resin resulted in a lower amount of attacked fibers, which could be an explanation for the higher strength values of the third and fourth variation.

For fiber volume fraction, a clear effect can be seen in that both modulus and strength (slightly) decrease when the fiber volume fraction is lowered. This is in line with literature, and in line with the rule of mixtures: since the strength and modulus of the fiber are dominant over that of the matrix, the material strength and modulus decrease when the amount of fibers decreases.

Lastly, considering fiber type, also a clear relationship can be observed, with both modulus and strength greatly increasing when using pitch fibers compared to PAN fibers. This is in line with what is reported in literature, as described in subsection B.4.2. Because of the more graphitized nature of the pitch fibers, they have better matrix interphase and they get attacked less by the silicon. Thus, they retain their strength properties better. Also, they have greatly increased stiffness, which translates to the higher material stiffness.

Now also the influence of the test section on strength and stiffness can be analyzed. The influence of cross-section on modulus for variations 1 and 5 can be seen in Figure 5.14, while the influence on strength can be seen in Figure 5.15. In both images, the data from all individually tested samples are plotted in a scatter plot. Samples originating from the same plate are given the same colour. The plate names are listed in the legend. The following can be observed: For the samples of variation 1, no influence can be observed on either strength or stiffness. This is likely for two reasons. Firstly, the change in cross-section from the smallest to the largest sample is small, around 50%. Thus even if the effect was there, it might not be visible. Secondly, the sample width compared to the fiber length is large, namely width/length ≈ 3. This means that it is likely that already the fibers are distributed in a very homogeneous way and increasing the sample cross-section will not have an additional positive influence in this regard. For variation 5 some influence can be seen both for modulus and strength. Though the average value at higher cross-sections seems to be approximately the same, the scatter around this average value is much less than at lower cross-sections. This effect can be attributed to the width/length ratio described above. Since these fibers are 12 mm, the width/length ratio when using the 9 mm width prescribed by the standard is below 1. Thus, when the sample is made wider and the cross-section larger, this ratio will go up and above 1. This will greatly increase the likelihood that fibers are positioned in a more homogeneous way, thus bringing the results closer together.

5.6. Thermal properties

Here the thermal characterisation test done will be explained and the results shown and discussed. First, the methods used and the motivation behind these will be discussed. After this, the test procedure will be elaborated on. Lastly, the results of the tests will be shown and analysed.

As its high-temperature performance is one of the characteristic features of a CMC material, quantifying this is an important part of assessing a CMC material. Different properties exist and can be tested for, such as thermal conductivity and coefficient of thermal expansion (CTE). Both of these are very relevant for design purposes, especially in rocket nozzles. Thermal conductivity determines what temperatures the surrounding structure will experience. In general, this means that for nozzles inside a casing, a low conductivity is desired (to protect the casing material), while for nozzles in free air, high conductivity is more desirable (to increase radiative and convective cooling). Knowing the coefficient of thermal expansion is relevant for nozzle integration with other structures, as mismatches in thermal

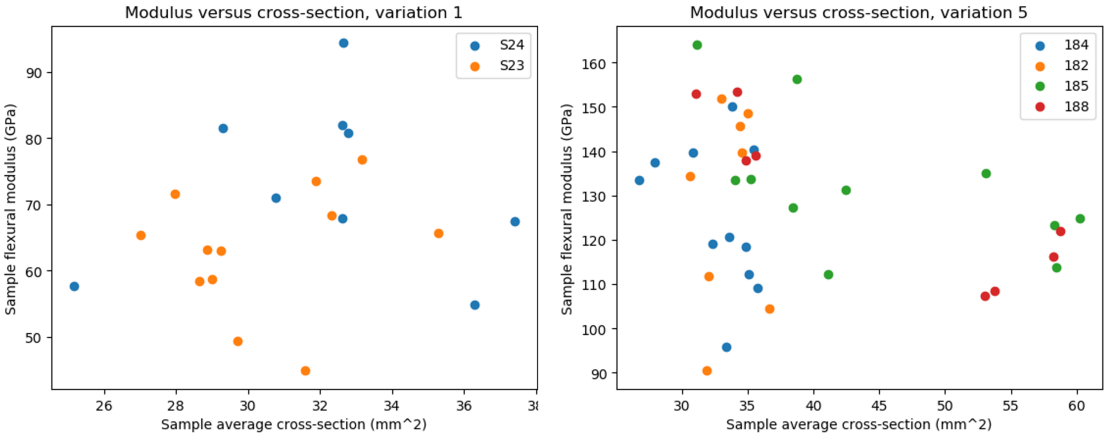

Figure 5.14: Influence of sample cross-section on flexural modulus

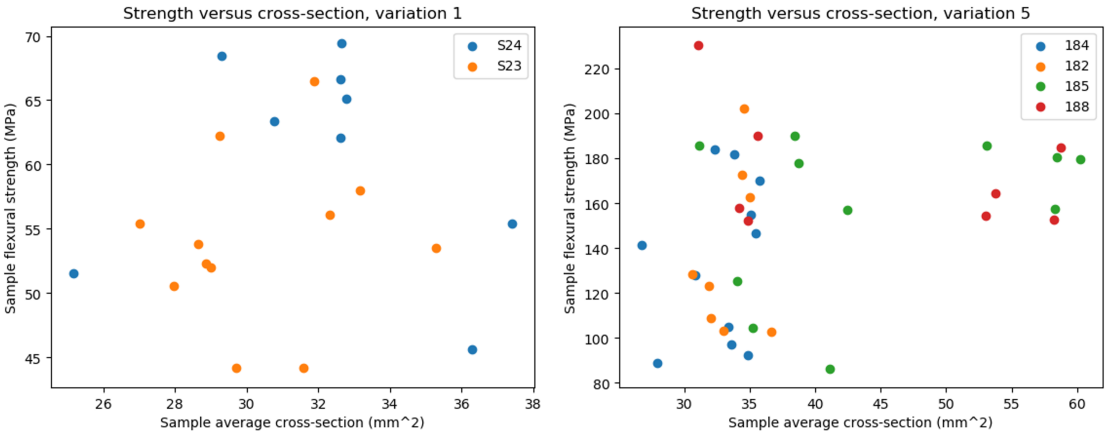

Figure 5.15: Influence of sample cross-section on flexural strength

expansion can induce high stresses in bonds when the structure is heated up or cooled down.

As part of this thesis research, only the coefficient of thermal expansion will be determined and compared. The reason for not measuring the conductivity is the complexity of measuring this, which made it unfeasible in the timeframe of the thesis. The most common way of measuring it is using laser flash analysis, which combined with differential scanning calorimetry can give a good estimate of the thermal conductivity. However, this equipment was not readily accessible, which meant a different and more complex setup would have been required, at which point it was decided to not perform these tests. The CTE however was determined. The methodology for this will now be explained.

Common ways of determining the CTE of a material are using a dilatometer or doing dynamic mechanical analysis. Both of these devices work on the principle of heating up a piece of material and measuring the change in length. For dynamic mechanical analysis, this is done in one dimension, while with a dilatometer it is sometimes also possible to determine the volumetric dimensional change. The change in length is determined using for example a laser distance sensor or a linear variable differential transformer. Both of these devices were available, however, in the end, they could not be used, due to maintenance or incompatibility with the CMC material. Therefore, to determine the CTE, a custom test setup was created and used. The principles of this test setup remained the same as with the methods described above. The heating-up part of the experiment was done simply by putting the part in an oven. The temperature determination of the part was done by using a thermal imaging camera. The measurement of dimensional change was performed using digital image correlation (DIC). The part was heated up in the oven to a desired temperature, after which it was taken out and passively cooled down to room temperature. During this cooling down phase, the difference in size of the plate was measured using the DIC system.

Some more detail on test methods will now be given. First of all, DIC will be elaborated on. Digital image correlation is a non-destructive measurement technique in which the change in the shape of objects is determined by optical means. It is done by setting up one or two cameras, which take repeated images of a specimen from a fixed position. The advantage of using two cameras is the ability to also determine out-of-plane displacements. To increase the resolution and ease of use of the technique, samples are prepared by painting them with a speckled, black-on-white, pattern. In an ideal case, the speckles are a few pixels in size, which can lead to sub-pixel accuracy in post-processing. The setup for this test was as follows. First, the samples were painted white and once dried, a black speckle pattern was applied. This was done using MoTip heat-resistant spray paint, which is rated to be usable up to 800 °C. The samples were then dried in an oven at 150 °C for 45 minutes to harden the paint. A test stand was made and fixed to a table for the measurements of the samples. Next to the table, two DIC cameras were fixed to a tripod and pointed at the test stand. A light source was put in between and behind the cameras. The aperture and focus of the cameras were set, after which great care was taken not to move the table or tripod anymore. The output of the cameras was connected to a computer running the VIC-snap software by Correlated Solutions, which was used to capture and process the DIC data. A calibration plate from this company was used in combination with the software to calibrate the cameras.

For measuring the temperature of the specimen during the test, a thermal imagining camera was used. This camera was set up on a tripod on the opposite side of the table, thus pointing at the back of the specimen. For this, the FLIR A655sc was used. This camera also was focused and connected to a computer, running dedicated FLIR software to capture the data. The camera has two measurement ranges, namely between -40 °C to 150 °C, and between 100 °C and 650 °C. Two test runs were done, one in both of these measurement ranges.

For the test, samples were heated up in an oven. All samples were stacked in the oven, after which it was programmed to heat up in 30 min or 1 hour. For the first test samples were heated to 160 °C, while for the second they were heated to 700 °C. By the time the samples were in the test stand, they had already considerably cooled down and were inside the test range of the thermal camera. For the test, first, the DIC and FLIR cameras were started, after which the sample was taken from the oven and carefully placed in the test stand. The temperature was tracked with the FLIR camera. When the tem-

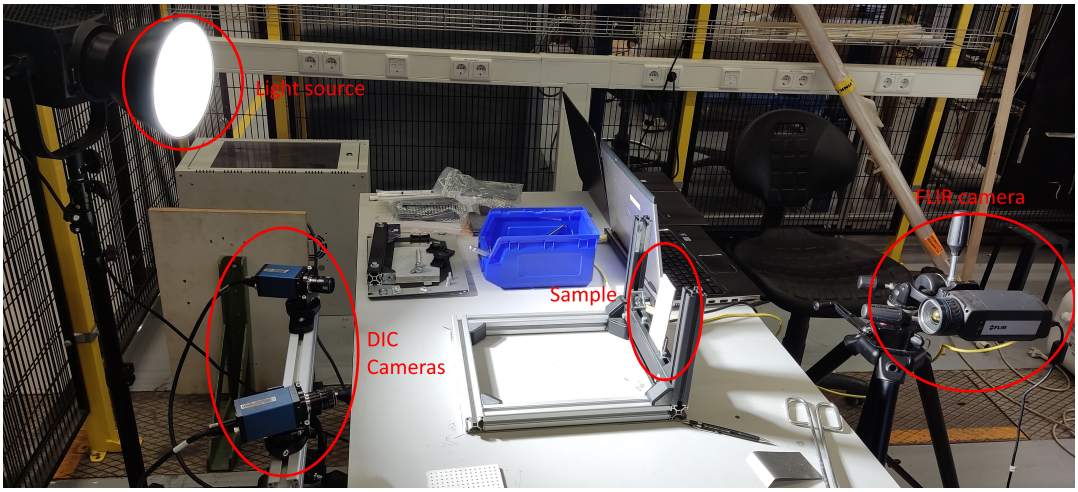

Figure 5.16: CTE measurement test setup

perature dropped below 40 °C for the first test or below 100 °C for the second test, the measurement was stopped. A picture depicting the test setup can be seen in Figure 5.16. After the test, the data was processed in the following way. For the DIC data, the VIC-3D software was used. In this software, both the calibration images and test images are loaded. The program will automatically detect the speckle pattern on the samples. After this, an area of interest is defined and the data processed, meaning that the program will determine the change in the shape of the specimen by tracking the movement of the speckle pattern, as explained above. After this, the strain over time can be exported from the program. Both strains in the x and strain in the y direction were considered, to check for inhomogeneous behaviour in the specimens. As region of interest, the top part of the specimen was taken, as this part is not in direct contact with the frame and thus cools down slower. Also, the lower part of the specimen was not always visible to the thermal camera, as sometimes a spacer was used here to hold up the sample in the test stand.

The FLIR data was processed using the FLIR research studio software. Also here a region of interest was taken, from which the average temperature over time was exported. However, determining the absolute temperature of the sample using a thermal camera was found to be non-trivial. It was noted during the test that the camera detected a large temperature difference between painted and non-painted parts, as can be seen illustrated in Figure 5.17. Note how the painted part number stands out, even though it is probably almost the same temperature as the surrounding material. The likely cause of this is a difference in emissivity. This is the most probable explanation, since the part was just taken from the oven, and since the detected areas of higher temperature were very localized to the painted areas. It is unlikely that there existed large actual temperature differences inside the part. Emissivity is a value that indicates how a material interacts with light, in this case infrared radiation. Three things can happen, namely reflection, absorption or transmission. In this case, since the part is not transparent or opaque in any way, the transmission will be 0. Therefore, all infrared radiation seen by the thermal camera is either emitted by the part or reflected by the part. The ratio between these two is captured by the emissivity value. This value will be very low for (polished) metal, and 1 for an ideal black body. The emissivity value can be inputted in the FLIR software, together with the distance to the specimen and reflected temperature to compensate for the reflection. However, the emissivity value of the samples was unknown and also differed between fiber and matrix dominated areas. Some literature data exists, however, it is often for a different temperature range [29][30][31]. However, these sources point to an emissivity value between 0.6 and 0.8, which is temperature dependent. To get an accurate temperature, an estimation of the emissivity was done for each sample. Emissivity can be determined in a few ways. One method is painting part of a sample with paint with a known emissivity value, after which the difference between the painted and non-painted areas can be compared. A second method is measuring the part temperature directly using for example a thermocouple and comparing this reading to the thermal camera reading. In the processing of the data, the first method was used for all samples in the following way. The average temperature of the painted area was deter-

mined at an emissivity value of 0.95 (a common value for white paint). Then, emissivity was decreased until the surrounding material area showed the same temperature as the painted area. This resulted in an emissivity of around 0.75 for most parts. To validate this approach, the second method was also used during the test, where a thermocouple was attached to a select number of samples, and its temperature reading was compared to the temperature reading of the thermal camera while the sample was cooling down. This led to an emissivity estimation of 0.8. Though not fully corresponding to the value determined by the first level, this author feels that this still validated the approach. One obvious reason for the discrepancy is the fact that the thermocouple only records temperature in a very specific location, likely either matrix of fiber dominated, while the thermal camera averages these regions.

After this, the temporal plots for strain and temperature were combined and the strain was plotted versus temperature. In these plots, a trendline was added. The slope of this trendline now gives the thermal expansion coefficient. The results of this can be found summarized in Table 5.5. The code used for this can be found in section A.4. All of the graphs can be found in section C.6. A number of things should be pointed out regarding these results.

Firstly the difference between the CTE in x direction and y direction. For almost all samples, this difference is very small, below 5%. However, for some, the difference is larger, notably variations 2 and 3 at the 150 degree test and variations 2, 3 and 4 at the 700 degree test. This can have several causes. Firstly, the fiber distribution might not be homogeneous inside the region of interest, leading to a non-isotropic material and thus a different CTE in different directions. However, it is also notable that these variations are also the ones with the lowest CTE values. Therefore, another likely cause is the inaccuracy of the measurement system, which will be most evident at the lowest strain values. This indeed can be seen when comparing the noise in both measurements, see Figure 5.18 and Figure 5.19.

Secondly, it can be noted when looking at the temperature versus strain curves, that, especially over large temperature ranges, the relationship becomes non-linear. For the boldly marked values in the table, this is really evident, but also for other samples, this non-linearity could be present, though to a lesser degree. Due to this non-linearity, the CTE is not a constant, but a changing value, dependent on temperature. This can be captured by using a trendline of higher order. An example of the resulting graph and CTE curve can be seen in Figure 5.20. It was decided to use trendlines of order two for the curve fitting, leading to linear CTE curves. Ideally, the order of the trendline is decided based on some underlying physical phenomena or theory. However, in this case, it was found that using trendlines of higher orders resulted in the trendlines following the noise in the data too much, leading to unrealistic CTE curves. Therefore, it was decided to keep it at this lower order, even though some of the data suggests that physics requires a higher-order relationship. For example: look at the region between 100 and 250 °C in the lastly mentioned graph: It seems as if there is also a curve here that is not captured by the trendline at this point. Another point to mention regarding trendlines is that because of the data spread, the low-temperature data has more weight on the trendline than the high-temperature data. This is because the sample cools down in an exponential fashion. This means that the sample spends exponentially more time at lower temperatures. Because the trendlines are time-based, this means that the lower temperatures have more weight than the higher temperatures.

Taking these considerations into account, the difference between CTE in low and high-temperature runs is also obvious: Firstly because the CTE curves are not linear, thus over the larger temperature range the average CTE will be different. And secondly, because the trendlines are skewed because of the datapoints, which can lead to less accurate CTE values for the high-temperature data. It is interesting to note that in general the CTE seems to increase with temperature. When considering rocket nozzles, this can be a positive effect: during operation the material will reach high temperatures, however, if the CTE is also high at these temperatures, the CTE mismatch with the connection structure will be lower, leading to lower stresses and less likelihood of failure.

Taking all of this into account, the different variations can be compared. Comparison is best done between single numbers, as then meaningful conclusions can be drawn. For that reason, the variations will be compared with the average of the CTE in the x and y directions for the low-temperature regime.

Table 5.5: CTE values for different variations. Bold numbers mark areas where CTE value is an average CTE over a region where CTE is not constant.

Variation (-)	CTE (E-6/K) between 40 and 150		CTE (E-6/K) between 100 and 650	
	X-direction	Y-direction	X-direction	Y-direction
1	3.0	2.8	3.6	3.7
1	2.9	2.9	**3.9**	**3.8**
2	2.5	1.9	**3.9**	**3.5**
2	1.5	1.3	**2.9**	**3.3**
3	1.0	1.6	**2.4**	**2.9**
4	1.8	1.8	**2.4**	**3.4**
4	1.5	1.7	1.9	2.0
5	2.8	2.8	4.3	4.5
5	3.5	3.5	5.4	5.3
6	3.0	3.1	4.6	4.6
7	3.9	3.7	5.5	5.4
8	3.2	3.4	5.1	5.1

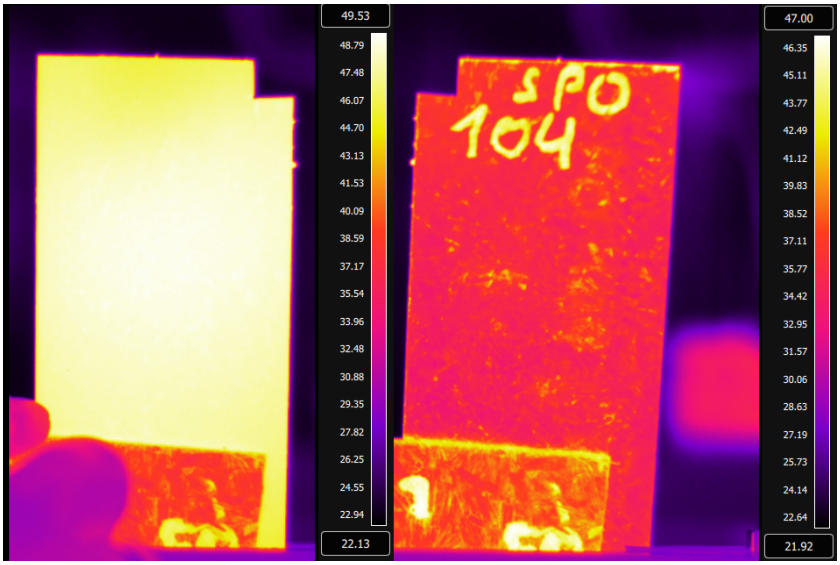

Figure 5.17: Difference in the thermal image between the painted front and the non-painted back of a heated sample

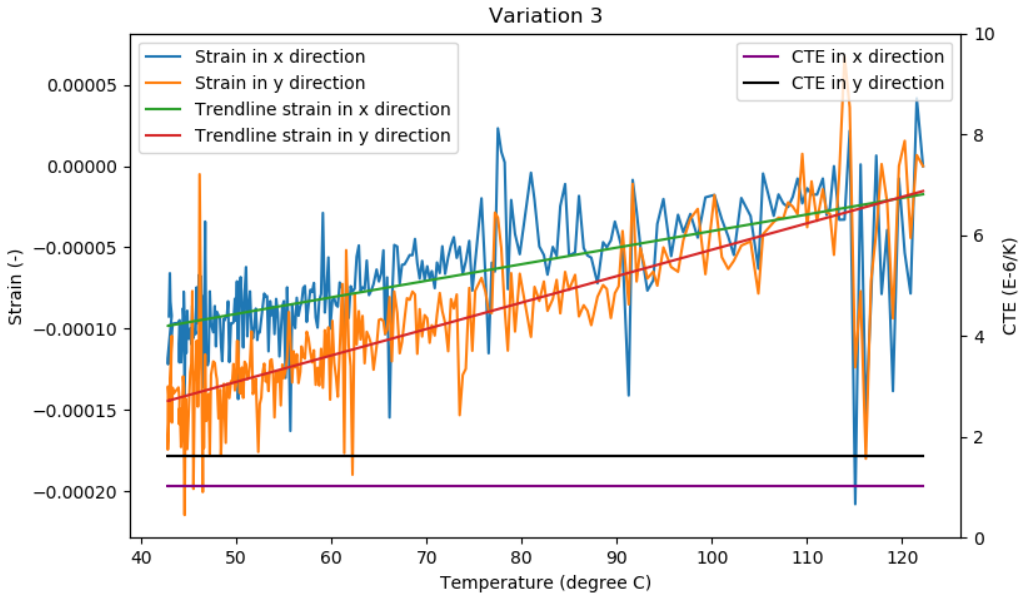

Figure 5.18: Strain versus temperature and CTE values, variation 3, low temperature

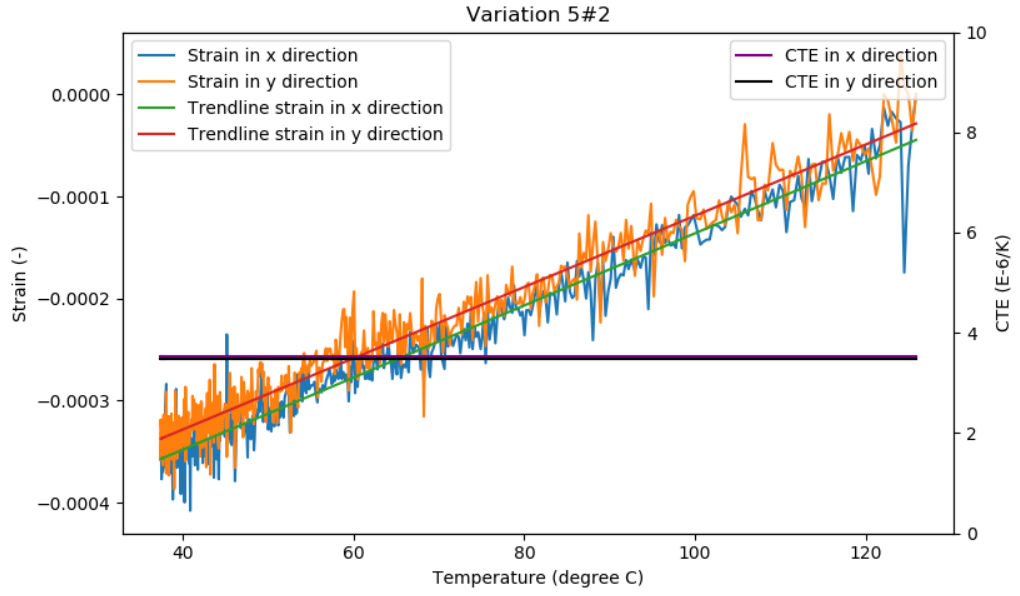

Figure 5.19: Strain versus temperature and CTE values, variation 5, sample 2, low temperature

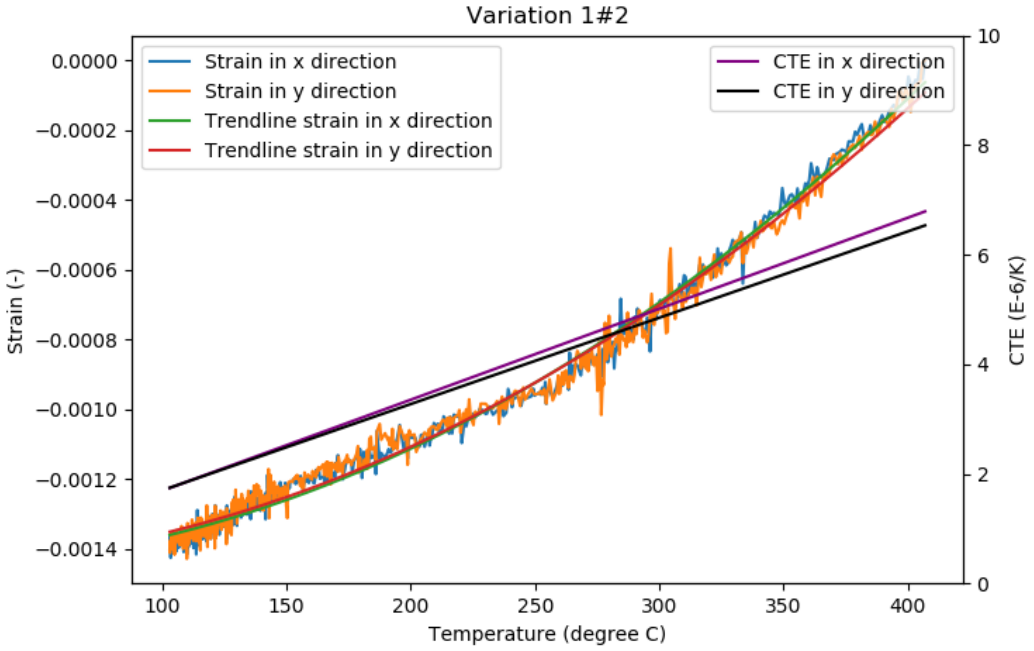

Figure 5.20: Strain versus temperature and CTE values, variation 1, sample 2, high temperature, non-linear

Table 5.6: Average low-temperature CTE values for different variations.

Variation	Average CTE (E-6/K)
1	2.9
2	1.8
3	1.3
4	1.7
5	3.2
6	3.1
7	3.8
8	3.3

The reason for this is that in this regime, the CTE presents the most linear behaviour and thus makes the CTE values more meaningful and accurate. The average CTE values can be found in Table 5.6. From this table, no clear conclusions can be drawn regarding the general influence of fiber length or resin type. However, the influence of fiber type is very clear: the Pitch based fibers all have a significantly higher CTE than their PAN-based equivalents. Also, the 3 mm and 12 mm PAN fibers, which came from different manufacturers, have very different CTE values. This leads to the hypothesis that the main factor influencing CTE is the exact fiber type and manufacturer. It can also be noted that the variations with higher fiber volume fractions have higher CTE values. This connects well with the hypothesis that the fibers dominate this property, as it shows that even if the fiber amount changes by just 15%, a noticeable change can be observed.

5.7. Summary

This section will summarize and collect all the test results and data from the sections above. Based on this, general statements and predictions can be made regarding the material properties, based on its components.

To test the effect of certain material components on material properties, 33 test samples were manufactured. Between these test samples, the material properties of fiber type, resin type, fiber length

Table 5.7: Complete test results summarized

	Density (kg/m^3)	Porosity (%)	Mass loss due to exhaust gasses (%)	Fiber bundle spreading	Phase distribution (%C/ %SiC/ %Si)	Infiltration	Flexural strength (MPa)	Flexural stiffness (GPa)	CTE (E-6/K)
1	2.31	1.03	3	Slighty spreadout	45/34/21	Good	57.0	67.4	2.9
2	2.17	2.94	-	Slighty spreadout	47/35/18	Good	70.4	63.1	1.8
3	2.04	1.94	-	Very compact	66/20/13	Good	98.6	58.5	1.3
4	1.99	1.73	-	Very compact	54/19/26	Good	86.8	50.9	1.7
5	2.67	2.45	1	Very spreadout	49/45/16	Good	143.2	128.0	3.2
6	2.37	0.81	-	Very spreadout	51/48/1	Good	88.1	55.4	3.1
7	2.51	11.71	-	Very spreadout	33/44/23	Mediocre	182.9	107.4	3.8
8	2.66	0.77	-	Very spreadout	29/48/23	Good	161.4	80.5	3.3

Table 5.8: Effect of material composition parameters on material properties

	Density (kg/m^3)	Porosity (%)	Mass loss due to exhaust gasses (%)	Fiber bundle spreading
Increase fiber length	No effect	Unknown	Unknown	No effect
15 % increase volume fraction	Increases	Increases	Unknown	No effect
Change from liquid to powder resin	No effect	Decreases	Unknown	Decreases
Change from PAN to pitch fiber	Increases (+20%)	Decreases	Decreases	Increases

and fiber volume fraction were changed, leading to 8 different variations. A number of relevant and important material properties were assessed for all of these variations. Specifically, the following measurements were done: Density and porosity determination, reaction to exhaust gasses, microstructural composition and phase distribution, infiltration based on X-ray imaging, flexural strength and stiffness and coefficient of thermal expansion. Now, all of these can be combined to give a complete overview of the attributes of each material variation, as seen in Table 5.7.

Based on these results and the discussion done in previous sections, the effect of each material composition parameter on material properties can be isolated. A summary of this can be seen in Table 5.8 and Table 5.9. These tables now act as a guideline and prediction tool for any new specimen that will be made. When a new material is to be designed, its desired properties can be compared with the actual measured properties in Table 5.7 and one can see how well these materials already fulfil the requirements. Then, if any requirements are not yet fulfilled, the other two tables can be used to determine what material properties can be changed to achieve the requirements.

Table 5.9: Effect of material composition parameters on material properties

	Phase distribution (%C/%SiC/%Si)	Flexural strength (Mpa)	Flexural stiffness (Gpa)	CTE (E-6/K)
Increase fiber length	Unknown	Increases (+25%)	Decreases (-10%)	Unknown
15 % increase volume fraction	More carbon (+15%)	Increases (+12%)	Increases (+20%)	Increases
Change from liquid to powder resin	More carbon	Unknown	Unknown	Unknown
Change from PAN to pitch fiber	More SiC (+30%)	Increases (+100%)	Increases (+100%)	Increases (+75%)

6

Nozzle development

6.1. Material selection

In this section, the material to be used for the nozzle will be selected, based on the results from the previous sections. A choice will be made between pitch and pan, fiber length and resin type.

For a nozzle, clear requirements can be set: Since it will experience high pressures and forces, both strength and stiffness should be high. Also, since it needs to be mated to a structure, a high CTE is desirable, though if not possible, mating it by using a container instead of a direct bond is also an option. Lastly, considering the hot exhaust gases, high ablation resistance is required. Using the tables in section 5.7, the following material is seen as ideal: 25 mm, pitch-based fibers with a powder resin. The reason for using 25 mm fibers is that they will give an increased mechanical strength for a small decrease in stiffness, which is desirable since stiffness will drive the design less than strength. This is because strength determines whether the nozzle fails or not, while stiffness might only impact its actual thrust output by some margin. Pitch-based fibers are chosen over PAN-based, as they are proven to have a much better ablation resistance, while also having an increased CTE. This does come at the expense of higher density, however again this is seen as a good trade-off: If the nozzle ablates too much it might fail, while if the weight is higher this only decreases performance by decreasing payload. Also, pitch-based fibers have a higher strength and a higher stiffness, which more than negates the stiffness loss due to the use of longer fibers. Lastly, powder is chosen because it decreases porosity in the final product, even though it also will compact the fibers slightly. The trade-off here was that decreased porosity will have positive effects for strength and stiffness, while the compacting effect on pitch-based fibers is likely minimal, looking at the SEM images of variation 6. Also, powder resin is generally easier to manufacture with, as mould filling is greatly simplified.

One of the factors to be considered when creating an actual product for the market is cost. It is important to realize that pitch fibers have a greatly increased cost compared to PAN fibers, thus for a commercial company the trade-off between PAN and pitch might be different. However, considering the research nature of this thesis, this is left out of consideration.

6.2. Production procedure

For the production of a rocket nozzle prototype, a dedicated mould is needed. The design of the mould which will be used is explained in this section. A cross-section of the mould can be seen in Figure 6.1. An outside view with all parts labelled can be seen in Figure 6.2. The part names and descriptions corresponding to the label can be found in Table 6.1.

This mould can be used in the following way. Parts 5 and 6 are connected, as well as parts 7, 1, 4, 9 and 8. Parts 2 and 3 are also connected and placed inside the aforementioned parts. Some parts are connected by threaded holes, while for others only alignment holes are used. After this is performed, mould filling can start. When the appropriate amount of material is placed as uniformly as possible in

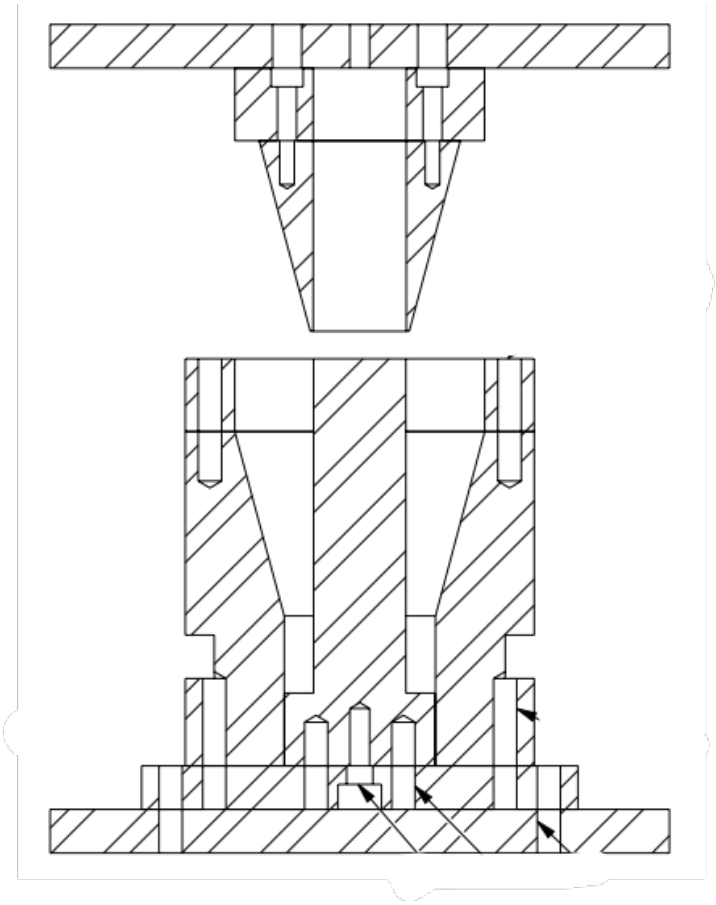

Figure 6.1: Cross-section of mould for nozzle manufacturing

Table 6.1: Labels and correlating part names for nozzle mould assembly

Part number	Part name
1	Base plate
2	Outer mould conical
3	Outer mould cylindrical
4	Mould core
5	Top plunger
6	Top plate
7	Ground plate
8	Clamping block
9	Clamping spacer

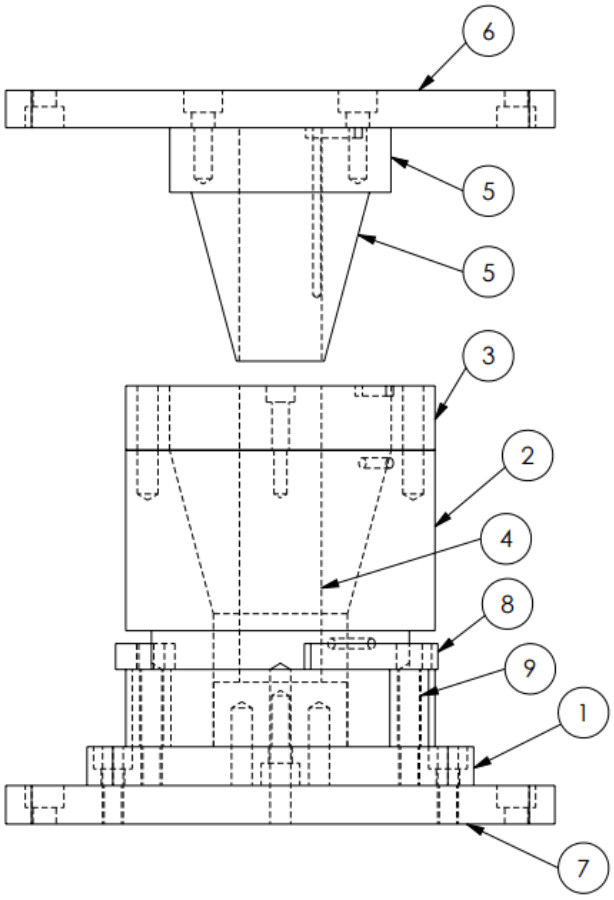

Figure 6.2: Labelled overview of the different nozzle mould parts

the mould, the top assembly can be placed over the core to close the mould. Due to the possibility of moving both the inside and outside mould parts up and down, the gap between them can be altered. During filling it will be large, giving enough space for material deposition. Then after closing it is reduced to the final part thickness. After closing, the mould is placed in a hot pressing device and connected to its plates. Also, the thermocouples are connected to the mould. The cycle is then started and no further action is necessary until demoulding. Demoulding is made easier due to the connection of the mould to the hot press, which means its hydraulic cylinders can be utilized to pull the parts apart.

Some notes can be made for this process. Firstly, it is evident that this mould does not utilize the more accessible oven technique anymore as described at the start of this report. The reasons for this are as follows. Though the mould for the oven technique would be largely similar, there are still some parts which make that a mould can only be used either inside a hot press or inside an oven. Therefore, a choice between these needed to be made. This mould is partly manufactured with the aim of series production in mind. This means that ideally, part quality should be high with minimal human intervention. This is best achieved by a hot press, as there pressure application is better controlled and can be programmed beforehand. Ideally, it would have been preferred to make the nozzle also using the oven technique, both to prove its feasibility and to better understand the process. However, in that case, two moulds would have to be made of which one would only be used in a few types. Thus, making dedicated moulds for prototyping with the oven technique was seen as too expensive and a waste of material.

Another note should be made on the temperature control features of this mould. As was discovered in the manufacturing research part of this thesis, the relation between the inside and outside temperature of a mould is very important. Therefore, this mould incorporates multiple locations for thermocouple insertion, such that this internal temperature can be monitored. This is especially relevant for this mould, as the complex shape could lead to internal temperature differences. One thermocouple can be inserted from the top into the core of the part, while a different one can be inserted from the side and a last one from the bottom. The locations are chosen such that the temperature in both parts very close to and very far from the edge of the mould can be monitored. This will greatly increase understanding of the moulding procedure.

6.3. Suggested production plan

Creating an actual nozzle prototype was found to be out of the scope of the thesis time-wise. However, still, some comments can be made regarding a plan for how this would have been done.

Many of the steps to be taken would have reflected the knowledge gained during the first part of the thesis. Firstly, the thermal characteristics of the mould would have to be measured. This is done by running a dummy program on the hot press while measuring the temperature at various locations on the inside of the mould using the aforementioned thermocouple holes. The difference between inside and outside temperatures could then be plotted, after which necessary changes to the program should be made to ensure that the inside cycle is as close as possible to the intended cycle. Once this is understood, the first samples can be made. It is recommended to first start with a 12 mm, PAN-fiber powder sample. The reason for this is that spreading and filling will be easier with 12 mm fibers, while it also will be less wasteful considering the lower cost of the PAN fibers. During the manufacturing of this part, note should be taken of any issues. Afterwards, the part density and porosity should be determined, as well as visual inspection performed. Based on these notes, changes can be made to the manufacturing process. Once, the manufacturing is well understood, possibly after a few samples, the change can be made from 12 mm PAN to 12 mm pitch samples. The same procedure should be followed to check if the result is any different. Lastly, after this, the change can be made to 25 mm pitch samples and likely after only a low amount of tries a successful prototype could be made. This of course then has to be pyrolyzed and siliconized. After this, more tests should be done, like tensile and compression tests and exhaust gas tests. When all of these are successful, the nozzle can be mounted on a rocket for a static fire and subsequently an actual test flight, which would validate the product.

7

Conclusion and recommendations

The aim of this report was to quantify and qualify the influence of manufacturing and material composition parameters on the properties of short fiber C/C-SiC material, specifically aimed at rocket nozzle applications. In the first part of the thesis, the manufacturing process was characterized and researched. A novel manufacturing technique was used, in which four major influencing parameters were found. The four major parameters which influenced the part quality were temperature cycle, moment of pressure application, excess resin amount and resin division. These were found to most influence part density and porosity, and it was researched and understood what values for these parameters resulted in the best material properties.

In the second part of the thesis, material composition parameters were researched. The influence of fiber length, fiber type, fiber volume fraction and resin type was investigated on various material properties. Through the evaluation of 33 samples of different compositions, some of the main conclusions were the following: Changing fiber type from PAN to pitch-based increases density, but also decreases porosity and greatly increases flexural strength, stiffness, coefficient of thermal expansion and ablation resistance of the material. Increasing fiber length mainly increases strength, while decreasing stiffness. Fiber volume fraction increases density and porosity, while it also slightly increases flexural strength, stiffness and coefficient of thermal expansion. Changing the resin type from liquid to powder causes lower porosity and a decrease in fiber bundle spreading.

In the final part of the thesis, the extensive knowledge gained was applied to rocket nozzle technology. Based on the second phase, it was decided that the optimal parameters for a rocket nozzle were 25 mm, pitch-based fibers with a powder resin. Using the knowledge from the first phase, a manufacturing procedure was designed. This resulted in a production and validation plan for a rocket nozzle prototype.

Of course, research is never finished and a number of new research avenues came up during this thesis. Regarding the first phase, recommendations are made to more thoroughly investigate the properties of phenolic resins, such as their many rheology characteristics and the calorimetry under applied pressure. These can then be correlated to manufacturing procedures to further understand the relationship between manufacturing quality and material properties. Also, investigation can be done into the thermal properties of cured samples, which can lead to a deeper understanding of pyrolysis and siliconization cycle design.

For the second phase, recommendations are made to research the influence of different material composition parameters, such as different matrix types or different fiber materials. Also the material composition parameters researched here can be further explored, especially in the area of fiber length, where also longer or shorter fibers can be considered. An especially interesting research field is the influence of the combination of different fiber lengths in a single sample.

Considering the third phase, more research is needed to determine the scalability of the process: can this same procedure be used for larger or thicker parts? Also, the material performance needs to be

determined more thoroughly. Recommendations are to perform microstructure tests, pressure tests, thermal tests and lastly full duration firing tests, as these best represents the applicable environment.

References

[1] Walter Krenkel. “Carbon fibre reinforced silicon carbide composites (C/SiC, C/C-SiC)”. In: *Handbook of ceramic composites* (2005), pp. 117–148.

[2] Bernhard Heidenreich. “Carbon fibre reinforced SiC materials based on melt infiltration”. In: 2007.

[3] Bernhard Heidenreich. “Manufacture and applications of C/C-SiC and C/SiC composites”. In: *Processing and Properties of Advanced Ceramics and Composites IV* 234 (2012), pp. 183–198.

[4] Qingmao Zhang and Guansheng Li. “A review of the application of C/SiC composite in thermal protection system”. In: *Multidiscipline Modeling in Materials and Structures* (2009).

[5] H Hald et al. “Development of a CMC nose cap system for X-38”. In: *Proceedings of the International Symposium on Atmospheric Reentry Vehicles and Systems, Arcachon, France*. 1999, pp. 16–18.

[6] Wolfgang Schäfer and Walter D Vogel. “Faserverstärkte Keramiken hergestellt durch Polymerinfiltration”. In: *Keramische verbundwerkstoffe* (2002), pp. 76–94.

[7] Francois Christin. “Design, fabrication, and application of thermostructural composites (TSC) like C/C, C/SiC, and SiC/SiC composites”. In: *Advanced engineering materials* 4.12 (2002), pp. 903–912.

[8] Eric P Bouillon et al. “Engine test experience and characterization of self sealing ceramic matrix composites for nozzle applications in gas turbine engines”. In: *Turbo Expo: Power for Land, Sea, and Air*. Vol. 36843. 2003, pp. 677–683.

[9] L Zawada, G Richardson, and P Spriet. “Ceramic matrix composites for aerospace turbine engine exhaust nozzles”. In: *Proceed. 5th Int. Conf. on High-Temperature Ceramic Matrix Composites, HTCMC*. Vol. 5. 2004, pp. 491–498.

[10] Kozo Nita, Yoji Okita, and Chiyuki Nakamata. “Experimental and numerical study on application of a CMC nozzle for high temperature gas turbine”. In: *Mechanical Properties and Performance of Engineering Ceramics and Composites VII* (2012), pp. 315–324.

[11] I. M. Low. “Advances in ceramic matrix composites: Introduction”. In: *Advances in Ceramic Matrix Composites: Second Edition* (Jan. 2018), pp. 1–7. DOI: 10.1016/B978-0-08-102166-8.00001-3.

[12] Walter Krenkel. “CMC materials for high performance brakes”. In: (1994).

[13] Mario Krupka and Andreas Kienzle. “Fiber reinforced ceramic composite for brake discs”. In: (2000).

[14] Sundar Vaidyaraman et al. “C/SiC material evaluation for aircraft brake applications”. In: *High temperature ceramic matrix composites* (2001), pp. 802–808.

[15] Ralph Renz and Walter Krenkel. “C/C-SiC composites for high performance emergency brake systems”. In: (2000).

[16] Ch Zuber and B. Heidenreich. “Development of a net shape manufacturing method for ventilated brake discs in single piece design”. In: *Materialwissenschaft und Werkstofftechnik* 37 (4 Apr. 2006), pp. 301–308. ISSN: 09335137. DOI: 10.1002/MAWE.200600996.

[17] W S Yang et al. “Fabrication of short carbon fibre reinforced SiC multilayer composites by tape casting”. In: *Ceramics International* 38 (2 2012), pp. 1011–1018. ISSN: 0272-8842.

[18] Daisy Julia Nestler et al. “An innovative production method for a C/C-SiC brake disc, suitable for a large-scale production”. In: Springer, 2015, pp. 605–627.

[19] Jonas Stiller et al. “New large-scale production method for C/C-SiC ceramics: Investigating the influence of chopped and nonwoven CF”. In: *Ceramics International* 45 (7 2019), pp. 9596–9603. ISSN: 0272-8842.

[20] Ralph Renz et al. “CMC Materials for Lightweight and low CTE Applications”. In: *High temperature ceramic matrix composites* (2001), pp. 839–845.

[21] D. Kopeliovich. “Advances in the manufacture of ceramic matrix composites using infiltration techniques”. In: *Advances in Ceramic Matrix Composites* (Jan. 2014), pp. 79–108. DOI: 10.1533/9780857098825.1.79.

[22] David P Stinton, Anthony J Caputo, and Richard A Lowden. “Synthesis of fiber-reinforced SiC composites by chemical vapor infiltration”. In: *American Ceramic Society Bulletin* 65.2 (1986), pp. 347–350.

[23] Martin Leuchs and August Mühlratzer. “CVI-Verfahren zur Herstellung faserverstärkter Keramik–Herstellung, Eigenschaften, Anwendungen”. In: *Keramische Verbundwerkstoffe* (2002), pp. 95–121.

[24] E Wong. “Solid rocket nozzle design summary”. In: *4th Propulsion Joint Specialist Conference*. 1968, p. 655.

[25] Stephan Schmidt et al. “Ceramic matrix composites: a challenge in space-propulsion technology applications”. In: *International Journal of Applied Ceramic Technology* 2.2 (2005), pp. 85–96.

[26] U. Papenburg et al. “Advanced ceramic matrix composites (CMC’s) for space propulsion systems”. In: *33rd Joint Propulsion Conference and Exhibit* (1997), pp. 1–9. DOI: 10.2514/6.1997-3391.

[27] Joseph R Davis. *Tensile testing*. ASM international, 2004.

[28] Stefan Flauder et al. “Size effect of carbon fiber-reinforced silicon carbide composites (C/C-SiC): Part 2-tensile testing with alignment device”. In: *Journal of the European Ceramic Society* 42 (4 2022), pp. 1227–1237. ISSN: 0955-2219.

[29] Davide Alfano et al. “Emissivity and catalycity measurements on SiC-coated carbon fibre reinforced silicon carbide composite”. In: *Journal of the European Ceramic Society* 29.10 (2009), pp. 2045–2051.

[30] Fuyuan Wang, Laifei Cheng, and Shuhua Liang. “Effects of pore on thermal diffusivity and thermal radiation properties of C/SiC composites at high temperatures”. In: *Applied Composite Materials* 26.5 (2019), pp. 1411–1422.

[31] Yufeng Zhang et al. “Effects of temperature on the spectral emissivity of C/SiC composites”. In: *Ceramics-Silikáty* 60.2 (2016), pp. 152–155.

[32] T Haug and K Rebstock. “Neue Werkstofftechnologien für Bremsen”. In: *FORTSCHRITT BERICHTE-VDI REIHE 12 VERKEHRSTECHNIK FAHRZEUGTECHNIK* (1999), pp. 40–52.

[33] Walter Krenkel, Bernhard Heidenreich, and Ralph Renz. “C/C-SiC composites for advanced friction systems”. In: *Advanced Engineering Materials* 4.7 (2002), pp. 427–436.

[34] Roger Naslain and Francis Langlais. “CVD-processing of ceramic-ceramic composite materials”. In: *Tailoring multiphase and composite ceramics*. Springer, 1986, pp. 145–164.

[35] Roland Weiss and Martin Henrich. “Short-Fiber Reinforced CMCS: Potentials and Problems”. In: *Mechanical Properties and Performance of Engineering Ceramics and Composites: Ceramic Engineering and Science Proceedings, Volume 26, Number 2* 26 (2005), pp. 351–359. DOI: 10.1002/9780470291221.ch42.

[36] Michael G Jenkins. “Wanted: CMC test standards, design codes, for next-generation nuclear power plants”. In: *American Ceramic Society Bulletin* 85.11 (2006), pp. 16–20.

[37] J. M. Hausherr, M. Eitel, and W. Krenkel. “Determination of material properties for short fibre reinforced C/C-SiC”. In: *MATEC Web of Conferences* 29 (Nov. 2015). ISSN: 2261236X. DOI: 10.1051/MATECCONF/20152900005.

[38] ASTM. “C1275-94: Standard Practice for Monotonic Tensile Strength Testing of Continuous Fibre-Reinforced Advanced Ceramics with Solid Rectangular Cross-Sections at ambient Temperatures”. In: (1994). ISSN: 2352-4928.

[39] J.P. Piccola Jr. and M.G. Jenkins. “Effect of test parameters on tensile mechanical behaviour of a continuous fibre ceramic composite (CFCC)”. In: vol. 16. 4. 1995, pp. 325–336. URL: https://www.scopus.com/inward/record.uri?eid=2-s2.0-0029338355&partnerID=40&md5=428d71ca0c3ec7754b6e86c145c401eb.

[40] J. Sankar, A.D. Kelkar, and J. Neogi. *Effect of sample test volume and geometry on the tensile mechanical behavior of SiC/SiC continuous fiber ceramic composites. Final report*. Oak Ridge Operations, Sept. 1998. DOI: 10.2172/663575.

[41] Michael G Jenkins and Edgar Lara-Curzio. “Standardized thermo-mechanical test methods for CFCCs(Continuous Fiber Ceramic matrix Composites)”. In: *Durability and damage tolerance* (1994), pp. 191–211.

[42] Sreeramesh Kalluri Anthony M Calomino. “An assessment of variability in the average tensile properties of a melt-infiltrated SiC/SiC composite”. In: vol. 280. John Wiley & Sons, 2009, p. 79. ISBN: 0470291583.

[43] Michael G. Jenkins and Larry P. Zawada. “Elastic modulus and proportional limit stress in ceramic matrix composites: Comparison of methods and results”. In: vol. 22. 3. 2001, pp. 503–512. URL: https://www.scopus.com/inward/record.uri?eid=2-s2.0-0035790018&partnerID=40&md5=a530f5fce6834ca759f1e16539424091.

[44] D Regener, M Henrich, and R Weiß. “Charakterisierung des Festigkeits□und Bruchverhaltens von kohlenstofffaserverstärktem Kohlenstoff (C/C) und siliziertem kohlenstofffaserverstärktem Kohlenstoff (C/C□SiC) unter Biegebeanspruchung”. In: *Materialwissenschaft und Werkstofftechnik: Entwicklung, Fertigung, Prüfung, Eigenschaften und Anwendungen technischer Werkstoffe* 33 (9 2002), pp. 524–533. ISSN: 0933-5137.

[45] Yuan Shi et al. “Influence of specimen geometry and surface quality on the bending strength of short fiber-reinforced C/SiC”. In: vol. 825-826. Trans Tech Publications Ltd, 2015, pp. 249–255. ISBN: 9783038355151. DOI: 10.4028/www.scientific.net/MSF.825-826.249.

[46] Yuan Shi, Kamen Tushtev, and Dietmar Koch. “Characterization of mechanical properties under shear load of a short-carbon-fiber-reinforced C/SiC ceramic”. In: *Journal of Ceramic Science and Technology* 6 (3 2015), pp. 183–190. ISSN: 2190-9385.

[47] M. Henrich, D. Regener, and R. Weiß. “Querschnittseinfluss beim Zugversuch von siliziertem kohlenstoffkurzfaserverstärktem Kohlenstoff (C/C-SiC)”. In: *Materialwissenschaft und Werkstofftechnik* 35 (1 Jan. 2004). 1,9, 13-16,19,20,21,22,23-28
, pp. 45–54. ISSN: 0933-5137. DOI: 10.1002/mawe.200300659.

[48] Tom Liensdorf, Nico Langhof, and Walter Krenkel. “Mechanical Properties of PEEK-Derived C/SiC Composites with Different Fiber Lengths”. In: *Advanced Engineering Materials* 21 (5 2019). DOI: 10.1002/adem.201800835. URL: https://doi.org/10.1002/adem.201800835..

[49] A Neubrand, B Thielicke, and A Kienzle. “Four Point Bending Tests of a C/SiC Material for Industrial Applications under Quasistactic and Cyclic Loading”. In: 2004, pp. 205–210.

[50] A Neubrand, B Thielicke, and E Hirsch. “Investigation of the notch sensitivity of short fibre reinforced C/SiC”. In: *Presented at the 5th International Conference on High-Temperature Ceramic Matrix Composites- HTCMC5*. 2004.

[51] A Neubrand et al. “Investigation of cutting-induced damage in CMC bend bars”. In: vol. 29. EDP Sciences, 2015, p. 00004.

[52] Jinguang Du et al. “A review on machining of carbon fiber reinforced ceramic matrix composites”. In: *Ceramics International* 45 (15 2019), pp. 18155–18166. ISSN: 0272-8842.

[53] Jan Marcel Hausherr et al. “Material characterisation of C/SiC: Comparison of computed-tomography and scanning electron microscopy”. In: 2006.

[54] Michael Krause et al. “Determination of the fibre orientation in composites using the structure tensor and local X-ray transform”. In: *Journal of Materials Science* 45 (4 2010), pp. 888–896. ISSN: 1573-4803.

[55] Michael Krause, Jan Marcel Hausherr, and Walter Krenkel. “Computing the fibre orientation from Radon data using local Radon transform”. In: *Inverse Problems & Imaging* 5 (4 2011), p. 879.

[56] J G Sun. “Thermal tomographic imaging for nondestructive evaluation of ceramic composite materials”. In: *Mechanical Properties and Performance of Engineering Ceramics and Composites V: Ceramic Engineering and Science Proceedings* 31 (2010), pp. 137–144.

[57] Yogesh P Singh et al. “Use of electrical resistance as a non-destructive evaluation tool in health monitoring and damage evaluation of ceramic matrix composites”. In: vol. 613. John Wiley & Sons, 2018, p. 89.

[58] Hui Mei and Laifei Cheng. “Damage analysis of 2D C/SiC composites subjected to thermal cycling in oxidizing environments by mechanical and electrical characterization”. In: *Materials Letters* 59 (26 2005), pp. 3246–3251. ISSN: 0167-577X.

[59] Craig E Smith, Gregory N Morscher, and Zhenhai Xia. “Electrical resistance as a nondestructive evaluation technique for SiC/SiC ceramic matrix composites under creep□rupture loading”. In: *International Journal of Applied Ceramic Technology* 8 (2 2011), pp. 298–307. ISSN: 1546-542X.

[60] Craig Smith and Andrew Gyekenyesi. “Detecting Cracks in Ceramic Matrix Composites by Electrical Resistance”. In: vol. 7983. SPIE, 2011, pp. 197–207.

[61] Gregory N Morscher, Christopher Baker, and Craig Smith. “Electrical resistance of SiC fiber reinforced SiC/Si matrix composites at room temperature during tensile testing”. In: *International Journal of Applied Ceramic Technology* 11 (2 2014), pp. 263–272. ISSN: 1546-542X.

[62] Jeongguk Kim and Peter K Liaw. “The nondestructive evaluation of advanced ceramics and ceramic-matrix composites”. In: *JOM* 50 (11 1998), pp. 1–15.

[63] M C Bhardwaj et al. “Contact□Free Ultrasound: The Final Frontier in Non□Destructive Materials Characterization”. In: Wiley Online Library, 2000, pp. 163–172.

[64] I Fischer, T Reimer, and H Weihs. “Design of a high temperature test device for bidirectional loading for CMC samples”. In: vol. 25. Wiley Online Library, 2004, pp. 275–281.

[65] Shu Qi Guo, Toshiyuki Nishimura, and Yutaka Kagawa. “Mechanical Properties of Short Carbon Fiber-Reinforced SiC-Matrix Composites and Correlation to Fibers”. In: vol. 512. Trans Tech Publ, 2012, pp. 798–803. ISBN: 3037854251.

[66] Shuqi Guo. “A Biaxial Flexural Test for Short Carbon Fiber□Reinforced SiC□Matrix Composites”. In: *High Temperature Ceramic Matrix Composites 8: Ceramic Transactions* 248 (2014), pp. 287–293.

[67] G Ojard et al. “Through thickness modulus (E33) of ceramic matrix composites: mechanical test method development”. In: *Mechanical Properties and Performance of Engineering Ceramics II: Ceramic Engineering and Science Proceedings* 27 (2006), pp. 331–338.

[68] Hanling Tang et al. “Effect of Short Carbon Fiber Content on the Mechanical Properties of Composite Csf/SiC”. In: *Journal - Chinese Ceramic Society* 35 (8 2007), p. 1057. DOI: 10.14062/j.issn.0454-5648.2007.08.023.

[69] L Li et al. “Mechanical properties and toughening mechanism of Csf/SiC ceramic composites”. In: *Information Science and Electronic Engineering* (2016), pp. 63–66.

[70] Federico De Bianchi et al. “Thermo-elastic properties in short fibre reinforced ultra-high temperature ceramic matrix composites: Characterisation and numerical assessment”. In: *Materials Today Communications* 29 (Dec. 2021), p. 102754. ISSN: 2352-4928. DOI: 10.1016/J.MTCOMM.2021.102754.

[71] Yusheng Ding et al. “Preparation of C/SiC composites by hot pressing, using different C fiber content as reinforcement”. In: *Journal of the American Ceramic Society* 89.4 (2006), pp. 1447–1449.

[72] Yutaro Arai et al. “Carbon fiber reinforced ultra-high temperature ceramic matrix composites: A review”. In: *Ceramics International* 45 (12 Aug. 2019), pp. 14481–14489. ISSN: 0272-8842. DOI: 10.1016/J.CERAMINT.2019.05.065.

[73] Wenqing Wang et al. “Additive manufacturing of Csf/SiC composites with high fiber content by direct ink writing and liquid silicon infiltration”. In: *Ceramics International* 48 (3 2022), pp. 3895–3903. ISSN: 0272-8842. DOI: https://doi.org/10.1016/j.ceramint.2021.10.176. URL: https://www.sciencedirect.com/science/article/pii/S0272884221033186.

[74] Walter Krenkel. “Microstructure Tailoring of C/C-Sic Composites”. In: *27th Annual Cocoa Beach Conference on Advanced Ceramics and Composites: B: Ceramic Engineering and Science Proceedings* (2003), pp. 471–476. DOI: https://doi.org/10.1002/9780470294826.ch68. URL: https://ceramics.onlinelibrary.wiley.com/doi/abs/10.1002/9780470294826.ch68.

[75] Thomas Reimer et al. “Fabrication and Characterization of C/C□SiC Material Made with Pitch□Based Carbon Fibers”. In: *Processing and Properties of Advanced Ceramics and Composites VII: Ceramic Transactions, Volume 252* (2015), pp. 277–293.

[76] Gerrit Hackl et al. “Reinforcing Effect of Carbon Short Fibers Coated with Pyrolytic Carbon in Ceramic Matrix Composites”. In: *Journal of composite materials* 41 (18 2007), pp. 2235–2243. DOI: 10.1177/0021998307075437.

[77] M E Westwood et al. “Oxidation protection for carbon fibre composites”. In: *Journal of Materials Science* 31 (6 1996), pp. 1389–1397. ISSN: 1573-4803. DOI: 10.1007/BF00357844. URL: https://doi.org/10.1007/BF00357844.

[78] M Labanti et al. “Evaluation of Damage by Oxidation Corrosion at High Temperatures of Coated C/C□SiC Ceramic Composite”. In: *High Temperature Ceramic Matrix Composites* (2001), pp. 218–223.

[79] W Krenkel et al. “Design, Manufacture and Quality Assurance of C/C-SiC Composites for Aeronautics and Space Transportation Systems”. In: LIDO-Berichtsjahr=2005, 2004. URL: https://elib.dlr.de/15142/.

[80] Wallace L Vaughn and Howard G Maahs. “Active-to-passive transition in the oxidation of silicon carbide and silicon nitride in air”. In: *Journal of the American Ceramic Society* 73.6 (1990), pp. 1540–1543.

[81] Bo Yan et al. “Effects of ablation at different regions in three-dimensional orthogonal C/SiC composites ablated by oxyacetylene torch at 1800° C”. In: *Journal of materials processing technology* 209.7 (2009), pp. 3438–3443.

[82] S. Mungiguerra et al. “Arc-jet wind tunnel characterization of ultra-high-temperature ceramic matrix composites”. In: *Corrosion Science* 149 (Apr. 2019), pp. 18–28. ISSN: 0010938X. DOI: 10.1016/j.corsci.2018.12.039.

[83] Yuan Shi et al. “Inspection of geometry influence and fiber orientation to characteristic value for short fiber reinforced ceramic matrix composite under bending load”. In: *Journal of the European Ceramic Society* 37 (4 2017), pp. 1291–1303. ISSN: 0955-2219.

[84] Husam Ahmad et al. “Influence of Initial Fibre Length and Content Used in The Injection Moulding of CFRP on the Properties of C/C and C/C-SiC Composites”. In: Trans Tech Publications Ltd, Aug. 2019, pp. 171–179. DOI: 10.4028/www.scientific.net/KEM.809.171. URL: www.scientific.net/KEM.809.171.

[85] Xiulan He et al. “Effect of sintering additives on microstructures and mechanical properties of short-carbon-fiber-reinforced SiC composites prepared by precursor pyrolysis–hot pressing”. In: *Ceramics international* 32 (8 2006), pp. 929–934. ISSN: 0272-8842.

[86] Rainer Gadow and Marcus Speicher. “Optimized morphological design for silicon infiltrated microporous carbon preforms”. In: Wiley Online Library, 2000, pp. 485–492.

[87] Jan Schulte-Fischedick et al. “The morphology of silicon carbide in C/C–SiC composites”. In: *Materials Science and Engineering: A* 332 (1-2 2002), pp. 146–152. ISSN: 0921-5093.

[88] Friedrich Raether, Jürgen Meinhardt, and Andreas Kienzle. “Oxidation behaviour of carbon short fibre reinforced C/SiC composites”. In: *Journal of the European Ceramic Society* 27 (2-3 2007), pp. 1217–1221. ISSN: 0955-2219.

[89] AW Adamson and AP Gast. “Physical chemistry of surfaces, John willey and sons Inc”. In: *New York* (1990).

[90] Giovanni Bianchi et al. “Influence of pyrolysis and Silicon infiltration on the properties of CMC parts shaped by composite flow molding”. In: *International Journal of Applied Ceramic Technology* 19 (1 2022), pp. 45–53. ISSN: 1546-542X.

[91] N Nier et al. “Influence of the Annealing Process Parameters in the Production of New Short-Fibre-Reinforced C/C-SIC Composites”. In: *Advances in High Temperature Ceramic Matrix Composites and Materials for Sustainable Development; Ceramic Transactions, Volume CCLXIII* 263 (2017), pp. 85–96.

[92] Erich Fitzer. “The future of carbon-carbon composites”. In: *Carbon* 25.2 (1987), pp. 163–190.

[93] Franck Lamouroux, Gerald Camus, and Jacques Thebault. “Kinetics and mechanisms of oxidation of 2D woven C/SiC composites: I, experimental approach”. In: *Journal of the American ceramic society* 77 (8 1994), pp. 2049–2057. ISSN: 0002-7820.

[94] Tang Hanling et al. “Research of Oxidation Resistance of Short Carbon Fiber Reinforced SiC Composite by Hot-pressing”. In: *Journal of Inorganic Materials* 24.2 (2009), pp. 305–309.

[95] Michael J Verrilli and Anthony Calomino. “Temperature Dependence on the Strength and Stress Rupture Behavior of a Carbon-Fiber Reinforced Silicon Carbide Matrix (C/SiC) Composite”. In: *27th Annual Cocoa Beach Conference on Advanced Ceramics and Composites: B: Ceramic Engineering and Science Proceedings*. John Wiley & Sons, Inc. Hoboken, NJ, USA. 2003, pp. 443–449.

[96] Ludovic Filipuzzi et al. “Oxidation mechanisms and kinetics of 1D□SiC/C/SiC composite materials: I, An experimental approach”. In: *Journal of the American Ceramic Society* 77 (2 1994), pp. 459–466. ISSN: 0002-7820.

[97] Bi□feng Zhang et al. “The Effects Originated from Low Earth Orbit Thermal Cycling and Atomic Oxygen on C/SiC Composites”. In: *Ceramic Transactions* 248 (June 2014), pp. 327–333. ISSN: 9781118932988. DOI: 10.1002/9781118932995.ch35.

[98] Lei Liu et al. “Effects of SiC addition on the ablation properties of C/C composites in different heat fluxes under oxyacetylene torch”. In: *Vacuum* 90 (2013), pp. 97–99.

[99] Yuan Shi et al. “Oxidation kinetics and its impact on the strength of carbon short fiber reinforced C/SiC ceramics”. In: *Advanced Engineering Materials* 15 (1□2 2013), pp. 19–26. ISSN: 1438-1656.

[100] Rüdiger Brandt, Martin Frieß, and Günther Neuer. “Thermal conductivity, specific heat capacity, and emissivity of ceramic matrix composites at high temperatures”. In: *High Temperatures - High Pressures* 35-36 (2 2003), pp. 169–177. ISSN: 00181544. DOI: 10.1068/htjr105.

[101] Fiona Kessel et al. “Wet-laid nonwoven based ceramic matrix composites: An innovative and highly adaptable short fiber reinforcement for ceramic hybrid and gradient materials”. In: *Journal of the European Ceramic Society* 41 (7 July 2021), pp. 4048–4057. ISSN: 0955-2219. DOI: 10.1016/J.JEURCERAMSOC.2021.02.040.

[102] Liyang Cao et al. “Thermal conductivity and bending strength of SiC composites reinforced by pitch-based carbon fibers”. In: *Journal of Advanced Ceramics* 11 (2 2022), pp. 247–262. ISSN: 2227-8508. DOI: 10.1007/s40145-021-0527-5. URL: https://doi.org/10.1007/s40145-021-0527-5.

[103] Daisy Nestler et al. “Development and characterisation of phenolic resin moulding materials for the production of new short fibre-reinforced C/C-SiC composites”. In: vol. 825. Trans Tech Publ, 2015, pp. 215–223. ISBN: 3038355151.

[104] G Ojard et al. “Durability Results from Ceramic Matrix Composite with Differing Porosity Levels”. In: *Mechanical Properties and Performance of Engineering Ceramics and Composites IX* (2014), pp. 27–36.

[105] Natalia Nier et al. “Evaluation of the moulding process for production of short-fibre-reinforced C/C-SiC composites”. In: *Journal of the European Ceramic Society* 40 (4 2020), pp. 1057–1066. ISSN: 0955-2219.

[106] Mrityunjay Singh and Stanley R Levine. “Low cost fabrication of silicon carbide based ceramics and fiber reinforced composites”. In: (1995).

[107] Fabian Breede et al. “Design and testing of a C/C-SiC nozzle extension manufactured via filament winding technique and liquid silicon infiltration”. In: *Design, Development, and Applications of Structural Ceramics, Composites, and Nanomaterials: Ceramic Transactions, Volume 244* (2014). ISSN: 1118770943.

[108] Li Zhuan et al. “Manufacture and properties of carbon fibre-reinforced C/SiC dual matrix composites”. In: *New carbon materials* 25.3 (2010), pp. 225–231.

[109] R Inoue et al. “Mode I fracture toughness of short carbon fiber-dispersed SiC matrix composite fabricated by melt infiltration process”. In: *Ceramics International* 39 (7 2013), pp. 8341–8346. ISSN: 0272-8842.

[110] Benedicta D Arhatari et al. “Local structural damage evaluation of a C/C–SiC ceramic matrix composite”. In: *Microscopy and Microanalysis* 23 (3 2017), pp. 518–526. ISSN: 1431-9276.

[111] R. Inoue et al. “Mixed-mode fracture criterion of short carbon fiber-dispersed SiC matrix composite”. In: *Journal of Ceramic Science and Technology* 8 (2 June 2017), pp. 223–232. ISSN: 2190-9385. DOI: 10.4416/JCST2016-00108. URL: https://tus.elsevierpure.com/en/publications/mixed-mode-fracture-criterion-of-short-carbon-fiber-dispersed-sic.

[112] Anthony G Evans and Frederick A Leckie. *The Processing and Mechanical Properties of High Temperature/High Performance Composites. Fatigue and Creep. Book 3*. 1994.

[113] S Zhu et al. “Monotonic tension, fatigue and creep behavior of SiC-fiber-reinforced SiC-matrix composites: a review”. In: *Composites Science and Technology* 59 (6 1999), pp. 833–851. ISSN: 0266-3538.

[114] A G Evans, F W Zok, and R M McMeeking. “Fatigue of ceramic matrix composites”. In: *Acta Metallurgica et Materialia* 43 (3 1995), pp. 859–875. ISSN: 0956-7151.

[115] Edgar Lara-Curzio et al. “The High Temperature Tensile Fatigue Behavior of a Polymer-Derived Ceramic Matrix Composite”. In: *Proceedings of the 19th Annual Conference on Composites, Advanced Ceramics, Materials, and Structures—A: Ceramic Engineering and Science Proceedings*. Wiley Online Library. 1995, pp. 341–349.

[116] S. Schmidt et al. “Advanced ceramic matrix composite materials for current and future propulsion technology applications”. In: *Acta Astronautica* 55 (3-9 Aug. 2004), pp. 409–420. ISSN: 0094-5765. DOI: 10.1016/J.ACTAASTRO.2004.05.052.

[117] Sufang Tang et al. “Ablation behaviors of ultra-high temperature ceramic composites”. In: *Materials Science and Engineering: A* 465.1-2 (2007), pp. 1–7.

[118] A Paul et al. “UHTC–carbon fibre composites: preparation, oxyacetylene torch testing and characterisation”. In: *Journal of the European Ceramic Society* 33.2 (2013), pp. 423–432.

[119] Xiang Zhang et al. “Morphology and microstructure of ZrB2–SiC ceramics after ablation at 3000 oC by oxy-acetylene torch”. In: *Ceramics International* 42.2 (2016), pp. 2798–2805.

[120] Fengjuan Zuo et al. “Ablative property of laminated ZrB2–SiC ceramics under oxyacetylene torch”. In: *Ceramics International* 39.4 (2013), pp. 4627–4631.

[121] D Sciti et al. “Design, fabrication and high velocity oxy-fuel torch tests of a C f-ZrB 2-fiber nozzle to evaluate its potential in rocket motors”. In: *Materials & Design* 109 (2016). ISSN: 0264-1275. DOI: 10.1016/j.matdes.2016.07.090. URL: http://dx.doi.org/10.1016/j.matdes.2016.07.090.

[122] R H Carter and J J Swab. “Internal pressure testing of structural ceramic tubes”. In: vol. 25. John Wiley & Sons, Inc. Hoboken, NJ, USA, 2004, pp. 295–300.

[123] David N Brewer, Michael Verrilli, and Anthony Calomino. “Ceramic matrix composite vane subelement burst testing”. In: vol. 42371. 2006, pp. 279–284. ISBN: 0791842371.

A

Appendix A - Code

A.1. Thermocouple data calibration code

```
#Imported packages
import pygame as pg
import cv2
import numpy as np



#Test image is imported
name='Test6.jpg'
img=cv2.imread(name)
size=img.shape[:2]

#Program is stared, image is loaded, text is defined, screen is loaded
pg.init()
image=pg.image.load(name)
txt=pg.font.SysFont('arialblack',40)
black=(0,0,0)
screen=pg.display.set_mode((4*size[1],4*size[0]))
image=pg.transform.scale2x(image)
#image=pg.transform.scale2x(image)
image_rect=image.get_rect()
image_rect.topleft=(0,0)


running = True

#Steps of all places to be clicked are defined
sequence=['Click on top left of the fourth digit of the top row',
          'Click on top left of the third digit of the top row',
          'Click on top left of the second digit of the top row',
          'Click on top right segment of the first digit of the top row',
          'Choose which digit number to use as reference',
          'Click on top segment of the chosen digit of the top row',
          'Click on top left segment of the chosen digit of the top row',
          'Click on top right segment of the chosen digit of the top row',
          'Click on middle segment of the chosen digit of the top row',
          'Click on bottom left segment of the chosen digit of the top row',
          'Click on bottom right segment of the chosen digit of the top row',
          'Click on bottom segment of the chosen digit of the top row',
          'Click on top left of the fourth digit of the bottom row',
          'Click on top left of the third digit of the bottom row',
          'Click on top left of the second digit of the bottom row',
          'Click on top right segment of the first digit of the top row',
          'Choose which digit number to use as reference',
          'Click on top segment of the chosen digit of the bottom row',
          'Click on top left segment of the chosen digit of the bottom row',
          'Click on top right segment of the chosen digit of the bottom row',
          'Click on middle segment of the chosen digit of the bottom row',
```

```
          'Click on bottom left segment of the chosen digit of the bottom row',
          'Click on bottom right segment of the chosen digit of the bottom row',
          'Click on bottom segment of the chosen digit of the bottom row',
          'done']

i=0
pos=np.zeros((25,2))
#Loop to run program, all places clicked are stored
while running:
    pg.event.pump()
    keys = pg.key.get_pressed()
    if keys[pg.K_ESCAPE]:
        running = False
    mouse = pg.mouse.get_pressed()
    if mouse[0]==1 and i!=4 and i!=16:
        pos[i,:]=pg.mouse.get_pos()
        pg.time.delay(100)
        i+=1
    if (i==4 or i==16) and (keys[pg.K_1] or keys[pg.K_2] or keys[pg.K_3] or keys[pg.K_4]):
        if keys[pg.K_1]:
            if i==4:
                key1=0
            if i==16:
                key2=0
        if keys[pg.K_2]:
            if i==4:
                key1=1
            if i==16:
                key2=1
        if keys[pg.K_3]:
            if i==4:
                key1=2
            if i==16:
                key2=2
        if keys[pg.K_4]:
            if i==4:
                key1=3
            if i==16:
                key2=3
        i+=1
    screen.blit(image,image_rect)
    txtsurf=txt.render(sequence[i],True,black)
    screen.blit(txtsurf,(image_rect[2]/2,20))
    pg.display.flip()
    if i>23:
        running = False
pg.quit()

#Calculating and saving all the results
pos=(pos/2).astype(int)
chosendigt1=3-key1
chosendigt2=3-key2
segmentlist1=pos[5:12,:]-pos[chosendigt1,:]
segmentlist2=pos[17:24,:]-pos[chosendigt2+12,:]
segments1=[]
segments2=[]
for k in range(7):
    segments1.append(tuple(segmentlist1[k,:]))
    segments2.append(tuple(segmentlist2[k,:]))

segment_pos1=np.zeros((4,2))
segment_pos2=np.zeros((4,2))
segment_pos1[0,:]=pos[3,:]-segmentlist1[2,:]
segment_pos2[0,:]=pos[15,:]-segmentlist2[2,:]
segment_pos1[1,:]=pos[2,:]
segment_pos1[2,:]=pos[1,:]
segment_pos1[3,:]=pos[0,:]
segment_pos2[1,:]=pos[14,:]
segment_pos2[2,:]=pos[13,:]
segment_pos2[3,:]=pos[12,:]

```

```
segment_pos1=segment_pos1.astype(int)
segment_pos2=segment_pos2.astype(int)
```

A.2. Thermocouple data processing code

```
#Importing all used packages
import cv2
from PIL import Image
import glob
import numpy as np
import cyclet, cycletemp, cyclets, cycletemps
from matplotlib import pyplot as plt
#Part of this code is based on and taken form https://pyimagesearch.com/2017/02/13/
    recognizing-digits-with-opencv-and-python/

#Defining the segment locations
"""
 7 segments indexes are:
 0: top,
 1: top left,
 2: top right,
 3: middle,
 4: bottom left
 5: bottom right
 6: bottom
"""
#Turning the segments into numbers
segments = {
    (1, 1, 1, 0, 1, 1, 1): 0,
    (0, 0, 1, 0, 0, 1, 0): 1,
    (1, 0, 1, 1, 1, 0, 1): 2,
    (1, 0, 1, 1, 0, 1, 1): 3,
    (0, 1, 1, 1, 0, 1, 0): 4,
    (1, 1, 0, 1, 0, 1, 1): 5,
    (1, 1, 0, 1, 1, 1, 1): 6,
    (1, 0, 1, 0, 0, 1, 0): 7,
    (1, 1, 1, 1, 1, 1, 1): 8,
    (1, 1, 1, 1, 0, 1, 1): 9,
    (0, 0, 0, 0, 0, 0, 0): 0
}

#Importing all pictures
names=glob.glob('Sample2/*.jpg')

#Taking the test length from the images and converting it into seconds
start=names[0][-16:-7]
end=names[-1][-16:-7]
length=len(names)
start=3600*int(start[0:2])+60*int(start[3:5])+int(start[6:8])
end=3600*int(end[0:2])+60*int(end[3:5])+int(end[6:8])
s=3600*24-(start-end)
t=np.linspace(0,s,length)

#Defining black and white color
white=(255,255,255)
black=(0,0,0)

#Definition for finding clostest value in a list
def closest(lst, K):

     lst = np.asarray(lst)
     idx = (np.abs(lst - K)).argmin()
     return lst[idx]

#Definition for transforming one image type into another
def cv2_2_pil(cv2img, transform=cv2.COLOR_BGR2RGB):
    return Image.fromarray(cv2.cvtColor(cv2img, transform))

#Definition for getting the a number from an image, based on which segments are identiefied
```

```
def get_digit1(img):
    segment_pos = segments1
    active = map(lambda x: int(np.count_nonzero(get_dig_sub(img, x[0], x[1], 4, 4)) > 8),
        segment_pos)
    #print(list(active))
    return segments.get(tuple(active), 'x')

#Definition for getting a number from an imag, based on which segments are identiefied
def get_digit2(img):
    segment_pos = segments2
    active = map(lambda x: int(np.count_nonzero(get_dig_sub(img, x[0], x[1], 4, 4)) > 8),
        segment_pos)
    #print(list(active))
    return segments.get(tuple(active), 'x')

#Definition for isolating one number from the entire image
def get_dig_sub(img, x, y, width=30, height=60):
    return img[y:y + height, x:x + width]

#Definition for turning an image into 4 numbers for the first row
def thermo_image_to_temp1(img,level):
    imgray = cv2.cvtColor(img, cv2.COLOR_BGR2GRAY)
    ret, imthresh = cv2.threshold(imgray, level, 255, cv2.THRESH_BINARY_INV)
    imthresh = cv2.dilate(imthresh, np.ones((2, 2), np.uint8), iterations=1)
    #cv2_2_pil(imthresh, cv2.COLOR_GRAY2RGB).show()
    dig1 = get_dig_sub(imthresh, segment_pos1[0,0]-2, segment_pos1[0,1])
    dig2 = get_dig_sub(imthresh, segment_pos1[1,0], segment_pos1[1,1])
    dig3 = get_dig_sub(imthresh, segment_pos1[2,0], segment_pos1[2,1])
    dig4 = get_dig_sub(imthresh, segment_pos1[3,0], segment_pos1[3,1])
    #dig1=cv2.rectangle(dig1,segments1[5],segments1[5],white,4)
    #cv2_2_pil(dig1, cv2.COLOR_GRAY2RGB).show()
    return "{}{}{}.{}".format(*map(get_digit1, [dig1, dig2, dig3, dig4]))

#Definition for turning an image into 4 numbers for the second row
def thermo_image_to_temp2(img,level):
    imgray = cv2.cvtColor(img, cv2.COLOR_BGR2GRAY)
    ret, imthresh = cv2.threshold(imgray, level, 255, cv2.THRESH_BINARY_INV)
    imthresh = cv2.dilate(imthresh, np.ones((2, 2), np.uint8), iterations=1)
    #cv2_2_pil(imthresh, cv2.COLOR_GRAY2RGB).show()
    dig1 = get_dig_sub(imthresh, segment_pos2[0,0]-5, segment_pos2[0,1])
    dig2 = get_dig_sub(imthresh, segment_pos2[1,0]-2, segment_pos2[1,1])
    dig3 = get_dig_sub(imthresh, segment_pos2[2,0], segment_pos2[2,1])
    dig4 = get_dig_sub(imthresh, segment_pos2[3,0], segment_pos2[3,1])
#     dig3=cv2.rectangle(dig3,segments2[0],segments2[0],black,4)
#     dig3=cv2.rectangle(dig3,segments2[1],segments2[1],white,4)
#     dig3=cv2.rectangle(dig3,segments2[2],segments2[2],black,4)
    #dig3=cv2.rectangle(dig3,segments2[3],segments2[3],black,4)
    #dig3=cv2.rectangle(dig3,segments2[4],segments2[4],black,4)
#     dig3=cv2.rectangle(dig3,segments2[5],segments2[5],white,4)
#     dig3=cv2.rectangle(dig3,segments2[6],segments2[6],black,4)
    #cv2_2_pil(dig3,cv2.COLOR_GRAY2RGB).show()
    return "{}{}{}.{}".format(*map(get_digit2, [dig1, dig2, dig3, dig4]))

#Lists for all digits, as well as light level settings
digs1=[]
digs2=[]
level1=85
level2=75

#Loop which goes trough all images and generates the numbers. Also prints progress
for i in range(len(names)):
    if i%189==0:
        print(str(i/length*100)+'%')
    if i==2161:
        level1=80
        level2=90
    digs1.append(thermo_image_to_temp1(cv2.imread(names[i]),level1))
    digs2.append(thermo_image_to_temp2(cv2.imread(names[i]),level2))
#     if i>=446 and i<=455:
#         print(digs[-1])
#         img=cv2.imread(names[i])
```

```
#         imgray = cv2.cvtColor(img, cv2.COLOR_BGR2GRAY)
#         ret, imthresh = cv2.threshold(imgray, 133, 255, cv2.THRESH_BINARY_INV)
#         imthresh = cv2.dilate(imthresh, np.ones((2, 2), np.uint8), iterations=1)
#         cv2_2_pil(imthresh, cv2.COLOR_GRAY2RGB).show()
#

#Lists for processed numbers
realdigs1=[]
time1=[]
realdigs2=[]
time2=[]

#Loop for going through all numbers to correct any errors
for i in range(len(names)):
    if 'x' not in digs1[i]:
        realdigs1.append(float(digs1[i]))
        time1.append(t[i])
    if digs1[i][-1]=='x':
        temp=digs1[i][:-2]
        digs1[i]=temp
        if 'x' not in temp:
            realdigs1.append(float(temp))
            time1.append(t[i])
    if digs2[i][0]=='8':
        digs2[i]='1'+digs2[i][1:]
    if 'x' not in digs2[i]:
        realdigs2.append(float(digs2[i]))
        time2.append(t[i])
    if digs2[i][-1]=='x':
        temp2=digs2[i][:-2]
        digs2[i]=temp2
        if 'x' not in temp2:
            realdigs2.append(float(temp2))
            time2.append(t[i])

#Plotting the results
time1=np.array(time1)
time2=np.array(time2)
plt.plot(time1/60,realdigs1,label='Measured temperature inside mould')
plt.plot(time2/60,realdigs2,label='Measured temperture outside mould')
print(len(realdigs1),len(realdigs2),len(names))
tcycle=cyclet
tempcycle=cycletemp
plt.plot(tcycle,tempcycle,label='Intended cycle')



tcycler=cyclets
tempcycler=cycletemps
plt.plot(tcycler,tempcycler,label='Set cycle')
plt.xlabel('Time (min)')
plt.ylabel('Temperature (degree C)')
plt.title('Moulding temperature trial')

plt.legend()
```

A.3. Voltcraft data processing code

```
#Packages are imported
import numpy as np
from matplotlib import pyplot as plt
import cyclet, cycletemp, cycleti, cycletempi

#Data from dataloggers is imported
Inside=np.genfromtxt('IH13_Inside.CSV',skip_header=12,delimiter=',')
Outside=np.genfromtxt('IH13_Outside.CSV',skip_header=12,delimiter=',')

#Test time is defined
time1=np.linspace(0,len(Inside)/360,len(Inside))
```

```
time2=np.linspace(0,len(Outside)/360,len(Outside))

#Limit is set to make sure only interesting and useful data is plotted
lim=3550

#Data is plotted
plt.plot(time1[:lim],Inside[:lim,2],label='Measured temperature inside mould',color='purple')
plt.plot(time2[:lim],Outside[:lim,2],label='Measured temperature outside mould',color='orange
    ')

#Time of mould being out of oven (for closing) is defined
topen1=3
topen2=23

#Based on this, oven cycle is plotted
tsegments=cyclet
tcycle=np.cumsum(tsegments)
tempcycle=cycletemp
plt.plot(tcycle,tempcycle,label='Set cycle',color='green')

#Also intended cycle is plotted
tsegmentts=cycleti
tcycler=np.cumsum(tsegmentts)
tempcycler=cycletempi
plt.plot(tcycler,tempcycler,label='Intended cycle',color= 'blue')

#Times when oven was open are indicated in graph
a=np.array([20,np.max(tempcycle)])
plt.fill_betweenx(a,tcycler[3],tcycler[4],facecolor='lightgray',label='Oven open for mould
    operations')
plt.fill_betweenx(a,tcycler[7],tcycler[8],facecolor='lightgray')

#Axis labels, title and legend
plt.xlabel('Time (h)')
plt.ylabel('Temperature (degree C)')
plt.title('Sample curing cycle')
plt.legend()
```

A.4. CTE workout code

```
import numpy as np
import glob
from matplotlib import pyplot as plt

def nearest(array, value):
    array = np.asarray(array)
    idx = (np.abs(array - value)).argmin()
    return array[idx]

def nearestidx(array, value):
    array = np.asarray(array)
    idx = (np.abs(array - value)).argmin()
    return idx

#Create file storage paths
DICbasic=glob.glob('./DIC_basic/150/*.csv')+glob.glob('./DIC_basic/700/*.csv')
DIC_dat=glob.glob('./DIC_strain/*.csv')
FLIR_dat=glob.glob('./FLIR/*.csv')

#Define common points
CPFLIR1=np.array([[15,29,44],
                  [15,37,19.58],
                  [15,43,35.68],
                  [9,19,52.1],
                  [9,28,0.89],
                  [9,38,40.72],
                  [10,6,11.40],
                  [10,12,11.78],
                  [10,18,41.04],
```

```
                [10,26,16.48],
                [10,54,55.18],
                [11,4,17.06],
                [10,42,43.9],
                [12,29,39.04],
                [12,38,56.76],
                [12,47,59.92],
                [12,57,32.46],
                [13,10,41.66],
                [13,22,41.62],
                [13,27,27.98],
                [13,31,38.72],
                [13,37,9.16],
                [13,41,57.54],
                [13,47,20],
                [13,54,22.64]])
CPDIC1=np.array
    ([37,30,28,20,23,16,24,26,22,22,20,15,37,41,80,68,86,68,67,53,47,90,94,90,107])
SPDIC1=np.array
    ([37,37,29,39,49,23,25,27,26,38,21,25,40,42,142,264,105,87,91,102,131,99,96,116,109])

#Define variations
DIC_title=np.array([['Variation 7'],
                    ['Variation 4 #1'],
                    ['Variation 5#1'],
                    ['Variation 3'],
                    ['Variation 5#2'],
                    ['Variation 6'],
                    ['Variation 1#2'],
                    ['Variation 4#2'],
                    ['Variation 2#1'],
                    ['Variation 2#2'],
                    ['Variation 8'],
                    ['Variation 1#1'],
                    ['Variation 4 #1'],
                    ['Variation 1#1'],
                    ['Variation 4 #1'],
                    ['Variation 8'],
                    ['Variation 7'],
                    ['Variation 5#1'],
                    ['Variation 2#2'],
                    ['Variation 2#1'],
                    ['Variation 4#2'],
                    ['Variation 1#2'],
                    ['Variation 6'],
                    ['Variation 5#2'],
                    ['Variation 3']
])
for i in range(25):
    #Import files
    DIC_basic1=np.genfromtxt(DICbasic[i],delimiter=',',skip_header=1)
    DIC_150_1=np.genfromtxt(DIC_dat[i],delimiter=',',skip_header=2)
    FLIR_150_1=np.genfromtxt(FLIR_dat[i],delimiter=',',skip_header=1)
    FLIR_150_1_t=np.genfromtxt(FLIR_dat[i],delimiter=',',skip_header=1,dtype=str)

    #Convert FLIR time
    FLIR_150_1_HMS=np.zeros((len(FLIR_150_1_t),3))
    FLIR_150_1_HMS[:,0]=[x[11:13] for x in FLIR_150_1_t[:,1]]
    FLIR_150_1_HMS[:,1]=[x[14:16] for x in FLIR_150_1_t[:,1]]
    FLIR_150_1_HMS[:,2]=[x[17:22] for x in FLIR_150_1_t[:,1]]
    FLIR_150_1_time=FLIR_150_1_HMS[:,0]*3600+FLIR_150_1_HMS[:,1]*60+FLIR_150_1_HMS[:,2]

    #Check length
    LenFLIR=FLIR_150_1[-1,2]
    LenDIC=DIC_basic1[-1,3]-DIC_basic1[0,3]

    #Define common point
    CPFLIR=CPFLIR1[i]
    CPDIC=CPDIC1[i]

    #Convert to reltime
```

```
    CPDIC=DIC_basic1[CPDIC,3]-DIC_basic1[0,3]
    CPFLIR=CPFLIR[0]*3600+CPFLIR[1]*60+CPFLIR[2]
    CPFLIR=nearest(FLIR_150_1_time,CPFLIR)-FLIR_150_1_time[0]

    #Match
    RTDiff=CPDIC-CPFLIR


    #Define start point using DIC
    SPDIC=SPDIC1[i]
    SPFLIRAT=DIC_basic1[SPDIC,3]-DIC_basic1[0,3]-RTDiff+FLIR_150_1_time[0]
    SPFLIRIDX=nearestidx(FLIR_150_1_time,SPFLIRAT)

    #Common shared indextime
    LenFdat=len(FLIR_150_1)-SPFLIRIDX
    FLIRIdxT=np.linspace(0,len(DIC_150_1)-1,LenFdat)

    ##Plot temp and strains vs time
    #fix,ax1=plt.subplots(1,1)
    #ax2=ax1.twinx()
    #ax1.plot(FLIRIdxT,FLIR_150_1[SPFLIRIDX:,3],label='temp')
    #ax2.plot(DIC_150_1[:,0],DIC_150_1[:,1],label='exx')
    #ax2.plot(DIC_150_1[:,0],DIC_150_1[:,2],label='eyy')

    #Plot temp vs strains
    #Figure out reducing ratio FLIR data

    RIND=np.round(np.linspace(SPFLIRIDX, len(FLIR_150_1)-1, num=len(DIC_150_1))).astype(int)
    FLIRdatR=FLIR_150_1[RIND,3]
    if True:
        if i==9:
            fix,ax1=plt.subplots(1,1)
            ax1.plot(FLIRdatR[:164],DIC_150_1[:164,2],label='Strain in x direction')
            ax1.plot(FLIRdatR[:164],DIC_150_1[:164,3],label='Strain in y direction')
            #Trendlines
            Exline=np.polyfit(FLIRdatR[:164],DIC_150_1[:164,2],1)
            Eyline=np.polyfit(FLIRdatR[:164],DIC_150_1[:164,3],1)
            Pltxl=np.poly1d(Exline)
            Pltyl=np.poly1d(Eyline)
            ax1.plot(FLIRdatR[:164],Pltxl(FLIRdatR[:164]))
            ax1.plot(FLIRdatR[:164],Pltyl(FLIRdatR[:164]))
            #ax1.set_title(DIC_dat[i][13:-4])
            ax1.set_title(DIC_title[i][0])
            ax1.set_xlabel('Temperature (degree C)')
            ax1.set_ylabel('Strain (-)')
            #print(DIC_dat[i][13:-4],'Ex=',np.round(Exline[0]*1E6,3),'Ey=',np.round(Eyline
                [0]*1E6,3))
            #print(Exline,Eyline)
            ax2=ax1.twinx()
            Pltxld=np.polyder(Pltxl)
            Pltyld=np.polyder(Pltyl)
            ax2.plot(FLIRdatR[:164],Pltxld(FLIRdatR[:164])*1E6,label='CTE in x direction',
                color='purple')
            ax2.plot(FLIRdatR[:164],Pltyld(FLIRdatR[:164])*1E6,label='CTE in y direction',
                color='black')
            ax2.set_ylim([0,10])
            ax2.set_ylabel('CTE (E-6/K)')
            print(np.round(Exline[0]*1E6,3),np.round(Eyline[0]*1E6,3))
            ax1.legend()
            ax2.legend()
        else:
            fix,ax1=plt.subplots(1,1)
            ax1.plot(FLIRdatR,DIC_150_1[:,2],label='Strain in x direction')
            ax1.plot(FLIRdatR,DIC_150_1[:,3],label='Strain in y direction')
            #Trendlines
            Exline=np.polyfit(FLIRdatR,DIC_150_1[:,2],1)
            Eyline=np.polyfit(FLIRdatR,DIC_150_1[:,3],1)
            Pltxl=np.poly1d(Exline)
            Pltyl=np.poly1d(Eyline)
            ax1.plot(FLIRdatR,Pltxl(FLIRdatR),label='Trendline strain in x direction')
            ax1.plot(FLIRdatR,Pltyl(FLIRdatR),label='Trendline strain in y direction')
```

```
            #ax1.set_title(DIC_dat[i][13:-4])
            ax1.set_title(DIC_title[i][0])
            ax1.set_xlabel('Temperature (degree C)')
            ax1.set_ylabel('Strain (-)')
            ax2=ax1.twinx()
            Pltxld=np.polyder(Pltxl)
            Pltyld=np.polyder(Pltyl)
            ax2.plot(FLIRdatR,Pltxld(FLIRdatR)*1E6,label='CTE in x direction',color='purple')
            ax2.plot(FLIRdatR,Pltyld(FLIRdatR)*1E6,label='CTE in y direction',color='black')
            ax2.set_ylim([0,10])
            ax2.set_ylabel('CTE (E-6/K)')
            #print(DIC_dat[i][13:-4],'Ex=',np.round(Exline[0]*1E6,3),'Ey=',np.round(Eyline
                [0]*1E6,3))
            #print(Exline,Eyline)
            print(np.round(Exline[0]*1E6,3),np.round(Eyline[0]*1E6,3))
            ax1.legend()
            ax2.legend()
```

A.5. Mechanical testing workout code

```
import numpy as np
from matplotlib import pyplot as plt
from matplotlib.pyplot import cm

LBD=np.genfromtxt('LBD.csv',delimiter=',',skip_header=1)
LBDnames=np.genfromtxt('LBD.csv',dtype=str,delimiter=',',skip_header=1)
filenames=LBDnames[:,0]
length=0
testlen=np.zeros((len(filenames)),dtype=int)


L=LBD[:,7]
B=LBD[:,10] #average
D=LBD[:,9] #average

for i in range(len(filenames)):
    a=np.genfromtxt(filenames[i]+'.csv',delimiter=',',skip_header=3)
    testlen[i]=np.shape(a)[0]
    length=max(testlen)

data=np.zeros((len(filenames),length,2))
for i in range(len(filenames)):
    testdat=np.genfromtxt(filenames[i]+'.csv',delimiter=',',skip_header=3)
    data[i,:testlen[i],:]=testdat

datshape=np.shape(data)
strdat=np.zeros(datshape)
for i in range(len(filenames)):
    strdat[i,:testlen[i],1]=data[i,:testlen[i],1]*3*L[i]/(2*B[i]*D[i]*D[i])
    strdat[i,:testlen[i],0]=6*data[i,:testlen[i],0]*D[i]/(L[i]*L[i])

maxindex=np.zeros((len(filenames)),dtype=int)
for i in range(len(filenames)):
    maxindex[i]=np.argmax(strdat[i,:,1])

Startstress=3
startindex=np.zeros((len(filenames)),dtype=int)
for i in range(len(filenames)):
    startindex[i]=np.argmin(np.absolute(strdat[i,:,1]-Startstress))

firststrain=0.0004
secondstrain=0.0007
Elist=np.zeros((len(filenames)))
maxlist=np.zeros((len(filenames)))
for i in range(len(filenames)):
    firstindex=np.argmin(np.absolute(strdat[i,:,0]-firststrain))
    secondindex=np.argmin(np.absolute(strdat[i,:,0]-secondstrain))
    m=(data[i,secondindex,1]-data[i,firstindex,1])/(data[i,secondindex,0]-data[i,firstindex
        ,0])
```

```
    print(m,firstindex,secondindex)
    Elist[i]=0.25*L[i]**3*m/(B[i]*D[i]**3)/1000
    maxlist[i]=strdat[i,maxindex[i],1]

#for i in range(len(filenames)):
#    plt.plot(strdat[i,:testlen[i],0],strdat[i,:testlen[i],1],label=filenames[i])
#
#for i in range(len(filenames)):
#    plt.plot(strdat[i,:maxindex[i],0],strdat[i,:maxindex[i],1],label=filenames[i])

#q=10
#p=9
#
#plt.scatter(LBD[3:14,q]*LBD[3:14,p],Elist[3:14],label='184') #184 some removed
#plt.scatter(LBD[20:28,q]*LBD[20:28,p],Elist[20:28],label='182') #182 some removed
#plt.scatter(LBD[49:60,q]*LBD[49:60,p],Elist[49:60],label='185') #185
#plt.scatter(LBD[63:71,q]*LBD[63:71,p],Elist[63:71],label='188') #188
##plt.scatter(LBD[40:49,q]*LBD[40:49,p],Elist[40:49],label='S24') #S24
##plt.scatter(LBD[28:40,q]*LBD[28:40,p],Elist[28:40],label='S23') #S23
#plt.xlabel('Sample average cross-section (mm^2)')
#plt.ylabel('Sample flexural modulus (GPa)')
#plt.title('Modulus versus cross-section, variation 5')
#plt.legend()

#whatplot=range(len(filenames)) #all
#whatplot=np.arange(3,14) #184 some removed
#whatplot=range(len(filenames[:28])) #184 and 182
#whatplot=np.arange(19,28) #182 some removed
#whatplot=np.arange(28,40) #S23
#whatplot=np.arange(40,49) #S24
whatplot=np.arange(28,49) #S23 and S24
#whatplot=np.arange(49,60) #185
#whatplot=np.arange(63,71) #188


color = cm.gist_ncar(np.linspace(0, 1, len(whatplot)+2))

f=0
for i in whatplot:
    plt.plot(strdat[i,startindex[i]:maxindex[i],0]-strdat[i,startindex[i],0],strdat[i,
        startindex[i]:maxindex[i],1],label=filenames[i],c=color[f])
    f+=1


plt.legend()

firststrain=0.0004
secondstrain=0.0007
Elist=np.zeros((len(filenames)))
maxlist=np.zeros((len(filenames)))
for i in range(len(filenames)):
    firstindex=np.argmin(np.absolute(strdat[i,:,0]-firststrain))
    secondindex=np.argmin(np.absolute(strdat[i,:,0]-secondstrain))
    m=(data[i,secondindex,1]-data[i,firstindex,1])/(data[i,secondindex,0]-data[i,firstindex
        ,0])
    print(m,firstindex,secondindex)
    Elist[i]=0.25*L[i]**3*m/(B[i]*D[i]**3)
    maxlist[i]=strdat[i,maxindex[i],1]
print(np.average(Elist))
```

B

Appendix B - Literature Study

B.1. Introduction

In the last ten years, interest in spaceflight has skyrocketed. The number of rocket launches per year has doubled, reusable rocket systems have been successfully developed and more and more commercial companies have started developing their own launch systems. Part of the reason why this is possible is the continual research into new materials and new applications. By increasing performance of materials and decreasing their cost, space is becoming more accessible every day. One of the most important and extreme parts of a rocket is the nozzle, here many disciplines such as chemistry, aerodynamics and structural mechanics come together. This is one of the most stressed parts of a rockets, with high pressures and often both very high and very low temperatures next to each other. Also in this area improvements have been and need to be made. A promising next step for rocket nozzles is the application of ceramic matrix composites, instead of the currently used super-alloys. Ceramic matrix composites are composite materials that combine the advantages of ceramics (high temperature resistance, high hardness) with composites materials (high strength, high stiffness, low density, good toughness). These materials have the potential to increase the performance of nozzles, by increasing temperatures, while decreasing weight and cooling requirements. However, to be successfully applied, these materials need to be well understood and the gap between research and industry needs to be bridged.

This report aims to summarize the research surrounding ceramic composite materials and their application in rocket nozzles. Specific focus shall be on C/C-SiC, as this is a very promising material for this application. To bridge the gap between research and industry, the manufacturing process has to be well understood. Therefor, the research question has been stated as: What is the effect of manufacturing parameters on the performance of a short carbon fiber C/C-SiC ceramic matrix composite rocket nozzle? To support the answering of this question, the following sub-questions are devised:

- What effect do testing parameters have on testing results and thus what testing procedures should be used?
- What material composition parameters are there and what is their effect?
- What processing parameters are there and what is their effect?
- What material properties are there, and which should be assessed?
- What parameters determine rocket nozzle performance?

The aim of the report will be to answer this question and its sub-questions in the most complete and clear way.

The report will be structured in accordance with the sub-questions. Each chapter will focus on one of the sub-questions, where the sections discuss different aspects. Before all of this a chapter with background information will be given to familiarize the reader with the topics discussed in the rest of the report. After this will be the chapter about the effect of testing parameters, followed by chapter

four about different material composition parameters. Chapter five talks about processing parameters, while chapter six discusses material properties. Chapter seven will go into more depth on the topic of rocket nozzle performance. The report is ended with a concluding chapter.

B.2. Background information

In this chapter some relevant background information will be given, to ensure the reader knows the necessary terminology to understand the rest of the document. In the first section, a short summary will be given of what ceramic matrix composites are, as well as their common properties and major uses. In the second section, the most common manufacturing routes will be explained. In the last section, a summary will be given of rocket nozzle design considerations.

B.2.1. Ceramic matrix composites

Ceramic matrix composite materials (CMCs), are a type of composite material in which the matrix phase consists of a ceramic material. This in contrast with the polymer material used in the more commonly known CFRP or GFRP materials. This material type aims to combine the desirable properties of both ceramics and CFRP materials. The desirable properties of the ceramic are its high scratch-resistance and its superior high temperature behavior. The fibers support in providing additional strength, as well as providing ductility in the otherwise too brittle ceramic material class. Also, this combination gives high specific properties due to the strength and stiffness of the carbon fiber and the relatively low density of the ceramic matrix. This often makes it an improvement over metal based alternatives.

As with other composite materials, the choice of fiber and matrix are very important and together determine the material characteristics. For the matrix, either oxide or non-oxide based matrices can be used. In the first category alumina oxide is a commonly used material, while for non-oxide CMCs, silicon carbide (SiC) is prevalent. Of course, many other options are possible, most notably the combination of elements such as zirconium, hafnium or boron. These increase the working temperature of the material even more and are therefor often described as ultra high temperature ceramic matrix composite materials (UHTCMCs).

As is the case for polymer based composites, also in ceramic matrix composites carbon fiber is the most commonly used reinforcement. It can be used in multiple forms, with a notable distinction to be made between continuous fibers, often in the form of fabric materials or filament winding, and short fibers. Here the first category provides more strength and stiffness, however can be harder to use and is more expensive, compared to short fibers. Apart from carbon fibers, other fibers are also used, such as SiC fibers. These are most commonly applied in high temperature, oxidizing settings, as they do not have the risk of deterioration in air which carbon fiber does have. However, this performance benefit comes with a large increase in material cost.

The unique properties make that the material can be and has been applied in a number of different fields. Some examples are the following, as described by Krenkel [1] and Heidenrich [2][3].

- Spacecraft thermal protection systems: Shielding a re-entry vehicle with the necessary protection from the high thermal and mechanical load environment. In this application CMCs excel, especially on the highest stress locations such as nose cones and leading edges[4]. Here not many other alternatives exist. An example of this is the experimental NASA X-38 plane, where the nose cap and body flaps were made from CMC material [5].
- Rocket and jet engine components: Again the high temperature resistance ability of the CMC is applied here. Examples of applications are vanes in rocket exhaust which act as thrust vector control or nozzle and nozzle extensions, for example the one used on the Ariane 5 rocket [6]. Also, jet engine components and gas turbine applications have been developed [7][8] [9] [10]. A specific example of this is the LEAP engine, which is used in aircraft such as the Airbus A320neo and Boeing737 Max. Here CMC components eliminated the need for cooling and thus increased the efficiency of the engine [11].
- Friction systems: This is the first application in which serial production has been seen for CMC components. Good tribological properties and the ability to maintain these under high temperatures, have lead to the development of CMC brake disks [32] [33] , which have since been

applied in high performance sports cars[12], racing cars[13] and aircraft[14], as well as emergency brakes[15] for elevators, cranes and trains. In this application, the use of short fibers was crucial, due to their lower cost. Using short fibers, complex components such as ventilated brake discs, were made in near-net shape, cost efficient way [16]. Next to this, the processes used to create short fiber based parts are easier to automate, which gave the possibility for cheap and easy series production. Several ways of doing this have been proven to work, such as tape laying [17] and injection moulding [18][19].

- High precision structures: Another important property of CMCs is a very low coefficient of thermal expansion. This combined with their high stiffness and low weight, makes them ideal for high precision structures. Applications in the past have been calibration plates [20] and telescope tubes, such as the one used on the TerraSAR-X. CMCs offer major advantages over other low CTE materials, such as lower density, less susceptibility to environmental conditions and absence of hysteresis and low heat capacity.
- Refractory industry: Here also the high temperature characteristics and high durability are the key to successful application. In the refractory industry high production numbers are achieved and moving parts such as slide gates have to be replaced often. CMCs have the potential to replace these parts and greatly increase their lifespan.

B.2.2. Manufacturing routes

Multiple manufacturing routes exist for the creation of CMC materials, with three of them being used on an industrial scale. In this section the routes will be discussed for the C/C-SiC material, though routes are similar for other CMC types. The three main routes are chemical vapour infiltration (CVI), polymer infiltration and pyrolysis (PIP) and liquid silicon infiltration (LSI). These will be discussed in the following subsections. It should be noted that the manufacturing technique has major influence on the properties of the final part, as different routes lead to different microstructures in the final product. To illustrate this point, material properties achieved using different methods can be found in Table B.1, as taken from Heidenrich [2]. The explanations in the following sections will be based on the work of Krenkel[1], Heidenrich [3] and Kopeliovich [21], who all give good and detailed overviews of the different manufacturing routes.

Table B.1: "Typical material properties of C/SiC and C/C-SiC materials in dependence of the manufacturing method.", taken from Heidenrich [2]

Manufacturing route		CVI	CVI	LPI	LSI	LSI	LSI
Material		C/SiC	C/SiC	C/SiC	C/C-SiC	C/C-SiC	C/SiC
Manufacturer		SPS (SNECMA)	MT Aerospace	EADS	DLR	SKT	SGL (9)
Density	g/cm^3	2.1	2.1-2.2	1.8	1.9-2.0	>1.8	2/2.4
Porosity	%	10	10-15	10	2-5	-	2/<1
Tensile strength	MPa	350	300-320	250	80-190	-	110/20-30
Strain to failure	%	0.9	0.6-0.9	0.5	0.15-0.35	0.23-0.3	0.3
Young's Modulus	GPa	90-100	90-100	65	50-70	-	65/20-30
Compression strength	MPa	580-700	450-550	590	210-320	-	470/250
Flexural strength	MPa	500-700	450-550	500	160-300	130-240	190/50
Inter-laminar shear strength	MPa	35	45-48	10	28-33	14-20	-
Fiber content	Vol. %	45	42-47	46	55-65	-	-
Coefficient of thermal expansion ||	E-6/K	3(1)	3	1.16(4)	-1-2.5(2)	0.8-1.5(4)	-0.3/1.8(5)
Coefficient of thermal expansion □	E-6/K	5(1)	5	4.06(4)	2.5-7(2)	5.5-6.5(4)	-0.03-1.36(6) /3(7)
Thermal conductivity ||	W/mK	14.3-20.6(1)	14	11.3-12.6(2)	17.0-22.6(3)	12-22	23-12(8) /40-20(8)
Thermal conductivity □	W/mK	6.5-5.9(1)	7	5.3-5.5(2)	7.5-10.3(3)	28-35	-
Specific heat	J/kgK	620-1400	-	900-1600(2)	690-1550	-	-

Chemical Vapour Infiltration

In CVI the composite is created by depositing the matrix on a carbon preform using a gaseous carrier. This technique usually consists of the following steps. First a dry carbon fiber preform is created, for example by densifying fibers in a mould, or by using winding or braiding methods. This creates a porous carbon preform. After this, the interphase between the fibers and the matrix is created. The interphase is important, as it dictates many of the toughness and fracture behavior properties of the material. Using chemical vapour deposition, a thin layer of (pyrolytic) carbon is deposited to act as an interphase. After this, the preform is put in the infiltration chamber, heated up and a gas carrying the SiC matrix is introduced. Most commonly, methyltrichlorsilane (MTS) is used, which can be reacted with hydrogen gas to form solid SiC. Since in this process only carbon fiber and a minimal amount of interphase is present, this material is referred to as C/SiC, with C pointing to the reinforcement and SiC to the matrix.

Two types of CVI can be identified. Firstly isothermal CVI [34], in which the entire chamber is a uniform temperature, around 800-900 °C. A pressure of 50-100 hPa is used and deposition happens through diffusion alone. This results in very good properties and there are no restrictions on part shape. However, part thickness is limited to around 3 mm, as by then pores start to close and further infiltration is halted. To continue infiltration, pores have to be mechanically opened and then the infiltration step can be repeated. The main disadvantage of this type of CVI is the long duration: as only diffusion is present as mechanism, time to infiltration of thick parts can take weeks or months.

The second type of CVI [22][23] prevents this problem by speeding up infiltration through the use of a pressure or temperature gradient, commonly applied by heating one end of the part to a higher temperature than the other end, usually in the range of 1000-1100 °C. This way, process time can be reduced to less than a week. However, the need to create this gradient over the part does limit the complexity of the parts that can be used and therefor it is mostly used on simple shapes like tubes.

Some advantages and disadvantages of the CVI process can be listed. The advantages being high quality and purity matrix material, as well as very good mechanical, thermal and oxidation properties. Next to this the interphase and matrix material can be controlled very well. The disadvantages however are the long process time with high associated costs. Also due to the slow nature of infiltration and the closing of the surface pores, full densification is almost never achieved and thus resulting porosity is often high, around 10-15%.

Polymer Infiltration and Pyrolysis

Polymer infiltration and pyrolysis, also called liquid polymer infiltration (LPI), is a manufacturing technique in which ceramic polymers are used as precursors, which are later converted to a ceramic matrix by pyrolysis. This process is usually done using the following steps. First both fibers and resin are prepared. Similarly to what was described above, the fibers are first coated to ensure a good interphase. The used resin is often a preceramic precursor, like polycarbosilane or polysilane polymers. To increase ceramic yield, SiC particles can be added to the polymer to form a slurry. After this the fibers and resin are combined, after which prepreging or wet filament winding is performed to create the final preform. This is then cured in an autoclave. Afterwards a pyrolysis step is done, in which the precursors is converted to a ceramic matrix. This is done at temperatures between 1100 °C and 1600 °C, where higher temperatures lead to a less porous matrix. Still, due to the release of organic volatiles and the shrinking of the part, the resulting porosity is large. To reduce the porosity the part is re-infiltrated with the polymer and the pyrolysis is repeated. This is done 4-10 times to attain a high density and desired porosity of below 10%. This can take multiple weeks up to several months.

The advantages of this route are good control over the matrix material, relatively low temperatures, meaning no damage to the fibers and near-net shape manufacturing leading to the possibility of large and complex parts. The disadvantages are mainly the expensive materials used, as well as the very long (and thus expensive) process, caused by the need for multiple re-infiltration cycles. Also the resulting porosity is still high for the final part, reducing the mechanical properties.

Liquid Silicon Infiltration

Liquid silicon infiltration is a form of reactive melt infiltration, where the ceramic matrix is formed by the chemical reaction between liquid silicon and a carbon/carbon preform. This manufacturing route often uses the following steps. First a CFRP preform is created, which can be done using most of the currently commercially available techniques, like warm pressing, filament winding or resin transfer moulding. The fibers used can be pretreated using CVI or PIP, however this is not always necessary. The resin used is required to have a high carbon yield and often phenolic resins are used. The second step is the pyrolysis of this preform. Here the resin matrix is partially vaporized and partial converted to carbon. The thermal expansion mismatch between the fiber and the matrix causes microcracking of the part. Both of these processes result in a porous and microcracked C/C part. Here the reinforcement used and shape of the part determine the process parameters. For highly anisotropic, woven reinforcements, the non-uniform shrinkage can lead to delaminations and faults and thus slow heating rates are required, especially for thick parts. For randomly orientated short fibers, fast heating rates can be used. The resulting time for pyrolysis is thus between one to two days to one to two weeks. In the last step this part is infiltrated using liquid silicon, meaning at temperatures above 1414 °C. The infiltration happens due to capillary forces, often aided by vacuum. During the infiltration, the liquid silicon will react with the carbon to form the SiC matrix of the CMC. As the pores are closed the infiltration stops and some amount of unreacted carbon as well as residue silicon will remain in the part. The fact that both carbon fibers and unreacted carbon are present lead to the term C/C-SiC. Due to the presence of unreacted silicon, the more correct terminology would be C/C-SiSiC, however this is not commonly used. The full siliconization step is often done in one or two days.

The advantage of this technique are the following. Firstly less steps and less expensive materials are needed, making this cheaper than other available methods. This effect is compounded by the greatly reduced processing times. With the infiltration process low porosity can be achieved, often below 4%. Next to this there is no real limit to part size and shape, which can be made in near net size. An additional advantage is the ability to create complex shapes by joining them after pyrolysis. This is

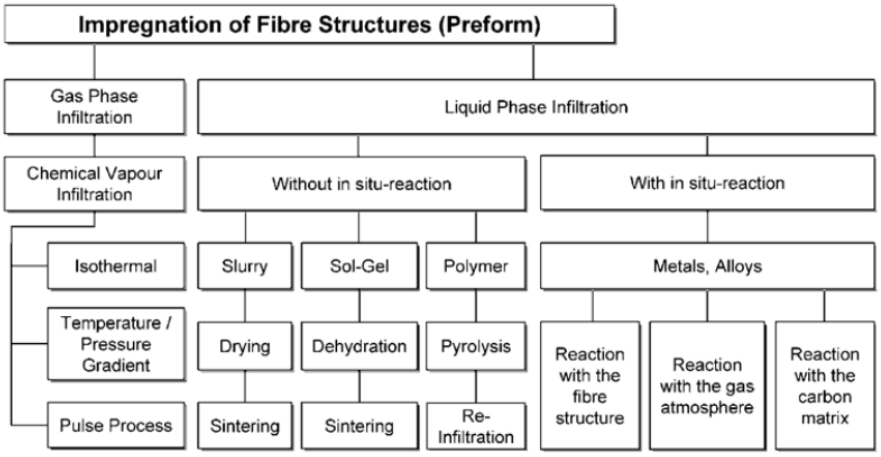

Figure B.1: "General overview of the manufacturing processes for CMC materials", taken from Krenkel [1]

done by taking to pyrolyzed parts, joining them with a carbonaceous paste or felt and then siliconizing them together, leading to a strongly bonded part. The disadvantage is the lower control over the resulting micro-structure. If done incorrectly, the silicon can react with carbon fibers, greatly reducing the materials strength. Also, due to the nature of the micro-structure, with unreacted carbon and silicon, the mechanical properties are most of the time inferior to those of parts made by other methods.

Other techniques

The above described methods are the most commonly used ones and also the only ones that have been used on a industrial scale. However, of course also other alternatives exist. These will now be shortly summarized. A good overview of all the different methods and their relations was drawn up Krenkel, and can be seen in Figure B.1, as taken from Krenkel [1].

Direct melt oxidation is a technique similar to LSI, however here the molten metal reacts with the gas which is present in the part. This method is often used when making aluminum oxide based parts.

Slurry infiltration is a method were ceramic powders are mixed in a solvent to form a slurry. This slurry is then infiltrated in a fiber, after which a preform is made. This preform is then pressed and sintered to form the CMC part. This method can be used when making alumina, silica or glass based parts, though also experiments for using it with silicon carbide or nitride have been performed.

Sol-gel infiltration is similarly to slurry infiltration, however now sols are used. These liquids with particles in them turn into gels at higher temperatures, thus the name sol-gel. This gel can then be converted into a ceramic at low temperatures. The process is thus the infiltration of fibers by a sol, after which a preform is made. Gelation and drying follows. Since the ceramic yield is quite low, this part is re-infiltrated with sol and the gelation and drying is repeated. In the end the part is fired in an oven to form the final part.

Lastly there are combined methods. Many of the above mentioned methods can be combined in an attempt to get the best of both methods. Examples of this are slurry infiltration combined with LSI or PIP, combining CVI with LSI or combining PIP with LSI. The details of these methods are further explained in the referenced literature, however are less relevant for this literature review (as these methods are rarely used) and therefor not included here.

B.2.3. Rocket nozzles

Rocket nozzle serve to convert heat into kinetic energy and thus produce thrust for a rocket. This inherently means that these nozzles experience uniquely extreme thermal and mechanical loads during their operation. Here it will be shortly explained what the main concerns are in rocket nozzle design and the use of ceramic matrix composites in this.

In general it can be stated that the exact loads exerted on the nozzle will be greatly depended on the nozzle and motor design. The main design drivers are given as this[24]. First of all will be the performance characteristics such as exhaust gas temperature and composition, firing time, thrust level

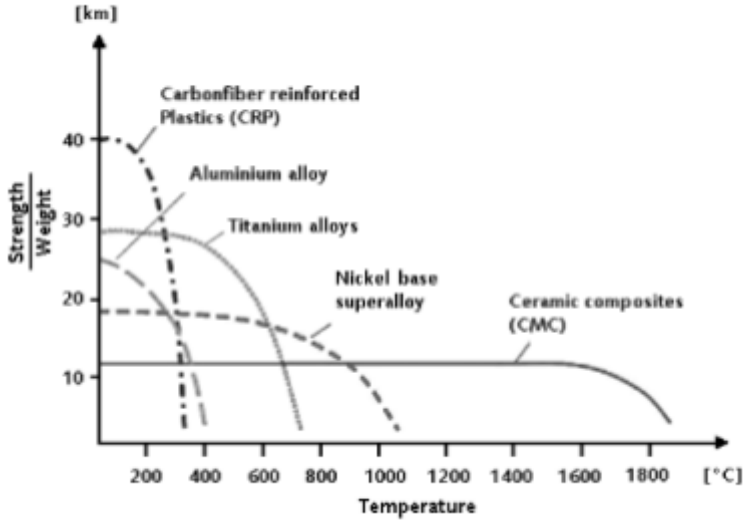

Figure B.2: Comparison of strength to weight ratio over temperature for different nozzle materials, taken from Schmidt et al.[25]

and chamber pressure. Next to this the aerodynamic design will dictated a very specific (inside) shape for the nozzle, especially around the throat area. Lastly, also a weight and size limitation will be present. These requirements will have to be converted to stresses to form the design of the nozzle. Apart from the obvious pressure and working temperature requirements, other design drivers will be high shear stresses and high thermal gradients inside the material. Based on these requirements, different materials will be considered, such as graphite, ceramics or refractory metals.

The potential for CMC materials in rocket nozzle applications has been researched for some time. The major advantages of CMCs compared to other materials are the following. Compared to metals, they will have a greatly increased working temperature range, while retaining their strength and stiffness and while having a lower density. This can be seen well illustrated in Figure B.2 as taken from Schmidt et al.[25]. This often leads to reduced cooling requirements or even removal of a cooling subsystem, which increases performance. Next to this, CMC materials can withstand much higher thermal gradients than their metal counterparts. Compared to ceramic materials they show higher damage tolerance and increased toughness. The weaknesses of CMCs lie in their lower strength at room temperature, as well as their corrosion characteristics. This last one is mostly relevant for uncoated carbon based CMCs in gas flows with high amount of oxygen or oxygen derivatives. It should be noted though that metal or graphite components can also suffer from problems in these types of flow. One of the major contributors in development of CMC nozzle components is the company DASA (later Astrium, later EADS-ST, currently Airbus Group). They developed both rocket nozzle and rocket nozzle extensions as well as combustion chambers out of CMC material and tested these under real life conditions during extended test fires [25][26]. They found that CMC components can satisfactory handle the mechanical and thermodynamic loads, while having lower mass and cooling requirements than other alternatives.

B.3. Effect of testing procedures

In this chapter the first sub-question will be discussed. This question was stated as: What effect do testing parameters have on testing results and thus what testing procedures should be used? This question is especially relevant for short-fiber ceramic matrix composite materials. Though for CFRP and continuous fiber reinforced CMCs extensive standards for testing exist, this is not the case for short fiber reinforced CMC [35] [36]. Many authors simply use standards for continuous fibers CMCs [37], however this can lead to unwanted consequences, as will now be explained. Firstly the investigation into testing procedure effects on continuous fiber reinforced CMCs will be elaborated. Following this, the step to short-fiber reinforced CMCs will be made. In the third section different ways of data collection during testing will be discussed. Lastly, alternative testing procedures are explored in the fourth section.

B.3.1. Continuous fiber reinforced

First the development of testing standards for continuous fiber CMC will be considered, as well as what influence test parameters have on outcomes when using these standards. Early work on the influence of testing parameters was performed by Piccola et al. on continuous fiber SiC/SiC composites, especially regarding the ASTM C1275-94 standard [38]. They found no significant effect of test rate and test mode (displacement versus load control) on the strength values. Geometry however did influence ultimate tensile strength values, with lower gauge volume leading to higher strength values [39]. Sankar et al. did similar experiments and found the same relation, as well as finding higher ultimate stress for faster loading rates. Next to this, lower fracture strengths were found under displacement control mode. This fracture strength corresponded with the ultimate strength for load control mode test and faster displacement control tests (>0.03 mm/s), but for slower tests (0.003 mm/s) an unloading region formed in the stress-strain curve [40] [41]. The reason that these effects were not found by Piccola while similar test were performed is as follows. Piccola found similar tendencies of his specimen, however using ANOVA test found that these were not significant ($p>0.05$), due to the relatively small number of tested specimen (8). It has been shown that often more than 10 samples are needed to even reach the 10% confidence interval range [42]. Sankar did not do any statistical analysis and therefor drew different conclusions. However, the fact that these effects were observed in both studies strengthens the hypothesis that these effects are at play, though more tests should be done to prove this with a good statistical significance.

Next to parameters such as gauge volume and test rate, other parameters were also found to influence test results.

The ASTM C-1275 standard mentioned before is also used for determining elastic modulus and proportional limit stress. A study by Jenkins et al. using Nicalon (SiC) fibers found that even while using the standard, user choices, such as the choice of stress range used for calculation, can still influence the values of the coefficients by up to 40% [43]. Next to this, Regener et al. did extensive flexural testing on continuous C/C-SiC samples with different sizes, fiber types and orientations. They found a number of factors influencing the flexural strength data when using samples with a thickness below three millimeter. These factors included the machining of the sample and the orientation of the top layer. Also a large influence of pores and defects was found when using small cross-section samples [44].

So summarizing it can already be said that even in continuous fiber CMC material, a lot of parameters during testing can result the measured test values. It means that great care should be taken to control and document all steps taken. Now the step to short-fiber based CMC material can be made.

B.3.2. Short-fiber reinforced

In short-fiber based C/C-SiC another complication arises with regard to determination of material properties. The reason is as follows. The short fibers cause the material to be on average isotropic, however when small testing samples are cut from big plates, local fiber distribution is often not homogeneous. This leads to large scattering of material data, meaning a high number of samples are required to give statistically significant results for the material properties [37] [3] [45][46].

Henrich et al. were one of the first to look at the effect of testing parameters in short fiber based C/C-SiC. They focused on the influence of differing testing cross-section on resulting tensile strength, modulus and elongation. They found significant differences with different cross-sectional areas. They also found that especially for samples with small cross-sections, i.e. around 3 by 10 mm^2, that a large data spread was formed, with values for maximum stress, maximum strain and E-modulus varying wildly between samples. They therefor recommend bigger samples, as well as carefully noting doing all procedures used [47].

This increase in sample width however does mean that the continuous fiber standards cannot be used anymore. The advantage however is that it has been shown that material data spread can be greatly reduced. For example, a significant reduction of scattering can be achieved by increasing the width of the sample from 10 mm to 30 mm. This is the reason why Hausherr et al. recommend using a sample

width of at least 5 times the fiber length [37]. However, another study found that even with more than 4 times the fiber length as width, scatter was still large in three-point bending tests, so other measures to reduce the scatter should also be considered. This study proposes to use four-point bending tests instead of three-point bending tests, which was found to also greatly help with the reduction of material data scatter [45][46]. A similar recommendation was done after studies by Liensdorf et al. [48] and Neubrand[49].

Henrich together with Weiß later expanded on this work by also doing short fiber C/C-SiC cross-section influence test with regard to flexural and tensile strength. Here they found no difference in value for flexural strength, though for tensile strength it was found that tensile strength decreased with smaller test gauge volumes. Also the finding of higher standard deviation for smaller samples was reproduced [35]. The tensile strength relation was later confirmed again by Shi et al. who found that for tensile tests, the measured test value cannot said to be geometry independent, even for very high test sample cross-sections [45][46]. Flaunder et al. however, did a similar test, evaluating the size effect for tensile C/C-SiC samples, but found no significant size effect [28]. This even though a very large sample set of 190 specimens was used. Reason for this different result can be that the change in specimen volume used was small (20%) compared to the previously mentioned studies (100%). Also a very high confidence interval was used of 99% to determine statistically relevant results. Even with this high confidence interval, the error ranges of the maximum strength values for the different gauge volumes just slightly overlapped (160.0 to 163.8 MPa and 162.0 to 166.6 MPa). This again leads to the conclusion that likely the size effect is present, however hard to detect with statistical significance. As Flaunder et al. already mentioned, more tests are needed ideally with a sample set size of at least 3 times larger than they used.

Another way to reduce the scatter was proposed by Flaunder et al., who argued that the high spread of strength data in CMC testing is due to the fact that often flexural testing is used. Flexural tests create complex load conditions, combining tension, compression and shear loading, meaning different failure mechanisms might be at work. Therefor, they suggest using uni-axial (tensile) testing, though they do acknowledge the problems with gripping and alignment present in these tests. They avoided these issues by using a complex self-alignment tool and intricate edge and face gripping system [28].

Another solution to the large spread of material data is by aligning all the short fibers in one direction during manufacturing. This leads to a plate with orthotropic properties, which can then be tested accordingly. The measured orthotropic values can then be used to predict the properties of samples with randomly distributed short fibers [37].

Considering other potential sources of error, it was found that the short fiber C/C-SiC material has very low notch sensitivity in tensile loading. It was also confirmed that specimen surface quality did not significantly influence measured values. [50][45][46]. Also the cutting method was investigated using continuous fiber CMC. Here it was found that only laser cutting significantly increased scatter, which should thus be avoided [51]. A recent review of machining found that when using proper tools, conventional milling and cutting gives good quality. However, waterjet cutting combined with laser cutting also has great potential for fast and high quality cuts [52].

Summarizing it can be said that though short-fiber testing is complex due to the inherently large scatter of data, multiple solutions to this exist which can greatly reduce the scatter. Next to this, as was also the case for continuous fiber testing, great care should be taken to control and document every step, as many parameters will have an influence on the measured test values.

B.3.3. Data collection techniques

Now, the best way to collect data from these kind of tests should also be considered and investigated. Firstly, micro-structural analysis is very important in CMCs to see the phase composition and the effect it has on material performance .The most common method of inspection of the micro-structure is by using scanning electron microscopy (SEM), which can give good insight into composition, especially in combination with EDX. However, next to this in some cases CT scanning can be a powerful complementary tool to give a more complete overview of the sample and identify interesting areas which can

then be further analysed using SEM [53]. CT scanning can also be used to assess fiber orientation and the amount of defects, which can even be automated by using a structure tensor approach [37] [45][46] [54]. Another way of determining orientation is using Radon data with a local radon transform [55].

Another important reason for looking at the micro-structure is the detection of voids and other defects. Though this is often also done using SEM, other options are also available. A different way for detecting defects in CMCs was developed by Sun, who used thermal tomographic imaging to successfully identify delaminations and voids in SiC-SiNC material [56].

Also, during tensile or flexural tests as much information as possible should be collected. In recent years, next to more standard inspection techniques such as strain gauges, extensometers and ultrasonics, the use of electrical resistance measurements has also been shown to have great promise for detecting damage during testing and service life. This method is easy to implement and is a reliable way to measure crack initiation and growth [57], even in dynamic conditions such as wet thermal cyclic testing [58]. Also reliable functioning at high temperatures, up to 1300 °C, has been proven [59][60]. At this temperature, it is one of the only viable options for possible future structural health monitoring. Even with some amount of residual silicon in the CMC, this method can still be used, even though in that case the silicon also becomes a major conductor [61]. It also has the advantage of being able to measure cracks through thickness and in transverse directions, while most other methods fail to detect these. Note is made that all these experiments were done on continuous fiber reinforced CMCs. Though the electric properties of the constituents in short and continuous fiber composites are the same, still some more research is required before fully implementing this on short fiber CMCs.

Another datastream which can be utilized during testing is that of ultrasonics. Though it cannot be used during testing, it is valuable in detecting defects in ther material afterwards or prior to testing. Also by using the speed of sound, the moduli of the material can be determined [62]. Though coupling agents such as gel or water are often used other options such as a polymer sheet as coupling or even contactless ultrasonics are also possible [63].

B.3.4. Alternative testing techniques

Tests different from the tensile of flexural variants are also possible, though less common. Fischer et al. looked into more complex stress states by creating a device to combine torsion and tensile loading, resulting in a multi-axial stress failure curve. They also included a way to do high temperature test, from which they confirmed that at high temperature, shear strength increase with up to 60% [64]. Other test have shown that flexural strength also greatly increases at elevated temperatures, especially at high fiber volume fractions [65]. Increases of flexural strength up to 150% were observed, depending on specific material composition. Another way to investigate a more complex stress state is by using a ring on ring test, which creates a biaxial flexural load. Guo found this to be more valuable than the standard three or four point bending tests, since it leads to a very low amount of data scattering [66]. Also, measurement of through thickness properties have shown to be possible, but were found to be complex and require large amounts of material [67].

B.4. Material composition parameters

Now the second sub-question will be discussed. This question is stated as: What material composition parameters are there and what is their effect? The final material properties are dictated by the way the material is created. The major influences on the material properties can be captured in a number of parameters. What parameters exist, what material properties they influence and what the relation is between the parameters and material properties is vital knowledge for understanding the behavior of the material. The parameters identified and researched for C/C-SiC will now be discussed. As the manufacturing route to create CMC's often starts with creating a CFRP body, as described in the introduction, many of these parameters will have to do with properties of this CFRP green body.

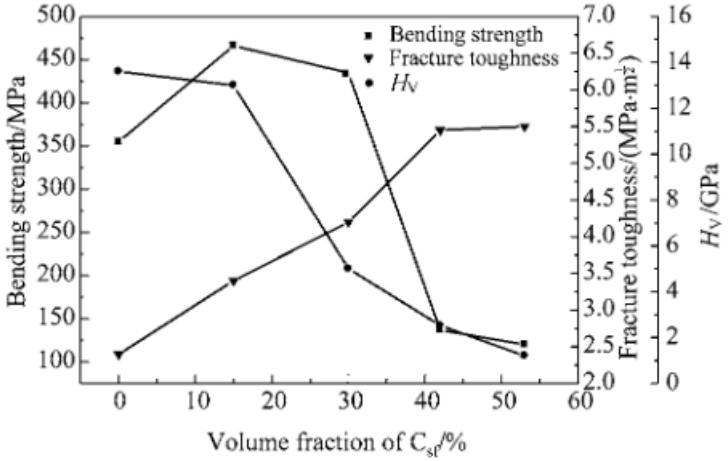

Figure B.3: Effect of fiber volume fraction on mechanical properties, by Tang et al [68]

B.4.1. Fiber volume fraction

Firstly fiber volume fraction will be discussed. Tang et al. were one of the first ones to study the effect of this in short fiber based C/C-SiC composites. Some of the mechanical properties they tested for were flexural strength, fracture toughness and Vickers hardness. The results of this can be seen in Figure B.3[68]: As can be seen, both Vickers hardness and flexural strength go down as fiber volume fraction is increased, while fracture toughness goes up. The reason for increased toughness is explained by the authors through the phenomena of fiber pullout, fracture of fibers and crack guiding, which are all phenomena which give the composite the ability to absorb energy without shattering. The decreasing hardness is explained by the fact that fibers have a much lower hardness than the SiC material, thus the higher the amount of fibers, the lower the overall hardness. The flexural strength first reaches a maximum, after which it drastically decreases. According to the authors, the peak is caused by the strengthening effect of the fibers, as they have higher ultimate properties than the SiC material. The decrease is explained by fiber bridging: the fibers crossing each other form a skeleton and make densification harder, leader to lower mechanical properties. It should be noted that the authors used a hot sintering process to produces this composite, where they combined SiC powder with 3 mm short carbon fibers, which were then milled. The results from this process have later been replicated [69], finding similar curves for toughness and flexural strength. This study also identified fiber pullout and debonding of fibers to be the major contributors to the increase in toughness. Research done on a different type of short carbon fiber CMC made using the sintering way also showed decreasing values of thermal expansion and elastic modulus for increasing fiber volume fractions [70]. Also if continuous fibers are used instead of short fibers in this sintering process, the flexural strengths keeps increasing with higher fiber volume fractions, as was shown by Ding et al. [71]. While using different techniques, the results can differ. When using melt infiltration it was found that the flexural strength can go up as well as down in the fiber volume fraction region of 30-50%, depending on the type of fiber used [65]. This study also found that thermal conductivity can go up or down with increasing fiber volume fraction, again depending on the specific fiber used. When considering through thickness thermal conductivity, it was found that it goes down with increasing fiber volume fraction, as the fibers start acting as a thermal barrier [72]. A recent study by Wang et al. used direct ink writing, a form of additive manufacturing, combined with liquid silicon infiltration. They found increasing values for tensile and flexural strength and modulus when testing in the fiber volume fraction range of 30-40% [73].

B.4.2. Fiber type

Next different fiber types can be discussed. The type of fiber, mainly determined by their pretreatment, has large effects on the properties of the final CMC product [48]. This was clearly explained Krenkel [74]. The interface between the fiber and the matrix greatly dictates the physical properties of the material, especially the amount of ductility shown in the fracture behavior. Krenkel showed that the pretreatment temperature dictates the strength of the interface between the CFRP matrix and fiber. This

bond strength then influences the pyrolysis and siliconization steps. When pretreatment temperatures increase, the bonds becomes weaker, which leads to more shrinkage and cracking of the matrix and less shielding of the fibers. This leads to more fibers coming in contact with silicon in the siliconization step, which causes them to become converted to SiC. This conversion then increases SiC content and decreases mechanical properties, as well as ductile fracture behavior, i.e. the material becomes more brittle. This logic can be further expanded when looking at pitch versus PAN based fibers. These are the two main types of fibers, which are made from different raw materials. Due to this, they also have different manufacturing routes, which then leads to different properties. Pitch based fibers have more crystalinity and because of this have higher stiffness and thermal conductivity. However, most importantly in this case, pitch based fibers are graphitized to a much higher degree[75]. Due to the increased layer of carbon on the outside of pitch based fibers, the fibers are protected against deterioration due to conversion to SiC [66]. A notable difference can also be seen in the microstructure. For pitch based fibers, silicon is able to get in between the fiber bundles, while for PAN based fibers the bundles often remain isolated. This can be clearly seen in Figure B.4 from Reimer et al. [75].

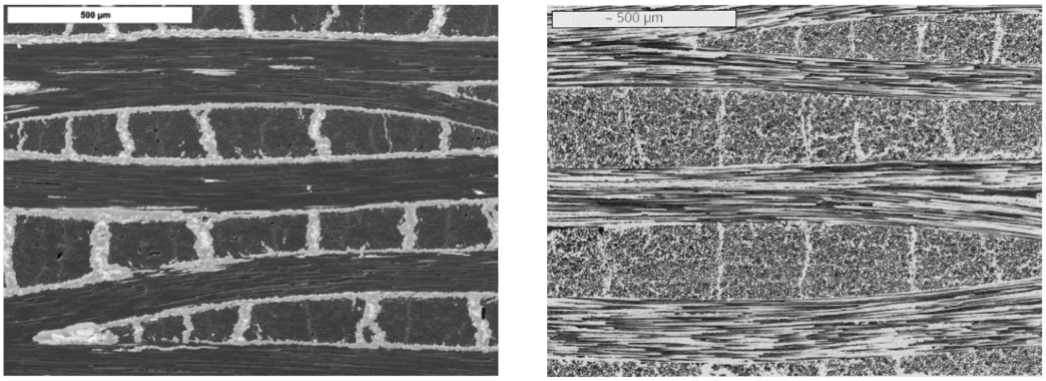

Figure B.4: Microstructure of (a) standard PAN based C/C-SiC and (b) of Pitch based C/C-SiC [75]

This effect can lead to higher ablation resistance for the pitch based fibers, as they are better shielded inside the matrix. Also, since the silicon is more completely infiltrated, porosity is often lower, leading to improved mechanical properties [66]. Next to this, the graphitized layer has a large and positive influence on the fracture behavior of the material. This is due to the following mechanism: The graphite provides an low-strength cleavage plane, as the layers are weakly bonded. These layers are positioned in between the SiC and the carbon fibers and thus called the interphase. Due to this weak interphase, fibers are able to move within the matrix when load is applied. This prevents fibers breaking and increases toughness. If this interphase is lacking, the SiC will be bonded directly to the fibers, leading to a brittle fracture behavior, as fibers will not be able to slide under load. Also, fibers will be attacked by the Si during infiltration, leading to a decrease in mechanical properties [21]. Lastly, since their inherent thermal conductivity is higher, the CMC thermal conductivity also increases with pitch based fibers[65][72]. Another way of influencing the fiber matrix interface strength is by fiber coatings. It was shown that with the right amount of pyrolytic carbon coating on fibers, flexural strength could be increased by 30% and failure strain by up to 900 % [76].

B.4.3. Coating

A different option is the coating of the entire composite. This would mainly be done to shield the carbon fibers from oxidizing in a high temperature oxidizing environment. Westwood et al. reviewed many possible options for this, and concluded that a multilayer coating consisting of silicon based material, combined with a functional, self-healing, boron-based layer offers the best performance. However, exact coating choice of course depends on other requirements such as working range and cost [77]. When these coatings were investigated for performance at higher temperatures (>1000 °C) for an extended period of time, it was found that none provided excellent protection, especially when heating up cycles were involved [78]. Later yttrium silicates were used in combination with SiC and titanium dioxide, which showed promising results, even at high temperature cyclic tests [79]. It has however

been noted that coatings still have major drawbacks, mainly in the cases where delaminations can happen, leading to a loss of coating and rapid deterioration of the material afterwards. Also, considering C/C-SiC composites specifically, it was found that the SiC matrix gives the same oxidation protection as a common coating would [72] [80] [81]. This gives an upper working temperature of around 1800 °C. To improve that even more, a switch from SiC to different, ultra high temperature ceramics is required, such as Zr- or Hf- based ceramics [72]. These have been proven to be able to withstand reentry conditions with temperatures exceeding 2400 K [82].

B.4.4. Fiber length

Another important parameter is the fiber length used. From Shi et al. it can be seen that higher fiber length greatly increases flexural strength [83]. Ahmad et al. suggests a similar trend while using a completely different manufacturing technique, however their results are not statistically significant [84]. The increase in strength was also confirmed by Liensdorf et al., using both three and four point bending tests. They also found that differing the fiber length has little to no effect on density, porosity, Young's modulus and failure strain [48]. An interesting additional finding from this study was that mixing different fiber lengths often leads to even higher flexural strength, as the homogeneity of the material is increased. Another study with very different manufacturing techniques also found increasing strength, as well as increasing modulus. However, this is likely a cause of the manufacturing technique, where fibers are not randomly distributed but aligned [17], also there was poor sintering, leading to problems with the matrix material, possibly invaliding some of the results.

B.4.5. Additives

Additives can have large effects on the properties of the material, as they can influence the interphase and improve density and mechanical properties [85]. However, the major drawbacks are the often high material cost of used additives, as well as the added complexity (and thus complexity) in the manufacturing stage.

B.5. Processing parameters

The third sub-question was stated as: What processing parameters are there and what is their effect? Meant by this is: What steps taken during manufacturing of the CFRP part, as well as what parameters used during the pyrolysis and siliconization stages are present and which influence the final part properties in a major way. In the first subsection the process parameters around infiltration will be elaborated, while in the second subsection the post-cure step will be discussed. Lastly some general remarks on the curing cycle will be made in the last subsection.

B.5.1. Infiltration

Though infiltration is not a well-defined process parameter in itself, it is a good subject to discuss a lot of other small changes which influence the final part properties significantly through their influence on the infiltration process. As will be explained in more detail in subsection B.6.3, infiltration and porosity are closely linked. Therefor, any parameters that influence porosity, will influence infiltration and therefore the final product properties. This was shown by Gadow et al. who added SiC powders to the CFRP stage. This led to a bimodal porosity distribution, which then led to ideal infiltration conditions and thus a dense CMC part [86]. Siliconization temperature is a measurable parameter which also effects the material properties. One of the major ways in which this can be observed, was discussed by Schulte-Fischedick et al. [87]. They proposed a hypothesis for an infiltration mechanism and concluded that at the current common temperatures, first a layer of β-SiC forms with small grains and a high number of defects, followed by larger grained β-SiC. It is suggested that β-SiC will turn into α-SiC when temperatures are increased, as this transition is seen in other manufacturing methods were temperatures upwards of 2000°C are used. These two types SiC are fundamentally different, as they have different crystal structures. This also means that they differ in their properties, such as melting temperature, hardness and conductivity [1]. This will then also influence the final material properties of the CMC. Another way in which infiltration temperature can influence material parameters is described by Raether et al. [88]. They show that close to the melting point of silicon, SiC formation controlled the infiltration

[1] https://www.satnanomaterial.com/blog/what-is-the-difference-between-alpha-sic-and-beta-sic-in-silicon-carbide-powder-_b30, date accessed: 04-10-2022

rate, while at higher temperatures, infiltration kinetics were better described by the Washburn equation [89] for infiltration of porous bodies. This meant that small increases in infiltration temperature can lead to large decreases in infiltration time, which are not proportional to the change in viscosity, surface tension and carbon solubility of the silicon. For example, an increase in temperature from 1485°C to 1700 °C, leads to an decrease in infiltration time by a factor of 12, while viscosity and surface tension only change with 10-30%. Shorter infiltration times are preferable from a cost and manufacturing time point of view. This is thus likely the reason why often siliconization happens around 1650 °C. It has already been noted before that properties such as viscosity, reactivity and wetting need to be considered regarding their influence on material properties [1]. Extensive research into this and other siliconization parameters has recently been preformed by Bianchi et al. [90]. Both pyrolysis and infiltration temperature influence was assessed, as wel as dwell time at these temperatures. It was found that an increase in pyrolysis temperature will decrease the residual mass of the matrix, which thus increase the porosity in the C/C stage, which then increases the mass gain during siliconization. An increase in infiltration temperature also lead to an increase in silicon uptake, as the silicon viscosity is lower. This then leads to a higher silicon and SiC content in the final product, as well as low porosity and more and larger SiC grains. An increase in dwell time was found to also give more and larger SiC grains, as well as lower toughness, as more silicon became attached to the carbon fibers, thus decreasing the ability for fiber pullout. Increases in temperatures for infiltration and pyrolysis also decreased failure strain and toughness and increased flexural strength. For flexural modulus the maximum was found at a balance point, as too low temperatures gave too much porosity which decreased flexural modulus, while too high temperatures lead to too much fiber deterioration, decreasing the modulus. A good illustrations of the differences caused by these parameters can be seen in the micro structure, as shown in Figure B.5 below from the paper [90]. All of these observations make sense from a physics standpoint and line up well with earlier research [1].

B.5.2. Postcure

A postcure step is the action during CFRP manufacturing to put the created part back in the oven after demoulding at a high temperature for several hours. In general it is recommended to do a postcure step when working with phenolic resins. This because postcuring is needed to fully finish the polymerization process of the resin [1]. However, later research showed that an annealing or post-cure step in the CFRP stage has little influence on the mechanical properties of the final C/C-SiC component, though the properties of the intermediate products did improve [91]. This is possibly due to the fact that the final parts of the polymerization are burned away during the pyrolysis anyway and thus do not have any effect anymore when the siliconization happens.

B.5.3. Cycle determination

Most of the process steps that can be taken are during the manufacturing of the CFRP part. However, little can be said about this in general terms, as the cycle used is often prescribed by the manufacturer of the resin. The cycle of each resin is very different and depended on factors like possible solvents used and the type of resin in general. Nevertheless, it can be recommended to always look at the cycle and figure out what each steps intention is. For example, a low temperature dwell is possibly to boil off any solvent in the resin system. By determining the purpose of each step, a better understanding of the cycle will be achieved and finding the source of possible errors or optimizing the manufacturing process will be made easier.

B.6. Material properties

Here the fourth sub-question will be discussed. The question was stated as: What material properties are there, and which should be assessed? The main aim of this question is determining what material properties are most relevant for assessing the quality of a CMC material, based on what properties are mentioned and evaluated in literature. In the first section the property of recession behavior will be elaborated. This is followed by a section on thermal conductivity. In subsection B.6.3 porosity is discussed. After this in section four fracture toughness is described. Lastly in section five fatigue and creep properties are elaborated on. Of course general mechanical properties like flexural strength are also important, however this is already discussed in detail in section B.3.

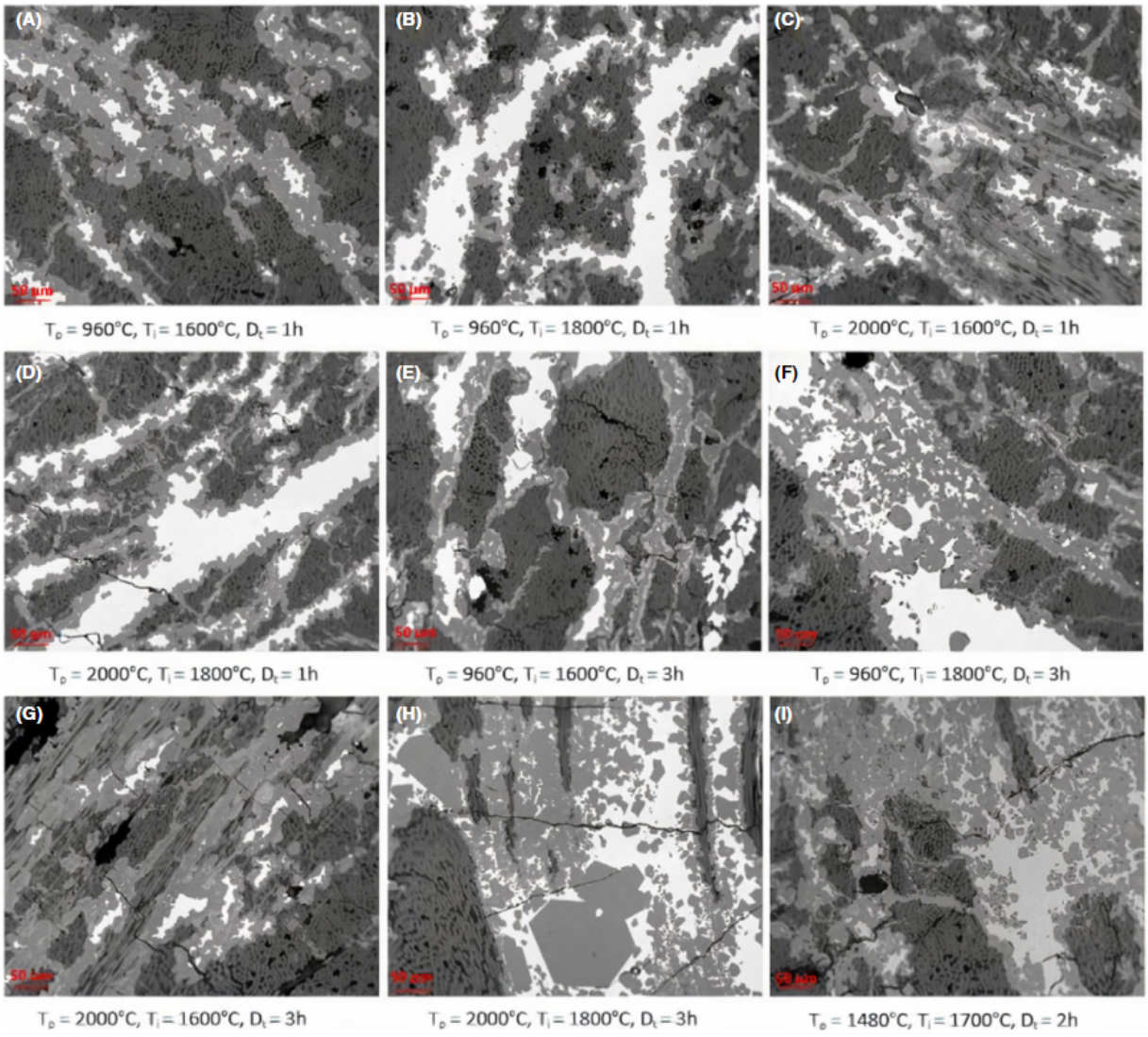

Figure B.5: Microscope images of C/C-SiC prepared at different pyrolysis temperatures T_p, infiltration temperatures T_i, and dwell times D_t, taken from Bianchi et al. [90]

B.6.1. Recession behavior

Recession behavior is a relevant material property, though less easily caught in a single number and more dependent on the environment. Recession behavior has to do with how well the material can handle high temperatures, pressures and aggressive environments. As explained before, for C/C-SiC composites the main point to consider here is oxidizing environments, as these limit the working temperature. In inert atmospheres, carbon material retains its properties up to 2500 °C [92]. It should be noted here that when considering extremely high temperature performance, a ”perfect” composite is considered with no residual silicon content. This because the melting point of silicon is around 1400 °C. Because of this, when creating C/C-SiC composites for high temperature applications, an additional processing step is done in which any residual silicon is removed. As discussed before, to avoid recession behavior, often coatings are used. One of the coatings which still represents to an extent the original C/C-SiC material is a SiC coating. For samples with this coating, a test was performed where they were exposed to temperatures of 1200 °C in static air for 200 to 400 hours. It was found that the samples lost up to 10% of their weight and that ultimate strength decreased by 30-80%. It was found that the critical temperature for these specimens was around 750 °C. Interestingly, recession at high temperatures was found to be minimal, if the intermediate temperatures could be avoided. It was hypothesized that this was due to the closed of cracks in the SiC coating and matrix, preventing any recession behavior [78]. This lines up well with the theories of Lamouroux et al., who identified three regimes, namely low (<800°C), where carbon-oxygen reactions dominate, intermedeiate (between 800 and 1100°C), where diffusion causes oxidation, and high (>1100 °C), where oxidation is halted due to SiC seal-coating microcracks [93]. These claims were confirmed by Hanling et al., who also determined the temperature at which oxidation is the highest to be at 900 degrees [94]. Later research done on uncoated SiC samples found similar results. [95]. Indeed, SiC based composites have been described to have self-healing characteristics at high temperatures [96]. Importantly, the oxidation has been confirmed to slow down in low earth orbit environments, where minimal oxidation was observed, even while the material was in contact with atomic oxygen[97]. This also lines up well with Lamouroux et al., who hypothesized that oxidation was proportional to the amount of oxygen encountered by the material [93].

It is notable that also tests on the ablation behavior of the composite were performed under the very high temperature and oxygen rich conditions of a oxyacetylene torch [98]. It was found that a cut-off point could be found after which C/C performed better than C/C-SiC, which was set around 3.6 MW/m^2.

An important distinction which was found was that between continuous and short fiber CMCs. The hypothesis being that short fiber CMCs are more protected by the SiC matrix against oxidation than continuous variants. Tests showed that this was indeed the case and that oxidation along protruding fibers became the dominant recession mechanism [88]. This led to experiments with different fiber lengths, where it was found that shorter fibers give better recession behavior, as the oxidation path becomes longer [99].

B.6.2. Thermal conductivity

Knowledge on thermal properties is crucial for this material, especially when used in rocket nozzle applications. It was found early on that the conductivity of the composite relies heavily on the chosen fiber, as well as the resin material [100]. Especially pitch fibers can greatly increase the conductivity, due to the fact that their conductivity is up to two orders of magnitude higher than that of their PAN based equivalents. These phenomena were confirmed to also be present in short fiber based C/C-SiC [65], where it was also determined that increases in fiber volume content, increases thermal conductivity. This is as expected, considering that fibers contribute the biggest part to the conductivity. It should be noted that the order of magnitude difference in pitch and PAN based fibers does not carry over to the final product, where the difference reduces to two to five times higher. This is due to the fact that the final conductivity remains a function both of the conductivity of the fiber, as well as the matrix. A way to estimate this is found in [75]:

$$\lambda_{comp,long} = 0.5FVC\lambda_{fiber} + 0.5FVC \cdot 0.236\lambda_{fiber} + (1 - FVC)\lambda_{matrix} \tag{B.1}$$

Where $\lambda_{comp,long}$ represents the conductivity of the composite, while λ_{fiber} and λ_{matrix} represent the conductivities of the fibers and matrix respectively. FVC stands for the fiber volume fraction. In the through-thickness direction, the conductivity is found to often be much lower, as it is dominated by the

matrix values. Also, conductivity perpendicular to fiber directions is often unknown and could be much lower than along the fiber[75]. Lastly, the fiber and matrix interfaces form a thermal barrier, meaning that with increasing fiber volume fraction, the conductivity decreases [72]. It is also notable that the conductivity of the material increases significantly with increasing temperature [100][75][101]. Cao recently did more research into the effect of different processing parameters on conductivity and found that infiltration temperature has a large effect, with an optimum found around 1600 °. However, resin carbon content had little effect [102]. This makes sense as this mainly influences the matrix properties, which have a minor effect on the total conductivity if the fiber volume fraction remains the same, as described above.

B.6.3. Porosity

Porosity is the amount of voids present in the material. This can be considered both in CFRP, C/C and CMC state. The void amount is an important parameter, as it influences the material properties, but also because it is easy to measure using the Archimedes method. Understanding the influence of voids can thus give a good first estimation on the quality of the material. Porosity is linked to material properties by the infiltration process. The pores present in the CFRP material are a starting point for pores in the C/C stage. These pores are vital during the siliconization, as they form the pathways through which the silicon is absorbed in the material. Additional voids form in the C/C stage, due to the mismatch in thermal expansion coefficient between the fibers and the matrix. Apart from total pore volume, pore size also plays a role: with small pore sizes the formation of SiC will quickly block any further silicon flow and therefor halt infiltration [44]. Thus, low amounts of porosity and small pore sizes in the CFRP stage lead to low amounts of silicon infiltration, meaning the final product will have a high carbon content [86]. This is advantageous when high strength and stiffness, is required, as a large number of the fibers remain intact [18][103]. However, in high ablation environments, a higher SiC content is desirable. Porosity in the final product should also be monitored, as here porosity will influence the mechanical properties. High levels of porosity will lead to reduced tensile strength [104]. It should be noted that fatigue life seems less sensitive to porosity, and is more a function of pore distribution and size. The porosity in the final product is also influenced by the porosity in the CFRP and C/C stage. It should be noted that minimizing this porosity is about striking a balance, while also keeping in mind the previous comments made about resulting element distribution: too high porosity in the C/C stage will lead to incomplete siliconization and remaining pores, while also producing a high amount of residue silicon in the material. Meanwhile, too low porosity in the C/C stage leads to channels being blocked off early in the siliconization and thus also remaining pores and unconverted areas of C/C [75][105]. Optimal siliconization is achieved by a combination of both wide and small pores, combining high silicon mass flow with capillary action [86]. Ways to influence the porosity are filler materials in the CFRP stage, pyrolysis of additional resin in the C/C-stage [106][107] or using a CVI process [108]. Though ideally, one should try to optimize the porosity in the CFRP production steps instead of using these additional processes, as these will increase process time, complexity and cost.

B.6.4. Fracture toughness

Fracture toughness is an important material property, explaining how the material behaves under the influence of damage, specifically in the presence of a sharp notch. It can be described as the area under the stress-strain curve of the material. It is important to measure for CMCs, as fracture toughness is one of their main defining characteristics, especially in comparison with ceramics, which are known and avoided for their low fracture toughness. It has been found through research that the fracture toughness of a CMC is highly connected to the interphase between the matrix and the fiber. A weak interphase is needed to provide the material with mechanisms for fracture toughness [72]. The mechanisms through which toughness is introduced in the material are fiber pullout, fiber bridging, crack deflection, microcracking, and fiber debonding [109][68]. If the bonding between matrix and fiber is too strong, these mechanisms will not happen and the fiber will break at the same time as the matrix, that is in a brittle way [21]. Based on this some findings can be explained. Firstly it was found that high toughness was linked to a high carbon content in the material[1]. This is logical, as in that case the matrix fiber bond will be weak. Also, the other way around it was found that areas rich in SiC showed low fracture toughness [110], which again can be explained by noting that fiber matrix bonding will be high there, leading to brittle failure.

For short-fiber based C/C-SiC some special observations can be done. Tang et al. changed the fiber volume fraction and found the toughness to be increasing with the fiber volume fraction with a maximum of 5.5 MPa $\sqrt{m}$ at 53% fiber volume fraction, as can be seen in Figure B.3[68]. This means that the fracture toughness is a factor of two higher than in pure SiC. This was tested by indentation. The result was later replicated by Li et al. who found a value of 4.9 MPa $\sqrt{m}$ at 55%. They also found that the main energy absorption mechanisms were debonding and pullout, with fiber pullout absorbing the largest amount of energy [69]. Some tests were also performed to find the difference between mode I and mode II fracture toughness using the Brazilian disk method, with the first one being found to be around 1.5 times lower than the second one (3.5-4.1 MPa $\sqrt{m}$ vs 4.7 to 5.7 MPa $\sqrt{m}$ respectively)[109][111]. The reason for this given in the paper was the large influence of T-stress acting in compression parallel to the notch.

B.6.5. Fatigue and creep

Fatigue and creep, while not necessary connected, are both material properties related to failure over time with loads below the failure stress. In case of fatigue it is caused by cyclic loading, while in case of creep it is caused by a continually present load, usually in combination with heat. Especially this last case is relevant, as the material considered is often applied in high temperature applications. But also fatigue is relevant, for example in the case of powerful vibrations present in a nozzle during a rocket launch.

First of all fatigue is considered. It was already found early on that fatigue for CMC materials can also be captured by the well known S-N curve [112]. In creating these curves it was found that CMC materials have good fatigue properties, with a fatigue limit of 80% when tested at room temperature [113], later confirmed by Weiß et al. to be between 60% and 80% after one million cycles [35]. However, at temperatures above 1000 °C, fatigue life was found to decrease above a certain load [113]. This has to do with the mechanism of fatigue in CMCs, which is stated as the degradation of the sliding resistance of the interphase [112][114][113][115]. At high temperatures this sliding resistance degrades faster and thus fatigue life decreases, also likely under the influence of creep. Also, at high temperatures carbon fibers in the material can start degrading as they come into contact with hot air after the formation of microcracks [112][114]. As fatigue happens under the influence of cracks, first cracks have to form. This firstly means that fatigue will not happen if the stress is too low to form cracks. Also that fatigue resistance will go up with a strong interphase and an optimal porosity distribution [113][104].

Surrounding creep in CMCs the following has been found. In general CMC materials have high creep resistance [116]. The creep of the matrix will control the creep of the composite, and this creep is very depended on the load case, especially considering uniaxial or multiaxial loading [113]. In this last case creep resistance was found to be much lower. Again creep resistance can be improved by having a strong interphase which can resist crack and cavity growth.

B.7. Rocket nozzle performance

The last sub-question, which will be discussed in this chapter, was stated as: What parameters determine rocket nozzle performance? To answer this, first nozzle performance will be discussed in section one, after which the determination methods of this performance will be discussed in section two.

B.7.1. Nozzle performance

Many factors are taken into consideration when determining nozzle performance. Firstly, the load rating of the nozzle is crucial information. This will be both mechanical loads, due to the pressure inside the nozzle, as well as thermal loads, caused by the high temperature of the gasses. Also thermal shock resistance and thermal expansions ratios need to be taken into account. Next to these loads, the chemical rating of the nozzle is also important. This explains how well the nozzle deals with different kinds of propellants and their byproducts. Deterioration and ablation needs to be taken into account here. Lastly weight is, as always in aerospace, a driving factor. High specific properties leading to low mass is vital for commercial success of any thruster type. CMC contain many desirable properties in this regards and have for that reason already been explored as thruster material for missiles, satellites and large liquid propellant engines, for more than 20 years [26]. Prototypes have been fabricated and tested

in the past and have proven that the concept works [116]. The properties that make CMCs desirable are specifically that they have a low density, while maintaining high strength and stiffness. They also have good chemical resistance and are able to withstand high temperatures and large thermal shocks[10]. Currently, in most nozzle applications copper or nickel based superalloys are used. Compared to these, CMC materials have much lower density and greatly increased working temperatures. This means performance will be gained both by reduction in weight, as well as reduction in cooling requirements.

B.7.2. Nozzle performance determination

To determine whether or not the developed nozzle will have the desired characteristics, a test plan should be made. Of course, the most representative test is a static fire, in which the nozzle is placed on the end of a rocket, which is then fired for the full flight duration. However, these tests are expensive both due to the high material cost, as well as complex setup. Next to this, the nozzle will likely be damaged or at least need refurbishment after this, meaning it cannot be easily sold. Therefor, other methods should also be considered. Firstly, microstructural analysis can be considered: Density and porosity can be determined, which give information about the composition of the material. Also, when density and porosity determination is done in the C/C stage, estimations can be made about the infiltration quality. For example, some papers aimed for a porosity of <15% in the C/C stage to avoid residual silicon in the final product [107]. The importance of porosity is explained in more detail in subsection B.6.3. Next to this, CT scanning can be used to determine the dimensional accuracy of the nozzle and to see if any warping or other deformation happened during the high temperature processing steps. Other important tests are shaker tests, to see if the nozzle can withstand the mechanical loads experienced during operation, and leakage tests, which can be done for example using helium.

To determine the recession behavior of the nozzle, oxyacetylene torch tests can be performed. These are often performed on pellets, after which the ablation can be determined [117] [118] [119] [120]. Another option is using a high velocity oxygen fuel facility, in which supersonic flame conditions can be replicated [121]

For the pressure testing of the nozzle, relevant work has been done by Carter et al. They investigated the pressure strength of ceramic gun barrels using a compressed elastomer test. This has the advantage of being safer than tests with fluid or air as pressurant and easier to setup [122]. No examples of this method being applied to nozzle testing could be found, so this provides an interesting research gap. More conventional pressure testing using compressed air has been performed on CMC samples in the past, and shown to have great promise in determining failure modes and relevant material strengths [123].

B.8. Conclusion

In this report many aspects of ceramic matrix composites and their application in rocket nozzles have been studied. A literature search was performed and all relevant literature was summarized, compared and assessed. This was done to answer the main question stated as: What is the effect of manufacturing parameters on the performance of a short carbon fiber C/C-SiC CMC rocket nozzle?
Firstly the history of ceramic matrix composites and rocket nozzles was discussed, as well as their main manufacturing routes with their advantages and disadvantages. After this testing procedures were considered, where the difficulties of testing ceramic matrix composites materials were summarised, especially with regard to the short fiber variant. For this one, no testing standard exist, though some suggestions for good testing practices have been done. In the material composition parameters section the influence of fiber volume fraction, fiber type, length and coating on the final properties was discussed, together with a theoretical framework supporting this. This was followed by an elaboration on the influence of different infiltration, postcure and cycle parameters, which were found to be needed to have a proper understanding of the material. Different material properties like recession behavior, thermal conductivity and porosity were also considered, which were found to be well relatable to the composition parameters of the material. Lastly rocket nozzle performance and the determination thereof was explored.

Concluding it can be said that after this research the most important manufacturing and processing parameters were discovered and a good theoretical understanding of the material was established. Based on this research the current state of the art surrounding ceramic matrix composites and rocket

nozzles was found, which can be used to build upon for further research.

C

Appendix C - Pictures

This appendix features images taken during the manufacturing and testing stages of the thesis and thus aims to provide a better understanding of the procedure of sample production and evaluation.

C.1. Production

C.1.1. Prepreg production

Figure C.1: Gathering of mould parts

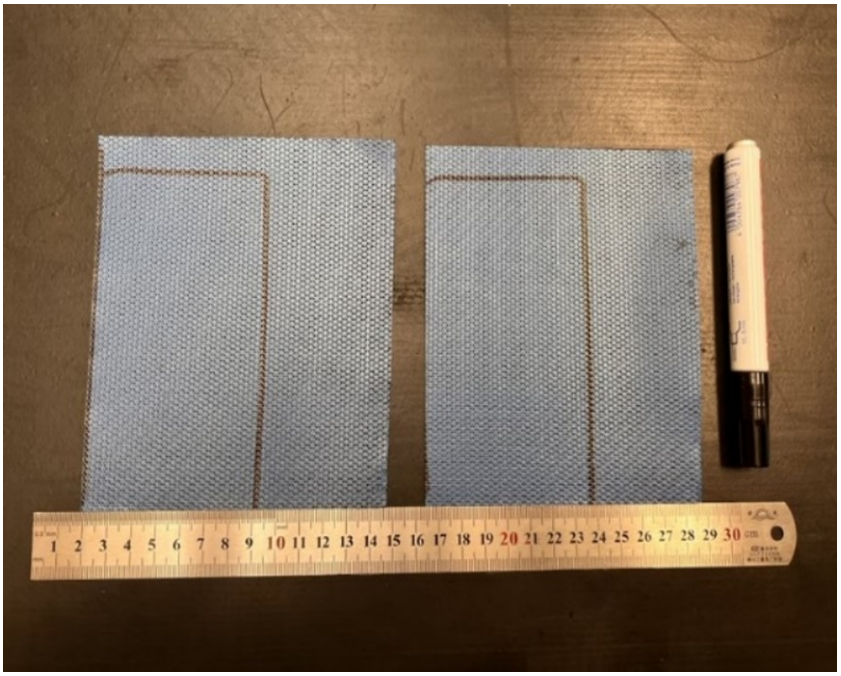

Figure C.2: Measuring and marking of prepreg layers

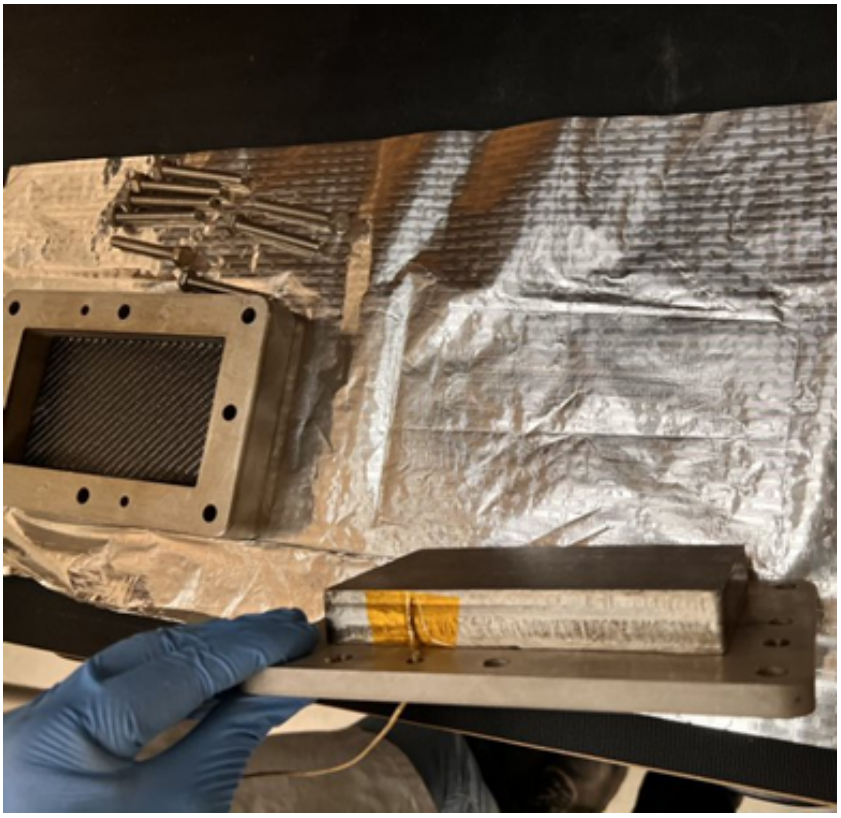

Figure C.3: Placing of the thermocouple inside the mould

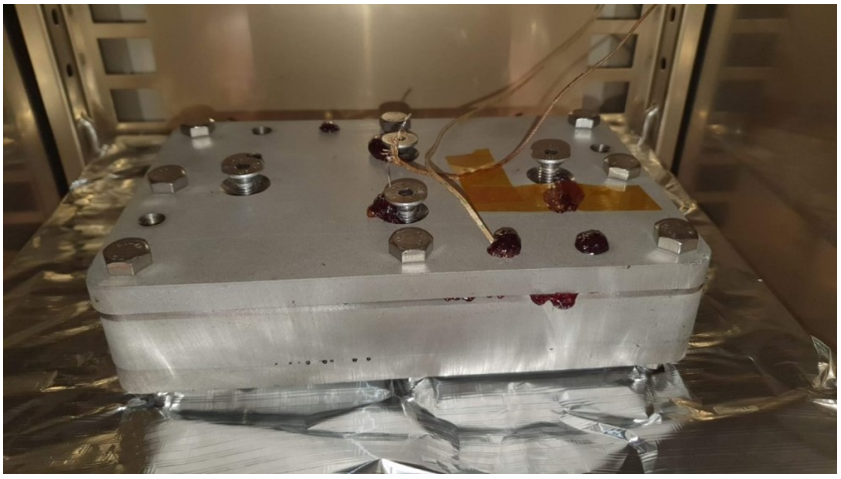

Figure C.4: Placing of the thermocouple outside the mould

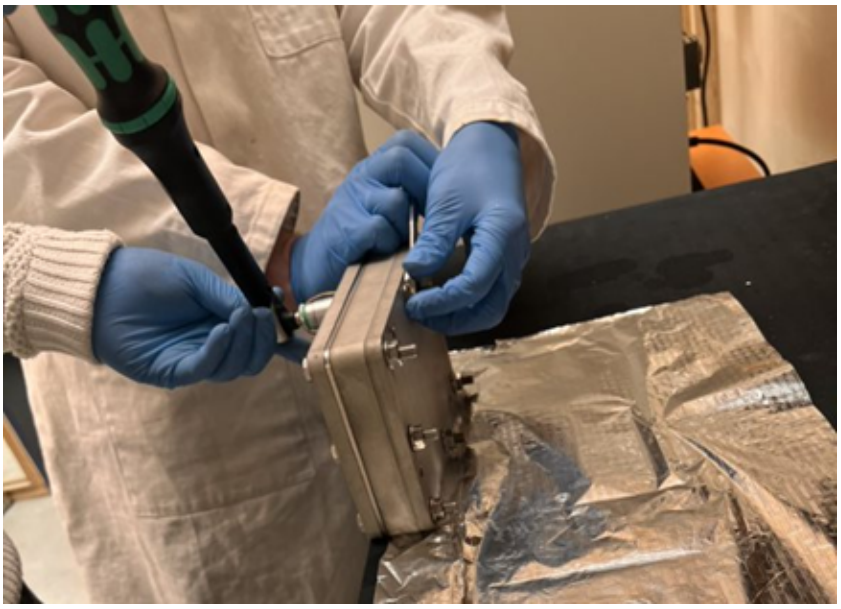

Figure C.5: Applying pressure to the mould

Figure C.6: Post-curing setup

C.1.2. Short-fiber production

Figure C.7: Measuring resin weight

Figure C.8: Creating a uniform resin layer

Figure C.9: Measuring fiber weight

Figure C.10: Filling fibers in the mould

Figure C.11: Filling the middle resin layer

Figure C.12: Filling the top fiber layer

Figure C.13: Placing the top resin layer

Figure C.14: Placing the mould in the oven

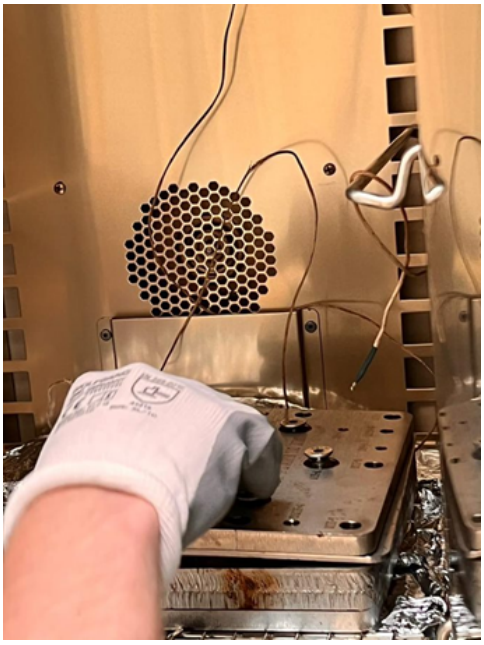

Figure C.15: Closing the mould after the first cycle part

Figure C.16: Closing the mould and applying pressure

C.2. Density and porosity testing

Figure C.17: Samples put in labeled cups

Figure C.18: Samples submerged in demineralized water

Figure C.19: Cups covered with perforated foil

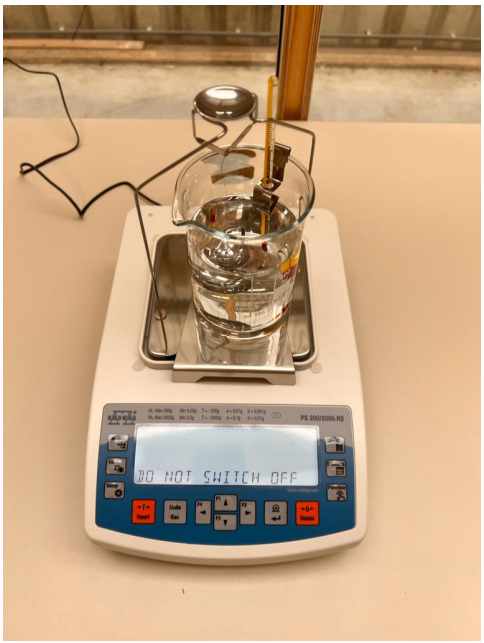

Figure C.20: Scale with density measurement setup

Figure C.21: Taking sample submerged mass

Figure C.22: Taking sample wet mass

C.3. Samples

C.3.1. Prepreg samples

Manufacturing phase

Figure C.23: Prepreg sample 1

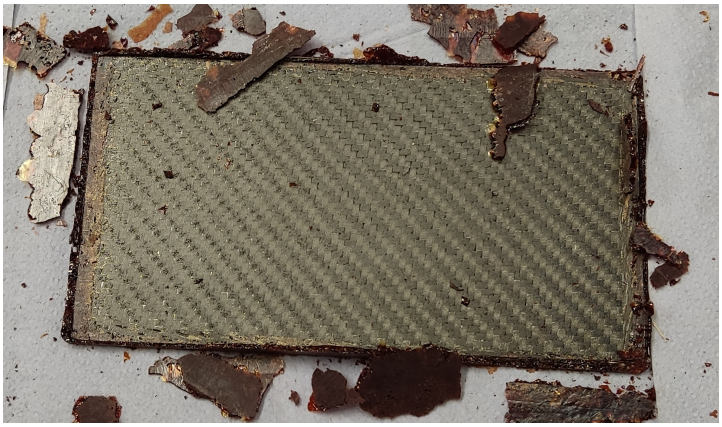

Figure C.24: Prepreg sample 3

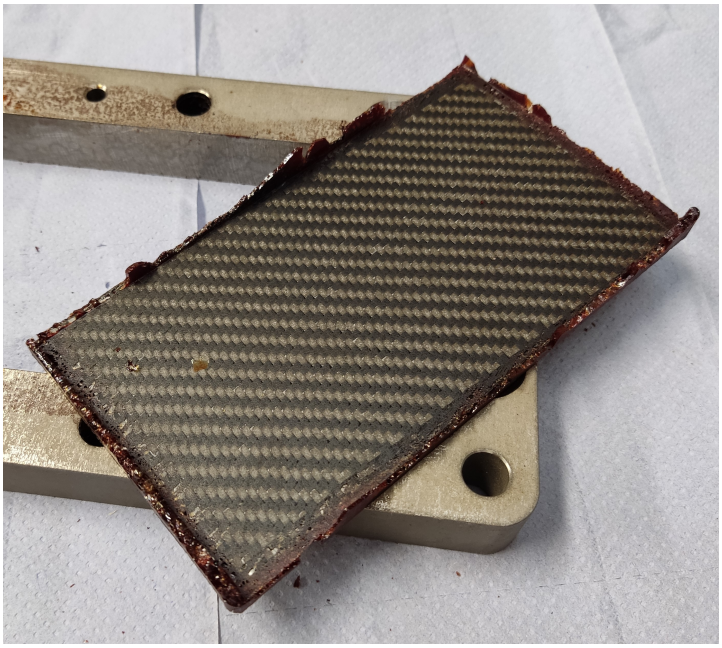

Figure C.25: Prepreg sample 5

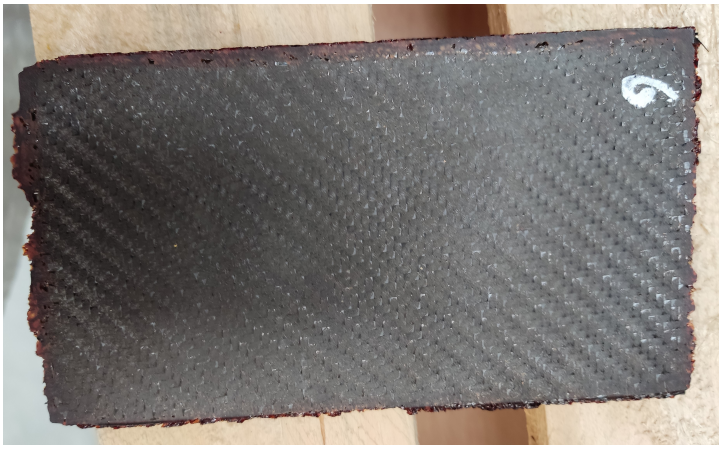

Figure C.26: Prepreg sample 6

Figure C.27: Prepreg sample 7

C.3.2. Short fiber PAN samples

Manufacturing phase

Figure C.28: PAN short fiber sample 1

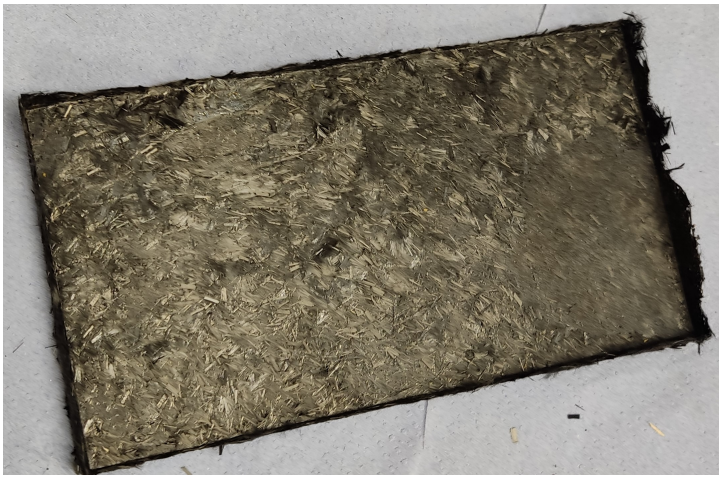

Figure C.29: PAN short fiber sample 2

Figure C.30: PAN short fiber sample 3

Figure C.31: PAN short fiber sample 4

Figure C.32: PAN short fiber sample 5

Figure C.33: PAN short fiber sample 6

Figure C.34: PAN short fiber sample 7

Figure C.35: PAN short fiber sample 8

Figure C.36: PAN short fiber sample 9

Material composition phase

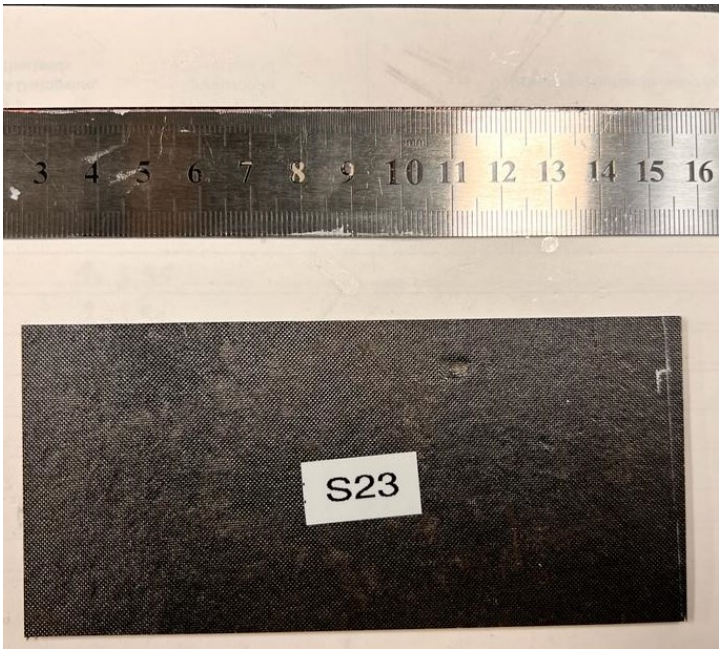

Figure C.37: Variation 1, sample 1

Figure C.38: Variation 1, sample 2

Figure C.39: Variation 1, sample 3

C.3.3. Short fiber pitch samples

Manufacturing phase

Figure C.40: Pitch short fiber sample 1

Figure C.41: Pitch short fiber sample 5

Figure C.42: Pitch short fiber sample 6

Figure C.43: Pitch short fiber sample 7

C.4. SEM

C.4.1. PAN short fiber

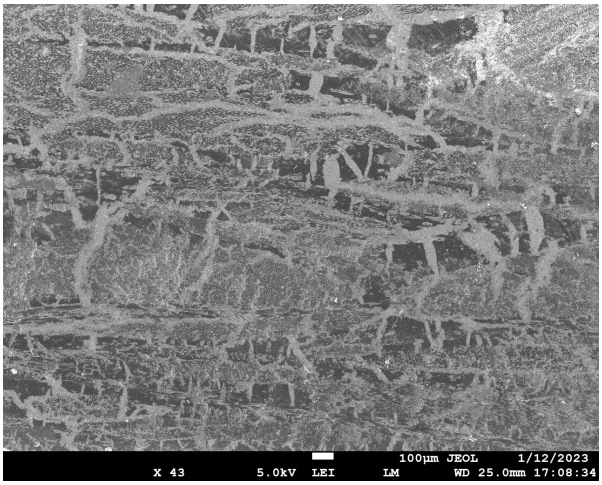

Figure C.44: Overview SEM image, variation 1

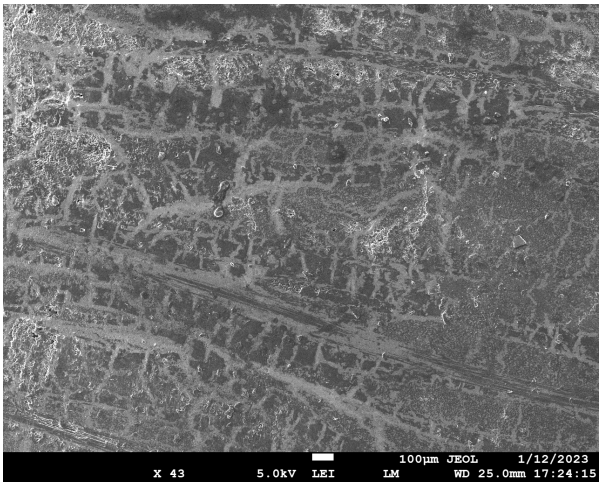

Figure C.45: Overview SEM image, variation 1

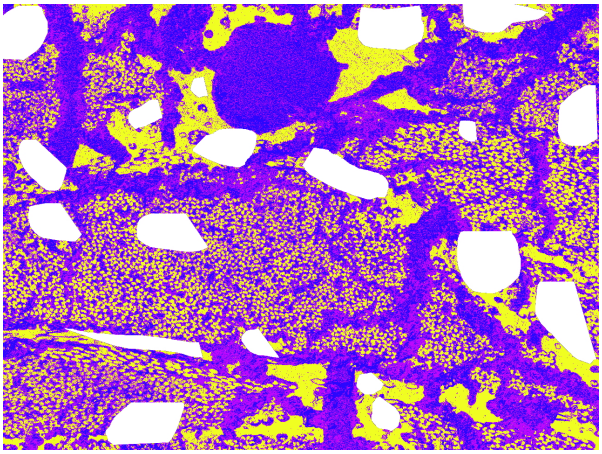

Figure C.46: Processed SEM image, variation 1

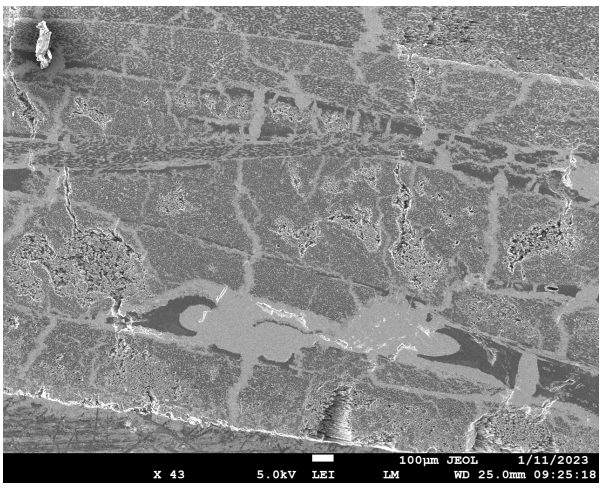

Figure C.47: Overview SEM image, variation 2

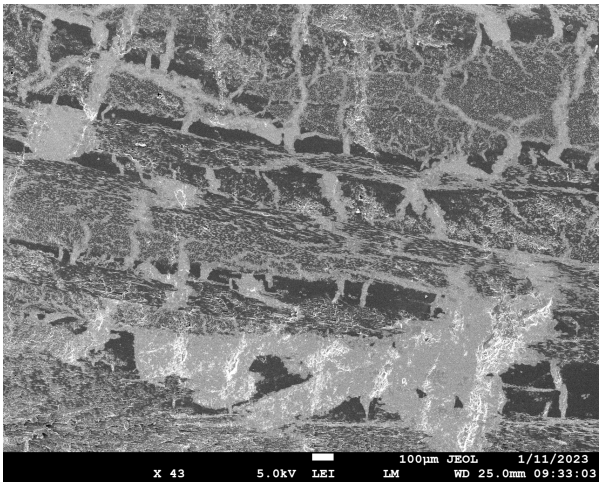

Figure C.48: Overview SEM image, variation 2

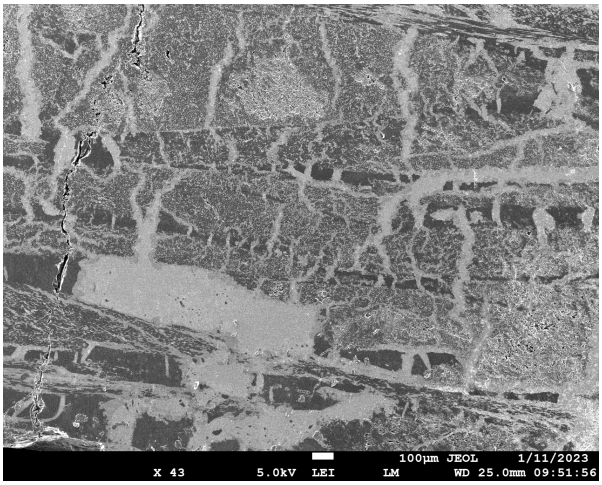

Figure C.49: Overview SEM image, variation 2

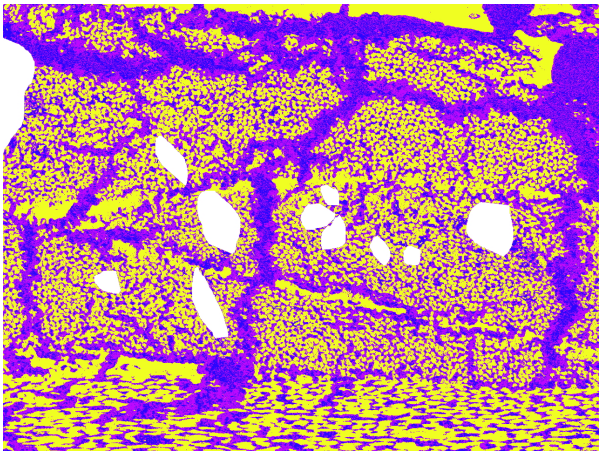

Figure C.50: Processed SEM image, variation 2

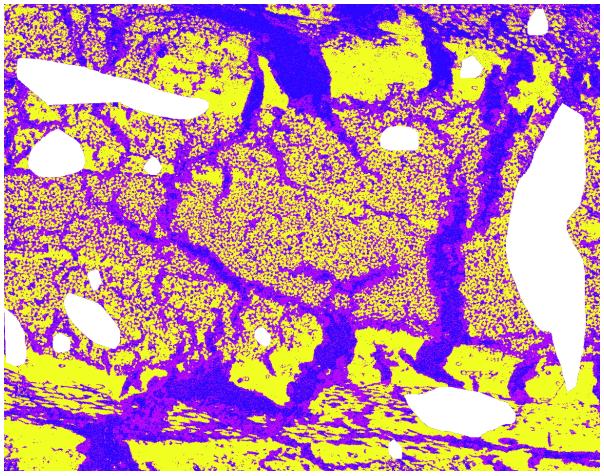

Figure C.51: Processed SEM image, variation 2

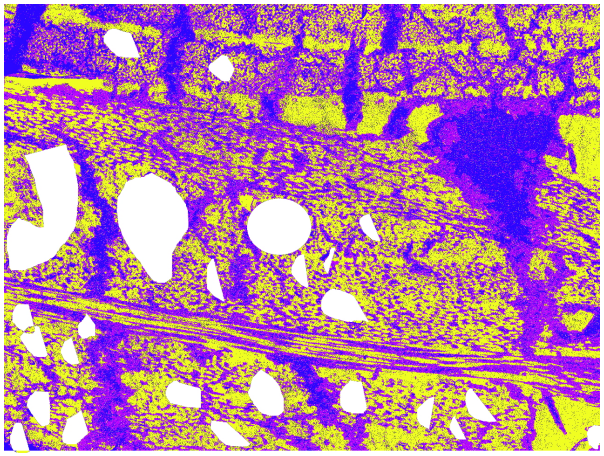

Figure C.52: Processed SEM image, variation 2

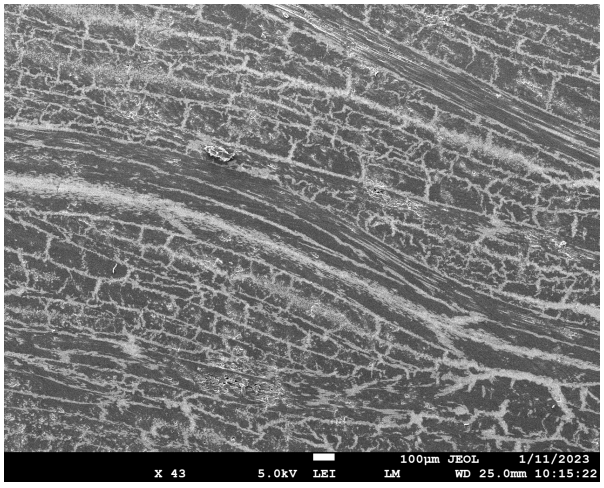

Figure C.53: Overview SEM image, variation 3

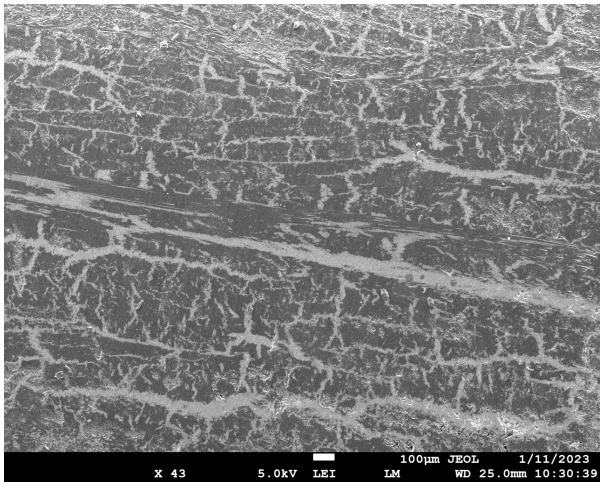

Figure C.54: Overview SEM image, variation 3

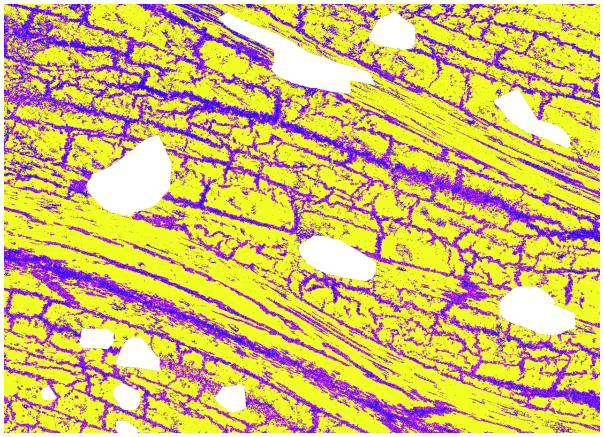

Figure C.55: Processed SEM image, variation 3

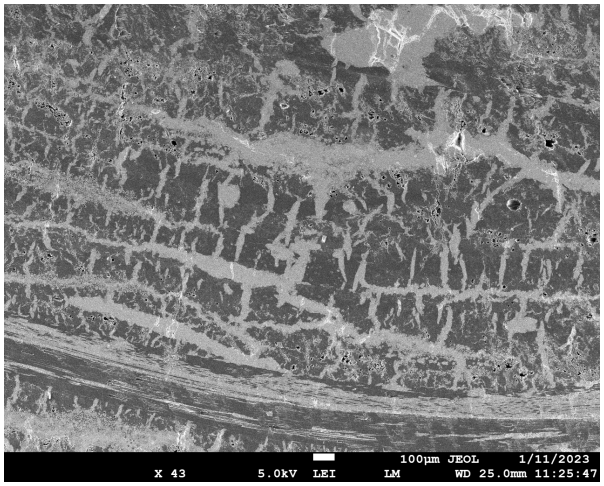

Figure C.56: Overview SEM image, variation 4

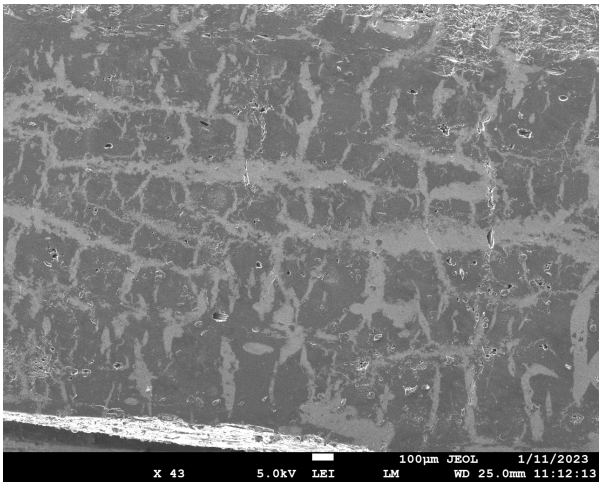

Figure C.57: Overview SEM image, variation 4

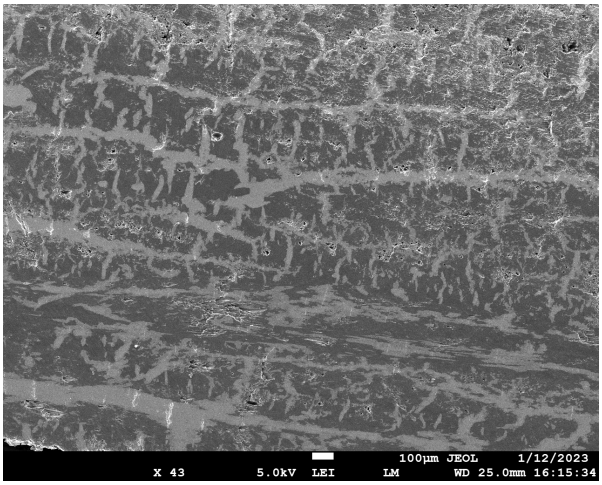

Figure C.58: Overview SEM image, variation 4

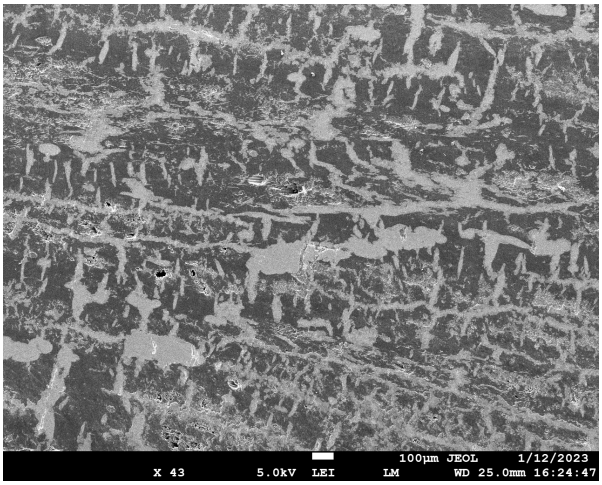

Figure C.59: Overview SEM image, variation 4

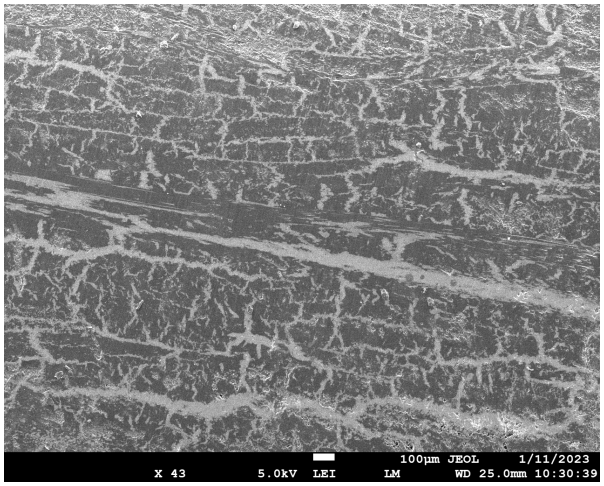

Figure C.60: Overview SEM image, variation 4

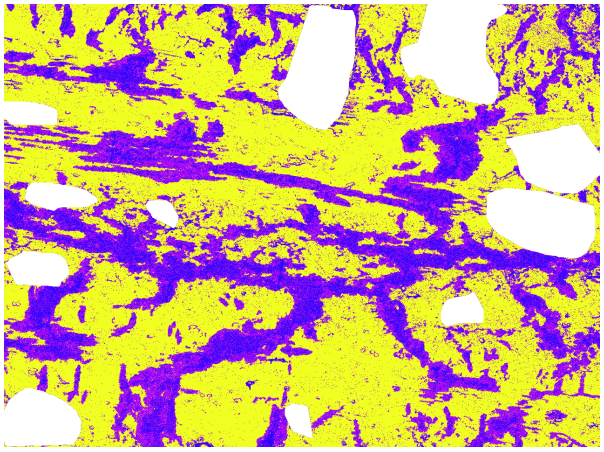

Figure C.61: Processed SEM image, variation 4

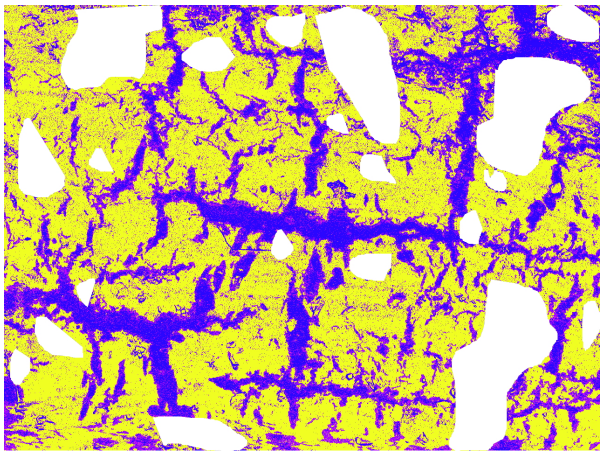

Figure C.62: Processed SEM image, variation 4

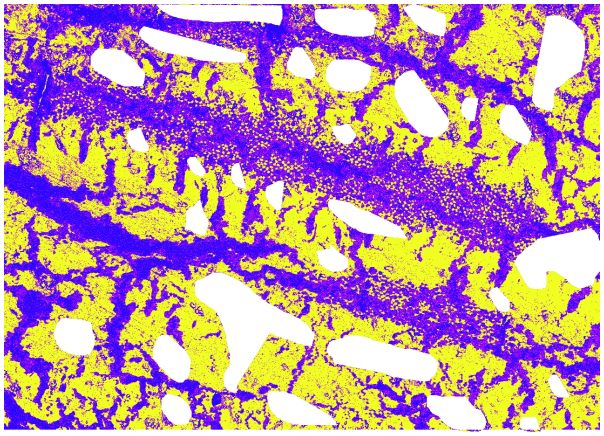

Figure C.63: Processed SEM image, variation 4

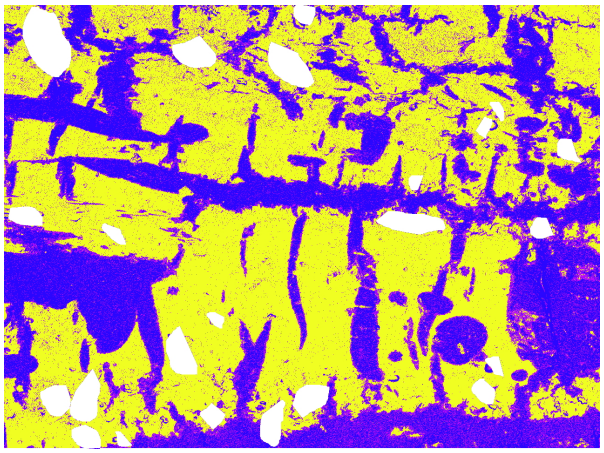

Figure C.64: Processed SEM image, variation 4

C.4.2. Pitch short fiber

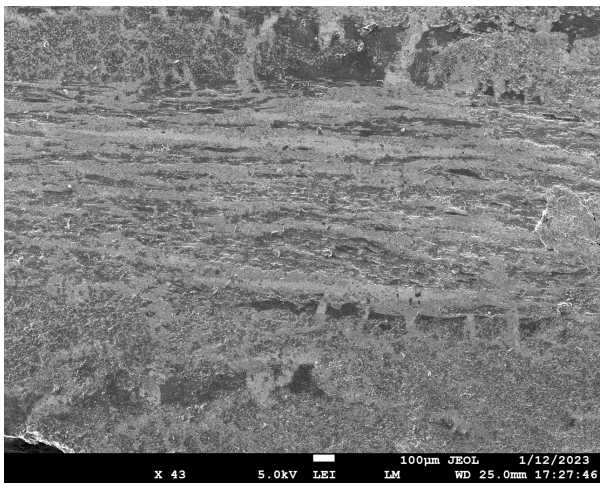

Figure C.65: Overview SEM image, variation 5

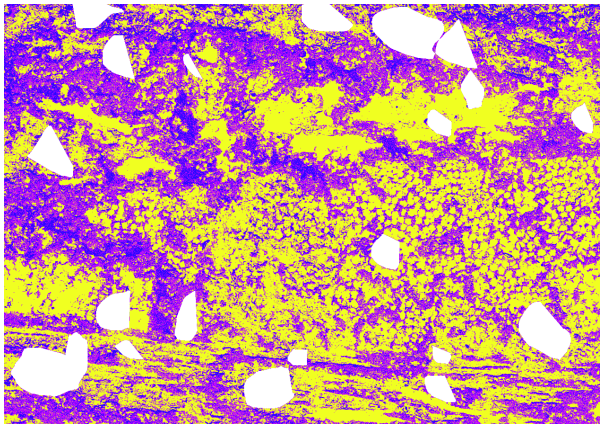

Figure C.66: Processed SEM image, variation 5

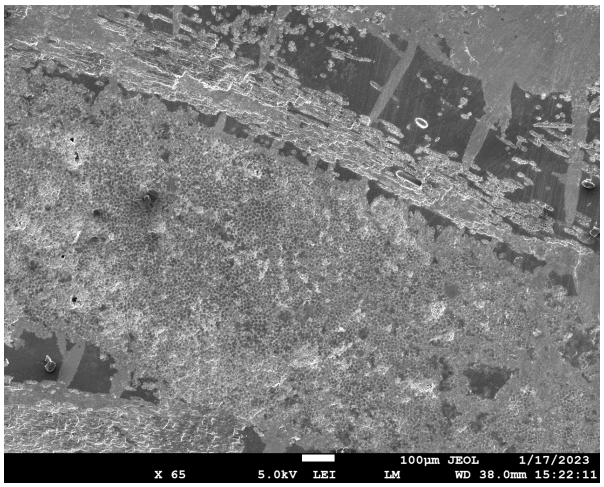

Figure C.67: Overview SEM image, variation 6

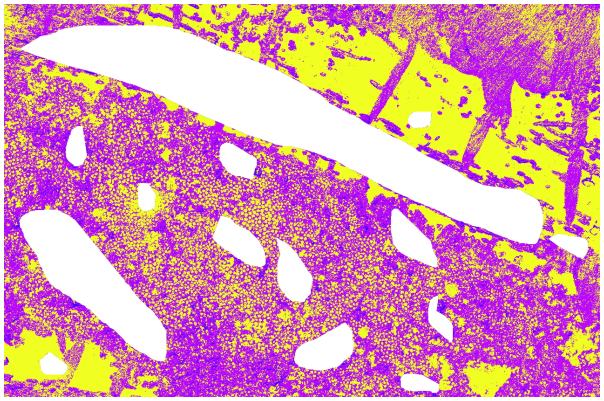

Figure C.68: Processed SEM image, variation 6

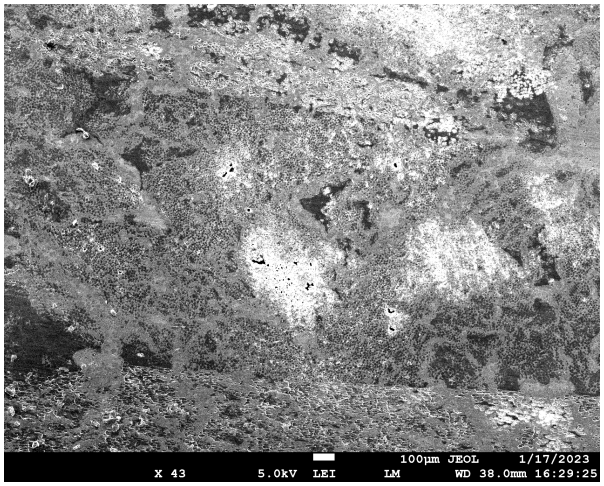

Figure C.69: Overview SEM image, variation 7

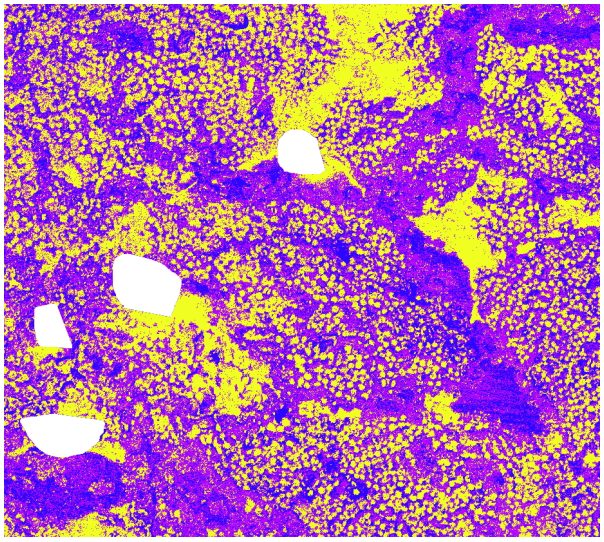

Figure C.70: Processed SEM image, variation 7

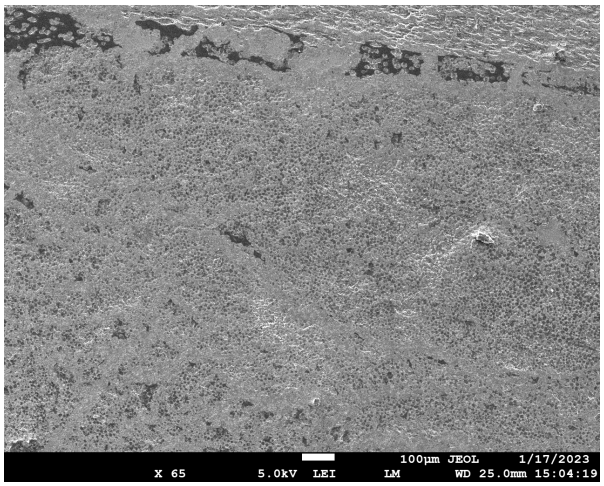

Figure C.71: Overview SEM image, variation 8

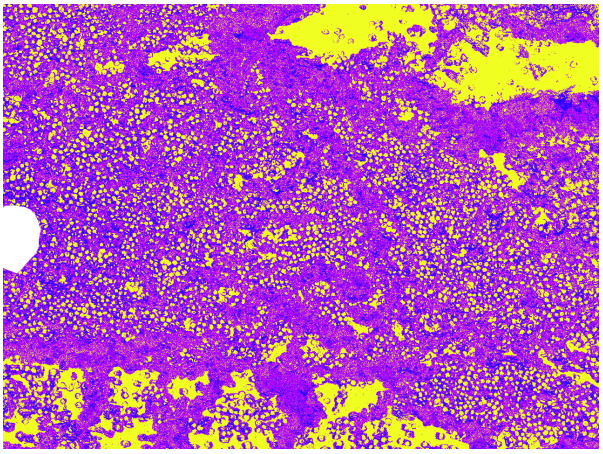

Figure C.72: Processed SEM image, variation 8

C.5. X-ray

C.5.1. PAN short fiber

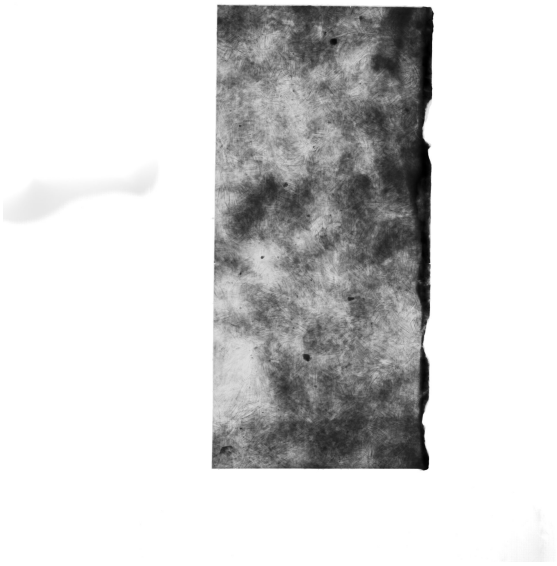

Figure C.73: X-ray, variation 1, sample 1

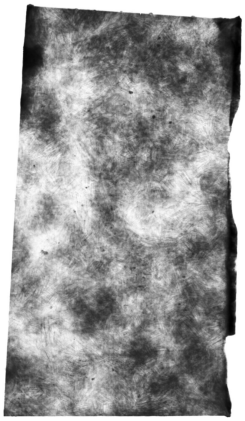

Figure C.74: X-ray, variation 1, sample 2

Figure C.75: X-ray, variation 1, sample 3

Figure C.76: X-ray, variation 1, sample 4

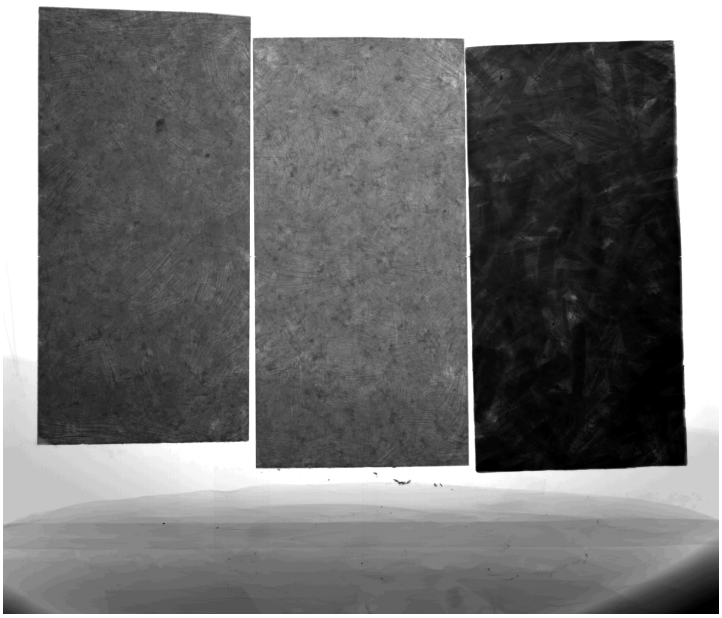

Figure C.77: X-ray, middle: variation 2, sample 8, left: variation 2, sample 9. Both 5 mm in thickness

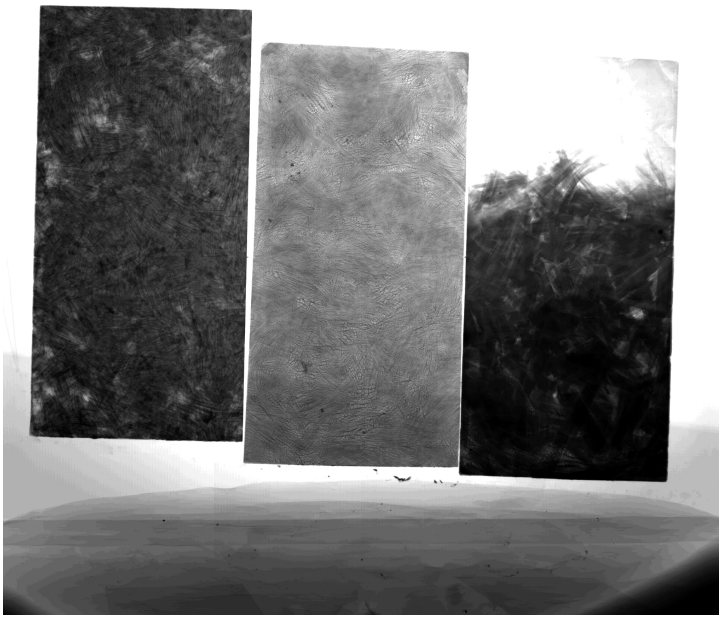

Figure C.78: X-ray, middle: variation 4, sample 5, left: variation 2, sample 10

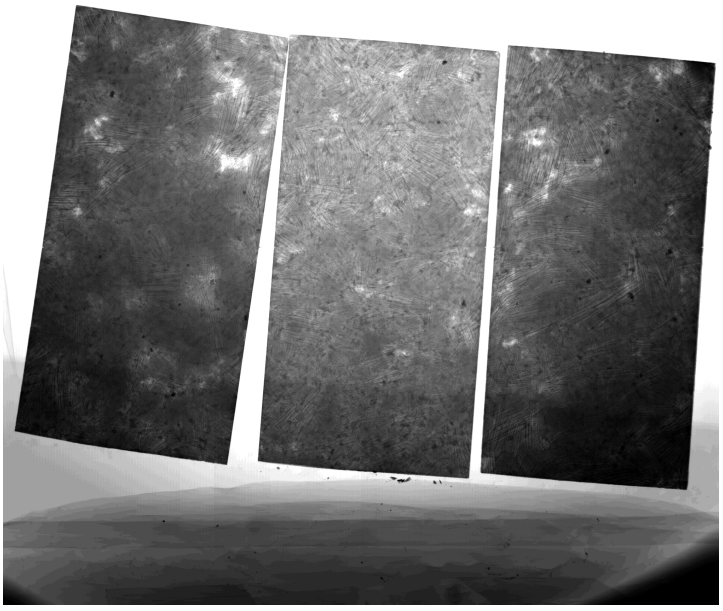

Figure C.79: X-ray, right: variation 2, sample 2, middle: variation 2, sample 3, left: variation 2, sample 4

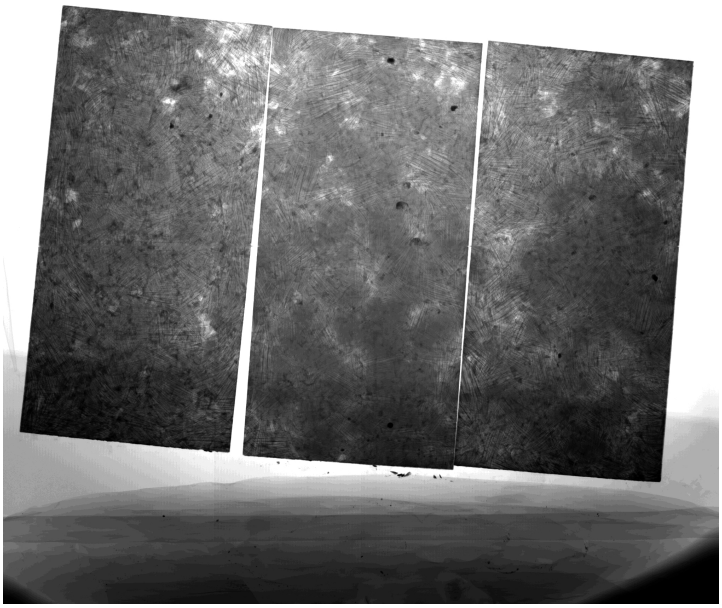

Figure C.80: X-ray, right: variation 2, sample 5, middle: variation 6, sample 3, left: variation 2, sample 7

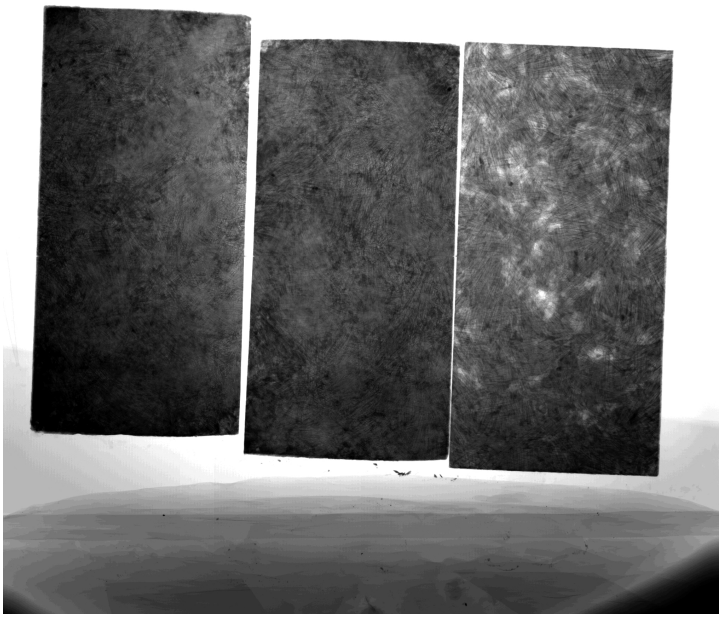

Figure C.81: X-ray, right: variation 2, sample 11, middle: variation 4, sample 1, left: variation 4, sample 2

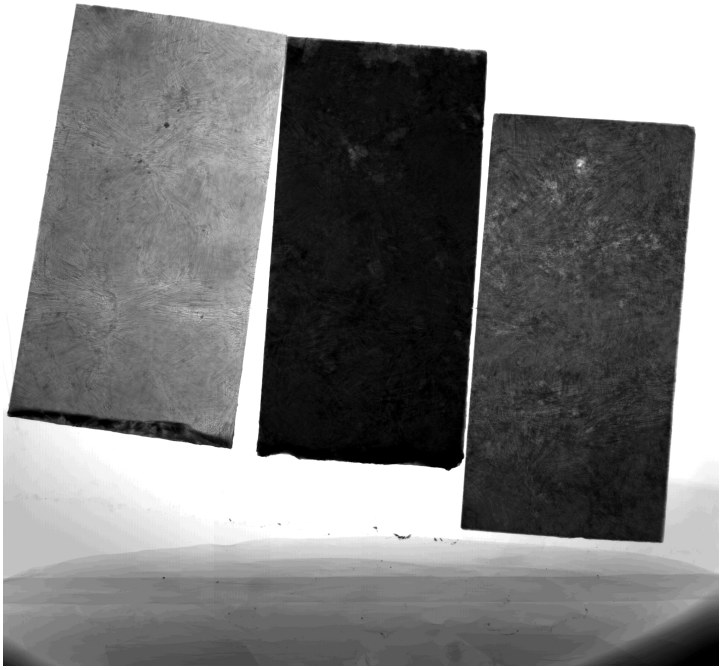

Figure C.82: X-ray, right: variation 4, sample 3, middle: variation 4, sample 4, left: variation 4, sample 6

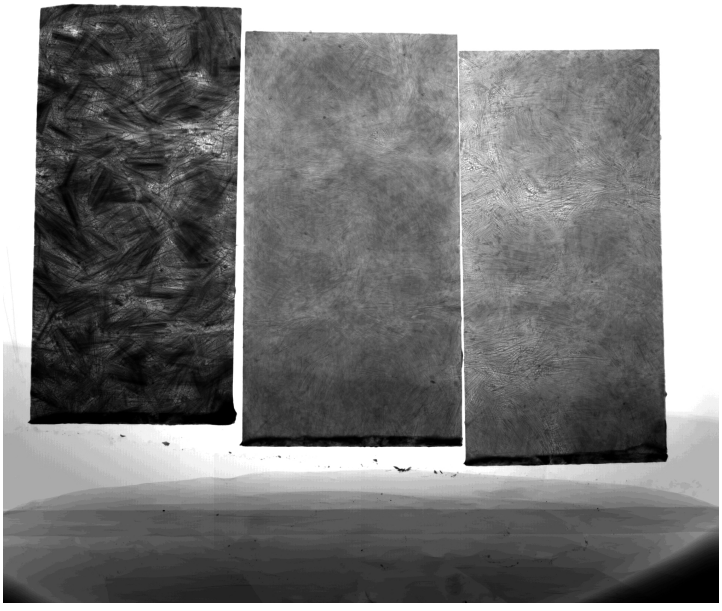

Figure C.83: X-ray, right: variation 4, sample 7, middle: variation 3, sample 1

C.5.2. Pitch short fiber

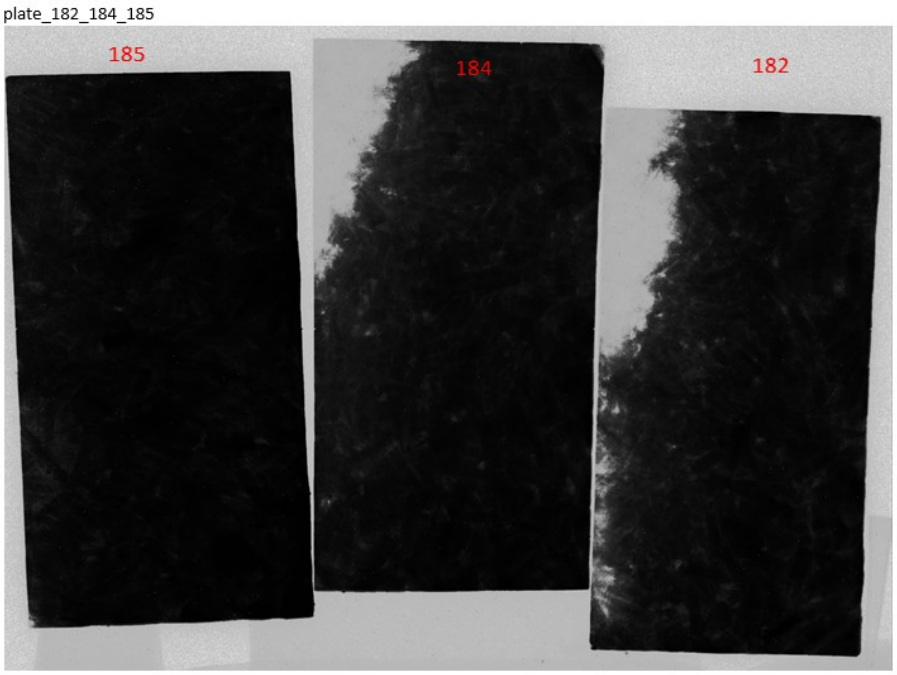

Figure C.84: X-ray, variation 5, sample 3, 2, 1

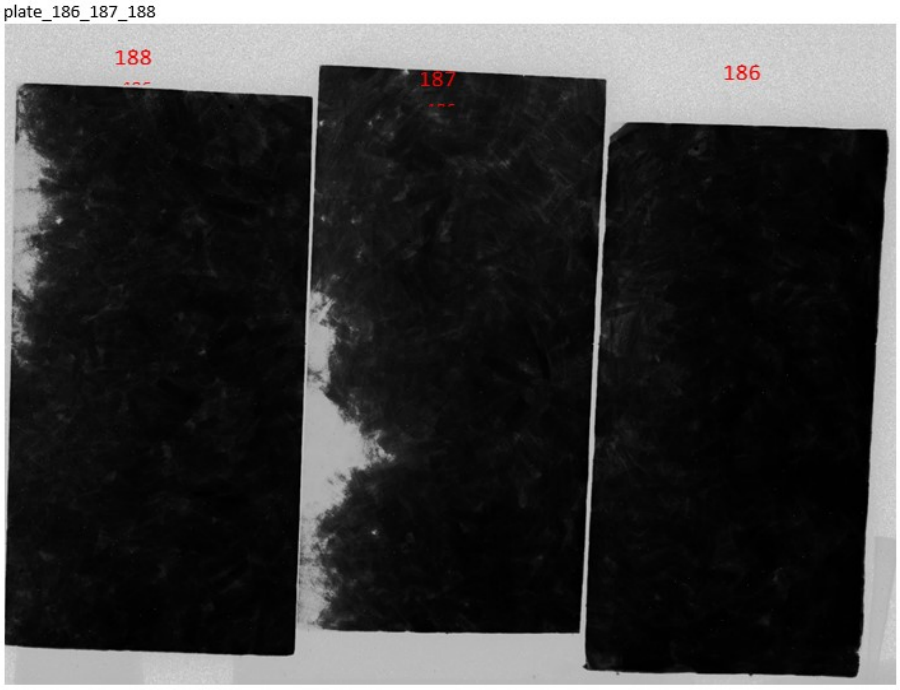

Figure C.85: X-ray, variation 5, sample 6, 5, 4

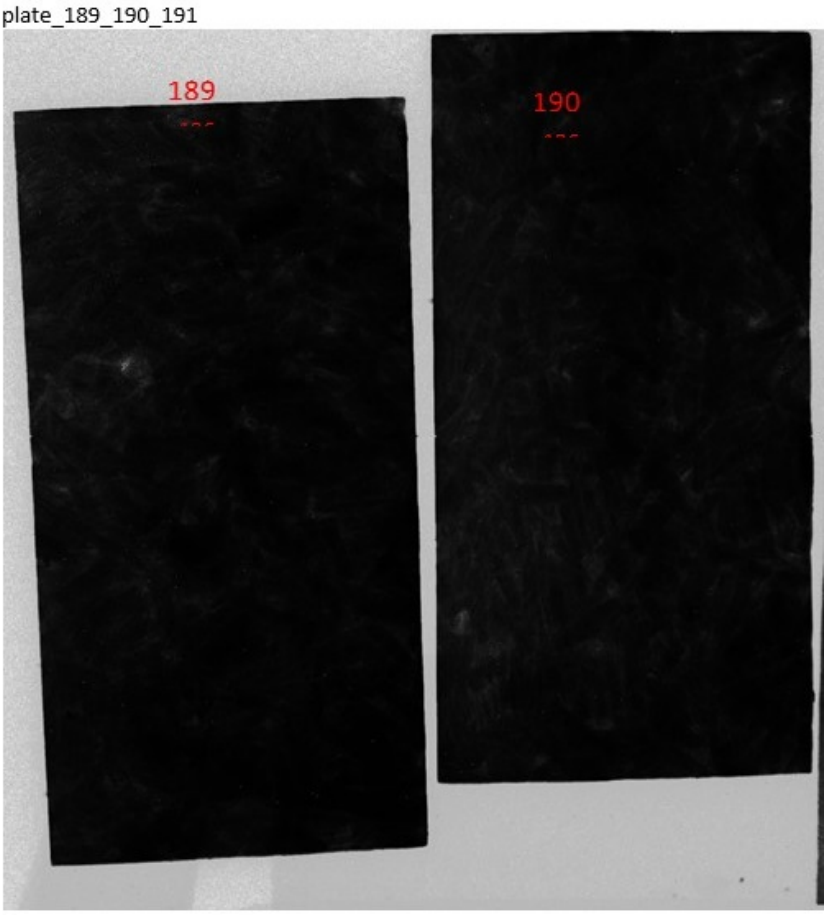

Figure C.86: X-ray, variation 5, sample 7,8

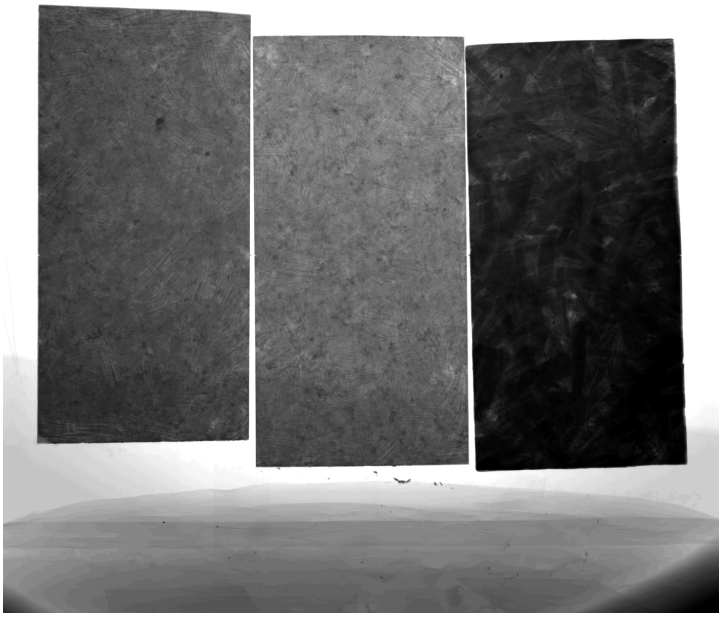

Figure C.87: X-ray, right: variation 8, sample 1

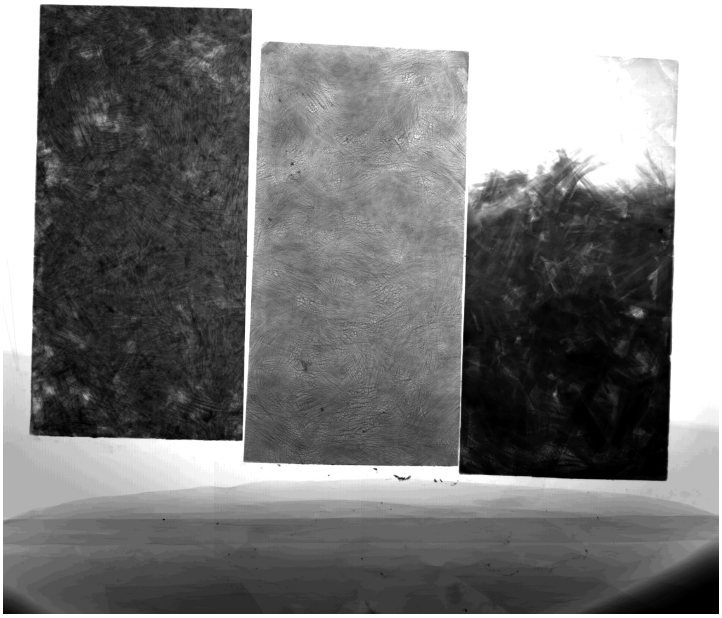

Figure C.88: X-ray, right: variation 7, sample 1

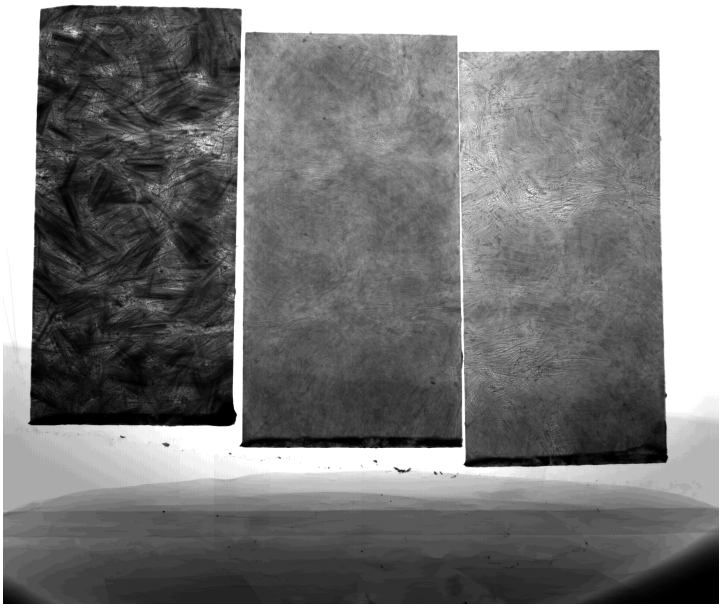

Figure C.89: X-ray, left: variation 6, sample 1

C.6. CTE graphs

C.6.1. Low temperature

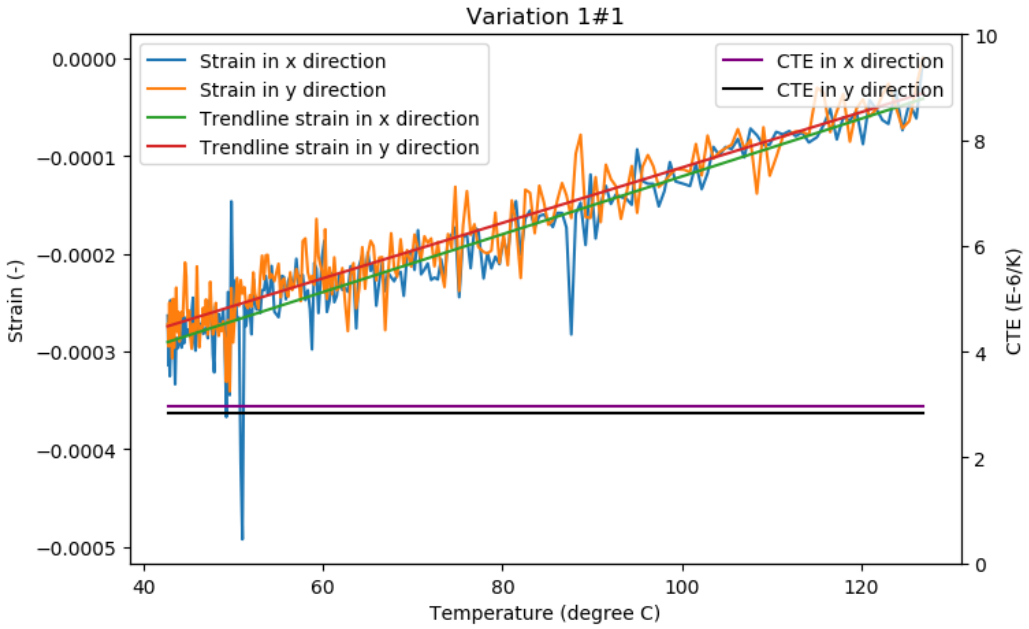

Figure C.90: Strain versus temperature and CTE values, variation 1, sample 1, low temperature

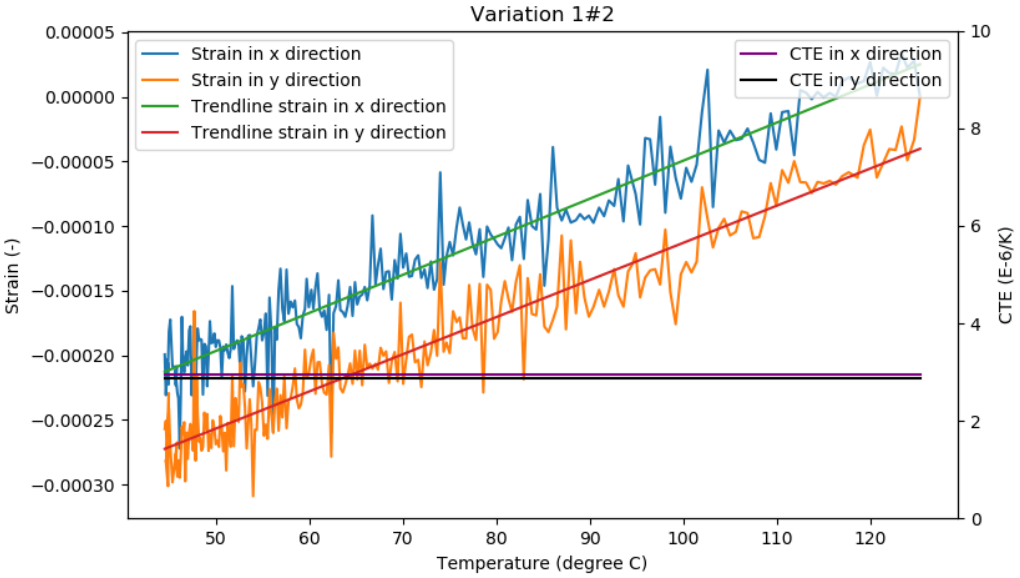

Figure C.91: Strain versus temperature and CTE values, variation 1, sample 2, low temperature

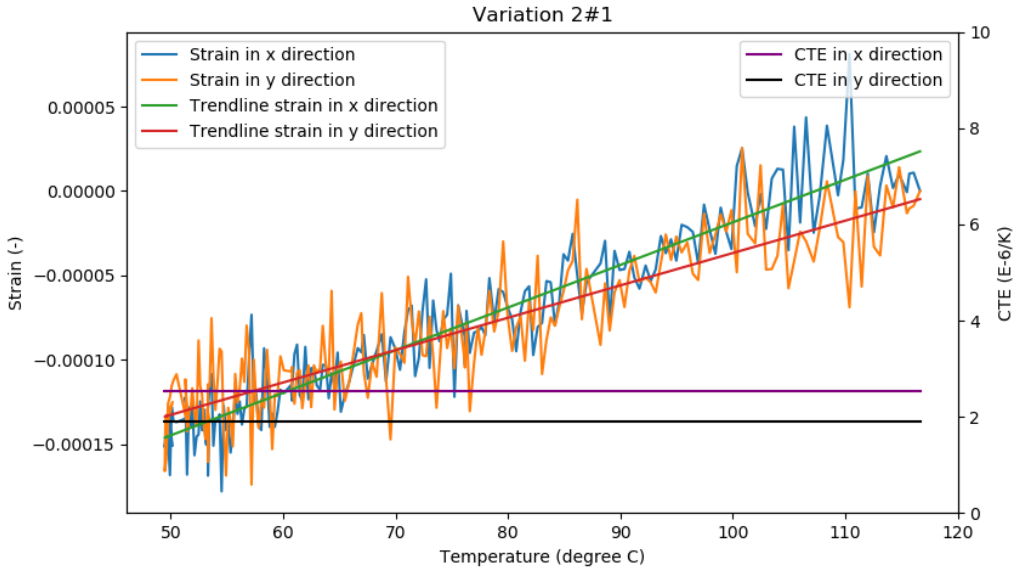

Figure C.92: Strain versus temperature and CTE values, variation 2, sample 1, low temperature

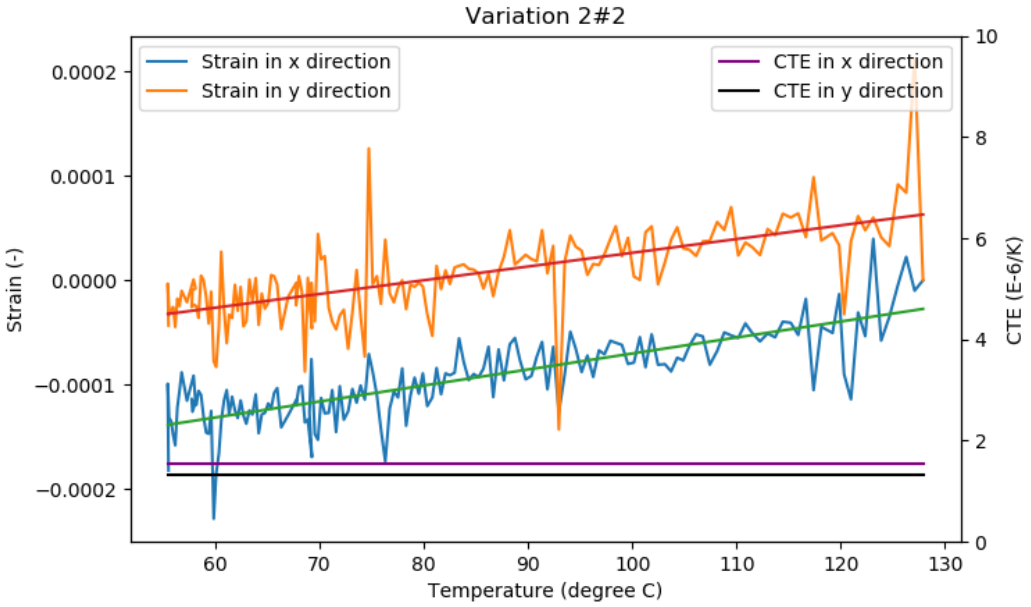

Figure C.93: Strain versus temperature and CTE values, variation 2, sample 2, low temperature

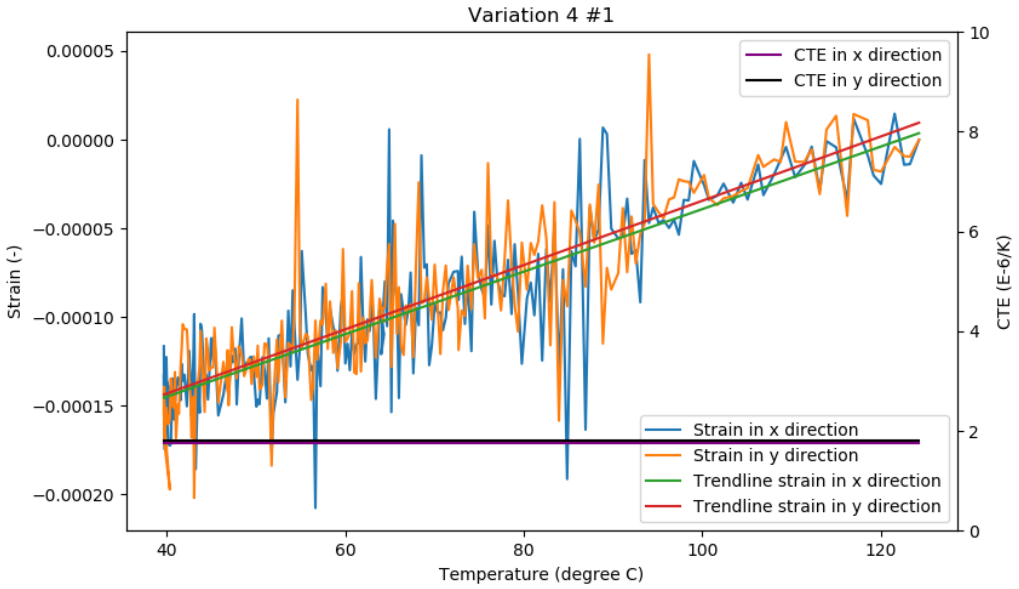

Figure C.94: Strain versus temperature and CTE values, variation 4, sample 1, low temperature

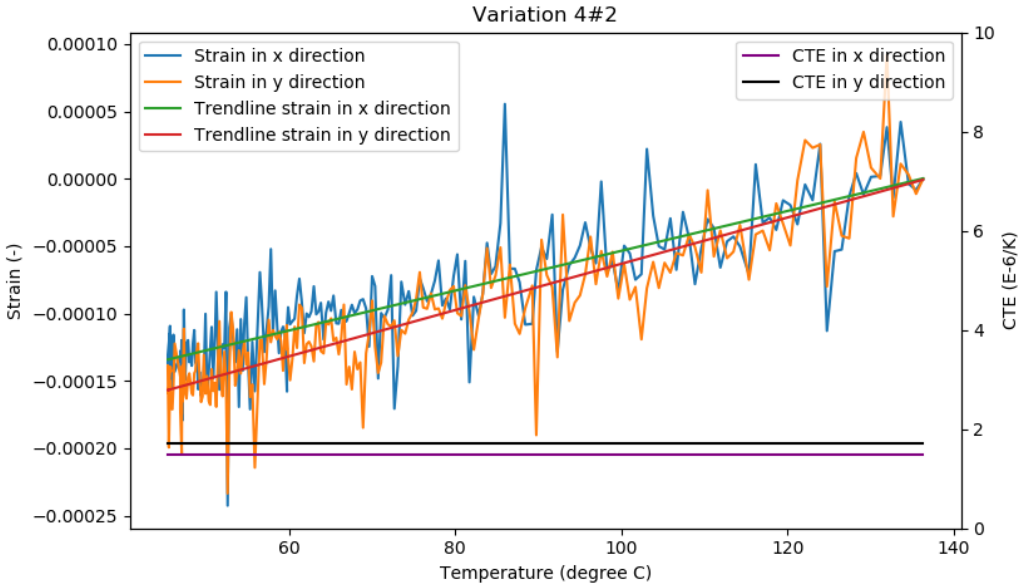

Figure C.95: Strain versus temperature and CTE values, variation 4, sample 2, low temperature

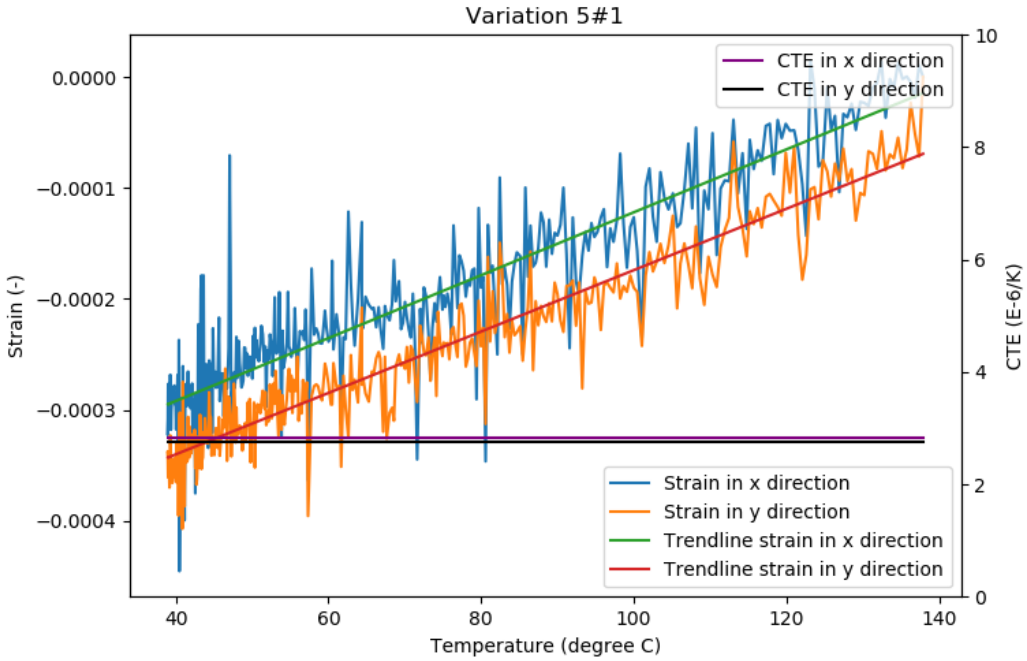

Figure C.96: Strain versus temperature and CTE values, variation 5, sample 1, low temperature

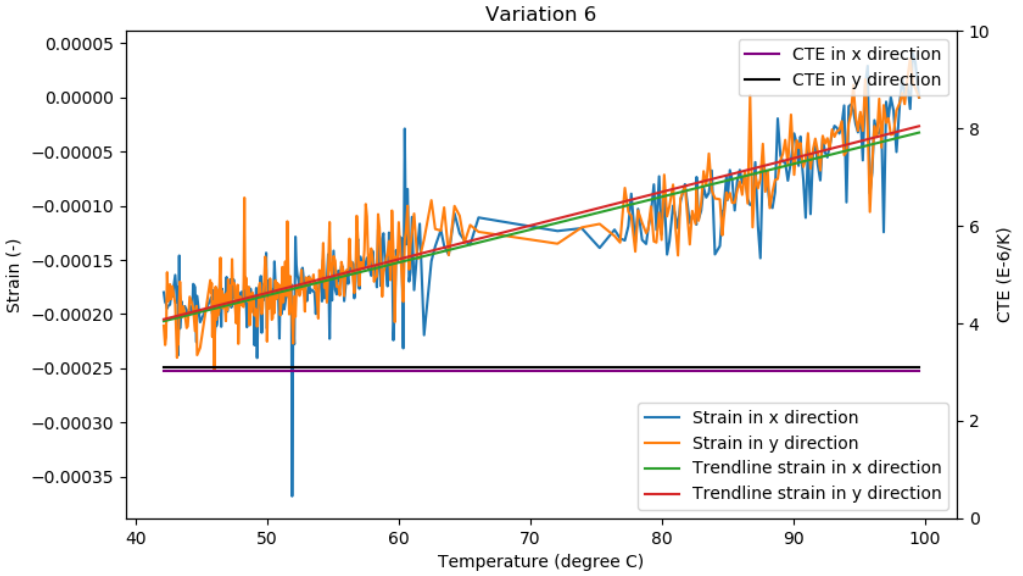

Figure C.97: Strain versus temperature and CTE values, variation 6, low temperature

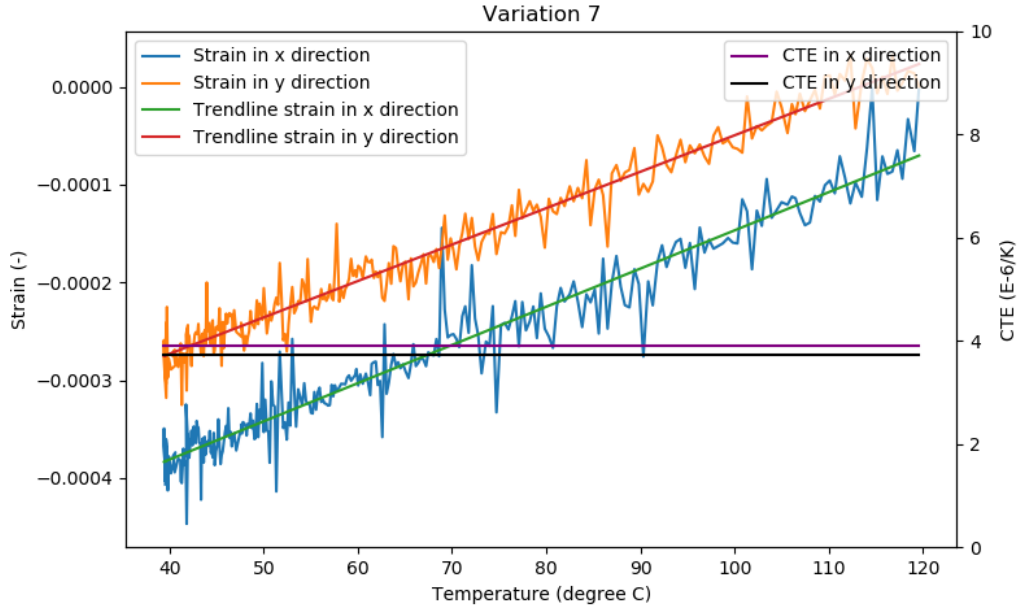

Figure C.98: Strain versus temperature and CTE values, variation 7, low temperature

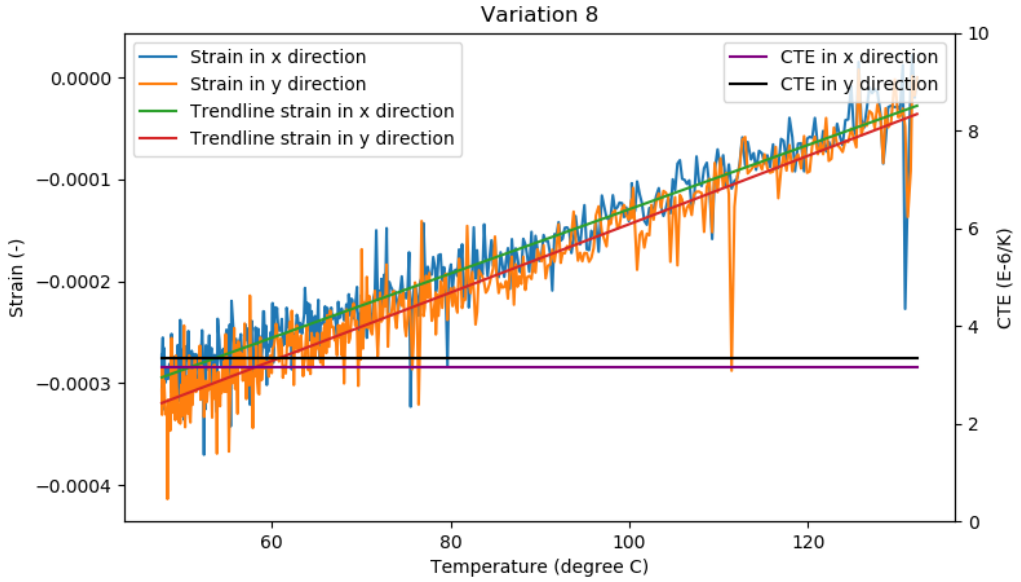

Figure C.99: Strain versus temperature and CTE values, variation 8, low temperature

C.6.2. High temperature

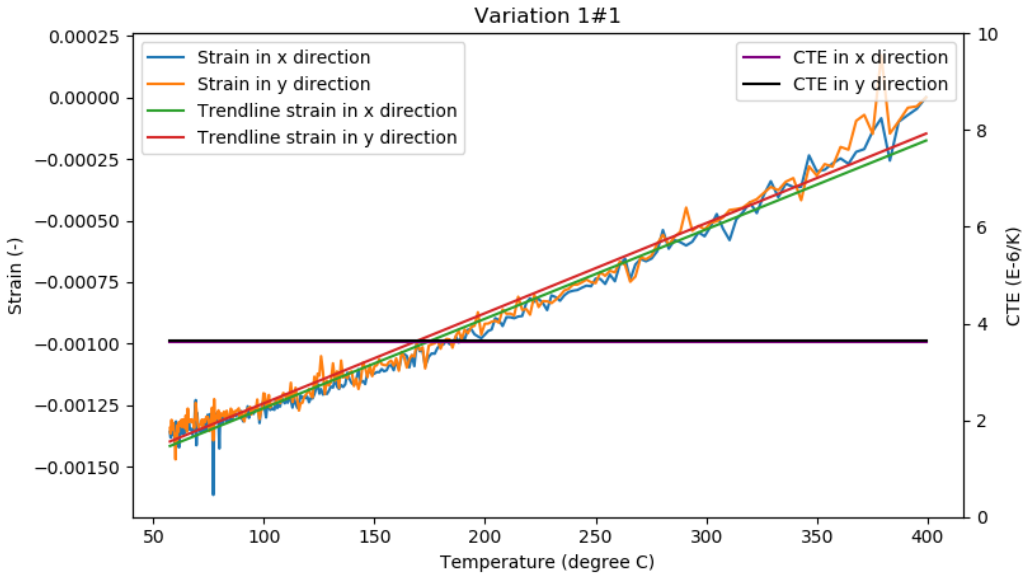

Figure C.100: Strain versus temperature and CTE values, variation 1, sample 1, high temperature

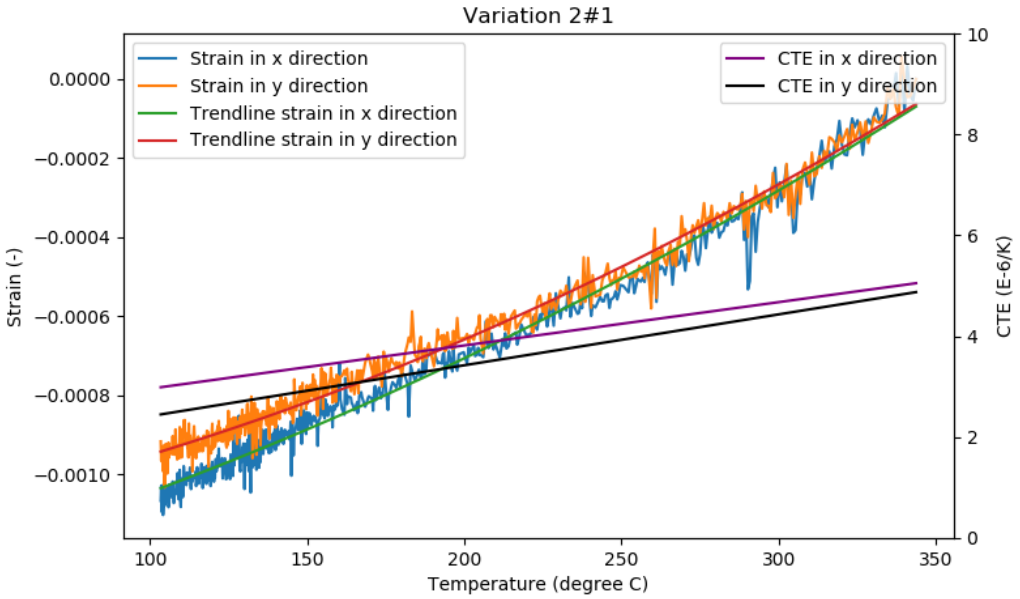

Figure C.101: Strain versus temperature and CTE values, variation 2, sample 1, high temperature

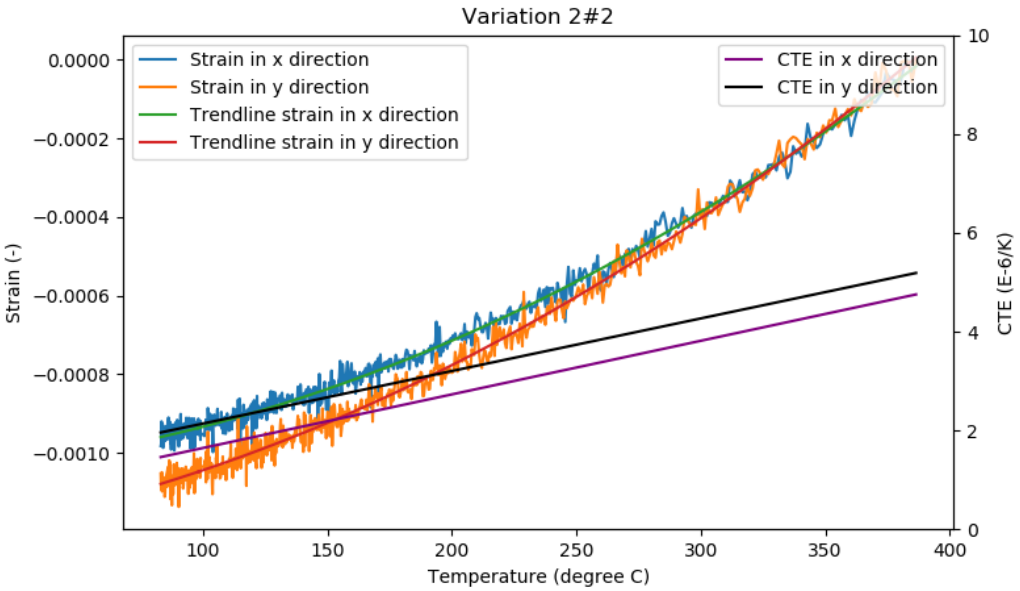

Figure C.102: Strain versus temperature and CTE values, variation 2, sample 2, high temperature

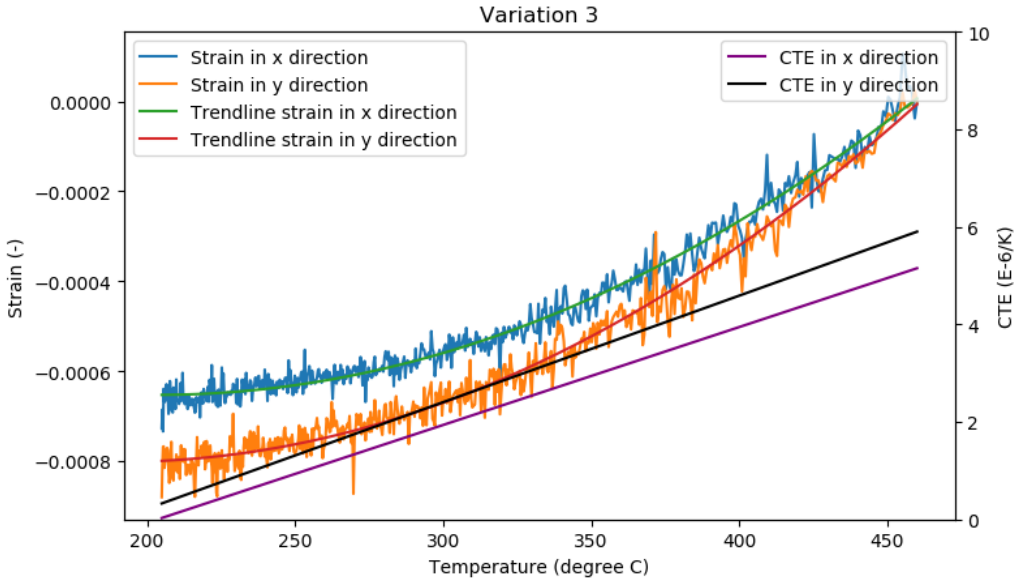

Figure C.103: Strain versus temperature and CTE values, variation 3, high temperature

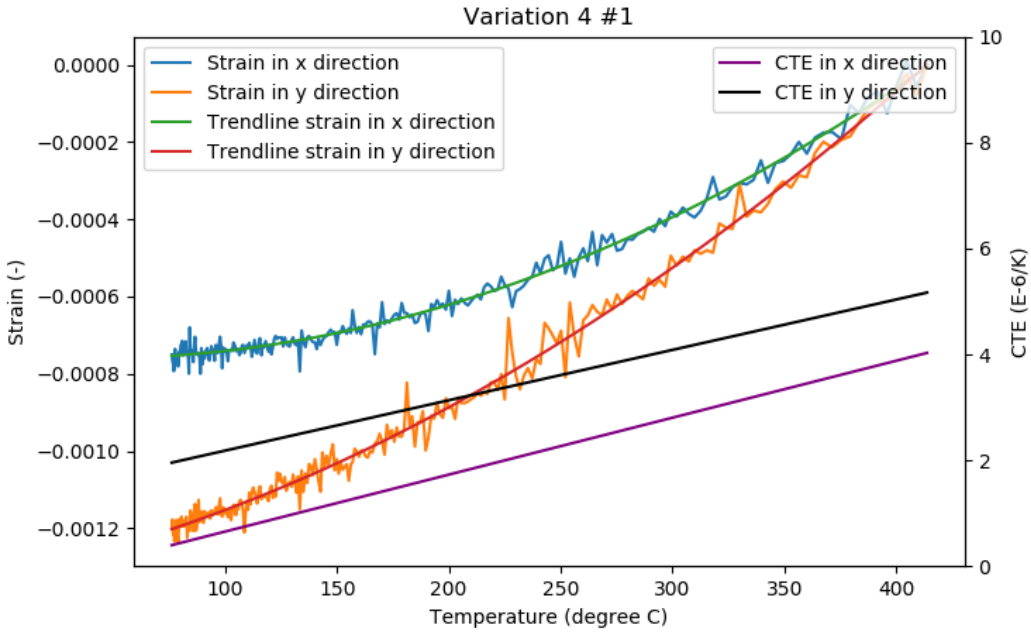

Figure C.104: Strain versus temperature and CTE values, variation 4, sample 1, high temperature

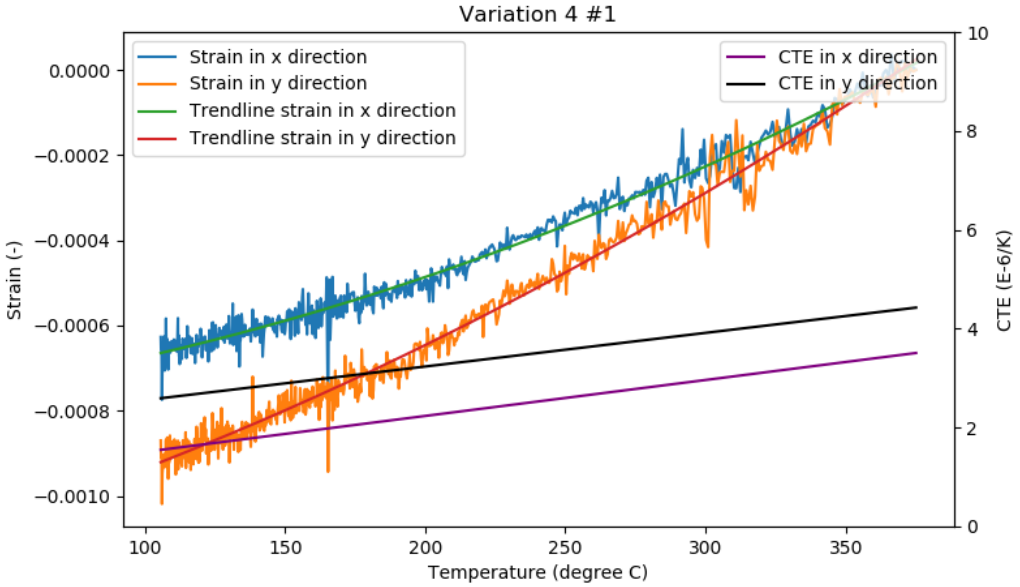

Figure C.105: Strain versus temperature and CTE values, variation 4, sample 1, high temperature

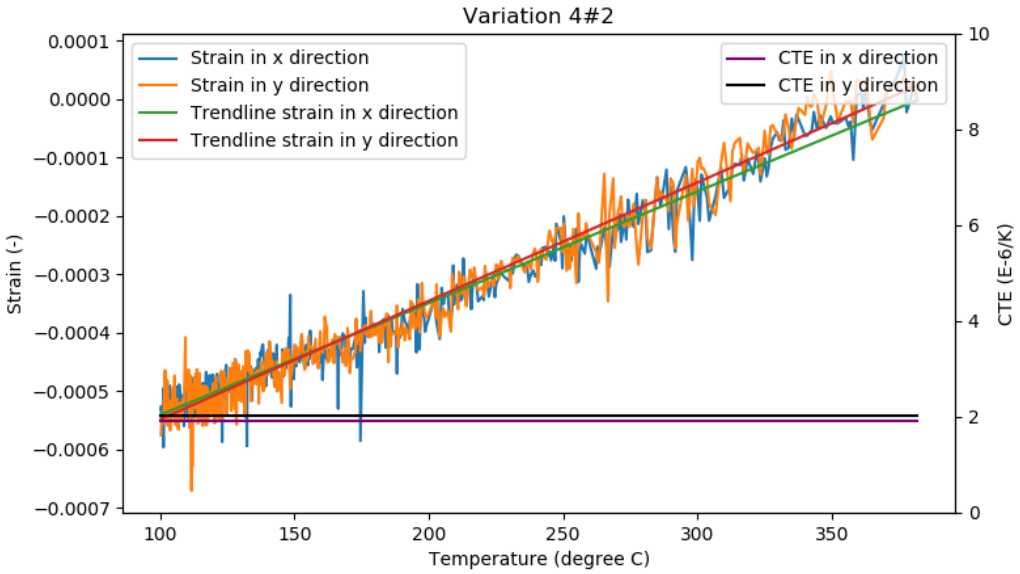

Figure C.106: Strain versus temperature and CTE values, variation 4, sample 2, high temperature

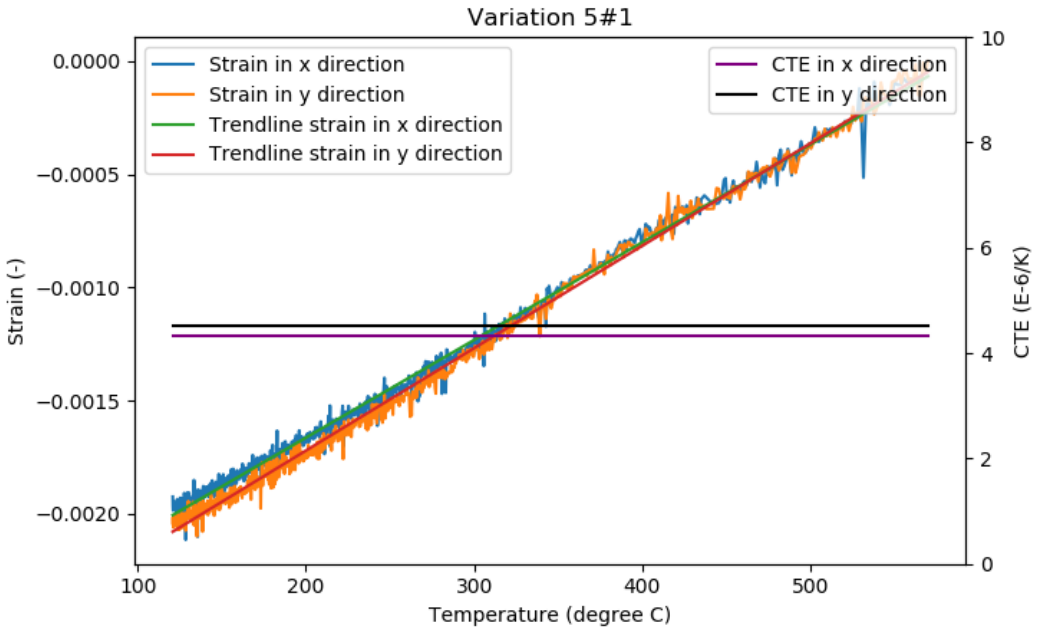

Figure C.107: Strain versus temperature and CTE values, variation 5, sample 1, high temperature

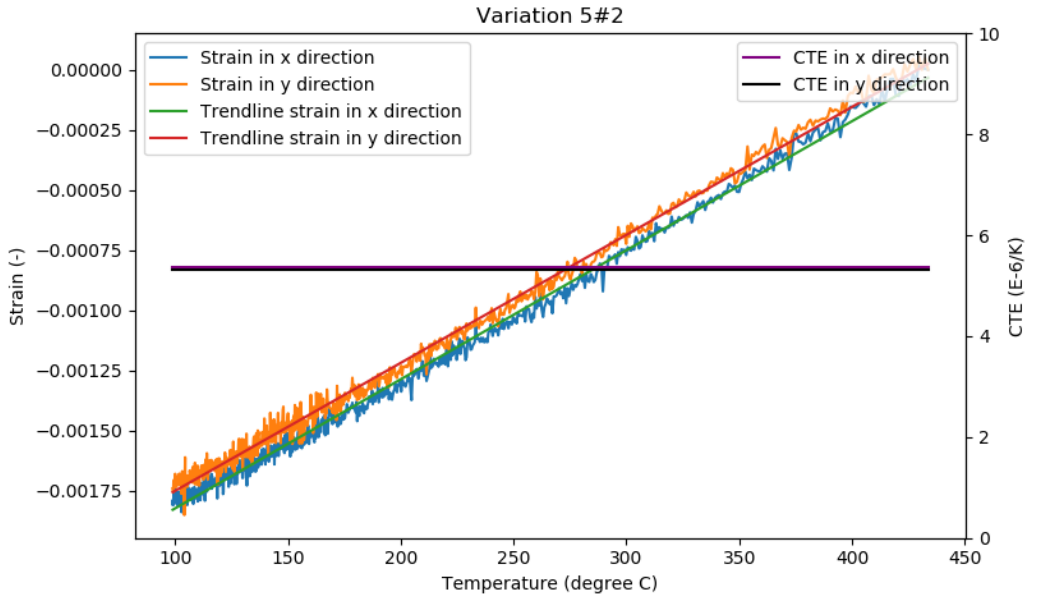

Figure C.108: Strain versus temperature and CTE values, variation 5, sample 2, high temperature

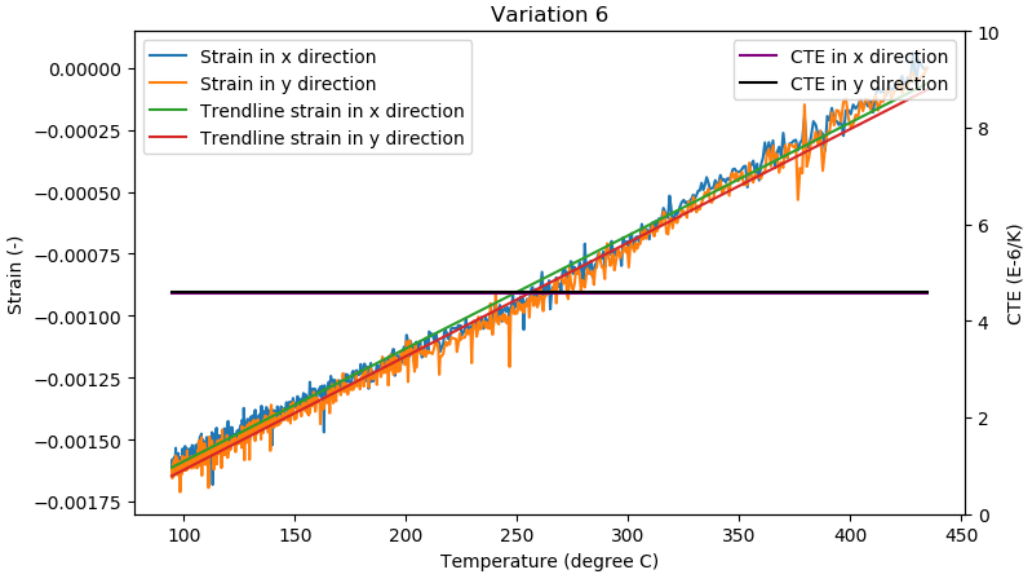

Figure C.109: Strain versus temperature and CTE values, variation 6, high temperature

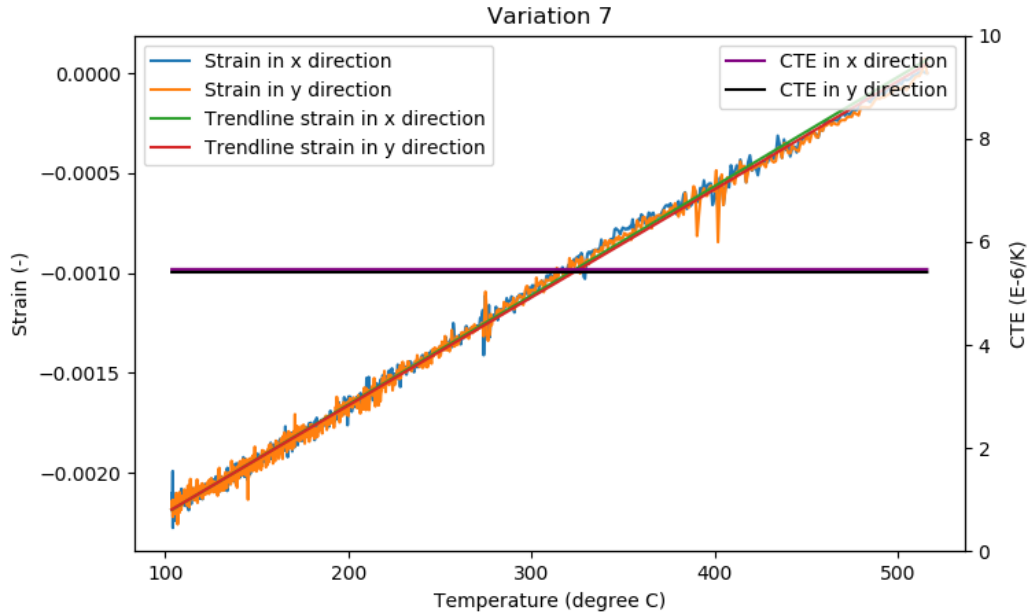

Figure C.110: Strain versus temperature and CTE values, variation 7, high temperature

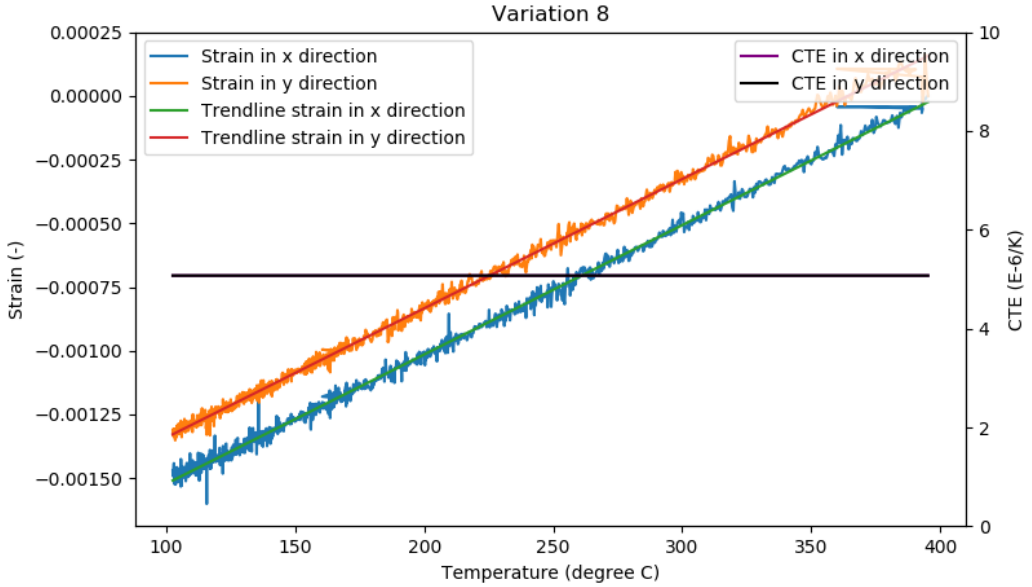

Figure C.111: Strain versus temperature and CTE values, variation 8, high temperature